



TECHNISCHE UNIVERSITÄT MÜNCHEN

Lehrstuhl für Anorganische Chemie mit Schwerpunkt Neue Materialien

**Polar Intermetallics at the Border Between
Hume-Rothery and Zintl Phases:
Investigations in the Systems Alkali Metal – Tin with
Late Transition and *p*-Block Metals**

Marina Boyko

Vollständiger Abdruck der von der Fakultät für Chemie der Technischen Universität
München zur Erlangung des akademischen Grades eines

Doktors der Naturwissenschaften (Dr. rer. nat.)

genehmigten Dissertation.

Vorsitzender: Prof. Dr. Shigeyoshi Inoue

Prüfer der Dissertation:

1. Prof. Dr. Thomas F. Fässler
2. Prof. Dr. Tom Nilges

Die Dissertation wurde am 07.08.2019 bei der Technischen Universität München
eingereicht und durch die Fakultät für Chemie am 11.09.2019 angenommen.

Der experimentelle Teil dieser Arbeit wurde in der Zeit von September 2015 bis August 2019 am Lehrstuhl für Anorganische Chemie mit Schwerpunkt Neue Materialien der Technische Universität München unter wissenschaftlicher Leitung von Herrn Prof. Dr. Thomas F. Fässler durchgeführt.

Ich erkläre hiermit an Eides statt, dass ich die vorliegende Arbeit ohne unzulässige Hilfe Dritter und ohne Benutzung anderer als der angegebenen Hilfsmittel angefertigt habe. Die aus anderen Quellen direkt oder indirekt übernommen Daten und Konzepte sind unter Angabe des Literaturzitats gekennzeichnet.

Garching, den 07.08.2019

“Miracles, in fact, are a retelling in small letters of the very same story which is written across the whole world in letters too large for some of us to see.”

C.S. Lewis

Acknowledgements

First of all, I would like to thank **Prof. Dr. Thomas F. Fässler** for giving me an opportunity to work on this project and his valuable guidance and expertise.

Throughout the whole time working on this dissertation I have received a great deal of support and assistance. I would like to acknowledge **Dr. Viktor Hlukhyy** for introducing me to the special aspects of the experimental work, constructive discussion, his help with the various crystallographic problems, guidance while solving single crystal structures and LMTO calculations as well as proofreading this dissertation.

I would also like to thank **Manuela Donaubauer**, the heart of our chair, for her amazing ability to know all there is to know about everything, including all kinds of bureaucratic affairs. Many thanks for her amazing patience and being always ready to help with any organizational question.

My sincere thanks also go to all my colleagues:

- **Maria Müller** for measuring EDX and hours spent together while He-transport, being my biggest helper with the SQUID magnetometer.
- **Ingrid Werner** for helping to maintain the SQUID magnetometer.
- **Dr. Wilhelm Klein** for his quick help with various diffractometer problems and for the ability to face them with humor.
- **Dr. Iryna Kurylyshyn** for her help with frustrating (not only for foreigners) bureaucratic procedures during my first steps in Germany.
- **Dr. Alexander Henze** for introducing me to the project, **Dr. Lavinia Scherf** and **Henrik Eickhoff** for their useful advice and helpfulness in every aspect of the experimental work.
- **Dr. Kerstin Mayer**, **Dr. Sabine Frischhut** for the lovely company outside of the lab, sharing adventures sport activities and our creative projects.
- **Christoph Wallach**, **Thomas Wylezich**, **Benedikt Witzel**, **Stefan Strangmüller**, **David Müller** and **Dr. Felix Geitner** for their team spirit and ability to ensure that our life never got boring.
- **Tassilo Restle** for the pleasure of sharing the office with me and providing a great working atmosphere and constructive discussions, as well as performing DSC measurements.

- **Christoph Wallach** and **Dr. Sebastian Geier** for performing Raman measurements.
- **Thomas Braun** for peaceful coexistence in the lab and his great help with LMTO calculations.
- **Jasmin Dums, Michael Giebel** for their friendly attitude.
- Master student **Fiorello Buzi** and intern **Po-Yuan Huang** for their experimental work.
- **Group of Prof. Dr. Tom Nilges** for participation in the group seminar, **Patrick Walke** for measuring DSC of various samples and **Claudia Ott** for supplying coffee.

There are all my old and new friends, who were of great support in deliberating over the problems and successfully distracting my mind from the research. A thank you to **Solomiia** and **Alina** for staying in touch despite the distance between us, **Nate, Phoebe, Andy**, and my flatmates **Johanna** and **Kami** for finding a way into my life.

I am extremely grateful to all my family, especially my parents **Natalia** and **Alexander** for the encouragement and support, their love and sacrifices for educating and preparing me for my future.

And finally, my special thanks to **Sebastian** for staying by my side in good and bad times. I am excited to experience what the future brings us.

Abstract

Impressive variety and complexity of polar intermetallic compounds as well as their unique properties are the sources of inextinguishable interest in modern chemistry. Relationships between structure, composition, and properties, rationalized by chemical bonding are not losing their importance in the understanding of metallic systems. In the course of this work substitution and addition effects in binary alkali metal-tin systems were systematically investigated in order to obtain a better understanding of the bonding principles behind the formation of the polar intermetallics at the Zintl border. The aim of the present work was to develop a rational approach in the syntheses of new polar intermetallic phases in Na-Ag-Sn, Na-Sn-Bi, *A-T-Sn* (*A* = Na, K; *T* = Ru, Rh, Pd, Os, Ir, and Pt) and *K-Tr-Pn* (*Tr* = Ga, In; *Pn* = As, Bi) ternary systems, using reactions between diverse elements with widely different electronegativities and facing unpredictable behavior of intermetallic compounds.

The different solid-state synthesis routes for the various novel polar intermetallic compounds were described in this work. The characterization of the obtained compounds was performed using powder and single crystal X-ray diffraction methods and Raman spectroscopy for structural analysis; energy dispersive X-ray analysis, differential scanning calorimetry and magnetometry measurements for determination of the composition, thermal and magnetic behavior, respectively. For selected compounds, band structure calculations were carried out.

As the outcome of the substitution of tin atoms by silver in Na-Sn binary system icosahedral phases $\text{Na}_{29}\text{Ag}_{21}\text{Sn}_{39}$, $\text{Na}_{13}\text{Ag}_{5.5}\text{Sn}_{21.2}$ and $\text{Na}_{230.45}\text{Ag}_{274}\text{Sn}_{136}$, as well as an open framework compound $\text{Na}_5\text{Ag}_{3.74}\text{Sn}_{8.26}$ were obtained. The structure of the $\text{Na}_{29}\text{Ag}_{21}\text{Sn}_{39}$ features a polyanionic network of interconnected clusters units: heteroatomic empty icosahedra and Na-centered 20-atom clusters (hexagonal prism with all faces capped) as well as tin triangles. The polyanionic substructure of $\text{Na}_{29}\text{Ag}_{21}\text{Sn}_{39}$ can be described as a hierarchical relative of the CaCu_5 structure type in which specific atoms are replaced by certain cluster units. Compounds $\text{Na}_{13}\text{Ag}_{5.5}\text{Sn}_{21.2}$ and $\text{Na}_{230.45}\text{Ag}_{274}\text{Sn}_{136}$ comprise endohedral fullerene clusters (empty in $\text{Na}_{13}\text{Ag}_{5.5}\text{Sn}_{21.2}$ and Ag-centered in $\text{Na}_{230.45}\text{Ag}_{274}\text{Sn}_{136}$) and spaces fillers. Both compounds contain similar clusters consisting of four concentric shells with the outer shell built of fullerene-like 60 (in $\text{Na}_{13}\text{Ag}_{5.5}\text{Sn}_{21.2}$) or both 60 and 80 atoms (in $\text{Na}_{230.45}\text{Ag}_{274}\text{Sn}_{136}$). These compounds are formally Frank Kasper phases, but could also be seen as Hume Rothery phases, diluted by alkali metals.

The fourth compound in Na-Ag-Sn ternary system is $\text{Na}_5\text{Ag}_{3.74}\text{Sn}_{8.26}$ with a three-dimensional open framework of four-bonded Sn and Ag atoms and Na cations located in the voids.

Both compounds in Na-Sn-Bi ternary system $\text{Na}_{13}\text{Sn}_{25.73}\text{Bi}_{1.27}$ and $\text{Na}_{27}\text{Sn}_{45.63}\text{Bi}_{0.57}$ comprise three-dimensional tin network where bismuth is partially substituting 2-bonded Sn atoms and, in case of $\text{Na}_{13}\text{Sn}_{25.73}\text{Bi}_{1.27}$, additionally containing rather isolated Bi atoms. Na atoms filling the voids, as in other compounds with polyanionic networks.

In K-Sn system, where K atoms are significantly larger than Na, the substitution by elements of the platinum group allowed to obtain endohedrally filled nine atom tin clusters with Ru, Rh, Pd, Os, and Pt. These results were confirmed by powder X-ray diffraction, Raman spectroscopy and energy dispersive X-ray analysis. For the compound $\text{K}_{12}\text{Pd}_{0.47}\text{Sn}_{17}$ the crystal structure was fully characterized, showing partial occupancy of the clusters by palladium atoms.

Finally, the complete substitution of tin by the combination of the group 13 and 15 elements (Ga and Bi or In and As) led to the formation of four new compounds: $\text{K}_{20}\text{Ga}_6\text{Bi}_{13.294}$, $\text{K}_7\text{In}_4\text{As}_6$, K_3InAs_2 , and $\text{K}_{144}\text{In}_{192}\text{As}_{37}$. Two of them, $\text{K}_7\text{In}_4\text{As}_6$ and K_3InAs_2 , are electron balanced Zintl phases with expected for these compositions tetrahedral coordination of In atoms. In $\text{K}_7\text{In}_4\text{As}_6$ homoatomic In-In bonds are present along with heteroatomic In-As. $\text{K}_{20}\text{Ga}_6\text{Bi}_{13.294}$ comprises planar $\{\text{Ga}_3\text{Bi}_6\}$ fragments and $\{\text{Bi}_2\}$ dumbbells, with remarkably short Bi-Bi distances. The In-rich compound $\text{K}_{144}\text{In}_{192}\text{As}_{37}$ consists of interconnected $\{\text{In}_{12}\}$ icosahedra, with six As handles and isolated by potassium As atoms.

Zusammenfassung

Beeindruckende Vielfalt und Komplexität von polaren, intermetallischen Verbindungen sowie deren einzigartige Eigenschaften sind die Quelle für ein ungebrochenes Interesse in der modernen Chemie. Beziehungen zwischen Struktur, Zusammensetzung und Eigenschaften, begründet durch chemische Bindungen, verlieren nie ihre Bedeutung für das Verständnis von metallischen Systemen. Im Laufe dieser Arbeit wurden Substitutions- und Additionseffekte in binären Alkalimetall-Zinn-Systemen systematisch untersucht, um ein besseres Verständnis für die Bindungsprinzipien, die der Formation von polaren Intermetallika an der Zintl-Grenze zugrundeliegen, zu erlangen. Das Ziel der vorliegenden Arbeit war es, eine rationale Herangehensweise an die Synthese von neuen, polaren, intermetallischen Phasen in den ternären Systemen Na-Ag-Sn, Na-Sn-Bi, *A-T-Sn* (*A* = Na, K; *T* = Ru, Rh, Pd, Os, Ir, Pt) und *K-Tr-Pn* (*Tr* = Ga, In; *Pn* = As, Bi). Dies wurde durch die Nutzung von Reaktionen zwischen diversen Elementen mit stark unterschiedlichen Elektronegativitäten und unterschiedlichem chemischen Verhalten intermetallischer Komponenten erreicht.

Die verschiedenen Festphasen-Syntheserouten zu den zahlreichen neuen, polaren, intermetallischen Komponenten werden in dieser Arbeit beschrieben. Die Charakterisierung der erhaltenen Komponenten wurde unter Verwendung von pulver- und einkristallröntgendiffraktometrischen Methoden sowie Raman-Spektroskopie zur Strukturanalyse und dynamischer Differenzkalometrie und magnetometrischen Messungen zur Bestimmung der Zusammensetzung sowie des thermischen und magnetischen Verhaltens durchgeführt. Für ausgewählte Verbindungen wurden Berechnungen der Bandstruktur durchgeführt.

Als Ergebnis der Substitution von Zinnatomen durch Silberatome im binären Na-Sn-System wurden die ikosaedrischen Phasen $\text{Na}_{29}\text{Ag}_{21}\text{Sn}_{39}$, $\text{Na}_{13}\text{Ag}_{5.5}\text{Sn}_{21.2}$ und $\text{Na}_{230.45}\text{Ag}_{274}\text{Sn}_{136}$, sowie $\text{Na}_5\text{Ag}_{3.74}\text{Sn}_{8.26}$, eine Verbindung mit offenem Netzwerk, erhalten. Die Struktur von $\text{Na}_{29}\text{Ag}_{21}\text{Sn}_{39}$ weist ein polyanionisches Netzwerk von untereinander verbundenen Clustereinheiten auf: Heteroatomare, leere Ikosaeder und Na-zentrierte Cluster mit 20 Atomen (allseitig überkapptes hexagonales Prisma), sowie Zinn-Dreiecke. Die polyanionische Unterstruktur von $\text{Na}_{29}\text{Ag}_{21}\text{Sn}_{39}$ kann als hierarchisch verwandt zum CaCu_5 -Strukturtyp, in dem spezifische Atome durch Clustereinheiten ersetzt sind, angesehen werden. Die Verbindungen $\text{Na}_{13}\text{Ag}_{5.5}\text{Sn}_{21.2}$ und $\text{Na}_{230.45}\text{Ag}_{274}\text{Sn}_{136}$ bestehen aus

endohedralen Fulleran-Clustern (leer in $\text{Na}_{13}\text{Ag}_{5.5}\text{Sn}_{21.2}$ und Ag-zentriert in $\text{Na}_{230.45}\text{Ag}_{274}\text{Sn}_{136}$). Beide Verbindungen beinhalten ähnliche Cluster, aufgebaut aus vier konzentrischen Schalen, wobei die äußere Schale fullerenähnlich aus 60 (in $\text{Na}_{13}\text{Ag}_{5.5}\text{Sn}_{21.2}$) oder sowohl 60 als auch 80 Atomen (in $\text{Na}_{230.45}\text{Ag}_{274}\text{Sn}_{136}$) zusammengesetzt ist. Diese Verbindungen sind formell Frank-Kasper-Phasen, können aber auch als Hume-Rothery-Phasen, die mit Alkalimetallen durchsetzt sind, gesehen werden.

Die vierte Verbindung im ternären Na-Ag-Sn-System ist $\text{Na}_5\text{Ag}_{3.74}\text{Sn}_{8.26}$, mit einem dreidimensional offenen Netzwerk von vierbindigen Sn- und Ag-Atomen und Na-Kationen in den Leerstellen.

Beide Verbindungen im ternären Na-Sn-Bi-System, $\text{Na}_{13}\text{Sn}_{25.73}\text{Bi}_{1.27}$ und $\text{Na}_{27}\text{Sn}_{45.63}\text{Bi}_{0.57}$, bestehen aus einem dreidimensionalen Sn-Netzwerk, in dem Bismut partiell zweibindige Sn-Atome substituiert und, im Fall von $\text{Na}_{13}\text{Sn}_{25.73}\text{Bi}_{1.27}$, zusätzlich isolierte Bi-Atome enthält. Na-Atome füllen, analog zu anderen Verbindungen mit polyanionischen Netzwerken, die Leerstellen.

Im K-Sn-System, mit K-Atomen signifikant größer als Na-Atome, erlaubte die Substitution durch Elemente der Platingruppe endohedral gefüllte, neunatomige Zinncluster mit Ru, Rh, Pd, Os und Pt zu erhalten. Diese Ergebnisse wurden durch Pulverdiffraktometrie, Raman-Spektroskopie und energiedisperive Röntgenanalyse bestätigt. Für die Verbindung $\text{K}_{12}\text{Pd}_{0.47}\text{Sn}_{17}$ wurde die Kristallstruktur vollständig charakterisiert. Eine partielle Besetzung der Cluster durch Palladium-Atome wurde gezeigt.

Die vollständige Substitution von Zinn durch eine Kombination von Elementen der Gruppen 13 und 15 (Ga und Bi oder In und As) führte schließlich zur Bildung von vier neuen Verbindungen: $\text{K}_{20}\text{Ga}_6\text{Bi}_{13.294}$, $\text{K}_7\text{In}_4\text{As}_6$, K_3InAs_2 , und $\text{K}_{144}\text{In}_{192}\text{As}_{37}$. Zwei davon, $\text{K}_7\text{In}_4\text{As}_6$ und K_3InAs_2 , sind Zintl-Phasen mit erwartet tetraedrischer Koordination der In-Atome. In $\text{K}_7\text{In}_4\text{As}_6$ sind homoatomare In-In-Bindungen sowie heteratomare In-As-Bindungen vorhanden. $\text{K}_{20}\text{Ga}_6\text{Bi}_{13.294}$ beinhaltet planare $\{\text{Ga}_3\text{Bi}_6\}$ -Fragmente und $\{\text{Bi}_2\}$ -Hanteln, mit bemerkenswert kurzen Bi-Bi-Abständen. Die In-reiche Verbindung $\text{K}_{144}\text{In}_{192}\text{As}_{37}$ besteht aus untereinander verbundenen $\{\text{In}_{12}\}$ -Ikosaedern, mit sechs As exo-Bindungen.

List of Abbreviations

0-D	Zero-dimensional
1-D	One-dimensional
2-D	Two-dimensional
3-D	Three-dimensional
Å	Angstrom
A	Alkali metal
ADPs	Anisotropic displacement parameters
$a, b, c, \alpha, \beta, \gamma$	Crystallographic parameters
bcc	Body-centered cubic
calc.	Calculated
d	Interatomic distance
DFT	Density Functional Theory
DOS	Density Of States
DSC	Differential Scanning Calorimetry
e^-	Electron
EDX	Energy Dispersive X-Ray Analysis
E_F	Fermi energy
e.g.	exempli gratia
etc.	et cetera
exp.	Experimental
F	Structure factor
fcc	Face-centered cubic
g	Gram

Goof	Goodness of fit
hcp	Hexagonal close packed
h, k, l	Miller indices
HP	High pressure modification
HT	High temperature modification
I	Intensity
K	Kelvin
LMTO	Linear Muffin Tin Orbital
Occ.	Occupancy
Pn	Pnictogens (P, As, Sb, Bi)
ppm	Parts per million
PXRD	Powder X-Ray Diffraction
Ref.	Reference
RT	Room temperature
SCXRD	Single Crystal X-Ray Diffraction
S. O. F.	Site occupancy factor
SQUID	Superconducting Quantum Interference Device
T	Transition metal
Tr	Triel elements (Ga, In, Tl)
Tt	Tetrel elements – Si, Ge, Sn, Pb
VEC	Valence Electron Consetrtion
XRD	X-Ray Diffractometry
Wyck.	Wyckoff position

Z	Number of formula units per unit cell
λ	Wavelength
D	Density
$\%$	Percentage

Content

1	Introduction: Intermetallic Compounds.....	1
1.1	Electron Compounds (Hume-Rothery phases)	4
1.2	Size Packing Phases.....	5
1.3	Grimm-Sommerfeld Phases	6
1.4	Zintl Phases	7
1.5	Electron-Poor Polar Intermetallic Phases.....	9
1.6	Scope and Outline	11
2	General Experimental Procedures and Analytical Methods	12
2.1	Synthesis.....	12
2.1.1	Sample Handling and Starting Materials.....	12
2.1.2	Sample Preparation and Reaction Conditions	13
2.1.2.1	Arc-Melting: Precursor Preparation	13
2.1.2.2	High Temperature Synthesis and Selecting the Temperature Program	13
2.1.2.3	Flux Synthesis	15
2.2	Characterization	16
2.2.1	X-Ray Diffraction Experiments	16
2.2.1.1	Powder X-Ray Diffraction.....	16
2.2.1.2	Single Crystal X-Ray Diffraction.....	16
2.2.2	Differential Scanning Calorimetry	17
2.2.3	Energy-Dispersive X-ray Spectroscopy	17
2.2.4	Magnetic Measurements	18
2.2.5	Raman Spectroscopy.....	18
2.2.6	Computational Methods	19
3	Results and Discussion	20
3.1	Substitutional Effects in the Na-Sn Binary System	20
3.1.1	Introduction	20
3.1.1.1	Na-Sn Binary System.....	20
3.1.1.2	Interactions in the Na-T-Sn Ternary Systems (T = late transition metals).....	22

3.1.2	Three Icosahedral Ternary Phases in the Na-Ag-Sn System: Na ₂₉ Ag ₂₁ Sn ₃₉ , Na ₁₃ Ag _{5.5} Sn _{21.2} and Na _{230.45} Ag ₂₇₄ Sn ₁₃₆	26
3.1.2.1	Na ₂₉ Ag ₂₁ Sn ₃₉ – a Cluster Interconnected Compound as a Hierarchical Variant of CaCu ₅ -type	26
3.1.2.2	Na ₁₃ Ag _{5.5} Sn _{21.2} and Na _{230.45} Ag ₂₇₄ Sn ₁₃₆ – Two Compounds Featuring Endohedral Fullerene Clusters	45
3.1.3	Na ₅ Ag _{3.74} Sn _{8.26} : a Compound with an Open Sn/Ag Anionic Framework	73
3.1.4	Substitution of Sn by Bi in the Na-Sn Binary System	84
3.1.4.1	A Zintl Phase Na ₁₃ Sn _{25.73} Bi _{1.27} Featuring Isolated Bi Atoms Encapsulated in 3-D Tin Network.....	86
3.1.4.2	Partial Substitution of Sn by Bi in the Binary Na ₇ Sn ₁₂ : Na ₂₇ Sn _{47.33} Bi _{0.57}	96
3.2	Solid-state Synthesis of the Endohedrally Filled Clusters with Transition Metals.....	102
3.2.1	Introduction	102
3.2.2	Ternary Phase K ₁₂ Pd _{0.47} Sn ₁₇ Featuring {Pd@Sn ₉ } ⁴⁻ Clusters.....	105
3.2.3	Other {T@Sn ₉ } Clusters Obtained as Neat Solids	118
3.2.3.1	{Ru@Sn ₉ } ⁶⁻ : Synthesis and Characterization of the K ₁₂ Ru _{1-x} Sn ₁₇	118
3.2.3.2	{Rh@Sn ₉ } ⁵⁻ : Synthesis and Characterization of the Na ₁₃ Rh _{1-x} Sn ₁₇	119
3.2.3.3	{Os@Sn ₉ } ⁶⁻ and {Pt@Sn ₉ } ⁴⁻	119
3.2.4	Raman Spectroscopy for the Characterization of the Endohedrally Filled Clusters	122
3.3	Ternary Compounds in K- <i>Tr</i> - <i>Pn</i> Systems (<i>Tr</i> = Ga, In; <i>Pn</i> = As, Bi).....	124
3.3.1	Introduction	124
3.3.1.1	Binary Phases	125
3.3.1.2	Existing Ternary Phases in A- <i>Tr</i> - <i>Pn</i> Systems (A = Na, K, Rb, Cs; <i>Tr</i> = Ga, In, Tl and <i>Pn</i> = P, As, Sb, Bi)	131
3.3.2	K ₂₀ Ga ₆ Bi _{13.294} – the First Compound in the A-Ga-Bi Ternary System.....	141
3.3.3	New Zintl Phase K ₇ In ₄ As ₆	147
3.3.4	An Electron Precise Zintl Phase K ₃ InAs ₂	155
3.3.5	Novel In-rich Icosahedral Phase K ₁₄₄ In ₁₉₂ As ₃₇	162
4	Summary and Conclusion.....	171
4.1	Na-Ag-Sn Ternary System	171

4.2	Compounds with Anionic Networks in the Na-Sn-Bi Ternary System.....	172
4.3	Endohedral Cluster Compounds in <i>A-T-Sn</i> Systems.....	174
4.4	New Ternary Compounds in <i>K-Tr-Pn</i> Systems.....	174
4.5	Conclusion	176
5	References	177
6	Appendix.....	184
7	List of Publications.....	209

1 Introduction: Intermetallic Compounds

As a result of the slow cooling of the liquid mixture of two (or more) metals, different equilibrium phases appear as a function of composition and temperature, summarized in a binary (ternary) phase diagram. The possible number of degrees of freedom in a closed system at the thermodynamic equilibrium in terms of the number of possible phases depending on the number of the components in the system was formulated by J. W. Gibbs [1]. The object of the solid-state chemistry is the solid region of a phase diagram, which usually contains several intermediate phases, in addition to the terminal solid solutions. In solid solutions the guest atoms randomly substitute positions in the host lattice, preserving the crystal structure of the host. Another possibility is interstitial solid solutions, in case the guest atoms are significantly smaller and therefore can occupy interstitial sites in the larger host-metal lattice. Contrarily, the crystal structure of the intermediate phase is unlike those of the component metals and has a narrow compositional range. These 'narrow' intermediate phases are commonly known as "**intermetallic compounds**" or simply "**intermetallics**" [2].

Many intermetallic compounds are known to have extraordinary functions and properties that are not observed in the individual metals and alloys. They have multiple applications due to their mechanical strength as well as magnetic properties, superconductivity, semiconductivity, hydrogen absorbing capability, etc. On the one hand, intermetallic compounds can be defined as those composed of two or more metallic elements, whereas in a wider sense, they may contain metallic and/or semi metallic elements, each featuring an ordered arrangement of two or more kinds of atoms. Various nature of the individual components within intermetallics results in various kinds of interatomic bonding, ranging from metallic to covalent or ionic bonding. Combination of the ordering of atoms and various strong interatomic bonding result in many attractive properties for intermetallic compounds [3].

According to J.D. Corbett [4] term "intermetallics" applies to compounds between two or more elements that are each metal, with this designation simply following the negative temperature dependence of the electronic conductivity of each. This interpretation is, again, rather loose and is not distinguishing whether the components are simple *s* or *d* metals or

post-transition metals or even whether the products themselves are metallic. For clarification, several general conditions were formulated [4].

First of all, intermetallic phases are required to have a unique structure in the solid-state, different from the structure of the individual components. In contrast to the most molecular and simple semiconductor materials, intermetallics have a lack of simple bonding or valence rules and closed-shell states (generally delocalized bonding of the valence electrons). This is natural in the presence of a surplus of valence orbitals and high coordination numbers for the most atoms. Depending on the nature of the elements involved, the structures and stoichiometry, the diverse bonding situation is another condition defining intermetallic phases. Among other, certain systems may still exhibit some characteristic, but unusual valence rules by approach closed-shell configurations (pseudo-gaps) at certain compositions, often reflecting electronic effects that are not well understood. These conditions helped to define the place of intermetallic compounds in modern chemistry.

Such materials are widely distributed over the periodic table, offering a huge amount of possible combinations and incredible potential for the experimental work.

Under the definition of the intermetallic compounds Ralph G. Pearson [5] separated three classes of intermetallics based on the most important factor that defined their crystal structures: (1) electron compounds governed by the valence electron concentration (Hume-Rothery phases); (2) size packing phases, governed by the geometric requirements (Frank-Kasper and Laves phases); (3) valence compounds, governed by the valence rules (8-N), e.g. Zintl phases. Additionally, there is another group of the intermetallic compounds, which combines properties of the Zintl and Hume-Rothery phases – polar intermetallics. Compounds of this class are in the focus of the present work.

Before going into the detailed classification, it is worth mentioning, that although there are no general rules governing stoichiometry, simple electron counting rules like the octet rule, the 18-electron rule, and Wade's rules provide guidance for stable the composition [6]. Electronic structure theory gives a theoretical justification for these simple rules, but the application of these quantum mechanical models requires knowledge of the structure, both actual and hypothetical. For example, to describe and understand the bonding patterns for intermetallic compounds comprising structural fragments in the forms of homo- or heteroatomic chains or clusters certain theories, like the Zintl-Klemm or the Hume-Rothery concept, have been developed.

In Figure 1.1 an overview of the selected reviews regarding compounds to which the Zintl–Klemm or the Hume–Rothery concept can be applied is presented in chronological order.

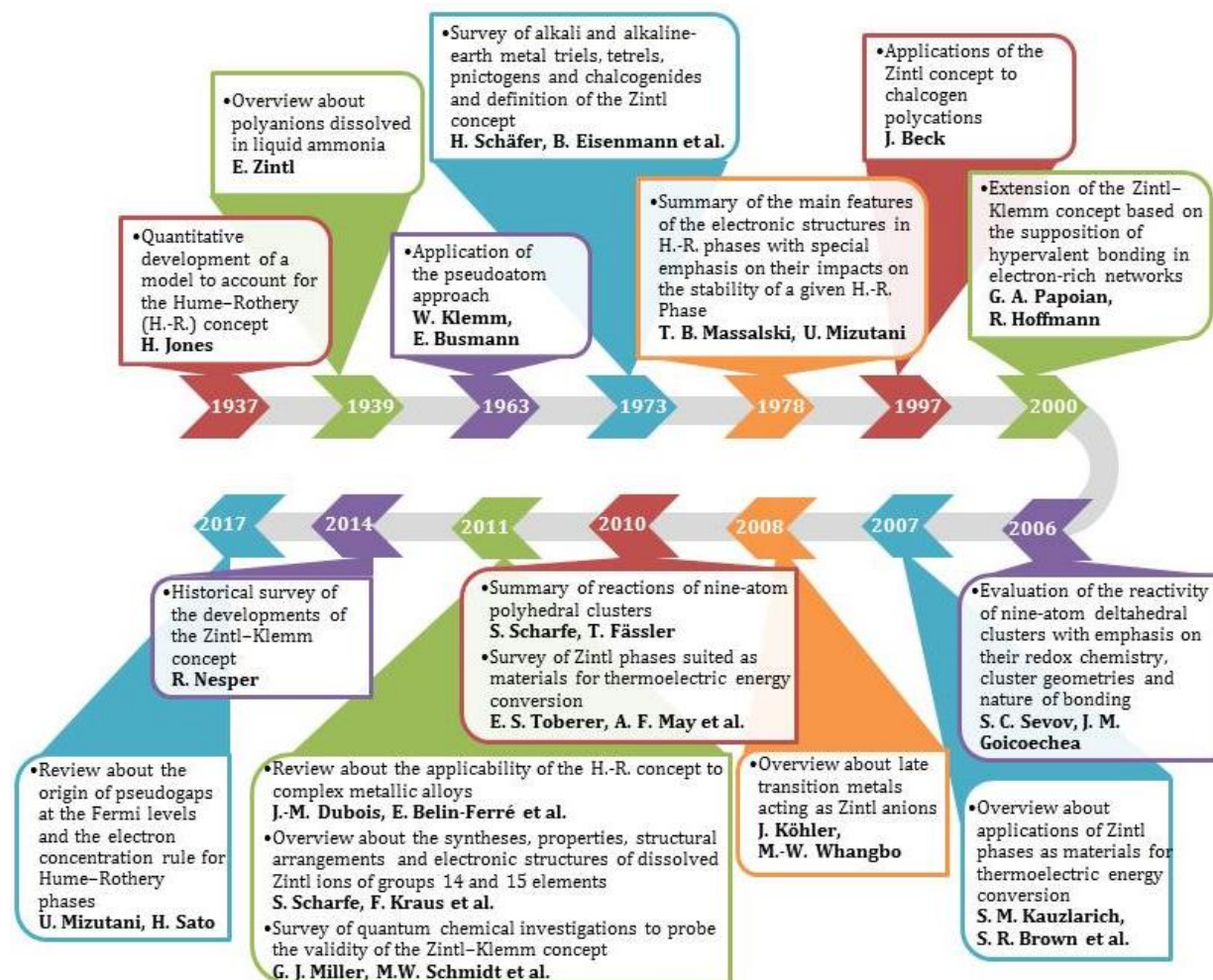


Figure 1.1 Overview of selected reviews regarding compounds to which the Zintl–Klemm or the Hume–Rothery concept can be applied. [7]

The Zintl–Klemm concept suggests that the electrons are transferred from the more electropositive to the more electronegative element that in consequence formally form anions. According to the Hume–Rothery theory, assigning certain types of structures to the specific valence electron concentrations is possible. Although the two aforesaid concepts help to understand the bonding motifs in quite a lot of intermetallic compounds, there is an emerging group of intermetallic compounds classified as polar intermetallic phases which comprise polar intermetallic bonds but lack in straightforward valence electron rules [8]. In these phases a certain degree of charge transfer exists, but the valence electron concentration (VEC per atom) is significantly lower, compared to those of the Zintl phases, going in the direction of the Hume–Rothery phases. The existence of such polar intermetallic phases raises the question of whether there are previously unknown fundamental directives

that help to classify and to forecast the nature of bonding in them, being a drive for the solid-state chemists over the last several decades.

1.1 Electron Compounds (Hume-Rothery phases)

British metallurgist William Hume-Rothery researched among other metal mixtures and created rules to predict whether two elements can form solid solutions, according to which an element might dissolve in a metal forming a solid solution ^[9]. Four factors were highlighted in his work: atomic size, crystal structure, valency and electronegativity.

Another even more important contribution of the British scientist, known as Hume-Rothery rule, empirically describing phase stabilization through the electron concentration. **Hume-Rothery phases** or **electron compounds**, following this rule, typically have defined composition and crystal structure that differ from the elements. The atoms in the compound are not ordered, but form statistical mixtures at each atomic position, especially at high temperatures (at low temperatures partial ordering can be observed). These phases can be defined as a transition state between solid solutions and a chemical compound. Basically Hume-Rothery defined the first clear border between alloys and intermetallic compounds.

Hume-Rothery made an important contribution to the understanding of intermetallics by proposing an electron counting scheme for compounds between the transition metals and *p*-metals, which resulted in specific valence electron concentrations (VEC, the ratio of valence electrons per atom) for different types of crystal structures. Correlation between the average number of valence electrons per atom and the crystal structures of Hume-Rothery phases resulted in specific valence electron concentrations (VEC) for different types of crystal structures: VEC of 1.38 for cubic α -phases (fcc), 1.48 for β -phases (bcc), 1.62 for γ -phases, and 1.75 for hexagonal ϵ -phases (hcp). It was shown later ^[10] that an accurate explanation of the Hume-Rothery rules is still incomplete and that *d*-orbital participation, and correlation for the ionic effects should be included. However, Lee ^[11] in 1991 demonstrated possible rationalizing the Hume-Rothery rules by the simple molecular orbital theory.

1.2 Size Packing Phases

Another important concept in the formation and stability of intermetallics is based on the sizes of the constituent atoms [2]. It was introduced by Laves [12] and formalized by Frank and Kasper [13]. It states that complex structures, found in the intermetallics, can be explained in terms of geometrical requirements of the sphere close-packing that are associated with the atomic radii ratio of the component atoms.

This is how the general definition for this class of intermetallics as **topologically close pack (TCP) phases**, also known as **Frank-Kasper (FK) phases** appeared. In 1958 Frank and Kasper in their original work investigating many complex alloy structures [13] showed, that non-icosahedral environments form an open-end network which they called the major skeleton. They came up with the methodology to pack asymmetric icosahedra into crystals using other polyhedra with larger coordination number and atoms. This allowed compounds of this class to maintain topological close packing.

Frank-Kasper phases represent one of the largest groups of intermetallic compounds and are characterized by the variety of their physical properties with application as high temperature structural (Laves, σ , χ and A15 phases [14]) and superconducting (A15 Nb₃Sn [15]) materials.

According to Frank and Kasper the coordination polyhedra exhibit the following features to avoid the formation of bigger octahedral voids (compared to tetrahedral voids): firstly, triangular faces due to effective tetrahedral close packing; secondly, convex polygon and, finally, five or six edges meeting at every edge [2]. The structure of the FK phases can be represented in terms of triangulated coordination polyhedra with coordination numbers of 12, 14, 15 and 16.

Laves further added that the geometrical factor formulated by Frank and Kasper is guided by three principles, namely: (1) the tendency to fill space as efficiently as possible; (2) the tendency to form arrangements of the highest possible symmetry; and (3) the tendency to form the closest connections between like atoms [2].

The class of intermetallics referred to as "**Laves phases**" was first discovered by James B. Friauf in 1927 [16] (compounds MgCu₂ and MgZn₂). In the 1930s, following that discovery, Fritz Laves [12a] initiated a comprehensive investigation of the characteristics and features of these materials. Subsequently, insightful interpretations of the crystal structure by Komura

in 1962, as well as the occurrence of the stacking variants in the intermetallic phase, have furthered the understanding of this class of materials. Accordingly, owing to the contributions of these three primary investigators, literature references to the intermetallic phases are FLK (Friauf–Laves–Komura) phases ^[17]. FLK phases are topologically close-packed, ordered, intermetallic compounds with the approximate formula AB_2 , where the A atoms are ordered in diamond, hexagonal diamond or a related structure and B atoms are forming tetrahedra around A atoms. Most of these intermetallics crystallize in one of the three crystal structure polytypes ^[18]: hexagonal C14 ($MgZn_2$) and C36 ($MgNi_2$), cubic C15 ($MgCu_2$). Recent thermodynamic studies on the prototypical Laves phases $MgZn_2$ and $MgCu_2$ strongly suggest the simultaneous existence of metallic, covalent and ionic bonding ^[19].

1.3 Grimm-Sommerfeld Phases

The **Grimm–Sommerfeld phases** are compounds that obey the Grimm–Sommerfeld rule ^[20], which states that in covalent compounds, the number of bonds formed depends on the total number of external electrons (isosteric). If in binary compounds the number of electrons / atoms (for intermetallic phases VEC) is the same, then the same number of bonds is formed, the same composition and mostly the same structure.

The only difference for the elements with the same VEC is that by increasing polarity a transition to the salts occurs. Binary compounds of elements of the $(N - k)$ - and $(N + k)$ -main groups possess the properties of the compounds of the N-main group, for example combination of the group 13 and 15 elements would result in the properties of the group 14 elements – a principle used in Chapter 3.3 of this work.

Grimm–Sommerfeld rule predicts that binary compounds with covalent character that have an average of 4 electrons per atom will have structures, where both atoms are tetrahedrally coordinated, which means they have a ZnS (wurzite/sphalerite) structure.

1.4 Zintl Phases

The Zintl–Klemm concept is another valence electron counting rule. **Zintl phases** are the class of intermetallics named after Edward Zintl who pioneered their exploration [7b, 21]. Due to some of the unusual properties of the intermetallics studied by Zintl, properties that included high melting points, high heats of formation, poor electrical conductivities notwithstanding their metallic luster, and increased brittleness, Zintl concluded that the network adopted by the ‘noble metal’ arose from charge (electron) transfer from the ‘active metal’ [22]. He explained the structural behavior of main-group binary intermetallics in terms of the presence of both ionic and covalent parts in their bonding. The original idea was to describe polar intermetallic compounds as salt-like species: on the one hand, the link between the metallic, alloy-type intermetallics, on the other hand, the typical valence compounds. This conjecture was also consistent with Pauling’s assessment of elemental electronegativities [23].

Zintl’s view applied to the classical Zintl phase NaTl [24] assumes complete electron transfer from the more electropositive sodium to the more electronegative thallium just as in genuine ionic salts such as NaCl. The difference is that the resulting anions do not necessarily achieve an electronic octet as isolated species but may rather bond to each other in order to do so. Thus, Tl⁻ in Na⁺Tl⁻ behaves like an element of the group to the right, group 14, and forms a diamond network, typical for the elements of that group, that is stuffed by the Na⁺ cations [25].

Klemm [26] and Busmann [27] generalized this powerful idea for such compounds and applied them to the other binary and ternary phases. Following the Zintl picture, Klemm developed a general description of the Zintl phases associating structure and bonding descriptions with the physical properties.

Compounds following this **Zintl–Klemm formalism** are called, in general, Zintl phases, which can range from extended solids through cluster compounds (i.e., containing cluster anions) to mono- or heteroatomic anions, which adapt salt-like structures. The principle of bonding in the Zintl phases is that there is a fairly large difference in the electronegativities between the two bonding partners, and thus initially adopts ionic concepts. The anionic substructure could be explained according to the rules for covalent compounds (8-*N* rule), so-called **Zintl–Klemm–Busmann concept**. In this case the bonding in the anionic substructure could be generalized.

Electron counting rules are useful for predicting the structures of the deltahedral clusters (e.g. borane and carborane). Originally formulated by Kenneth Wade [28] in 1971 and further developed by Michael Mingos [29] the **Wade-Mingos rules** provide a straightforward and eloquent rationalization of the shapes of “electron-deficient” cluster compounds in terms of the number of skeletal electron pairs (SEPs) these molecules possess. [30] Once the clusters were arranged into three families (*closo*, *nido* and *arachno*) it was clear that, structurally, a *nido* ($n - 1$)-vertex polyhedron and an *arachno* ($n - 2$)-vertex polyhedron were fragments of the appropriate parent *closo* n -vertex polyhedra. The structures of these parent polyhedra were exemplified by dianionic boranes $\{B_nH_n\}^{2-}$ and by the carboranes $C_2B_{n-2}H_n$ [30] and extended to intermetallic cluster compounds.

In the past three decades comprehensive research on Zintl phases has led to major discoveries that have immensely broadened our understanding of these systems with, often, complicated electronic structures. Undoubtedly, the most fascinating compounds among these are the compounds with delocalized bonding that elude description by simple valence rules but obey rather Wade's rules developed for electron counting in deltahedral boranes, $B_nH_n^{2-}$. Typical examples are the numerous isolated or linked deltahedral clusters of group 13 which, due to the only three valence electrons of the elements of this group, usually carry quite high negative charges. Similar isolated clusters of group 14 were discovered over the last three decades in the solid-state as well as crystallized from ethylenediamine or liquid ammonia solutions. Examples of these clusters in tin compounds with alkali metals are $\{Sn_4\}^{4-}$ in A_4Sn_4 [31] and $A_{12}Sn_{17}$ [32], $\{Sn_9\}^{4-}$ in A_4Sn_9 [33] and $A_{12}Sn_{17}$ [32] and $\{Sn_8\}^{6-}$ in $A_4Li_2Sn_8$ [34] all with delocalized bonding.

With the development of the molecular orbital theory, a quantum chemical approach allowed to describe the electronic structures of the Zintl phases. However, for the polar intermetallic phases often the results of this theory are initially unintuitive and require a complex and extensive analysis. To better understand and quickly interpret the geometric and electronic structures of the cluster compounds, simplified models have been developed. The most relevant are briefly presented below, followed by a discussion on the quantum-chemical analysis of bonding situations and the methods used. At this point it must be mentioned that the Wade Mingos rules and the Zintl-Klemm-Busmann concept can be used for the simple models, however, they quickly reach their limits.

1.5 Electron-Poor Polar Intermetallic Phases

The validity (or lack thereof) of the classical Zintl formalism as applied to less polar intermetallics, is nicely probed by electron-poor compounds [2]. The apparent electron deficiency in the chemical bonding of clusters compounds group 13 elements and substituted compounds of the group 14 elements (which are in the scope of this work) are offset by the formation of three-center-two electron bonds, following the classic Wade-Mingos rules for boranes and extended through isolobal analogies [2]. However, cluster-based intermetallic phases that violate even these rules have also appeared. These violations appear in extremely electron-poor compounds that featured closed deltahedral frameworks but did not exhibit their canonical polyhedral form. As examples of these could be named phase in K-In binary system (K_8In_{11} [35]), as well as compounds with transition metals, e.g. Cu, Zn or Cd (in $A_{12}Cu_{12}Sn_{21}$ [36] ($A = Na, K, Rb, Cs$), $Na_{29}Zn_{24}Sn_{32}$ [37] $Na_8K_{23}Cd_{12}In_{48}$ [38]). For compounds like that the term “**metallic Zintl phase**” has been proposed by Corbett [39] and is increasingly being recognized in describing many polar intermetallics that at the Zintl border.

Intermetallic compounds consisting of main group metals, can be broadly divided into three large groups according to the degree of charge transfer from electropositive to electronegative components. As it was shown recently [40], the relation between Hume-Rothery, polar intermetallic and Zintl phases exists, depending on the valence electron concentration per atom. The first group, Hume-Rothery phases can be characterized as condensed structures following the Hume-Rothery mechanism: minimal charge transfer and significant interatomic orbital overlap between the atoms. On the opposite side of the diagram are Zintl-phases with larger electronegativity difference, typically semiconductors with open framework and ionic bonding between polarized counterparts (e.g. alkali metal cations and polyanionic network formed by *p*-elements group 13-15; within the polyanionic network covalent bonding is also possible), following the Zintl–Klemm formalism.

Between these two types of intermetallic phases polar intermetallics are located, featuring complex structures and mixed bonding types with no obvious structure-bonding relations. They simultaneously possess ionic and covalent interactions, like Zintl phases, but the commonly accepted valence electron counting rules often fail to rationalize the structures and compositions of polar intermetallic phases, in particular for those containing transition metals.

In Figure 1.2 the position on the VEC diagram of the Hume–Rothery phases in the T -Sn ($T = \text{Cu, Ag}$) systems and Zintl phases in the A -Sn ($A = \text{Na, K, Rb, Cs}$) systems are shown, as well as expected VEC region for the intermediate class – polar intermetallics.

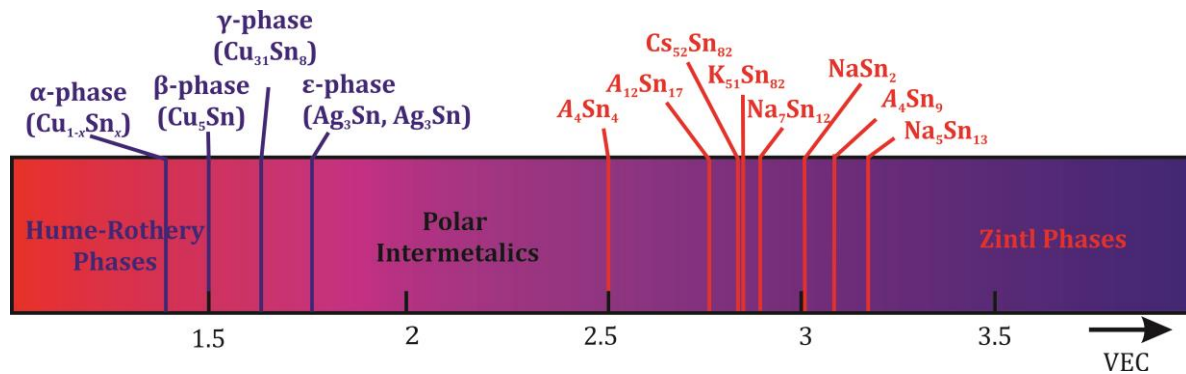


Figure 1.2 Positioning of the polar intermetallics between Hume–Rothery phases (illustrated by the examples from Cu-Sn and Ag-Sn binary systems) and Zintl phases (alkali metal-tin binary systems) on a scale of valence electron concentration per atom.

1.6 Scope and Outline

Impressive variety and complexity of polar intermetallic compounds are the huge source of interest in the modern chemistry. Homo and heteroatomic clusters mark a borderline between solid-state, solution based and gas phase chemistry in both intermetallic phases and soluble metal cluster compounds, with macroanionic networks and interconnected cluster units.

As it was stated by J. D. Corbett ^[4]: “Exploratory synthetic adventures regarding the inorganic chemistry of polar intermetallic phases have proven to be especially productive of novel compositions, new and unprecedented structures, and unusual bonding regimes.” Not only does it offer a wide area for exploring the many elements, but also provides a valuable testing ground for any new intuitive and innovative concepts of chemical bonding.

To quote Arnold M. Guloy ^[2]: “the synthesis of novel solids is as much an *art* as a *science*, it relies as much on empirical rules developed from past serendipitous as on intuitive discoveries”. Because the comprehension of the properties is worthwhile to tailor compounds with predictable features, there is a great desire to establish fundamental directives which allow distinguishing and predicting the relations between the crystal structures, electronic structures and physical properties in solid-state materials ^[41].

Thus, the aim of the present work is to develop a rational approach in the syntheses of new polar intermetallic phases in Na-Ag-Sn, Na-Sn-Bi, *A-T-Sn* (*A* = Na, K; *T* = Ru, Rh, Pd, Os, Ir, and Pt) and *K-Tr-Pn* (*Tr* = Ga, In; *Pn* = As, Bi) ternary systems. Starting with exploration of alkali metal-tin binary systems and introducing the substitution of the anionic component (tin) by *p*-block (Ga, In, As, Bi) or late *d*-block (Ru, Rh, Pd, Os, Pt, Ag) elements, it was expected to obtain structures with polyanionic clusters or networks of metals, paired with the corresponding monatomic alkali metal cations. Obtained results were presented in three groups: (1) modification of the Na-Sn binary system by adding third component (Ag or Bi), Chapter 3.1; (2) addition of the platinum group metal to the *A-Sn* systems (*A* = Na, K), Chapter 3.2; and finally (3) complete substitution of tin by the combination of the group 13 and 15 elements (Ga and Bi or In and As), Chapter 3.3.

2 General Experimental Procedures and Analytical Methods

2.1 Synthesis

2.1.1 Sample Handling and Starting Materials

Since some of the used starting materials and all of the products were air and moisture sensitive all the chemicals were stored and handled in an inert atmosphere inside of an Ar (Westfalen, purity grade 4.8) filled glovebox (H_2O and O_2 levels < 0.1 ppm; MBraun). All chemicals used in the syntheses were obtained commercially, some data concerning their specifications are given in Table 2.1. The alkali metals were washed in hexane, put into a Schlenk tube and dried under vacuum. Arsenic was purified by distilling commercially obtained pieces in an evacuated silica ampoule at 600°C for 12 hours. If needed Ru, Pd, Os, Ir or Pt powder was pressed in pallets. Before usage, potassium and sodium additionally were mechanically freed from surface oxide layers.

Table 2.1 Starting chemicals and their specifications.

Material	Purity (%)	Supplier	Shape
Na	99	Chempur	Rods
K	98	Merck	Pieces
Ag	99.9	Sigma Aldrich	Wire
Ru	99.999	Chempur	Powder
Rh	99.9	Chempur	Granules
Pd	99.9+	Chempur	Sponge
Os	99.9	Venton	Powder
Ir	99.9	Chempur	Powder
Pt	99.9	Sigma Aldrich	Powder
Sn	99.999	Merck	Granules
Sn	99.99	Aldrich	Powder
Ga	99.99	ChemPur	Pieces
Bi	99.999	ChemPur	Granules
In	99.99	Aldrich	Granules
As	99.9	AlfaAesar	Pieces

2.1.2 Sample Preparation and Reaction Conditions

2.1.2.1 Arc-Melting: Precursor Preparation

When fast high temperature reaction with no further annealing to achieve homogeneity was needed, the synthesis using arc melting furnace was chosen. It was used to ensure pre-reaction of the high-melting late transition metals (Ag, Ru, Rh, Pd, Os, Ir, Pt) with tetrel element (Sn). The obtained binary reguli containing one or more phases were used as a precursor for further reactions with alkali metal in order to obtain ternary compounds.

To guarantee inert reaction conditions arc melting was performed in the Ar-filled glovebox using Mini Arc Melting System, MAM-1, Johanna Otto GmbH with a generator operating in range from 5A (10V) till 200A (35V). It was supplied with water cooled copper sample holder and a moveable tungsten cathode. The procedure itself included melting elements (in form of granules, wire spirals, pieces or powder) pressed in pallets using the manual hydraulic press to form a homogenous alloy. The resulting reguli were turned upside down and arc melted at least three times in order to ensure homogeneity.

2.1.2.2 High Temperature Synthesis and Selecting the Temperature Program

The choice of the reaction container plays an important role in the high temperature synthesis. On one hand, alkali metal can diffuse into the container material such as glass or silica making it brittle. This could lead to breakage or in the worst case explosion of the reaction containers. On the other hand, *d*-metals such as Ag and elements of the platinum group are relatively chemically resistant, have a high melting point and reluctant to undergo reactions with other elements used in this work. Due to this fact, tantalum and niobium ampoules were used as reaction containers. They were prepared by cutting 2.5-5 cm long (depending on the sample size) pieces of a 2m long metal tube (10 mm external diameter, 0.5 mm wall thickness) as it is schematically shown in Figure 2.1, a. Fitted caps were punched of Nb and Ta sheets (thickness 0.5 mm) by the precision mechanics workshop (TU Munich). Metal tubes and caps were cleaned by sonification in acetone, glacial acetic acid, water, and acetone again (30 min per step). After cleaning tubes and caps were left in a drying oven at 120°C overnight and transferred in the glovebox where the caps were pressed (Figure 2.1, b) and arc-welded in the Ar atmosphere (water-cooled arc furnace, MAM-1, JOHANNA OTTO GmbH) to one side of each tube – Figure 2.1, c. After putting the reactants inside (Figure 2.1, d) the other end could be welded exactly the same way – Figure 2.1, e, or squeezed with the

tweezers and sealed along the occurred line– Figure 2.1, f. The order in which ampoules were filled was dependent on the melting temperature of the material: low-melting components were placed on the bottom and covered with the high-melting ones. Water cooling is important to prevent elements with low melting and boiling temperatures from evaporating and any reactions with the copper block holding the ampoule. If binary precursors were used for the reaction, they were ground in the agate mortar (if possible) or broken in the smaller pieces before loading them in the ampoule to ensure homogeneity of the mixture.

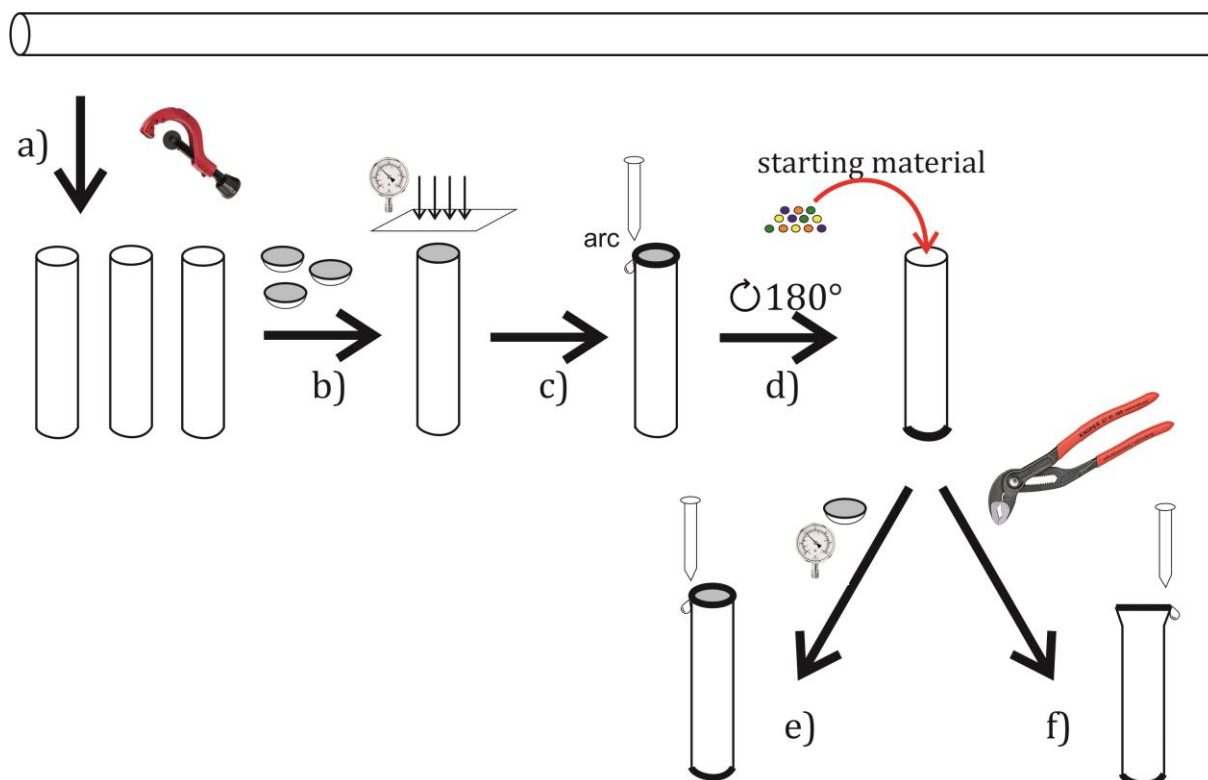


Figure 2.1 Assembling of the Ta/Nb reaction container: cutting the tube into smaller pieces (a); pressing caps on one end of the tubes (b); welding the caps one side with the arc melting furnace (c); filling the ampoule (d); pressing and sealing the cap on the other side of the ampoule (e) or squeezing the top of the ampoule and sealing it closed (f).

Since both Nb and Ta are oxidizing on the air above 300°C ampoules were placed under vacuum. To achieve that the ampoules were transferred into a silica tube (outer diameters 35mm, can be heated up to 1200°C) with a 40/45 ground glass joint with a stopcock. This is a practical solution since several ampoules can fit inside of one tube and the tube can be used multiple times. Silica tubes with Nb or Ta ampoules were evacuated and flushed with Ar at least three times, closed under vacuum and transferred into vertical resistance furnace (HTM Reetz LOBA 1200-40-600, Eurotherm 2416 controller). Temperature programs were selected individually for different samples.

2.1.2.3 Flux Synthesis

Flux method is a crystal growth technique from the solution, where the solvent is a low-melting metal. Excess of the solvent together with the starting materials is loaded in the reaction container and heated according to the selected temperature program above the melting point of the solvent long enough to form a solution. Then the container is cooled very slowly to make the desired material to precipitate. Flux method allows to grow congruently and incongruently melting materials is relatively simple and has a short grown time scale. It also needs a small amount of material. The negative side of this method is the relatively small size of obtained crystals, but they usually are big enough for the characterization using single-crystal XRD analysis.

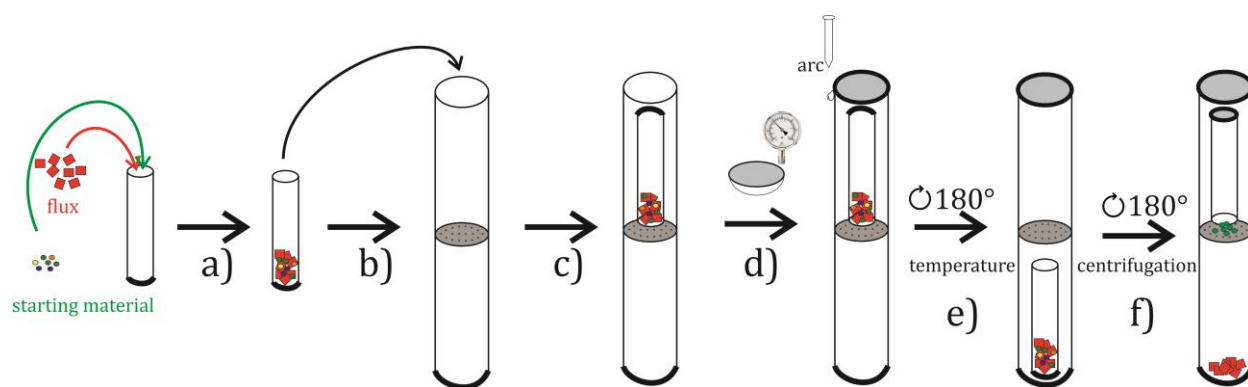


Figure 2.2 Schematic representation of the flux-synthesis: loading starting materials and flux into sealed from the bottom Ta ampoule (a); transferring the Ta ampoule inside of the bigger steel ampoule closed from the bottom (b) and turning it upside down (c); pressing and welding the cap on the open end the ampoule (d); turning container upside down (e) and putting it in the oven; separating crystals of the product from the flux (f).

In this work flux synthesis (as it is shown in Figure 2.2) was performed using custom stainless steel ampoules separated into two parts with a build-in sieve and the bottom cap welded on. As flux material, elemental Sn (melting temperatures of 231.93 C) was used. To prevent reaction with the ampoule starting materials were loaded first inside of another open from one side Ta ampoule (Figure 2.2, a), which was transferred upside down into the steel ampoule, closed from one side (Figure 2.2, b-c). In the next step stainless steel ampoule was sealed from the other side as well (Figure 2.2, d), turned once again upside down (Figure 2.2, e), enclosed in steel containers lined with silica wool and transferred into the muffle oven (Nabertherm, P330 controller). The temperature program was applied to heat the mixture to the reaction temperature and then cooled down to the temperature between the melting point of the desired compound and the flux material to initiate crystallization. The

reaction mixture was held at this temperature for at least one week. After crystallization, the ampoule was turned again upside down and put in the centrifuge (Heraeus Megafuge 1.0) for five minutes at 3000 rpm to separate the product from the excess of the flux material.

2.2 Characterization

2.2.1 X-Ray Diffraction Experiments

X-ray structural analysis is the method for studying the structure of a substance by distribution in space and intensities X-ray radiation scattered on the analyzed object. It is based on the interaction of the X-rays with the electrons of a substance, as a result of which diffraction of the X-rays is observed.

Analyzing the X-rays scattered by the atoms of the crystal, it is possible to recreate the spatial distribution of the electron density in the crystal. This gives the knowledge of the spatial arrangement of atoms in the molecules of which the crystal is built. As a result, the atomic structure of a substance can be determined.

2.2.1.1 Powder X-Ray Diffraction

For the powder X-ray diffraction (PXRD) analysis, obtained samples were finely grounded in an agate mortar, sealed in a glass capillary (inner diameter 0.3 mm, wall thickness 0.01 mm, Hilgenberg GmbH) using capillary wax (Hampton Research) and measured at room temperature using a STOE Stadi P powder diffractometer with Cu-K α ($\lambda = 1.54056 \text{ \AA}$) or Mo-K α ($\lambda = 0.07932 \text{ \AA}$) radiation, Ge (111) monochromator and a position sensitive Dectris MYTHEN DCS 1K solid-state detector. STOE WinXPOW program package ^[42] was used for phase analysis, indexing, and refining cell parameters for the obtained phases.

2.2.1.2 Single Crystal X-Ray Diffraction

Crystals suitable for single crystal X-ray diffraction (SCXRD) analysis were selected under a microscope inside a glovebox and transferred into glass capillaries (inner diameter 0.1-0.3 mm, wall thickness 0.01 mm, Hilgenberg GmbH) using a glass filament dipped in perfluoropolyalkyl ether (Galden Perfluorinated Fluid LSD 230, Solvay Specialty Polymers, viscosity 1800 cSt). The capillaries were then sealed airtight using capillary wax (Hampton Research) and mounted onto a single crystal X-ray diffractometer with Mo K α radiation ($\lambda = 0.71073 \text{ \AA}$). Single-crystal intensity data were collected at room temperature or in cold N₂ stream (150 K), using a Stoe Stadivari diffractometer equipped with a micro focus GeniX 3D

source (high flux Mo K α radiation) and a DECTRIS PILATUS 300K detector. Corrections of the raw data for background, polarization, and Lorentz effects were applied. Due to a Gaussian-shaped primary X-ray beam profile, a scaling procedure within LANA was applied along with the numerical absorption correction using X-Red [43] and X-Shape [44] software. The starting atomic parameters were usually obtained by Direct Method with the SHELXS-2014 [45]. The structure was refined using SHELXL-2014 (full-matrix least-squares on F_o^2) with anisotropic atomic displacement parameters for all atoms. In order to check the composition, the occupancy parameters were refined in separate least-squares cycles.

2.2.2 Differential Scanning Calorimetry

Differential scanning calorimetry is a universal, reliable and most demanded method of thermal analysis. It allows studying the change in the properties of materials under the influence of temperature. The principle of operation of the differential scanning calorimeter is based on measuring the temperature difference between the container (crucible) with the sample and the reference container. The DSC signal measured in this way is a measure of the heat flux absorbed or released by the sample under study during its heating or cooling, as well as in the isothermal mode.

In this work, Netzsch DSC 404 Pegasus apparatus was used for the DSC analysis, operated by Maria Müller, Dr. Lavinia Scherf, and M.Sc. Tassilo Restle. The powdered sample was placed in a custom build by mechanics workshop at TU Munich and pre-cleaned cylindrical niobium ampoule which was closed by crimping it and sealing inside of the glove box. An empty niobium ampoule closed in the same way and was used as a reference. During the experiment, the sample was heated in an argon flow with a heating/cooling rate of 10 K/min to 1000°C in two cycles. For data processing the program Proteus Thermal Analysis [46] was used.

2.2.3 Energy-Dispersive X-ray Spectroscopy

The elemental composition of the crystals was checked using energy-dispersive X-ray spectroscopy, measuring the energy of the X-ray emitted from the sample which is characteristic for each element. Crystals were tested qualitatively to verify the absence of elements heavier than sodium. Two types of measurements were performed at least twice for each crystal: a point measurement and a surface scan. The composition of each crystal was determined by semi-quantitatively, averaging the data of at least four measurements.

The crystals for the EDX analysis were mounted onto an Al stub using graphite tape inside of the Ar-filled glovebox and transferred to the measurement facility in a closed Ar-filled container. Unfortunately, contact with the air for a few seconds could not be avoided while loading the aluminum stub into the microscope, which resulted sometimes in the oxidizing of the crystal surface. EDX spectra were obtained using a JSM 7500F scanning electron microscope (JEOL) by Maria Müller and an Oxford X-Max EDX analyzer with internal Mn standard by Katia Rodewald at Wacker-Chair of Macromolecular Chemistry (TU Munich).

2.2.4 Magnetic Measurements

Magnetic measurements were performed using a Quantum Design MPMS 5 XL SQUID magnetometer with liquid Helium cooling. The measurements were performed in the temperature range between 2 and 300 K and magnetic fields up to 5 Tesla. The reciprocal sample option (RSO) mode was used. For each measurement 30-80 mg of the powdered sample was transferred into the gelatin capsule and fixed in the middle of the plastic straw, which was afterward directly attached to the sample rod. The centering scan and the adjustment of the position of the sample inside of the chamber were performed in the DC mode. The typical sequence included the measurement at an applied field of 1 Tesla over a temperature range of 2 – 300 K (step size of 2-5 K in sweep mode), as well as field dependent measurements between 0 and 5 Tesla at 300 K (step size of 500-1000 Oe in hysteresis mode). For all samples, the superconductivity test was performed using the zero-field cooled/field cooled method at the applied field of 15 Oe in the temperature range between 2 and 30 K.

The data, including the temperature (K), field (H), long moment (emu) and long scan standard deviation (emu), was collected using the MultiVu program [47]. The raw data was handled in OriginPro [48], where long moment was converted into molar magnetic susceptibilities (χ_{mol}) and subsequently corrected for the sample holder and diamagnetic contribution of the core electrons using Pascal's constants [49].

2.2.5 Raman Spectroscopy

Raman spectroscopy is used to identify unknown materials from their unique Raman spectral fingerprints, by which compounds can be identified typically using databases of known spectra. The sample is illuminated by the laser beam, which initiates the unelastic scattering of photons (Raman scattering).

Raman spectroscopy measurements were performed by Dr. Sebastian Geier and M. Sc. Christoph Wallach using a Renishaw inVia Raman microscope equipped with a CCD detector and three different lasers ($\lambda = 532$ nm, 633 nm, and 785 nm) with a maximum power of 500 mW. For operating the device, the software WiRe 4.2 ^[50] was used. Samples were ground in an agate mortar inside of a glovebox, filled into glass capillaries (inner diameter 0.3 mm, wall thickness 0.01 mm, Hilgenberg GmbH) which are sealed using capillary wax (Hampton Research). The data was processed using OriginPro ^[48].

2.2.6 Computational Methods

The electronic structure calculations for some of the obtained compounds were performed to point out the structural-properties relation and to better understand the nature of the chemical bonding. The band structure and DOS calculations were performed using the Linear Muffin-Tin Orbital (LMTO) method in the atomic sphere approximation (ASA) using the tight-binding (TB) program TB-LMTO-ASA ^[51]. The exchange-correlation term was calculated within the local density approximation (LDA) and was parametrized according to von Barth and Hedin ^[52]. The radii of the muffin-tin spheres were determined after Jepsen and Andersen ^[53].

If it was possible, the band structure calculations were performed on the structural model based on the single crystal data refinement. In case of compounds with mixed occupancies or defect positions, fully occupied and/or ordered theoretical models were used.

3 Results and Discussion

3.1 Substitutional Effects in the Na-Sn Binary System

3.1.1 Introduction

Recent investigations in the systems with the late transition, alkali metals and early *p*-elements (group 13 and 14) reveal an impressive number of compounds with various structural motifs, among which are complicated 3-D networks of atomic clusters within the anionic framework. A wide variety of structures can exist in these systems, including isolated fragments, dimeric units, two-dimensional polyanions and three-dimensional networks.

3.1.1.1 Na-Sn Binary System

According to the phase diagram ^[54] (Figure 6.1, a), there are eight compounds in the Na-Sn binary system: Na₁₅Sn₄, Na₃Sn, Na₉Sn₄, NaSn, NaSn₂, NaSn₃, NaSn₄, and NaSn₅. Over the last years detailed research allowed to improve and correct this data and to describe the crystal structure of the binary phases, shown in Table 3.1 and visualized in Figure 3.1. It is typical for compounds with alkali (or alkaline-earth) metals and group 13 or 14 elements, the electronegative elements are reduced by the electropositive elements. Most of the binary phases in Na-Sn system are Zintl phases (Na₄Sn₄, Na₇Sn₁₂, NaSn₂, Na₅Sn₁₃) and, in accordance with the Zintl-Klemm formalism, these compounds form anionic frameworks.

Table 3.1 Binary compounds in the Na-Sn binary system.

Compound	Space group	Cell parameters				Ref.
		<i>a</i> (Å)	<i>b</i> (Å)	<i>c</i> (Å)	<i>V</i> (Å ³)	
Na ₁₅ Sn ₄	<i>I</i> $\bar{4}$ 3 <i>d</i>	13.14	-	-	2268.75	[55]
Na _{14.8} Sn ₄	<i>Pnma</i>	9.82	5.57	22.79	1246.55	[56]
Na ₅ Sn ₂	<i>R</i> $\bar{3}$ <i>m</i>	5.4253	-	22.3912	570.76	[57]
Na ₉ Sn ₄	<i>Cmcm</i>	5.4217	9.3913	29.621	1507.47	[55]
Na ₄ Sn ₄	<i>I</i> 4 ₁ / <i>acd</i>	10.475	-	17.412	1910.54	[31]
Na ₇ Sn ₁₂	<i>P</i> 2/ <i>n</i>	13.375	9.3294	17.976	2243.05	[58]
NaSn ₂	<i>C</i> 2/ <i>m</i>	13.3916	$\beta=90.15^\circ$ 6.8541	15.4889	1387.83	[59]
Na ₅ Sn ₁₃	<i>Cmcm</i>	8.979	$\beta=102.5281^\circ$ 19.448	50.43	8806.27	[60]
NaSn ₅	<i>P</i> $\bar{4}$ 2 ₁ <i>m</i>	6.2850	-	8.794	347.37	[61]

In the Na-Sn binary system, as it is shown in Figure 3.1, a wide variety of Sn frameworks can exist, including isolated Sn atoms in $\text{Na}_{15}\text{Sn}_4$ and $\text{Na}_{14.8}\text{Sn}_4$; dimeric $\{\text{Sn}_2\}$ units in Na_5Sn_2 and Na_9Sn_4 ; two-dimensional polyanions in $\text{Na}_7\text{Sn}_{12}$ and NaSn_2 ; three-dimensional Sn-network in $\text{Na}_5\text{Sn}_{13}$ and NaSn_5 , as well as isolated tetrahedral cluster $\{\text{Sn}_4\}^{4-}$ in NaSn (Na_4Sn_4). Strong evidence [62] are suggesting that one more binary phase, $\text{Na}_{12}\text{Sn}_{17}$, similar to $\text{K}_{12}\text{Sn}_{17}$ [32], with isolated $\{\text{Sn}_9\}^{4-}$ and $\{\text{Sn}_4\}^{4-}$ clusters also exist in Na-Sn system, but the detailed crystal structure of $\text{Na}_{12}\text{Sn}_{17}$ has not been described until now.

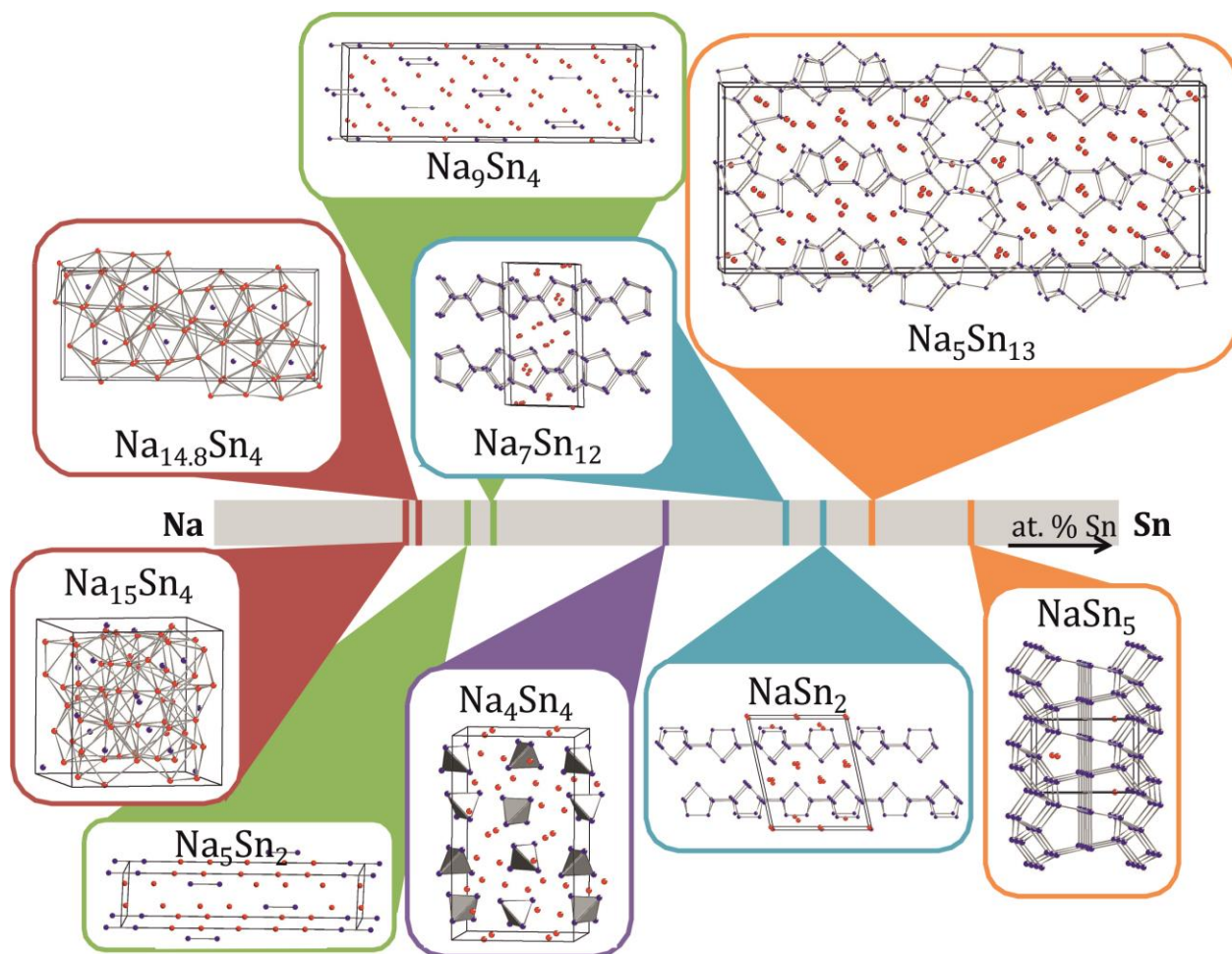


Figure 3.1 Fragments of the crystal structure of the binary phases in Na-Sn [31, 55-61] binary system, color-coded according to dimensionality of the Sn anionic frameworks: isolated Sn atoms – red rectangles; dimeric $\{\text{Sn}_2\}$ units – olive green; two-dimensional polyanions – aqua blue; three-dimensional Sn-network – orange; isolated clusters – purple.

3.1.1.2 Interactions in the Na-T-Sn Ternary Systems ($T = \text{late transition metals}$)

The substitution of the group 14 elements by transition metal introduces electron deficiency that leads to the condensation of the clusters and formation of new complicated networks, which could be shown through diverse interactions in the Na- T -Sn ternary systems (Table 3.2 visualized in Figure 3.2) resulting in complicated structures with various dimensionalities. In a row Zn (Cd, Hg)-Cu (Au)-Ni (Pd)-Co with decreasing electron number of transition metal a tendency in the building of polyanionic network to the filled isolated clusters can be observed.

For example, for transition metals Zn (Cd, Hg), Cu, Ni and Co the dimensionalities vary from linear anionic $\{\text{Sn-Zn-Sn}\}^{6-}$ in Na_6ZnSn_2 ^[63] to two-dimensional layered structures with hexagonal sheets in Na_2TSn ^[64] ($T = \text{Cd, Hg}$), as well as one-dimensional double walled nanorods $\{\text{Sn}_{0.6}@\text{Cu}_{12}@\text{Sn}_{20}\}^{12-}$ in $\text{Na}_{2.78}\text{Cu}_5\text{Sn}_{5.61}$ ^[65] or isolated two-shell matryoshka-clusters $\{\text{Sn}@\text{Cu}_{12}@\text{Sn}_{21}\}^{12-}$ in $\text{Na}_{12}\text{Cu}_{12}\text{Sn}_{21}$ ^[36], whereas both Co and Ni are forming $\{\text{Ni}@\text{Sn}_9\}^{4-}$ or $\{\text{Co}@\text{Sn}_9\}^{5-}$ along with $\{\text{Sn}_4\}^{4-}$ clusters in the structures of the $\text{Na}_{12}\text{Ni}_{0.93}\text{Sn}_{17}$ ^[66] or $\text{K}_{13}\text{CoSn}_{17}$ ^[66], respectively.

However, dominating among Na- T -Sn ($T = \text{late transition metal}$) are compounds with three-dimensional structures. NaPd_3Sn_2 ^[67] with CeCo_3B_2 -type structure is a ternary derivative from CaCu_5 -type with palladium atoms occupying the cobalt sites of CeCo_3B_2 and thus form a network of edge-connected trigonal prisms, in the centers of which the tin atoms are located.

In Na-Au-Sn system a diverse number of compounds are found: NaAuSn ^[68] being a variant of PbCl_2 -type and Na_2AuSn_3 ^[69] crystallizing in a ternary variant (Lu_2CoGa_3 -type) of the AlB_2 type. The tin atoms in Na_2AuSn_3 form the motif of a $\frac{1}{\infty}\{\text{Sn}_{3/3}\}$ tubular fragment of the hexagonal diamond structure and are connected to a framework structure via gold atoms with trigonal planar tin coordination and sodium atoms are placed in channel-like cavities of the Au-Sn partial structure. A special group within Na-Au-Sn ternary system form $\text{Na}_{26}\text{Au}_{55-x}\text{Sn}_x$ ($x = 13.45, 15.17$)^[70] and $\text{Na}_{30}\text{Au}_{39}\text{Sn}_{12}$ ^[71], both pure intermetallics and being classified as conventional Bergman-type structures, with bcc-packing of Samson polyhedra and Na-atoms as fillers between these clusters.

Within the Na-Zn-Sn ternary system all eight compounds were found and characterized in the group of T. F. Fässler^[72]. It was demonstrated that adding a small amount of transition

metal to alkali-rich Na-Sn alloy leads to the formation of ternary compounds with anionic substructures build up of four bonded atoms like those in clathrates or diamond. Compound Na_2ZnSn_5 ^[73] with tetrahedral framework structure is featuring temperature-dependent polymorphism: h- Na_2ZnSn_5 is metastable under standard conditions (obtained by fast cooling of a melt) and thermodynamically stable t- Na_2ZnSn_5 (obtained slow cooling of a melt or tempering hexagonal Na_2ZnSn_5). The structures of $\text{Na}_5T_{2+x}\text{Sn}_{10-x}$ ^[74] ($T = \text{Zn, Hg}$) consist of an anionic 3-D open framework of tetrahedrally coordinated Sn and T atoms interwoven with a cationic 2-D array of interconnected $\{\text{NaNa}_4\}$ tetrahedra. The framework can be partitioned into fragments of realgar-like units $\{\text{Sn}_{8-x}T_x\}^{2x-}$ and twice as many $\{\text{Sn-T}\}^{2-}$ dimers.

Table 3.2 Ternary compounds in the Na- T -Sn system (T = late transition metals).

Compound	Space group	Cell parameters			V (Å ³)	Ref.
		a (Å)	b (Å)	c (Å)		
Na-Ni-Sn						
$\text{Na}_{12}\text{Ni}_{0.93}\text{Sn}_{17}$	$P2_1/c$	23.7343	13.6799	44.620	14482.2	[66]
$\beta = 91.527^\circ$						
Na-Pd-Sn						
NaPd_3Sn_2	$P6/mmm$	5.772	-	4.23	122.05	[67]
Na-Cu-Sn						
$\text{Na}_{12}\text{Cu}_{12}\text{Sn}_{21}$	$Pn\bar{3}mZ$	16.6253	-	-	4595.24	[36]
$\text{Na}_{2.78}\text{Cu}_5\text{Sn}_{5.61}$	$Cmcm$	13.0075	22.3892	4.1852	1218.85	[65]
Na-Au-Sn						
$\text{Na}_{30}\text{Au}_{39}\text{Sn}_{12}$	$Im\bar{3}$	14.989	-	-	3367.58	[71]
Na_2AuSn_3	$P6_3/mmc$	9.585	-	7.516	598	[69]
NaAuSn	$Pnam$	7.476	8.088	4.53	273.91	[68]
$\text{Na}_{26}\text{Au}_{38.54}\text{Sn}_{13.45}$	$Im\bar{3}$	15.0194	-	-	3388.11	[70]
Na-Zn-Sn						
Na_6ZnSn_2	$C2/m$	10.077	5.4733	9.316	508.73	[63]
$\beta = 98.07^\circ$						
$\text{Na}_{20}\text{Zn}_8\text{Sn}_{11}$	$C2/c$	16.1505	9.2762	27.594	4028.55	[63]
$\beta = 102.969^\circ$						
$\text{Na}_{16}\text{Zn}_{13.54}\text{Sn}_{13.46}$	$Ibam$	27.4006	16.1004	18.4313	8131.16	[75]
$\text{Na}_{22}\text{Zn}_{20}\text{Sn}_{19}$	$Pnma$	16.4026	15.5975	22.6551	5796.07	[75]
$\text{Na}_{29}\text{Zn}_{24}\text{Sn}_{32}$	$P\bar{6}2m$	15.7121	-	9.4621	2022.96	[37]
$\text{Na}_5\text{Zn}_{2.28}\text{Sn}_{9.72}$	$Pbcn$	12.772	10.804	12.777	1763.1	[74]
h- Na_2ZnSn_5	$P6_122$	6.4510	-	6.2370	224.78	[73]
t- Na_2ZnSn_5	$I\bar{4}2d$	6.3360	-	22.3820	898.52	[73]
$\text{Na}_{34}\text{Zn}_{66}\text{Sn}_{38}$	$R\bar{3}mH$	16.95580	-	36.8607	9177.63	[75]
Na-Cd-Sn						
Na_2CdSn	$P6_3/mmc$	4.99	-	10.111	218.03	[64]
$\text{Na}_{49}\text{Cd}_{58.34}\text{Sn}_{37.69}$	$R\bar{3}mH$	16.034	-	50.64	11274.78	[76]

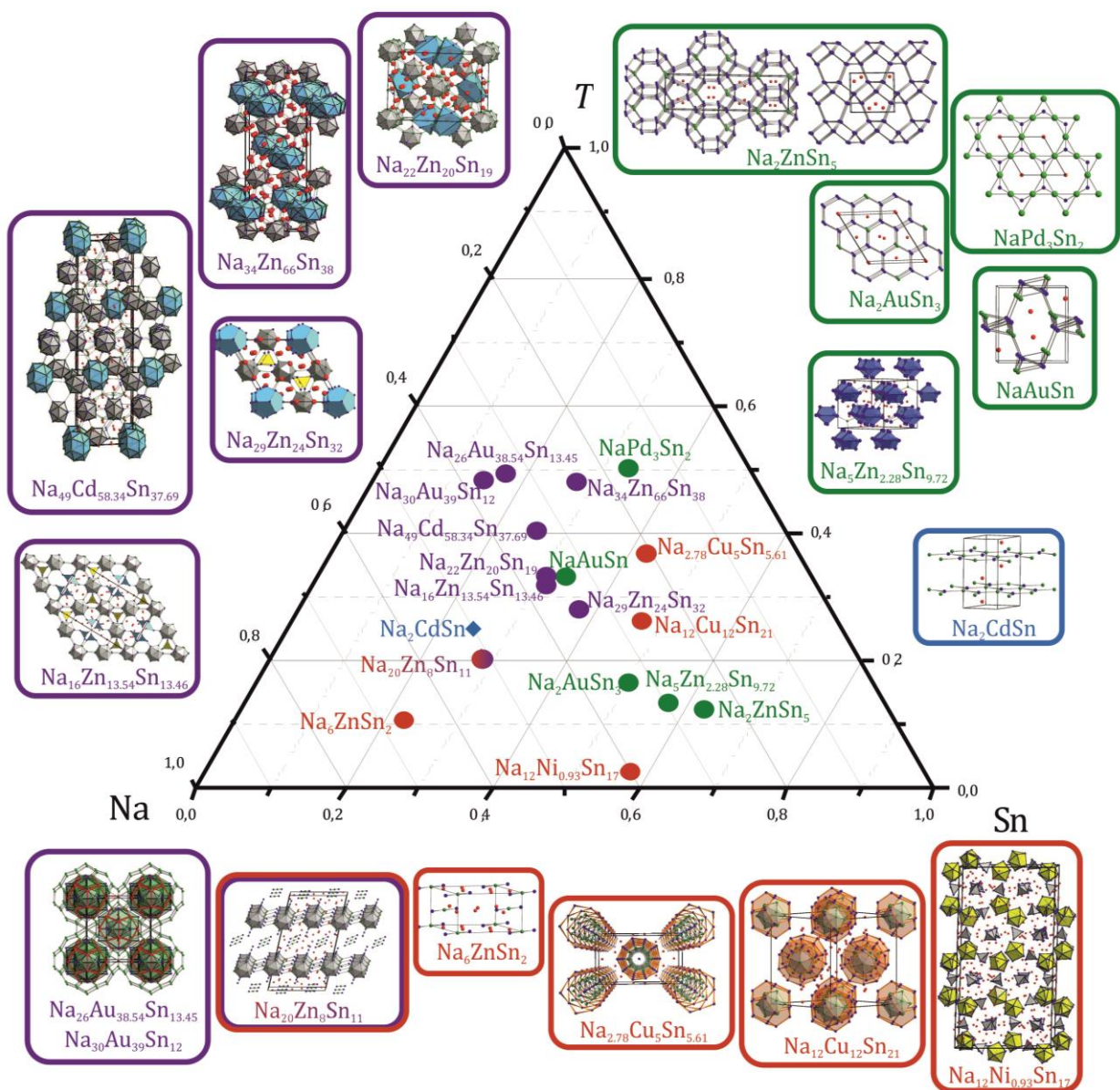


Figure 3.2 Structures of the compounds in Na-*T*-Sn ternary systems (*T* = late transition metals): phases with isolated clusters or fragments are marked with red rectangles, two-dimensional layered structures – blue, phases with three-dimensional networks – green and its subunits, phases with interconnected icosahedral networks in violet.

Among phases with three-dimensional structures, a special group is formed by the icosahedral phases. $\text{Na}_{20}\text{Zn}_8\text{Sn}_{11}$ [63] comprises layers of interconnected heteroatomic $\{\text{Zn}_7\text{Sn}_5\}$ icosahedra sheets combined with linear anions $\{\text{Sn-Zn-Sn}\}^{6-}$, as in Na_6ZnSn_2 .

In $\text{Na}_{29}\text{Zn}_{24}\text{Sn}_{32}$ [37] covalently linked $\{\text{Zn}_8\text{Sn}_4\}$ icosahedron coexist with a one-dimensional covalently bonded homoatomic tin substructure, containing an enneahedron $\{\text{Sn}_{14}\}$ and $\{\text{Sn}_3\}$ triangular fragments. Similarly, structures of $\text{Na}_{16}\text{Zn}_{13.54}\text{Sn}_{13.46}$ $\text{Na}_{22}\text{Zn}_{20}\text{Sn}_{19}$ $\text{Na}_{34}\text{Zn}_{66}\text{Sn}_{38}$ [75] consist of complex 3-D cluster networks of Zn and Sn atoms with the common motif of Kagome nets of heteroatomic $\{\text{Zn}_{12-x}\text{Sn}_x\}$ icosahedra. The structures have different fragments filling cavities of the Kagome nets: triangular units in $\text{Na}_{16}\text{Zn}_{13.54}\text{Sn}_{13.46}$, 15-atomic cages in $\text{Na}_{22}\text{Zn}_{20}\text{Sn}_{19}$ and pairs of triply fused icosahedra in $\text{Na}_{34}\text{Zn}_{66}\text{Sn}_{38}$. In Na-Cd-Sn system compound $\text{Na}_{49}\text{Cd}_{58.34}\text{Sn}_{37.69}$ [76] features a similar structure: $\{\text{Cd}_{12-x}\text{Sn}_x\}$ icosahedra forming Kagome nets with 18-atoms clusters in the voids.

Motivated by recently reported compounds in Na-Cu-Sn, Na-Au-Sn and Na-Zn-Sn ternary systems, in this Chapter the results of systematic investigation of introducing electron deficiency with Ag to Na-Sn binary phases are given. On the one hand, expecting structures with condensed cluster units, on the other hand, the filling of Hume-Rothery phases by alkali metal can help to better understand the electronic situation in polar intermetallic compounds. In this Chapter the synthesis and characterization of the first compounds in Na-Ag-Sn system are presented.

3.1.2 Three Icosahedral Ternary Phases in the Na-Ag-Sn System: $\text{Na}_{29}\text{Ag}_{21}\text{Sn}_{39}$, $\text{Na}_{13}\text{Ag}_{5.5}\text{Sn}_{21.2}$ and $\text{Na}_{230.45}\text{Ag}_{274}\text{Sn}_{136}$

3.1.2.1 $\text{Na}_{29}\text{Ag}_{21}\text{Sn}_{39}$ – a Cluster Interconnected Compound as a Hierarchical Variant of CaCu_5 -type

Synthesis and Characterization

The sample with the stoichiometry Na:Ag:Sn of 29:24:32 was prepared in a two step synthesis. First, binary Ag-Sn alloy was prepared by pre-melting 183.5 mg of Ag and 269.0 mg of Sn in an arc furnace to obtain a binary regulus. The obtained binary regulus was added to 47.3 mg of elemental Na for the synthesis of ' $\text{Na}_{29}\text{Ag}_{24}\text{Sn}_{32}$ ' in a niobium ampoule, which was sealed by arc welding from both ends. The ampoule was transferred into a silica tube, evacuated and placed into a vertical resistance tube furnace. It was heated to 800°C and tempered for 12 hours. Afterwards, the sample was cooled with a cooling rate of 0.1°C/min to 450°C and tempered for another 64 hours. Finally, the sample was cooled to room temperature with a cooling rate of 1°C/min. After the synthesis ampoule was opened in an argon atmosphere. The obtained product was a lustrous silver powder, sensitive to air and moisture.

The PXRD analysis of the sample ' $\text{Na}_{29}\text{Ag}_{24}\text{Sn}_{32}$ ' indicates an almost phase pure sample (Figure 3.4). The calculated hexagonal unit cell parameters obtained from the indexing of the X-ray powder diffractogram of the sample ' $\text{Na}_{29}\text{Ag}_{24}\text{Sn}_{32}$ ', measured at the room temperature for the title compound are $a = 15.992(2)$, $c = 9.841(1)$ Å and cell volume 2179.4(5) Å³ which slightly smaller than the cell parameter obtained as a result of the single crystal refinement at 150K (Table 3.4). This effect can be explained by a negative thermal expansion coefficient or phase width of this compound. To investigate the second possibility, a series of samples with the composition ' $\text{Na}_{32}\text{Ag}_{13+x}\text{Sn}_{55-x}$ ' with $x = 0, 7, 9, 13$ and 18 was prepared. All of the samples contained $\text{Na}_{29}\text{Ag}_{12.3+x}\text{Sn}_{48-x}$ as the main phase with the cell parameters listed in Table 3.3 and plotted in Figure 3.3. There is no clear dependency between the Ag content in the samples and the cell parameters of the phase $\text{Na}_{29}\text{Ag}_{12.3+x}\text{Sn}_{48-x}$, but the cell parameters of the sample ' $\text{Na}_{32}\text{Ag}_{26}\text{Sn}_{45}$ ' fit perfectly to that of the fully characterized sample ' $\text{Na}_{29}\text{Ag}_{24}\text{Sn}_{32}$ '.

Table 3.3 The cell parameters obtained from the PXRD of the samples with various Ag:Sn ratio.

Composition	a (Å)	c (Å)	V (Å ³)
'Na ₃₂ Ag ₁₃ Sn ₅₅ '	16.06(1)	9.754(7)	2178(2)
'Na ₃₂ Ag ₂₀ Sn ₄₈ '	16.050(7)	9.773(3)	2180(1)
'Na ₃₂ Ag ₂₂ Sn ₄₆ '	16.05(3)	9.78(1)	2183(6)
'Na ₃₂ Ag ₂₆ Sn ₄₅ '	15.992(2)	9.842(1)	2179.4(5)
'Na ₃₂ Ag ₂₉ Sn ₃₉ '	15.98(1)	9.833(9)	2175(1)

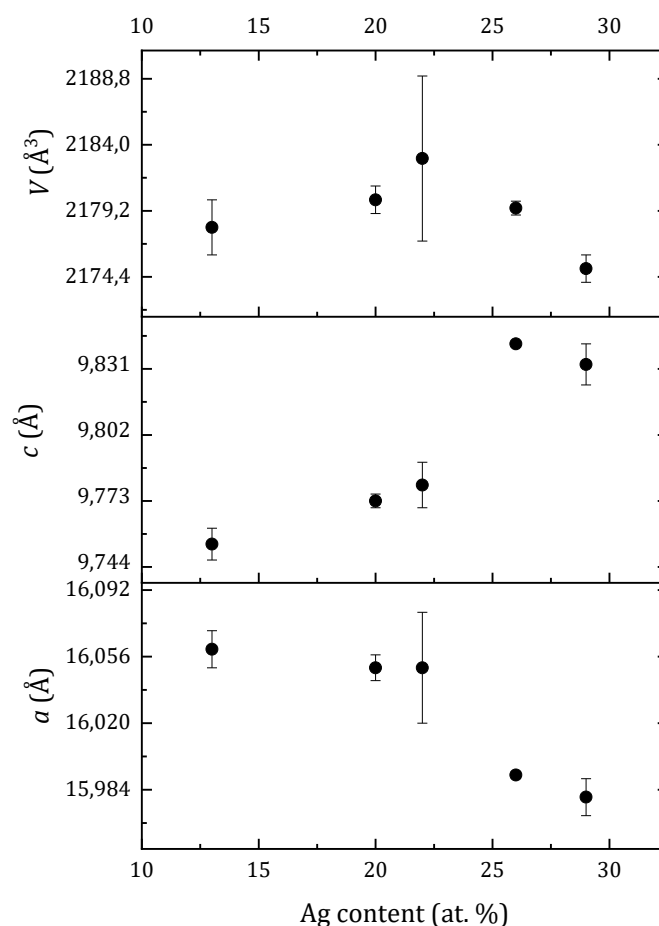


Figure 3.3 Dependency of the cell parameter from the Ag content in the samples containing the phase Na₂₉Ag_{12.3+x}Sn_{48-x}.

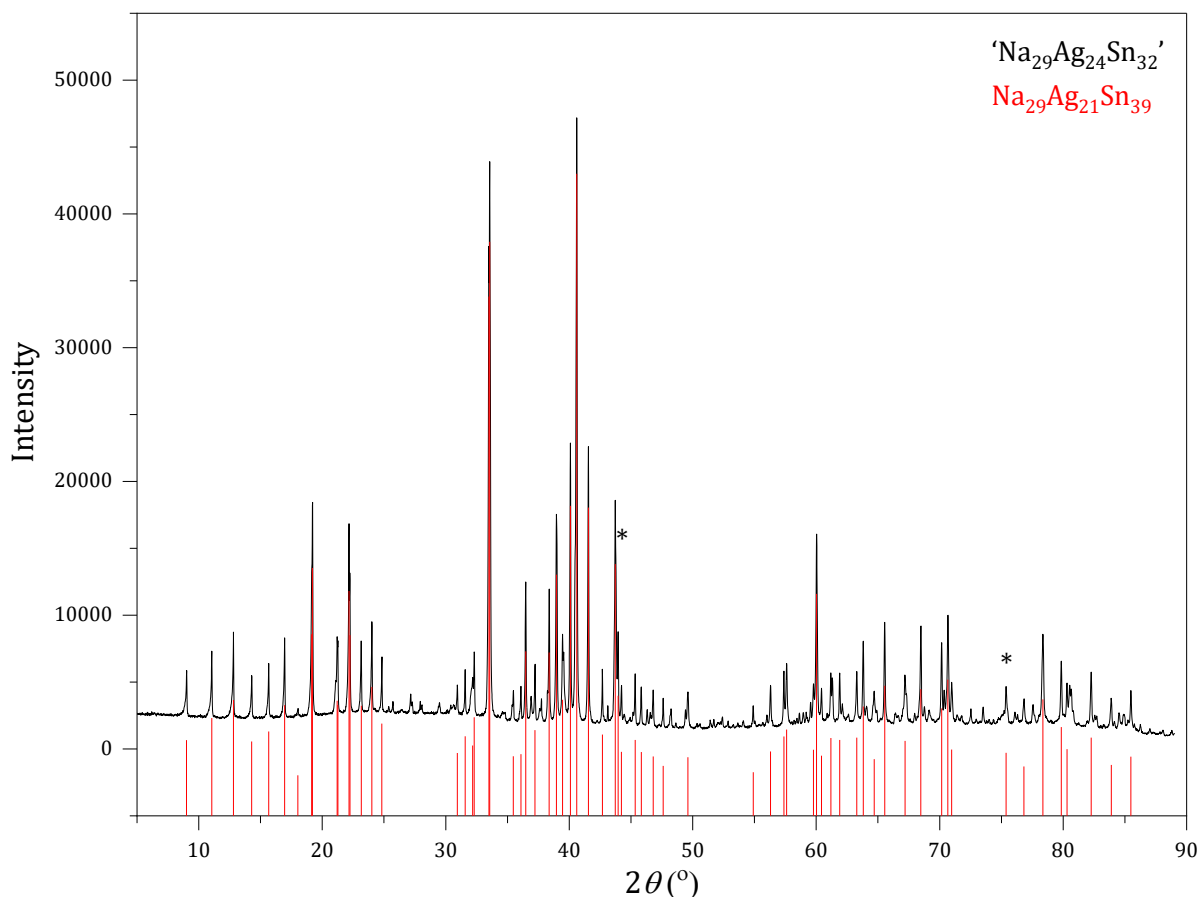


Figure 3.4 Experimental X-ray powder diffractogram of the sample ‘Na₂₉Ag₂₄Sn₃₂’ (black) with the theoretical pattern (red) of Na₂₉Ag₂₁Sn₃₉ (model obtained from single crystal data) and diamond (*) as internal standard.

For the structure determination of the new compound a suitable single crystal was selected, sealed in the capillary and measured at 150 K at Stoe Stadivari diffractometer. The structure was refined (results are shown in Table 3.4 and Table 3.5) using SHELXL-2014 (full-matrix least-squares on F_o^2)^[77] with anisotropic atomic displacement parameters for all atoms (Table 3.6).

In order to define the composition, the occupancy parameters were refined in separate least-squares cycles. Mixing of Ag and Sn was observed on the Wyckoff positions $6m$ and $12o$ (Sn₄/Ag₄, Sn₅/Ag₅, respectively). The largely elongated in ab -plane thermal ellipsoid for Sn₄/Ag₄ (Wyckoff position $6m$) can be described by the split in $12q$ position (site occ. 50 %). Positional and atomic displacement parameters (ADPs) for Ag and Sn were set to be equal at the respective atom sites. The refinement of the occupancy parameters led to 0.18/0.32(5) for Sn₄/Ag₄ and 0.60/0.40(5) for Sn₅/Ag₅. In the following discussion, we denote these sites as $M4$ and $M5$, respectively. The refinement revealed a defect on the Ag₂ positions $12n$ with

site occupancy factors of 0.859(4). No significant residual peaks were observed in the difference electron-density map. Relevant crystallographic data and conditions for the data collections and refinement procedure are listed in Table 3.4. Interatomic distances are shown in Table 6.1 (Appendix).

Table 3.4 Crystallographic data and selected details of structure refinement for the compound Na₂₉Ag₂₁₍₁₎Sn₃₉₍₁₎.

Formula	Na₂₉Ag₂₁₍₁₎Sn₃₉₍₁₎
Formula weight (g·mol ⁻¹)	7582.67
Space group	<i>P6/mmm</i> (no. 191)
<i>Z</i>	1
Unit cell parameters (Å)	<i>a</i> = 16.1231(9) <i>c</i> = 9.7387(6)
Volume (Å ³)	2192.4(3)
<i>D</i> _{calcd.} (g·cm ⁻³)	5.754
Abs. Coeff. (mm ⁻¹)	15.667
<i>F</i> (000) (e)	3271
Crystal shape/color	block/silver
Temperature (K)	150
θ range (deg)	2.527–27.495
Range in <i>hkl</i>	±20 ±20 ±12
Reflections collected	35564 (<i>R</i> ₆ = 0.0100)
Unique reflections	1042 (<i>R</i> _{int} = 0.0457)
Data / parameter	1042/61
GOF on <i>F</i> ²	1.093
<i>R</i> ₁ , <i>wR</i> ₂ (<i>I</i> > 2 σ (<i>I</i>))	0.0276, 0.0661
<i>R</i> ₁ , <i>wR</i> ₂ (all data)	0.0311, 0.0676
Largest diff. peak/hole (e Å ⁻³)	3.969 and -2.192

Table 3.5 Atom coordinates and equivalent isotropic displacement parameters (Å²) for the compound Na₂₉Ag₂₁₍₁₎Sn₃₉₍₁₎; *M* = statistical mixture of Sn and Ag.

Atom	Wyck.	S.O.F.	<i>x</i>	<i>y</i>	<i>z</i>	<i>U</i> _{eq}
Sn1	6 <i>m</i>	1	0.60493(3)	0.20985(5)	1/2	0.0163(2)
Sn2	12 <i>p</i>	1	0.49083(4)	0.15943(4)	0	0.01987(2)
Sn3	12 <i>n</i>	1	0.34601(4)	0	0.15979(6)	0.02203(2)
<i>M</i> 4	12 <i>q</i>	0.18/0.32(5)	0.24709(1)	0.10831(2)	1/2	0.0380(1)
<i>M</i> 5	12 <i>o</i>	0.60/0.40(5)	0.55101(2)	0.10203(4)	0.25151(6)	0.0217(2)
Ag1	2 <i>e</i>	1	0	0	0.1469(2)	0.0440(5)
Ag2	12 <i>n</i>	0.859(4)	0.17881(7)	0	0.26836(1)	0.0404(4)
Na1	4 <i>h</i>	1	2/3	1/3	0.1903(7)	0.0227(1)
Na2	1 <i>b</i>	1	0	0	1/2	0.031(3)
Na3	12 <i>o</i>	1	0.4280(3)	0.21399(1)	0.6966(4)	0.0272(8)
Na4	6 <i>l</i>	1	0.2642(4)	0.1321(2)	0	0.0333(1)
Na5	6 <i>k</i>	1	0.3813(4)	0	1/2	0.0338(1)

Table 3.6 Anisotropic displacement parameters (\AA^2) for $\text{Na}_{29}\text{Ag}_{21(1)}\text{Sn}_{39(1)}$. M = statistical mixture of Sn and Ag.

Atom	U_{11}	U_{22}	U_{33}	U_{12}	U_{13}	U_{23}
Sn1	0.0188(3)	0.0130(4)	0.0151(4)	0.000	0.000	0.0065(2)
Sn2	0.0208(3)	0.0164(3)	0.0227(3)	0.000	0.000	0.0095(2)
Sn3	0.0241(3)	0.0169(3)	0.0227(3)	0.000	0.0010(2)	0.0085(1)
M4	0.0258(7)	0.0269(2)	0.0494(9)	0.000	0.000	0.0042(7)
M5	0.0246(3)	0.0185(3)	0.0200(4)	-0.0003(2)	-0.0001(1)	0.0093(2)
Ag1	0.0520(8)	0.0520(8)	0.028(1)	0.000	0.000	0.0260(4)
Ag2	0.0459(5)	0.0233(5)	0.0446(6)	0.000	0.0093(4)	0.012(2)
Na1	0.0221(2)	0.0221(2)	0.024(3)	0.000	0.000	0.0111(9)
Na2	0.024(4)	0.024(4)	0.044(8)	0.000	0.000	0.012(2)
Na3	0.035(2)	0.026(1)	0.024(2)	-0.0022(8)	-0.0044(2)	0.018(1)
Na4	0.037(3)	0.028(2)	0.039(3)	0.000	0.000	0.018(2)
Na5	0.045(3)	0.032(3)	0.021(3)	0.000	0.000	0.016(2)

Table 3.7 Results of the EDX analysis of the crystal with the refined composition $\text{Na}_{29}\text{Ag}_{21}\text{Sn}_{39}$ from the sample ' $\text{Na}_{29}\text{Ag}_{24}\text{Sn}_{32}$ '.

	Na (at. %)	Ag (at. %)	Sn (at. %)
EDX	38(6)	24(4)	38(4)
$\text{Na}_{29}\text{Ag}_{21}\text{Sn}_{39}$	32.6	23.6	43.8

According to the EDX analysis of the crystal, previously characterized by the single crystal XRD (Table 3.7, deviation occurs as a result of averaging of four measurements: two point and two surface scans), the atomic ratios of Na:Ag:Sn, determined from several measurements and was 38:24:28, respectively. A significantly higher deviation of the sodium content in the crystal can be explained by oxidation of the surface of the crystal during the transport into the device.

Thermal Behavior of the Sample ' $\text{Na}_{29}\text{Ag}_{24}\text{Sn}_{32}$ '

The thermal behavior of the 65 mg of the sample ' $\text{Na}_{29}\text{Ag}_{24}\text{Sn}_{32}$ ' was determined with a Netzsch DSC 404 Pegasus apparatus. During the experiment, the sample was heated in an argon flow with a heating/cooling rate of $10^\circ\text{C}/\text{min}$ to 750°C in two cycles. The sample was recovered in an argon-filled glove box. Both recorded cycles were almost identical. In the courses of heating, one strong exothermic effect is visible at 499.71 and 498.07°C respectively. This effect appears as a result of the melting of the investigated phase. In the courses of cooling, one corresponding endothermic effect is found at 461.38 and 461.37°C (cycle 1,2), which results from the crystallization of the compound (Figure 3.5). No signs of any kind of phase transition were visible.

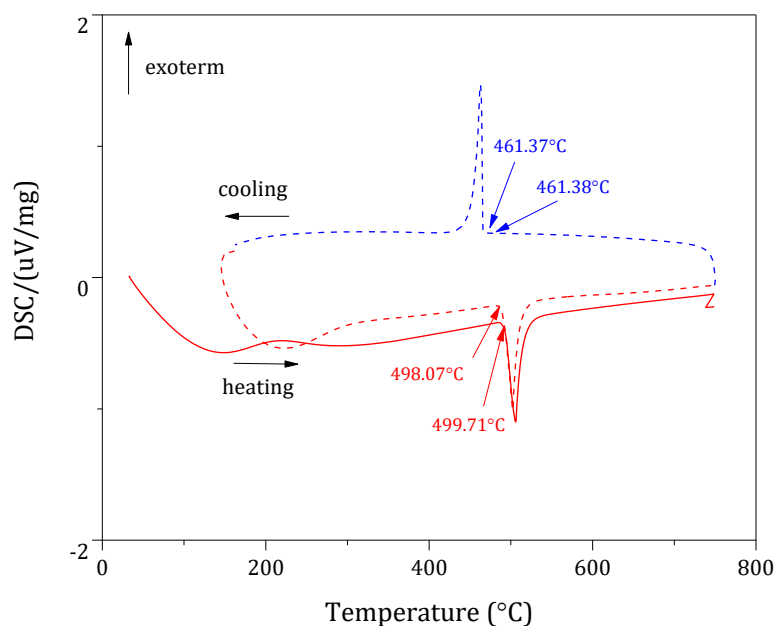


Figure 3.5 Thermogram of the sample ‘Na₂₉Ag₂₄Sn₃₂’. Heating curves are shown in red and cooling in blue (First cycle – solid line, second cycle – dashed line).

Magnetic Properties of the Sample ‘Na₂₉Ag₂₄Sn₃₂’

A powdered sample of ‘Na₂₉Ag₂₄Sn₃₂’ (24.78 mg) has been characterized by susceptibility measurements in external magnetic fields of 10 kOe and by magnetization isotherms at 300 K with fields up to 50 kOe. Obtained raw magnetization data were converted into molar magnetic susceptibilities (χ_{mol}) and subsequently corrected for the sample holder and diamagnetic contribution of the core electrons using Pascal’s constants (for Na⁺, Ag⁺ and Sn^{IV} [49]), Figure 3.6. Neither magnetic ordering, nor superconductive transition down to 1.8 K is found for Na₂₉Ag₂₁Sn₃₉. The upturn in the susceptibility curve at the temperatures below 20 K indicates the presence of paramagnetic impurities, in the amount below detectable by PXRD. The field dependence of the magnetization obtained at 300 K shows a linear decrease with the field, clearly indicating the diamagnetic character of the compound Na₂₉Ag₂₁Sn₃₉.

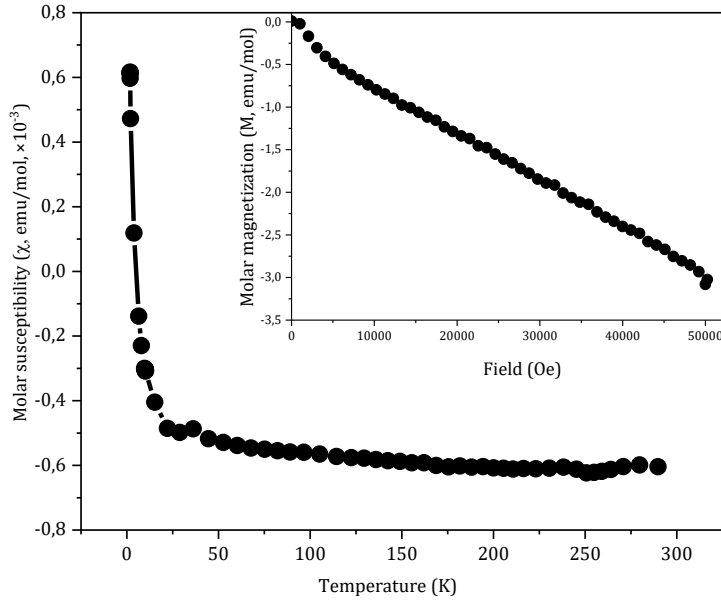


Figure 3.6 Molar magnetic susceptibility as a function of temperature at applied field of 10000 Oe and field-dependent magnetization measured at 300K (inset) for the sample 'Na₂₉Ag₂₄Sn₃₂'.

LMTO Calculations for the 'Na₂₉Ag₁₄Sn₄₈' and 'Na₂₉Ag₂₆Sn₃₆' Models

The electronic structure calculations were performed on the structural model based on the single crystal data refinement with the TB-LMTO-ASA method (Tight Binding Linear Muffin Tin Orbital) using the LMTO program package of Andersen *et al.* [51]

The exchange-correlation term was calculated within the local density approximation (LDA) and was parametrized according to von Barth and Hedin [52]. The radii of the muffin-tin spheres were determined after Jepsen and Andersen [53]. The following valence functions were used for the basis set for the short-ranged atom-centered TB-LMTOs: *s* valence function for Na; *s-d* valence functions for Ag, and *s, p* valence functions for Sn. Na-3*p* and Sn-3*d* orbitals were treated using a down folding technique [78].

The calculations were performed for the two hypothetical, fully ordered models 'Na₂₉Ag₁₄Sn₄₈' and 'Na₂₉Ag₂₆Sn₃₆', where Ag₂ (defect position in the compound Na₂₉Ag₂₁Sn₃₉) is fully occupied and both *M4* and *M5* positions occupied by one sort of atoms (Table 3.9). Additionally, to simplify calculations split position *M4* (12*q* Wyckoff position in Na₂₉Ag₂₁Sn₃₉) was considered as fully occupied 6*k* position.

Crystal Structure

The phase $\text{Na}_{29}\text{Ag}_{12.3+x}\text{Sn}_{48-x}$ was for the first time obtained by Alexander Henze [79], with the composition $\text{Na}_{29}\text{Ag}_{17.8}\text{Sn}_{43}$, showing lower Ag content compared to the results, presented in this work. The cell parameters for the $\text{Na}_{29}\text{Ag}_{17.8}\text{Sn}_{43}$ were slightly smaller compared to the title compound: $a = 16.0532(4)$ and $c = 9.7362(4)$ Å (measured at 130 K). The main difference between the two compounds is the occupancy of the four atomic sites: $2e$, $12n$, $12o$, and $12q$. In contrast to the $\text{Na}_{29}\text{Ag}_{21}\text{Sn}_{39}$, according to the single crystal XRD data for the $\text{Na}_{29}\text{Ag}_{17.8}\text{Sn}_{43}$ the $12q$ position ($M4$ in $\text{Na}_{29}\text{Ag}_{21}\text{Sn}_{39}$, Ag:Sn ratio of 0.18:0.32) is occupied only by the tin atoms. Instead, $12o$ ($M5$ in $\text{Na}_{29}\text{Ag}_{21}\text{Sn}_{39}$, Ag:Sn ratio of 0.60:0.40) and $2e$ (Ag1 in $\text{Na}_{29}\text{Ag}_{21}\text{Sn}_{39}$, fully occupied) positions are occupied by the atoms of the Sn/Ag statistical mixture with the Sn:Ag ratio of 0.56:0.44 and 0.60:0.40, respectively. The $12n$ position (Ag2 in $\text{Na}_{29}\text{Ag}_{21}\text{Sn}_{39}$, 85.9 % Ag) is defect as well with occupancy of the silver atoms of 0.90.

It is a common problem for the compounds containing Ag and Sn to crystallographically distinguish between both elements (electronically similar: only four electrons difference) while interpreting data obtained as a result of X-ray diffraction experiments. As it was mentioned, positions of tin atoms with the lack of electron density could be interpreted as defect (partially occupied by Sn atoms) or disordered (forming statistical mixture of Sn/Ag). The choice between these two options would significantly affect the refined composition while the quality of the refinement (R values) would stay the same. To decide which interpretation of the structure is the right one, the analysis of the interatomic distances was helpful. Because homoatomic Sn-Sn distances are on average longer than typical heteroatomic Sn-Ag (in β -Sn: $d_{\text{Sn-Sn}} = 3.115\text{-}3.350$ Å [80]; in Ag_3Sn : $d_{\text{Sn-Ag}} = 2.949\text{-}3.016$ Å [81]). Indeed, M -Sn (M = atoms of Sn/Ag statistical mixture) distances were on average shorter than Sn-Sn, which means that formation of the statistical mixture is more favorable than leaving vacancies in Sn positions.

To make a conclusive statement about the structure and composition of the crystal additional data is needed. The results of EDX analysis are filling this gap. In case of $\text{Na}_{29}\text{Ag}_{17.8}\text{Sn}_{43}$ [79], EDX analysis had a qualitative character: the presence of all three elements was confirmed, not the Ag:Sn ratio. Apart from that, comparing two refinements ($\text{Na}_{29}\text{Ag}_{21}\text{Sn}_{39}$ and $\text{Na}_{29}\text{Ag}_{17.8}\text{Sn}_{43}$ [79]), significantly better R values were obtained in the present work.

$\text{Na}_{29}\text{Ag}_{21}\text{Sn}_{39}$ is the first compound in the system Na-Ag-Sn. It crystallizes in its own structure type with the hexagonal space group $P6/mmm$ and lattice parameters of $a = 16.1231(9)$ and $c = 9.7387(6)$ Å. The structure of this compound features a polyanionic network of interconnected clusters units: empty $\{M_4\text{Sn}_8\}$ icosahedra ($M = \text{statistical Sn/Ag mixture}$); Na^+ -centered $\{M_6\text{Ag}_{14}\}$ clusters and $\{\text{Sn}_3\}$ triangles in a ratio 3:1:2 (Figure 3.7).

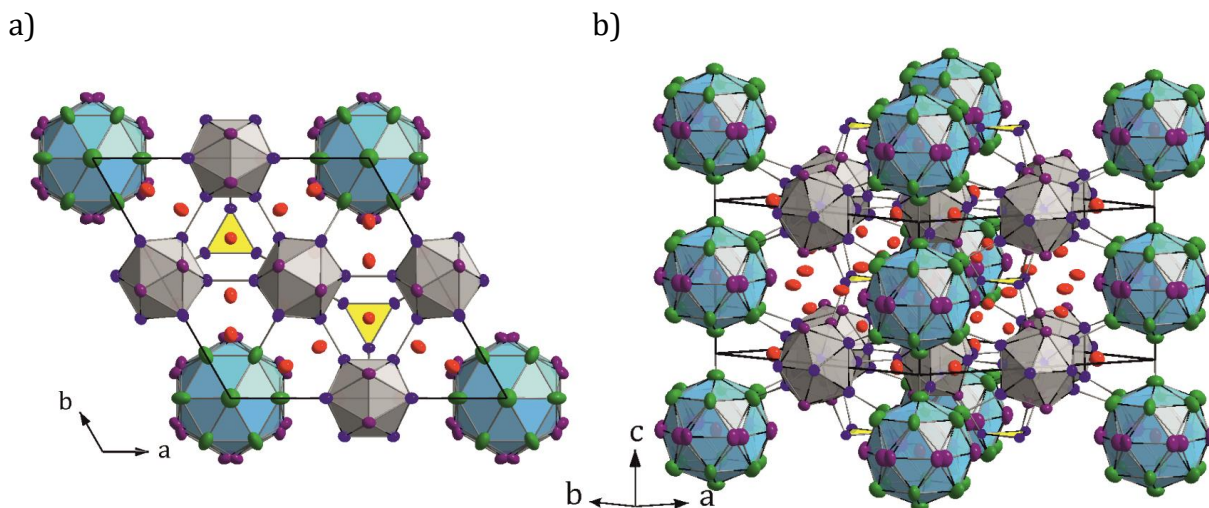


Figure 3.7 The view along $[001]$ direction of the unit cell of the $\text{Na}_{29}\text{Ag}_{21}\text{Sn}_{39}$ (a) and its structural fragment (b). The Na, Ag, Sn, and Sn/Ag atoms are shown in red, green, blue and violet, respectively. The displacement ellipsoids are drawn at a 90 % probability level.

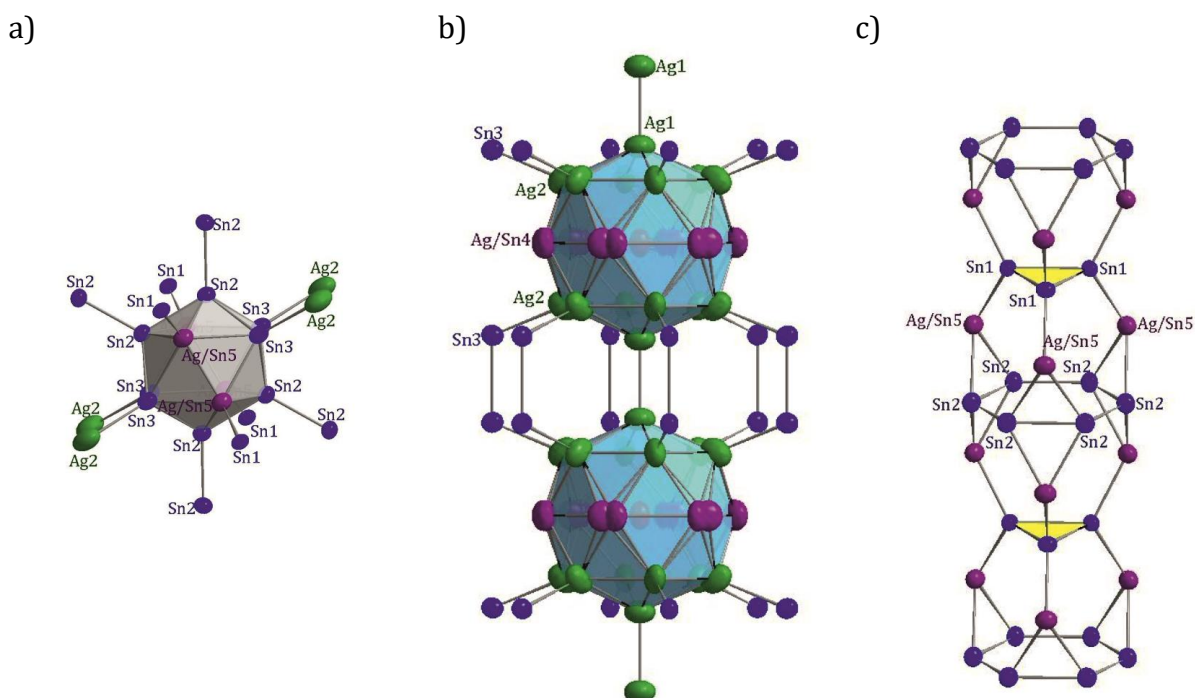


Figure 3.8 Structural fragments of $\text{Na}_{29}\text{Ag}_{21}\text{Sn}_{39}$: empty $\{M_4\text{Sn}_8\}$ icosahedron with 12 exobonds (a); strings of Na-centered $\{M_6\text{Ag}_{14}\}$ polyhedra (b); strings of stacked slightly distorted Friauf polyhedra formed by $\{\text{Sn}_3\}$ triangles and triangular faces of neighboring icosahedra (c). The Na, Ag, Sn, and Sn/Ag atoms are shown in red, green, blue and violet, respectively. The displacement ellipsoids are drawn at a 90 % probability level.

The $\{M_4Sn_8\}$ icosahedra (Figure 3.8, a) are build up by eight Sn atoms (in $12p$ and $12n$ positions) and four atoms of the statistical mixture $M5$ (position $12o$) with Sn to Ag ratio 0.60:0.40(5). The Sn-Sn interatomic distances in icosahedra are between $d_{Sn2-Sn2} = 2.866 \text{ \AA}$, showing covalent interaction along with metallicity (high coordination numbers), and $d_{Sn3-Sn3} = 3.112 \text{ \AA}$, which is on average longer than Sn-Sn distances α -Sn (2.353 \AA [80]) and shorter than in β -Sn (3.115 and 3.350 \AA [80]). The interatomic distance between atoms of the statistical mixture ($M5$) in the icosahedra are $d_{M5-M5} = 2.849 \text{ \AA}$, which is shorter than Sn/Ag-Sn distances ($d_{M5-Sn2} = 2.949$ and $d_{M5-Sn3} = 2.999 \text{ \AA}$). It is in good agreement with the Ag-Sn distances in the only binary compound in Ag-Sn system – Ag_3Sn (2.949 - 3.016 \AA [81]).

Each of the twelve atoms in icosahedron forms a covalent exo-bond to the neighboring Sn or Ag atom which results in a complex network: Sn2-Sn2 bonds with length of 2.773 \AA that connect icosahedra in Kagome net that form layers in ab -plane; four Sn3-Ag2 bonds ($d_{Sn3-Ag2} = 2.896 \text{ \AA}$) connect icosahedra to $\{M_6Ag_{14}\}$ clusters; atoms of statistical $M5$ mixture form another four bonds with Sn1 atoms ($d_{M5-Sn1} = 2.850 \text{ \AA}$) and connect icosahedra to $\{Sn_3\}$ triangles. Both $\{M_6Ag_{14}\}$ clusters and $\{Sn_3\}$ triangles are located between the layers of the Kagome net and occupy in the hexagonal and triangular channels, respectively.

In $\{M_6Ag_{14}\}$ clusters (Figure 3.8, b) twelve Ag2 atoms in a partially occupied (85.9 %) position form a hexagonal prism with Ag2-Ag2 distances of 2.883 \AA and height of 4.512 \AA , rectangular faces of which are centered by $M4$ atoms and hexagonal – by Ag1 atoms. $M4$ position is splitted, leading to a $12q$ Wyckoff position with an overall occupancy of 50% with 0.18:0.32 ratio of Sn to Ag (the distance between the two split positions is 0.491 \AA). It leads to $M4$ -Ag2 distances to be between 2.725 and 2.974 \AA . For another mixed $M6$ position the ratio of Sn to Ag is 0.11:0.89. $M6$ - $M6$ exo-bonds interconnect $\{M_6Ag_{14}\}$ clusters, which results in forming two-dimensional strings along c -direction. The $\{M_6Ag_{14}\}$ cluster, which has never been described before, is closely related to the 18-atom clusters – ‘drums’ – found in $Na_8K_{23}Cd_{12}In_{48}$ [38] and $Na_{30.5}Ag_{6.4}Ga_{53.6}$ [82], where hexagonal faces of the prism are not centered, consequently, the ‘drums’ are not interconnected.

The $\{Sn_3\}$ triangles (Figure 3.8, c) occupy the smaller, trigonal, voids of the Kagome nets neighboring with six icosahedra each connected via a Sn1- $M5$ bond to the $\{Sn_3\}$ triangle. This results in the formation of strings of stacked slightly distorted Friauf polyhedra in c -direction which share alternately the $\{Sn_3\}$ -fragment and the hexagonal ring build by Sn2 atoms of the

icosahedron. These Friauf polyhedra are all centered by a Na₄ atoms. The Sn1-Sn1 distance in the Sn₃ triangle is 2.986 Å, which is also shorter than the Sn-Sn distances in in β-Sn.

The polyanionic substructure of Na₂₉Ag₂₁Sn₃₉ can be described as a hierarchical relative of the CaCu₅ structure type in which specific atoms are replaced by certain cluster units. One layer (at $z = 1/2$) is Kagome net formed by {M₄Sn₈} icosahedra that take Cu₂ position in CaCu₅ structure; another layer (at $z = 0$) with {M₆Ag₁₄} cluster and {Sn₃} fragments taking Ca and Cu₁ positions in CaCu₅, respectively (Figure 3.9). The Kagome nets are stacked according to the primitive sequence AA along the *c*-axis.

The cationic partial structure of Na₂₉Ag₂₁Sn₃₉ (Figure 3.10) consists of a {Na₂₀} cage with the Na atoms capping the triangular faces of the icosahedra, therefore, forming a dual polyhedron – pentagonal dodecahedron as well as a {Na₃₀} cluster with six hexagonal, 12 pentagonal and 12 triangular faces encapsulating the {M₆Ag₁₄} cluster. The {Na₃₀} clusters are stacked along the *c*-axis by sharing their hexagonal faces with each other while the pentagonal faces are shared with the {Na₂₀} cluster. The {Sn₃} triangle is encapsulated in a {Na₁₄} cage with six pentagonal and six triangular faces which are shared with the {Na₂₀} and {Na₃₀} respectively. This way a complete space-filling is achieved. Additionally, the Na₂ position is centering the {M₆Ag₁₄} cluster. Selected interatomic distances are summarized in Table 3.8, for more details see Table 6.1 (Appendix).

Table 3.8 Selected interatomic distances in the compound Na₂₉Ag₂₁Sn₃₉. For the details see Table 6.1 (Appendix).

Atom types			Distance range(Å)			Atom types			Distance range(Å)		
Sn	-Sn	2.7727(1)-3.1123(8)	Na	-Sn	3.2140(2)-3.4997(4)	Na	-M	3.1791(4)-3.4589(3)	Na	-Ag	3.4387(2)-3.8293(6)
Sn	-Ag	2.8957(1)	Na	-M	3.1791(4)-3.4589(3)	Na	-Ag	3.4387(2)-3.8293(6)	Na	-Na	3.4548(7)-3.8276(9)
Sn	-M	2.8500(7)-2.9987(8)	Na	-Ag	3.4387(2)-3.8293(6)	Na	-Na	3.4548(7)-3.8276(9)			
M	-M	2.8493(8)									
Ag	-M	2.7254(2)									
Ag	-Ag	2.8612(3)-3.1162(1)									

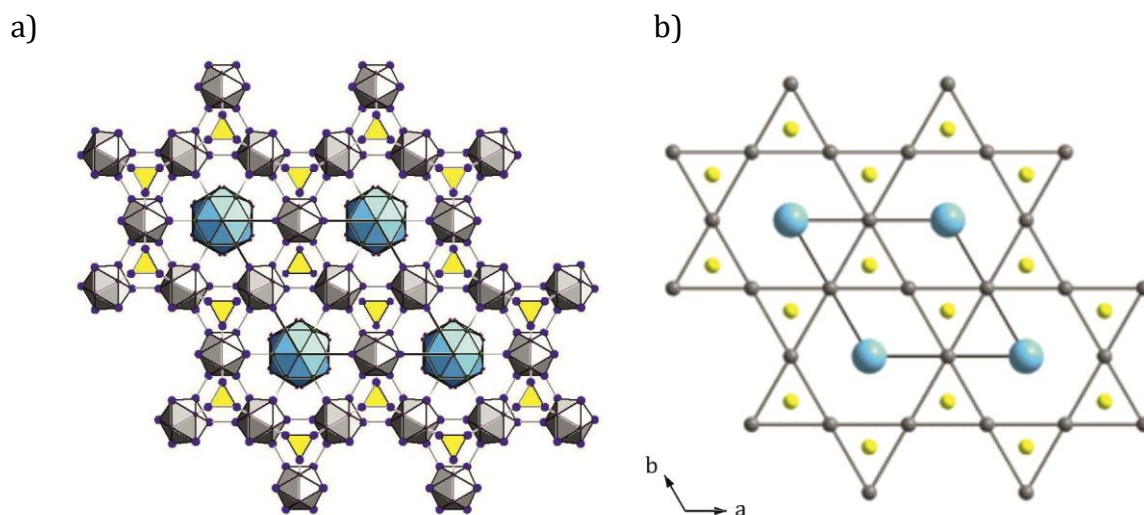


Figure 3.9 Relation of the $\text{Na}_{29}\text{Ag}_{21}\text{Sn}_{39}$ (a) compound to the CaCu_5 -structure type (b). Light blue – $M_8\text{Ag}_{12}$ polyhedra and Ca atoms in CaCu_5 , grey - $M_4\text{Sn}_8$ icosahedra in and Cu1 atoms, yellow - Sn_3 triangles and Cu2 atoms. The Na, Ag, Sn, and Sn/Ag atoms in the $\text{Na}_{29}\text{Ag}_{21}\text{Sn}_{39}$ are drawn in red, green, blue and violet, respectively.

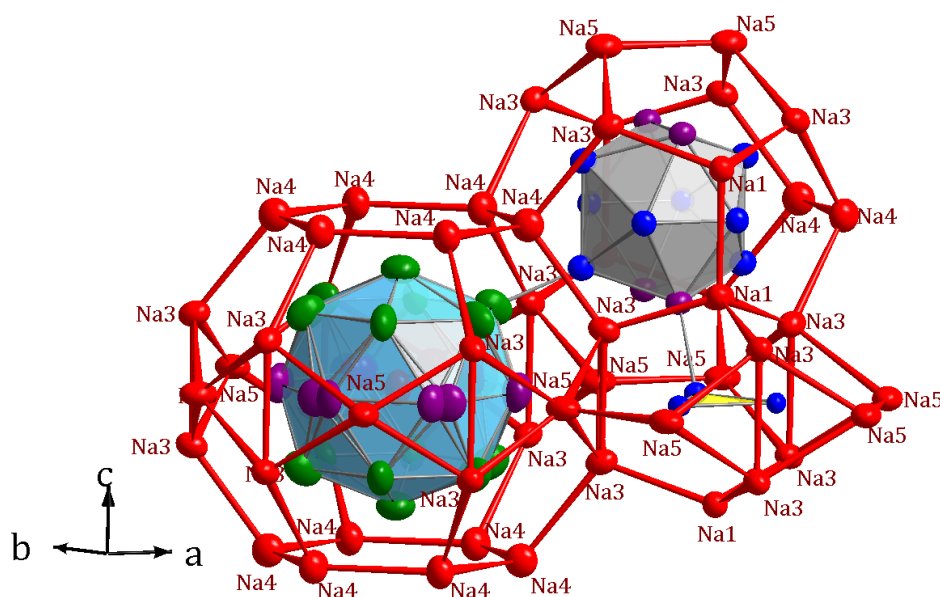


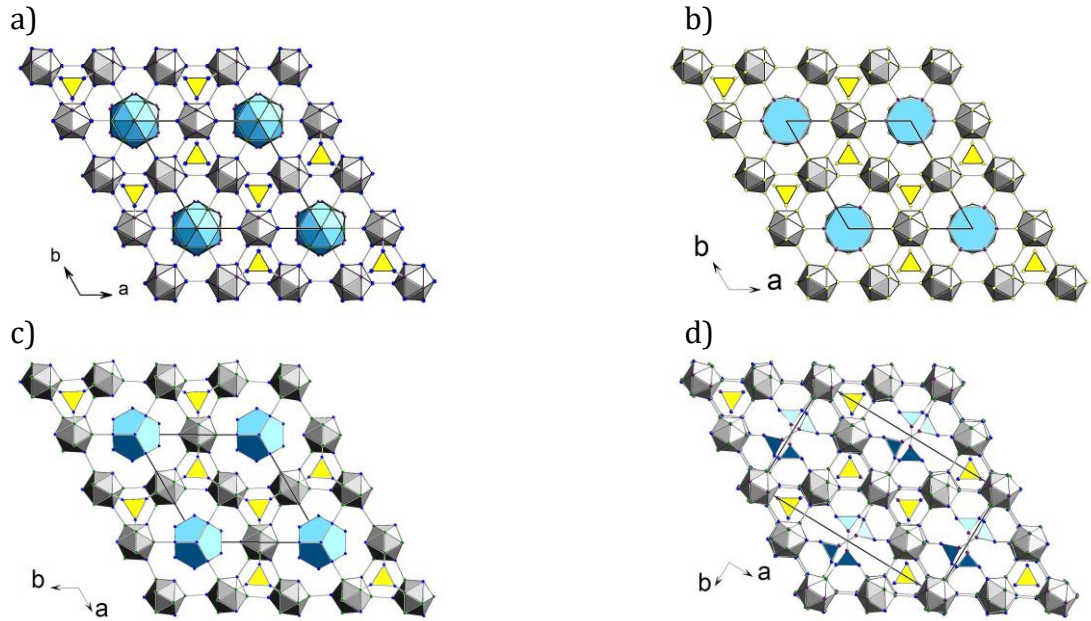
Figure 3.10 Cationic substructure of $\text{Na}_{29}\text{Ag}_{21}\text{Sn}_{39}$ around empty $\{M_4\text{Sn}_8\}$ icosahedron (gray), $\{\text{Na}@M_6\text{Ag}_{14}\}$ cluster (blue) and $\{\text{Sn}_3\}$ triangle (yellow). The Na, Ag, Sn, and Sn/Ag atoms are shown in red, yellow, blue and violet, respectively. The displacement ellipsoids are drawn at a 90 % probability level.

Formation of Kagome nets out of homo- or heteroatomic icosahedral fragments within a complicated network has been observed in a series of compounds group 13 and 14 elements, as it was mentioned earlier. Some of them are hierarchical variants of CaCu_5 structure type just like the title compound (Figure 3.11, a-d), with common features such as Kagome net formed by icosahedra and triangular fragments, but the polyhedra filling the hexagonal channels of the Kagome net can be quite different.

For example, in already mentioned isostructural compounds $\text{Na}_8\text{K}_{23}\text{Cd}_{12}\text{In}_{48}$ [38] and $\text{Na}_{30.5}\text{Ag}_{6.4}\text{Ga}_{53.6}$ [82] as well as in $\text{NaAu}_{0.18}\text{Ga}_{1.82}$ [83] the larger polyhedron (corresponds to Ca atoms in CaCu_5 -type) is a hexagonal prism with all the rectangular faces centered – so-called ‘drums’ (Figure 3.11, b), unlike enneahedra of Sn_{14} -atoms (Figure 3.11, c) in $\text{Na}_{29}\text{Zn}_{24}\text{Sn}_{32}$ [37]. In related compound $\text{Na}_{16}\text{Zn}_{13.54}\text{Sn}_{13.46}$ [75] the Ca position is taken by the interconnected triangles forming strings in [001] direction (Figure 3.11, c).

Among other icosahedral phases, the structures hierarchically related to Laves phase MgCu_2 -type exist, where Kagome nets of icosahedra are stacked along c -axis with the sequence ABC , as a result no hexagonal channels exist, but the ‘Friauf voids’. These voids are filled with different type of polyhedra like 15-atom spacer in $\text{Na}_{22}\text{Zn}_{20}\text{Sn}_{19}$ [75] (Figure 3.11, h), 16-atomic Frank-Kasper polyhedra in $\text{Na}_{36}\text{Ag}_7\text{Ga}_{73}$ [84] (Figure 3.11, i) or triicosahedra with different orientation in $\text{Na}_{34}\text{Zn}_{66}\text{Sn}_{38}$ [75], $\text{Na}_{17}\text{Zn}_{11.86}\text{Ga}_{38.18}$ [85] and $\text{Na}_{17}\text{Cu}_6\text{Ga}_{46.51}$ [86] (Figure 3.11, e-g).

CaCu₅-type of cluster packing



MgCu₂-type of cluster packing

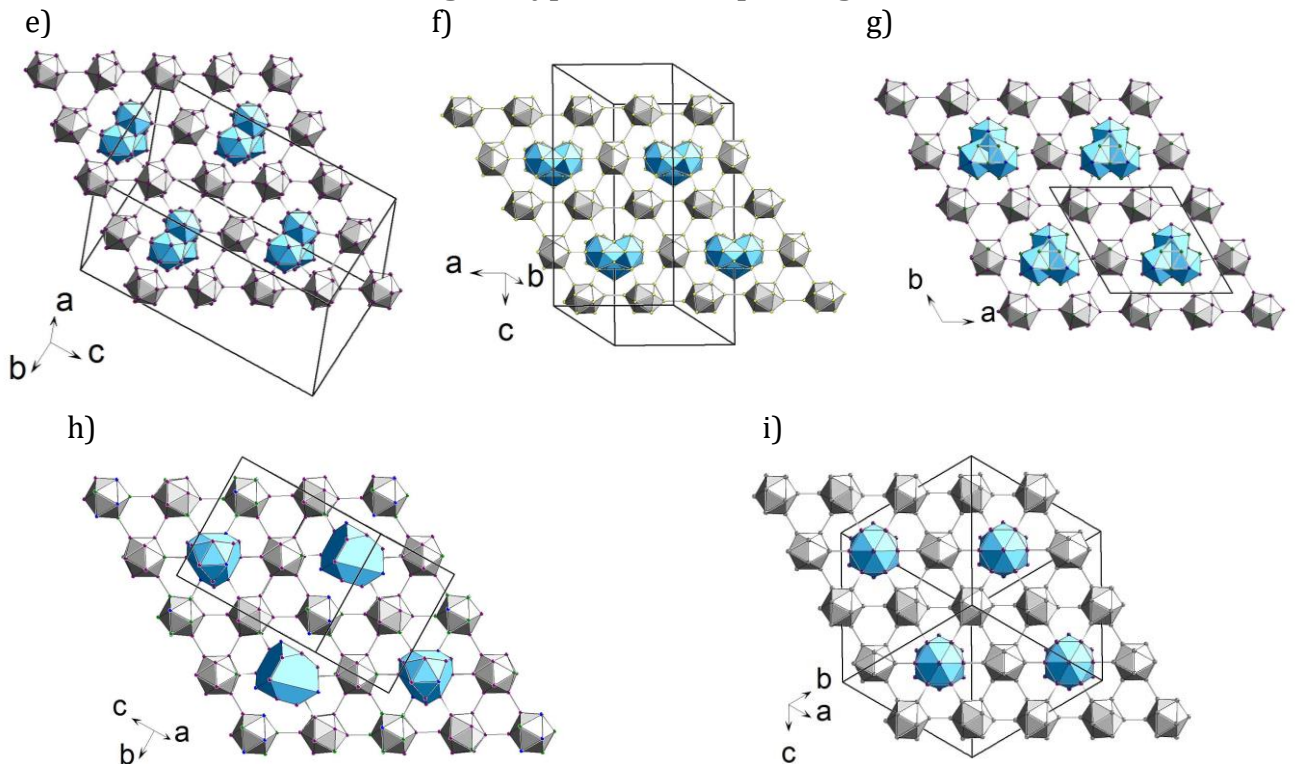


Figure 3.11 Comparison of structural motifs of the related to Na₂₉Ag₂₁Sn₃₉: compounds with Kagome nets out of icosahedral fragments. CaCu₅-type of cluster packing (compounds a-c) with different polyhedra filling hexagonal channels (Ca position in CaCu₅): {M₆Ag₁₄} polyhedra in Na₂₉Ag₂₁Sn₃₉'drums' (a) in Na₈K₂₃Cd₁₂In₄₈^[38], Na_{30.5}Ag_{6.4}Ga_{53.6}^[82] and NaAu_{0.18}Ga_{1.82}^[83] (b); Sn₁₄-eneahedra in Na₂₉Zn₂₄Sn₃₂^[37] (c); strings of interconnected triangles in Na₁₆Zn_{13.54}Sn_{13.46}^[75] (d). MgCu₂-type of cluster packing (compounds e-i) with different polyhedra filling hexagonal voids: 15-atom spacer in Na₂₂Zn₂₀Sn₁₉^[75] (h), 16-atomic Frank-Kasper polyhedra in Na₃₆Ag₇Ga₇₃^[84] (i) and triicosahedra clusters with different orientation in Na₁₇Zn_{11.86}Ga_{38.18}^[85] (e); Na₁₇Cu₆Ga_{46.51}^[86] (f) and Na₃₄Zn₆₆Sn₃₈^[75] (g). Alkali metal atoms are shown in red, transition metal – in green, tin atoms – in blue, atoms of the statistical mixtures – in violet, Ga and In – in yellow.

Electronic Situation in the Na₂₉Ag₂₁Sn₃₉

The mixed-occupied atomic positions in the {*M*₆Ag₁₄} cluster and {*M*₄Sn₈} icosahedra as well as the under occupancy of the Ag₂ position make it difficult to put reasonable formal charges using Wade's rule on the clusters, in the structure of Na₂₉Ag₂₁Sn₃₉. Problematic atomic positions in Na₂₉Ag₂₁Sn₃₉ are highlighted in Figure 3.12.

Therefore, for the investigation of the electronic structure of the disordered compound Na₂₉Ag₂₁Sn₃₉, the hypothetical, fully ordered models with no split in position *M*₄ (*6k* Wyckoff position was set for both models, in contrast to *12q* in Na₂₉Ag₂₁Sn₃₉), fully occupied Ag₂ position (*12n*, defect in Na₂₉Ag₂₁Sn₃₉) as well as assumption that atoms of only one type are occupying each site of the mixed *M*₄ and *M*₅ positions (*12q* and *12o*, respectively) were used, in hope to find an appropriate charge-balanced structural model (Table 3.9). These assumptions resulted in two possible models with the composition 'Na₂₉Ag₁₄Sn₄₈' and 'Na₂₉Ag₂₆Sn₃₆', the band structures and DOS for both were calculated and are shown in Figure 3.13 and Figure 3.14.

The low-lying bands between -12 and -4 eV predominantly correspond to the Sn 5*s* states. The main contribution to the DOS arises, as expected, from the Ag 4*d* orbitals, which are located between -6 and -1 eV and mix with the Sn-5*p* orbitals in all cases, indicating covalent contributions of the Ag-Sn interactions to the stabilization of the structure. There is no gap of the DOS located at the Fermi level or in its vicinity, meaning that the compound is metallic. The bands (generally Sn-*p*) cross the Fermi level underlying metallic character for both structural models.

The compound Na₂₉Ag₂₁Sn₃₉, contain 416e⁻ per formula unit (1×29+11×21+39×4), shown as a dashed violet line in Figure 3.14 and Figure 3.14, lies in the local minimum (model 2), indicating that deviation from the ordered composition by increasing Ag content is beneficial for the system.

Table 3.9 Comparison of the compound Na₂₉Ag₂₁Sn₃₉ with defect silver atoms (position Ag₂) and two positions with Sn/Ag statistical mixture (*M*₄ and *M*₅) and two hypothetical fully ordered models: 'Na₂₉Ag₁₄Sn₄₈' and 'Na₂₉Ag₂₆Sn₃₆'.

Na ₂₉ Ag ₂₁ Sn ₃₉				'Na ₂₉ Ag ₁₄ Sn ₄₈ '		'Na ₂₉ Ag ₂₆ Sn ₃₆ '	
Wyck.	Atom	S.O.F.	Wyck.	Atom	S.O.F.	Atom	S.O.F.
<i>12q</i>	<i>M</i> ₄	0.18/0.32(5)	<i>6k</i>	Sn ₄	1	Sn ₄	1
<i>12o</i>	<i>M</i> ₅	0.60/0.40(5)	<i>12o</i>	Sn ₅	1	Ag ₅	1
<i>12n</i>	Ag ₂	0.859(4)	<i>12n</i>	Ag ₂	1	Ag ₂	1

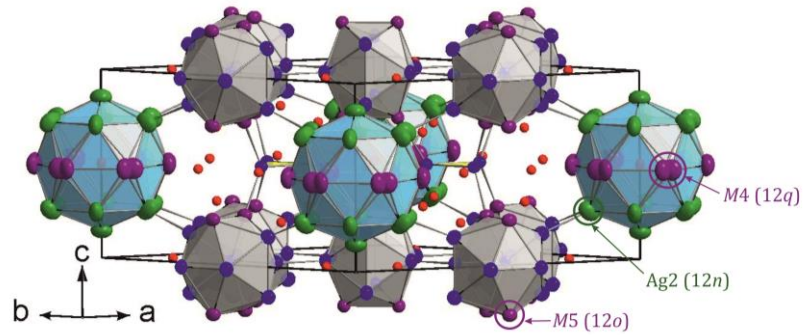


Figure 3.12 Atomic positions $M4$, $M5$ and $Ag2$ in the structure of the compound $Na_{29}Ag_{21}Sn_{39}$. The Na, Ag, Sn, and Sn/Ag atoms are shown in red, yellow, blue and violet, respectively.

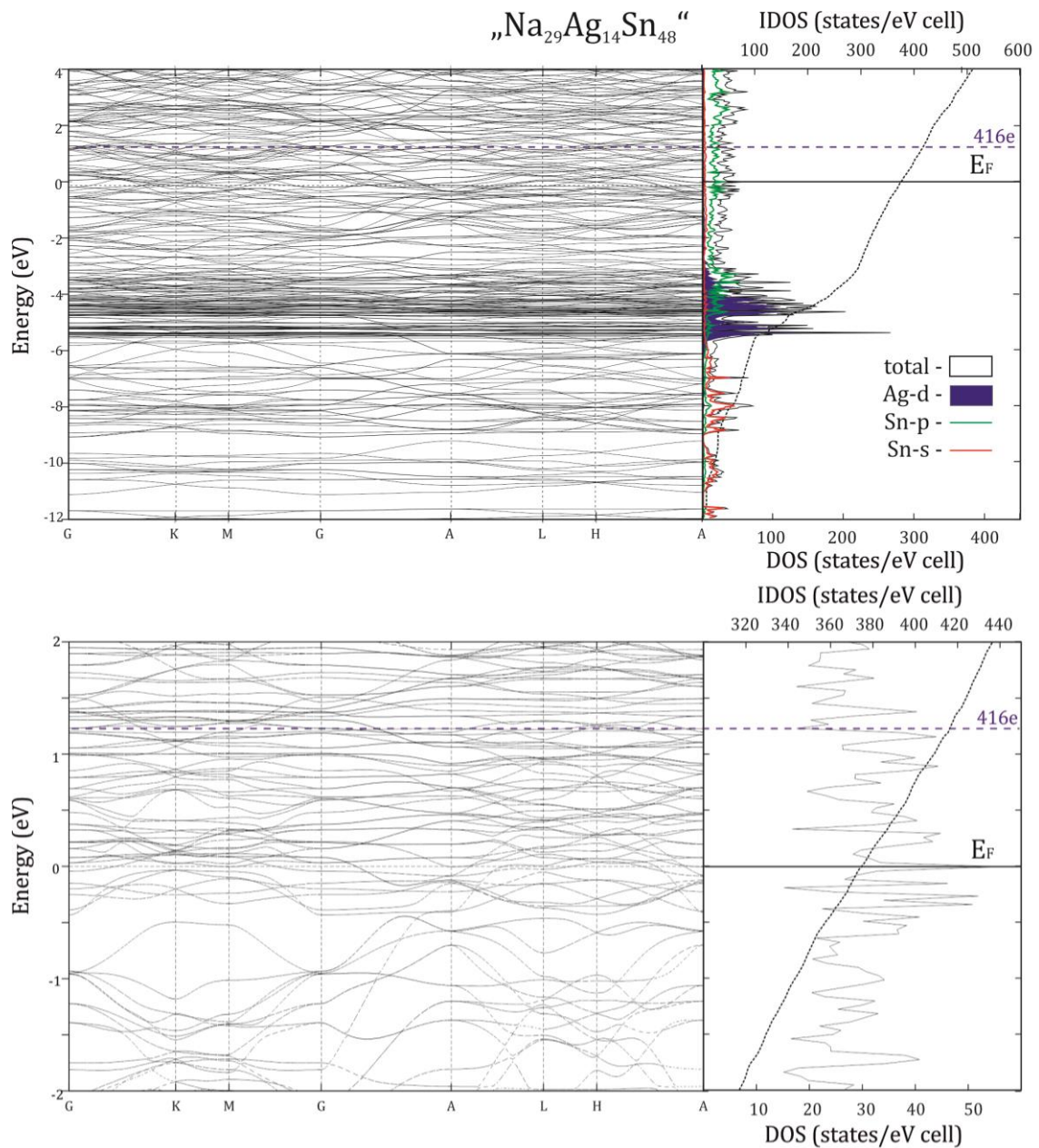


Figure 3.13 The band structure as well as the total Density of States (DOS) with orbital projected DOS calculated for the hypothetical, fully ordered model ' $Na_{29}Ag_{14}Sn_{48}$ ' (positions $12q$, $12o$ are occupied by Sn-atoms).

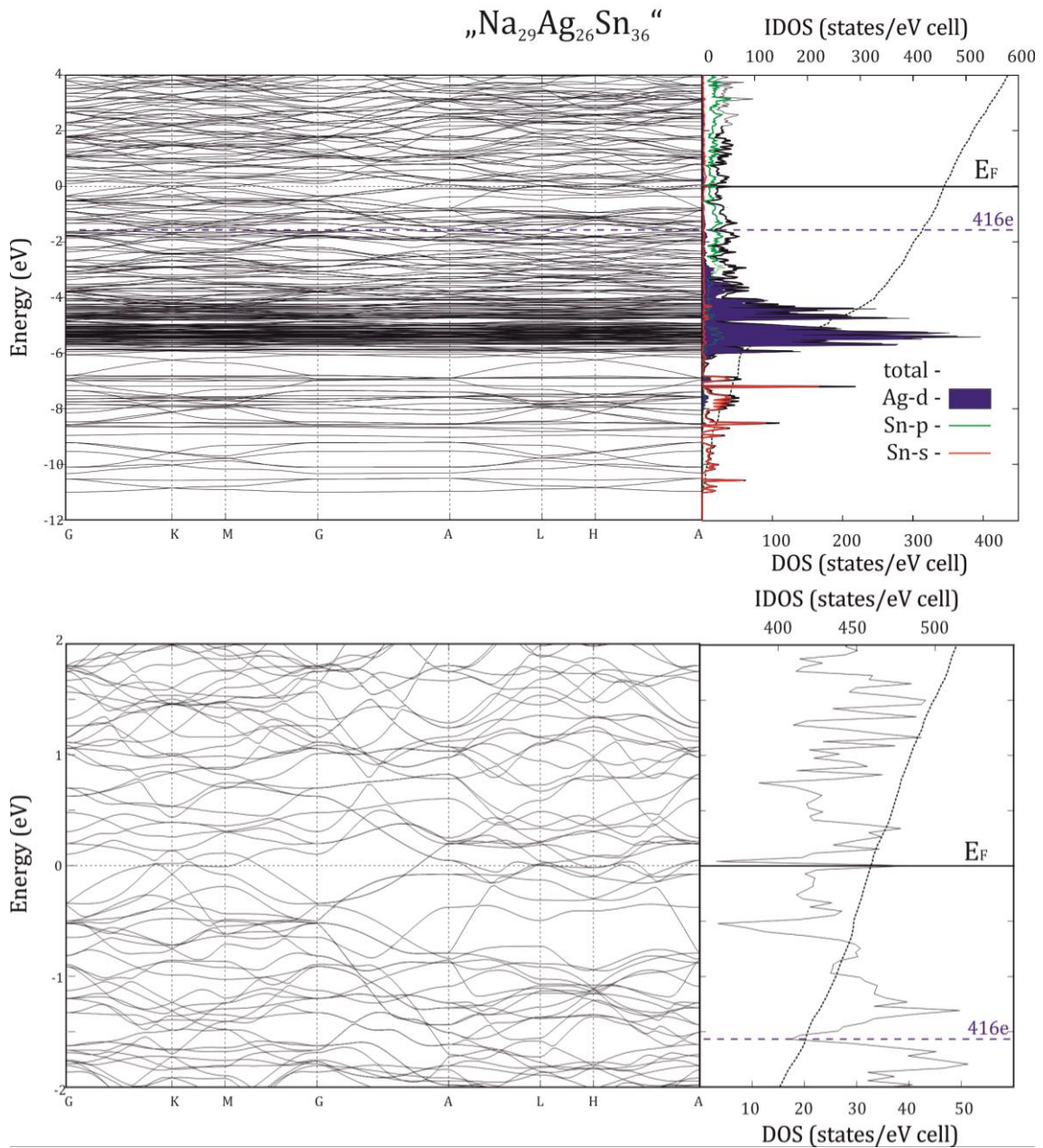


Figure 3.14 The band structures as well as the total Density of States (DOS) with orbital projected DOS calculated for the hypothetical, fully ordered model 'Na₂₉Ag₂₆Sn₃₆' (positions 12*q*, 12*o* are occupied by Sn and Ag-atoms, respectively).

Discussion

The title and related to it compounds with Kagome nets of interconnected icosahedra can be chemically considered as alkali-metal filled but structurally destroyed Hume-Rothery phases. However, like in pure Hume-Rothery phases constituted from 13-14-group element and 10-12-group metal, the valence electron concentration (VEC) per network atom in corresponding 'alkali-metal-filled' intermetallic compounds with covalently interconnected or condensed homo- and heteroatomic cluster networks play an important role in the structural stability.

The VEC per atom of anionic network of 3.43 for $\text{Na}_{29}\text{Ag}_{21}\text{Sn}_{39}$ fits nicely between other Sn or Ga-based compounds with CaCu_5 -type of cluster packing: compounds with 'drums' in hexagonal channels of Kagome nets (VEC of 3.30 and 3.32 for $\text{Na}_{30.5}\text{Ag}_{6.4}\text{Ga}_{53.6}$ and both $\text{Na}_8\text{K}_{23}\text{Cd}_{12}\text{In}_{48}$ and $\text{NaAu}_{0.18}\text{Ga}_{1.82}$) and $\text{Na}_{29}\text{Zn}_{24}\text{Sn}_{32}$ containing Sn_{14} -enneahedra in hexagonal channels with VEC of 3.66, the highest for this group of compounds (Table 3.10, Figure 3.15). It was shown that the linking of icosahedral units within structures is dependent on the number of valence electrons. In very reduced phases with high VECs and equal to the Wade polyhedral electron demand for naked clusters, on the other hand, phases with low VECs tend to form condensed clusters [87]. A good illustration of that principle are phases with oligomeric units, which are realized in twinned or triply fused icosahedra like in $\text{Na}_{34}\text{Zn}_{66}\text{Sn}_{38}$, $\text{Na}_{17}\text{Zn}_{11.86}\text{Ga}_{38.18}$, and $\text{Na}_{17}\text{Cu}_6\text{Ga}_{46.51}$ with the valence electron concentration (VEC) of 3.06 for Sn-based and 3.10 for both Ga-based phases.

Table 3.10 Phases with Kagome nets of icosahedral fragments, related to $\text{Na}_{29}\text{Ag}_{21}\text{Sn}_{39}$, and their VEC per atom of anionic network.

Compound	VEC/M	Polyhedra filling voids	Friauf	Type of cluster packing
$\text{Na}_{34}\text{Zn}_{66}\text{Sn}_{38}$	3.06			
$\text{Na}_{17}\text{Zn}_{11.86}\text{Ga}_{38.18}$	3.10	Triicosahedra		MgCu_2 -type
$\text{Na}_{17}\text{Cu}_6\text{Ga}_{46.51}$	3.10			
$\text{Na}_{30.5}\text{Ag}_{6.4}\text{Ga}_{53.6}$	3.30			
$\text{Na}_8\text{K}_{23}\text{Cd}_{12}\text{In}_{48}$	3.32	'drums'		CaCu_5 -type
$\text{NaAu}_{0.18}\text{Ga}_{1.82}$	3.32			
$\text{Na}_{36}\text{Ag}_7\text{Ga}_{73}$	3.28	16-atomic polyhedra	Frank-Kasper	MgCu_2 -type
$\text{Na}_{29}\text{Ag}_{21}\text{Sn}_{39}$	3.43	20-atom polyhedra		CaCu_5 -type
$\text{Na}_{22}\text{Zn}_{20}\text{Sn}_{19}$	3.54	15-vertex spacers		MgCu_2 -type
$\text{Na}_{16}\text{Zn}_{13.54}\text{Sn}_{13.46}$	3.59	strings of interconnected triangles		MgCu_2 -type
$\text{Na}_{29}\text{Zn}_{24}\text{Sn}_{32}$	3.66	Sn_{14} -enneahedra		CaCu_5 -type

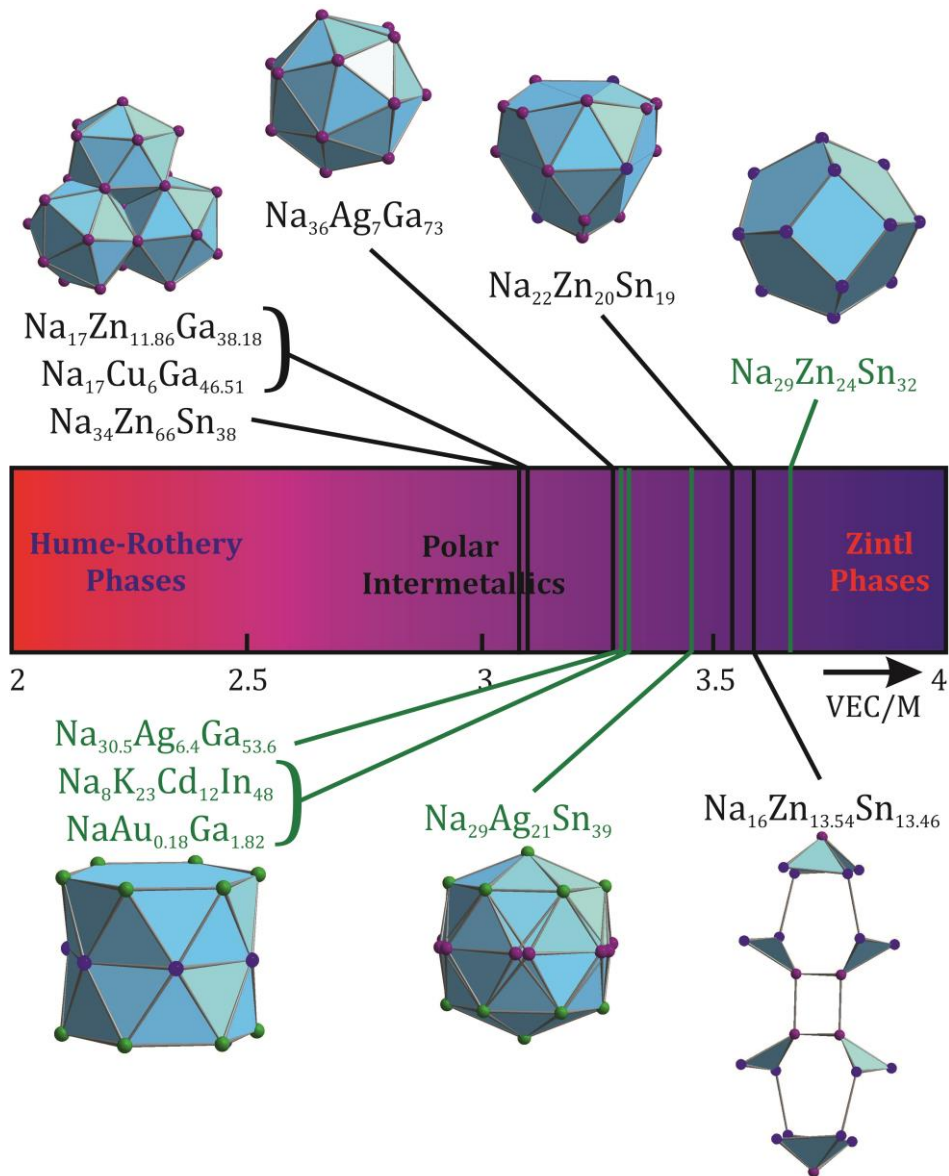


Figure 3.15 Position of the related to $\text{Na}_{29}\text{Ag}_{21}\text{Sn}_{39}$ compounds with Kagome nets out of icosahedral fragments relative to their VEC per atom of anionic network (M). The different polyhedra filling 'Friauf voids' (correspond to Mg position of MgCu_2 -type) and hexagonal channels (correspond to Ca position of CaCu_5 -type) are shown in black and green, respectively. For the details, see Table 3.10.

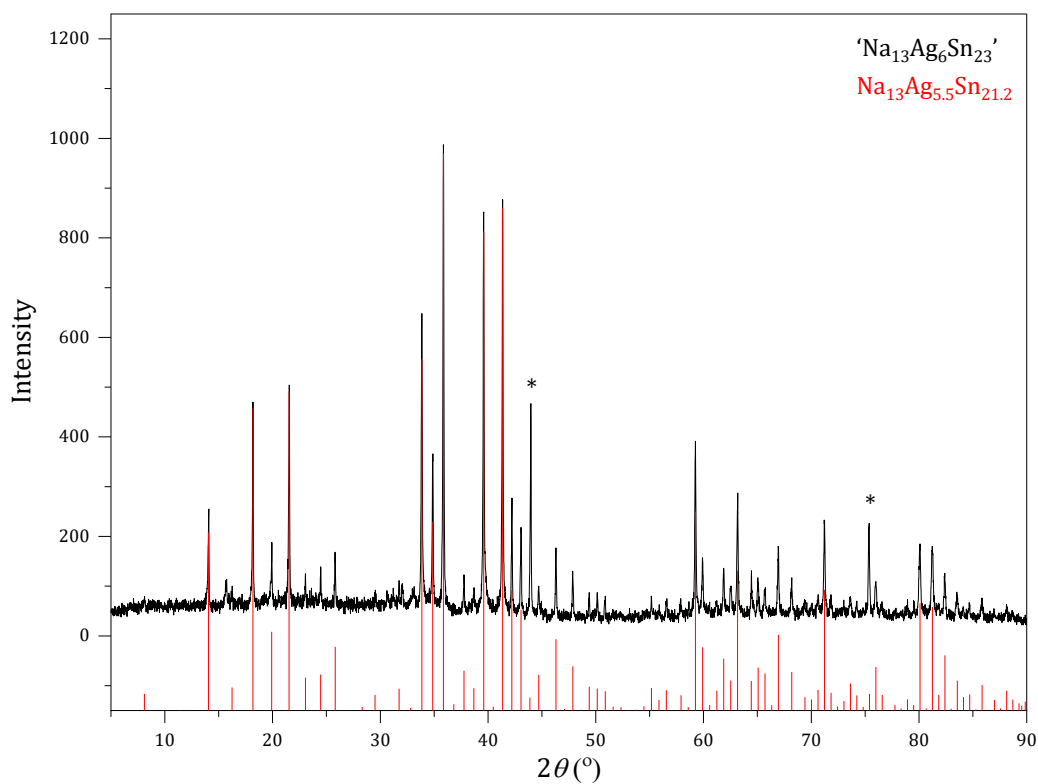
3.1.2.2 Na₁₃Ag_{5.5}Sn_{21.2} and Na_{230.45}Ag₂₇₄Sn₁₃₆ – Two Compounds Featuring Endohedral Fullerane Clusters

Synthesis and Characterization

Two ternary samples with Na:Ag:Sn ratio of 13:6:23 and 5:1:1 were obtained from the elements, preparing first a binary precursor from 88.0 mg Ag and 371.3 mg Sn for 'Ag₆Sn₂₃'; 197.9 mg Ag and 217.8 mg Sn for 'AgSn' as it was described oben and were temperature treated together with 40.6 mg of Na for 'Na₁₃Ag₆Sn₂₃'; 8.43 mg Na for 'Na₅AgSn' in niobium ampoule under the following program: heating up to 800°C with the rate of 4°C/min, holding the temperature for 12 hours; slowly cooling with rate of 0.1°C/min to 450°C and dwelling the sample for 64 hours and finally cooling with 1°C/min to room temperature. Obtained products were lustrous silver powders, sensitive to air and moisture. The first sample, 'Na₁₃Ag₆Sn₂₃', according to the PXRD analysis (Figure 3.16, a) contained almost phase pure new cubic compound with the cell parameter $a = 15.531(4) \text{ \AA}$ (obtained from indexing the powder diffractogram). The second sample, 'Na₅AgSn', contained two phases: new orthorhombic ternary compound and binary Na₉Sn₄ (Figure 3.16, b). Theoretical patterns for both compounds were obtained from the results of the single crystal X-ray diffraction, described below).

The single crystals, shiny and block-shaped (in case of the second sample having light blue luster) showed in addition to extreme air- light sensitivity, decomposing within a couple of hours under the microscope. To prevent the sample 'Na₅AgSn' from decomposing it was stored in the glass container packed in aluminum foil in the glovebox. Another challenge for the full structural characterization was the poor quality of the crystals from the sample 'Na₅AgSn'. To fix this problem tin-flux method for the crystal growth was applied, as it was described in the Chapter 2.1.2.3 Flux Synthesis. For this 0.426 mg of the sample 'Na₅AgSn' was finely grounded and pressed in a pallet. Together with almost fivefold excess (2.15 g) of tin, used as a flux, the pallet was loaded in Ta container and sealed in steel ampoule, which was hold at 350°C for two weeks. After separation of the excess flux through centrifugation, the single crystals of the new orthorhombic phase could be found growing on the pallet.

a)



b)

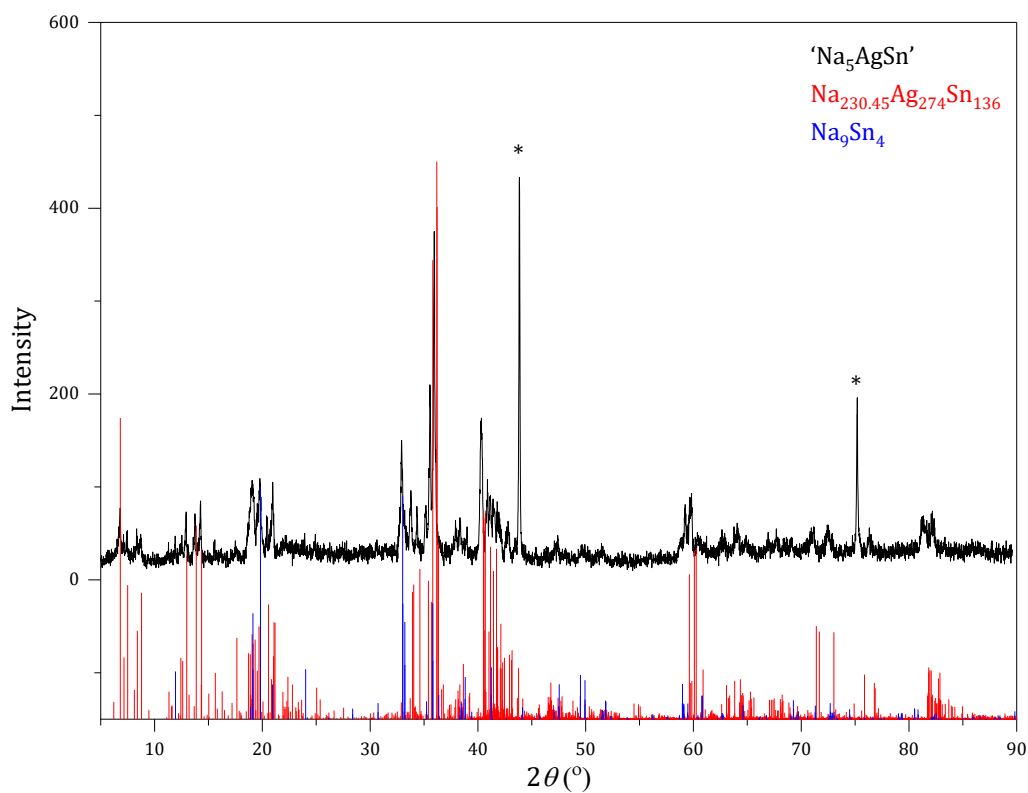


Figure 3.16 Experimental X-ray powder diffractograms: a) sample 'Na₁₃Ag₆Sn₂₃' (black) with the theoretical pattern (red) of Na₁₃Ag_{5.5(5)}Sn_{21.2(5)} b) sample 'Na₅AgSn' (black) with the theoretical pattern of Na_{230.45(4)}Ag₂₇₄₍₃₎Sn₁₃₆₍₃₎ (red) and additional phase Na₉Sn₄ (blue). Diamond (*) was used as internal standard.

Indexing the data, obtained from the measurement led to the cubic space group $Im\bar{3}$ for the first compound and orthorhombic $Immm$ for the second one. Corrections of the raw data for background, polarization, and Lorentz effects were applied. Due to a Gaussian-shaped primary X-ray beam profile a scaling procedure within LANA was applied along with the numerical absorption correction using X-Red and X-Shape software [43-44]. The starting atomic parameters for $Na_{13}Ag_{5.5}Sn_{21.2}$ and $Na_{230.45}Ag_{274}Sn_{136}$ were obtained by Direct Method with the SHELXS-2014[45]. The structures were refined using SHELXL-2014 (full-matrix least-squares on F_o^2) [77] with anisotropic atomic displacement parameters for all atoms. In order to check the composition, the occupancy parameters were refined in separate least-squares cycles. Results of the refinement, atomic coordinated and displacement parameters are presented in Table 3.11, Table 3.12, and Table 3.13, respectively.

Table 3.11 Crystallographic data and selected details of structure refinement for the compounds $Na_{13}Ag_{5.5(5)}Sn_{21.2(5)}$ and $Na_{230.45(4)}Ag_{274(3)}Sn_{136(3)}$.

Formula	$Na_{13}Ag_{5.5(5)}Sn_{21.2(5)}$	$Na_{230.45(4)}Ag_{274(3)}Sn_{136(3)}$
Formula weight (g·mol ⁻¹)	3408.807	50988.64
Space group	$Im\bar{3}$ (no. 204)	$Immm$ (no. 71)
<i>Z</i>	4	1
Unit cell parameters (Å)	<i>a</i> = 15.495(1)	<i>a</i> = 15.1995(2) <i>b</i> = 24.7063(3) <i>c</i> = 40.2152(6)
Volume (Å ³)	3720.4(9)	15101.7(4)
<i>D</i> _{calcd.} (g·cm ⁻³)	6.079	5.608
Abs. Coeff. (mm ⁻¹)	16.893	14.331
<i>F</i> (000) (e)	5840	22202
Crystal shape/color	block/silver	block/silver
Temperature (K)	150	150
θ range (deg)	1.859–29.954	2.850–30.000
Range in <i>hkl</i>	±21 ±21 ±21	–21 ÷ 18 ±34 ±56
Reflections collected	35517 (<i>R</i> ₆ = 0.0189)	185270 (<i>R</i> ₆ = 0.0322)
Unique reflections	1007 (<i>R</i> _{int} = 0.0589)	11774 (<i>R</i> _{int} = 0.0687)
Data / parameter	1007/43	8259/488
GOF on <i>F</i> ²	0.931	0.895
<i>R</i> ₁ , <i>wR</i> ₂ (<i>I</i> > 2 σ (<i>I</i>))	0.0175, 0.0244	0.0287, 0.0426
<i>R</i> ₁ , <i>wR</i> ₂ (all data)	0.0296, 0.0260	0.0561, 0.0470
Largest diff. peak/hole (e Å ⁻³)	0.873 and -0.917	3.655 and -1.401

Table 3.12 Atom coordinates and equivalent isotropic displacement parameters (\AA^2) for the compounds $\text{Na}_{13}\text{Ag}_{5.5(5)}\text{Sn}_{21.2(5)}$ and $\text{Na}_{230.45(4)}\text{Ag}_{274(3)}\text{Sn}_{136(3)}$; M = Sn/Ag statistical mixture, N = Ag/Na statistical mixture.

Atom	Wyck.	S.O.F.	x	y	z	U_{eq}
$\text{Na}_{13}\text{Ag}_{5.5(5)}\text{Sn}_{21.2(5)}$						
Sn1	24g	1	0.15325(2)	0	0.09399(2)	0.0133(1)
M2	48h	0.86/0.14(3)	0.30959(2)	0.09406(2)	0.34421(2)	0.01700(8)
M3	24g	0.81/0.19(3)	0.30971(2)	0	0.18158(2)	0.0188(1)
Ag4	12e	0.886(3)	0.40360(4)	0	1/2	0.0204(2)
Na1	12e	1	0.19786(2)	0	1/2	0.0190(5)
Na2	16f	1	0.18842(8)	0.18842(8)	0.18842(8)	0.0198(5)
Na3	24g	1	0.30576(2)	0.11608(1)	0	0.0208(4)
$\text{Na}_{230.45(4)}\text{Ag}_{274(3)}\text{Sn}_{136(3)}$						
Sn1	4i	1	0	1/2	0.11980(2)	0.00685(1)
Sn2	8i	1	0	0.21025(2)	0.22947(2)	0.00969(1)
Sn3	4i	1	1/2	0.38066(3)	0	0.00651(1)
Sn4	8i	1	0.19046(4)	0.11603(2)	0	0.00906(1)
Sn5	16i	1	0.81058(2)	0.31010(2)	0.31078(2)	0.00679(6)
Sn6	8i	1	1/2	0.18843(2)	0.07154(2)	0.00650(9)
Sn7	4i	1	0	1/2	0.26571(2)	0.00947(1)
Sn8	16i	1	0.19080(3)	0.30741(2)	0.07297(2)	0.00907(7)
Sn9	8i	1	1/2	0.38197(2)	0.38171(2)	0.00677(9)
Sn10	8i	1	0.28331(4)	1/2	0.05946(2)	0.00894(1)
Sn11	8m	1	0.68934(3)	0	0.11538(2)	0.00679(9)
Sn12	16o	1	0.16215(2)	0.37058(2)	0.19173(2)	0.01032(7)
Ag1	4f	1	0.17746(6)	1/2	0	0.01009(2)
Ag2	16o	1	0.59452(3)	0.38271(2)	0.44145(2)	0.00979(8)
Ag3	16o	1	0.18825(3)	0.78623(2)	0.03612(2)	0.00909(7)
Ag4	8l	1	1/2	0.09498(2)	0.03603(2)	0.00749(1)
Ag5	16o	1	0.34458(3)	0.24949(2)	0.07231(2)	0.00877(7)
Ag6	8l	1	1/2	0.29122(2)	0.11054(2)	0.01050(1)
Ag7	16o	1	0.59570(3)	0.19100(2)	0.13132(2)	0.00804(7)
Ag8	8l	1	1/2	0.28664(2)	0.03623(2)	0.00775(1)
Ag9	8n	1	0.34688(4)	0.44111(2)	0	0.00762(1)
Ag10	16o	1	0.80924(3)	0.40479(2)	0.34594(2)	0.00776(7)
Ag11	8n	1	0.34486(4)	0.05909(2)	0	0.00718(1)
Ag12	16o	1	0.34590(3)	0.44054(2)	0.38255(2)	0.00789(7)
Ag13	8m	1	0.90443(4)	1/2	0.32353(2)	0.00855(1)
Ag14	8m	1	0.09312(4)	1/2	0.06115(2)	0.00918(1)
Ag15	16o	1	0.18994(3)	0.59693(2)	0.03708(2)	0.00976(8)
Ag16	8m	0.928(2)	0.70716(4)	1/2	0.32118(2)	0.00953(2)
Ag17	8l	0.613(3)	0	0.30870(4)	0.19184(2)	0.0093(3)
Ag18	4g	0.839(5)	1/2	0.44072(4)	1/2	0.0129(3)
Ag19	8l	0.256(4)	0	0.90446(1)	0.24267(6)	0.0143(8)
Ag20	8l	0.195(5)	0	0.1052(2)	0.26677(2)	0.050(2)
Ag21	2b	0.764(6)	1/2	0	0	0.0053(5)
Ag22	8m	0.928(2)	0.89245(5)	0	0.23609(2)	0.01508(2)
Ag23	8m	0.073(2)	0.8358(8)	0	0.2629(3)	0.032(3)
Ag24	4i	0.073(2)	0	0	0.2223(4)	0.024(3)
Ag25	8m	0.069(4)	0.7987(8)	0	0.2833(3)	0.030(4)
Ag26	16o	0.292(7)	0.3276(2)	0.4190(3)	0.18495(2)	0.074(2)
Ag27	16o	0.141(7)	0.3479(1)	0.4279(4)	0.1955(3)	0.073(4)
Ag28	4i	0.116(5)	0	0	0.3077(2)	0.025(3)

M29	16o	0.387/0.613(3)	0.90290(3)	0.30811(2)	0.25087(2)	0.01242(8)
M30	8l	0.21/0.79(4)	1/2	0.28780(3)	0.34384(2)	0.0110(2)
M31	8l	0.56/0.44(4)	1/2	0.38690(2)	0.14557(2)	0.0156(2)
M32	8l	0.35/0.65(4)	0	0.40491(3)	0.22804(2)	0.0125(2)
M33	8m	0.14/0.86(4)	0.59494(4)	0	0.05803(2)	0.00800(2)
M34	16o	0.29/0.71(3)	0.09676(3)	0.30972(2)	0.13262(2)	0.01068(1)
M35	8l	0.38/0.62(4)	0	0.40469(2)	0.15565(2)	0.01057(2)
M36	16o	0.26/0.74(3)	0.65632(3)	0.24989(2)	0.30858(2)	0.01048(1)
N37	4g	0.259/0.741(6)	0	0.43714(9)	0	0.0135(8)
N38	8n	0.528/0.472(4)	0.10315(6)	0.31263(4)	0	0.0112(3)
N39	4i	0.073/0.928(2)	1/2	1/2	0.33930(1)	0.0328(1)
Na1	8l	1	0	0.37940(1)	0.30688(8)	0.0118(6)
Na2	8l	1	0	0.38103(1)	0.07544(8)	0.0139(7)
Na3	4i	1	1/2	1/2	0.42266(1)	0.0123(9)
Na4	8l	1	1/2	-0.07184(1)	0.11574(8)	0.0118(6)
Na5	16o	1	0.68686(2)	0.30617(9)	0.38039(6)	0.0121(4)
Na6	16o	1	0.18387(2)	0.42545(1)	0.11691(6)	0.0136(5)
Na7	8l	1	0	0.23699(1)	0.07701(8)	0.0121(6)
Na8	8n	1	0.3125(2)	0.31408(1)	0	0.0119(6)
Na9	8l	1	0	0.23581(1)	0.31048(8)	0.0144(6)
Na10	8m	1	0.1946(2)	0	0.04341(8)	0.0124(6)
Na11	16o	1	0.38259(2)	0.61970(9)	0.07201(6)	0.0126(4)
Na12	8n	1	0.6169(2)	0.18764(1)	0	0.0107(6)
Na13	8m	1	0.8869(2)	1/2	0.19128(9)	0.0169(7)
Na14	16o	1	0.80518(2)	0.19517(1)	0.26261(6)	0.0144(5)
Na15	8m	1	0.3936(2)	1/2	0.12345(8)	0.0158(7)
Na16	16o	1	0.68865(2)	0.30711(1)	0.14503(6)	0.0146(5)
Na17	4i	1	1/2	1/2	0.0413(1)	0.0125(9)
Na18	16o	1	0.31029(2)	0.11630(9)	0.07123(6)	0.0099(4)
Na19	4g	1	1/2	0.3126(2)	1/2	0.0113(9)
Na20	16o	1	0.68895(2)	0.92615(1)	0.23369(6)	0.0150(5)
Na21	16o	1	0.62173(2)	0.38137(9)	0.31070(6)	0.0140(5)

Table 3.13 Anisotropic displacement parameters (\AA^2) for $\text{Na}_{13}\text{Ag}_{5.5(5)}\text{Sn}_{21.2(5)}$ and $\text{Na}_{230.45(4)}\text{Ag}_{274(3)}\text{Sn}_{136(3)}$; $M = \text{Sn/Ag}$ statistical mixture, $N = \text{Ag/Na}$ statistical mixture.

Atom	U_{11}	U_{22}	U_{33}	U_{12}	U_{13}	U_{23}
$\text{Na}_{13}\text{Ag}_{5.5(5)}\text{Sn}_{21.2(5)}$						
Sn1	0.01249(2)	0.01395(2)	0.01335(2)	0.000	-0.00105(1)	0.000
M2	0.01963(1)	0.01564(1)	0.01572(1)	-0.00276(8)	0.00236(9)	-0.00025(8)
M3	0.02023(2)	0.01615(2)	0.01996(2)	0.000	-0.00567(1)	0.000
Ag4	0.0153(3)	0.0289(4)	0.0171(3)	0.000	0.000	0.000
Na1	0.0188(1)	0.0194(1)	0.0187(1)	0.000	0.000	0.000
Na2	0.0198(5)	0.0198(5)	0.0198(5)	-0.0017(5)	-0.0017(5)	-0.0017(5)
Na3	0.0216(1)	0.0220(1)	0.0190(9)	0.000	0.000	-0.0058(8)
$\text{Na}_{230.45(4)}\text{Ag}_{274(3)}\text{Sn}_{136(3)}$						
Sn1	0.0076(3)	0.0066(3)	0.0064(3)	0.000	0.000	0.000
Sn2	0.0085(2)	0.0121(3)	0.0084(2)	-0.00028(2)	0.000	0.000
Sn3	0.0053(3)	0.0051(3)	0.0092(3)	0.000	0.000	0.000
Sn4	0.0095(2)	0.0105(2)	0.0072(2)	0.000	0.000	0.00230(2)
Sn5	0.00635(2)	0.00752(2)	0.00650(2)	-0.00041(1)	-0.00007(1)	-0.00085(1)
Sn6	0.0066(2)	0.0063(2)	0.0066(2)	-0.00030(2)	0.000	0.000
Sn7	0.0106(4)	0.0089(3)	0.0089(3)	0.000	0.000	0.000
Sn8	0.00892(2)	0.00809(2)	0.01020(2)	0.00078(1)	0.00197(1)	0.00095(1)

Sn9	0.0053(2)	0.0069(2)	0.0082(2)	-0.00113(2)	0.000	0.000
Sn10	0.0088(2)	0.0100(2)	0.0080(2)	0.000	0.00024(2)	0.000
Sn11	0.0064(2)	0.0065(2)	0.0075(2)	0.000	-0.00029(2)	0.000
Sn12	0.01060(2)	0.01059(2)	0.00978(2)	-0.00004(1)	-0.00075(1)	0.00096(1)
Ag1	0.0095(4)	0.0131(4)	0.0077(3)	0.000	0.000	0.000
Ag2	0.00794(2)	0.01230(2)	0.00913(2)	0.00240(1)	-0.00164(1)	-0.00126(1)
Ag3	0.00857(2)	0.00960(2)	0.00910(2)	0.00168(1)	0.00002(1)	0.00087(1)
Ag4	0.0077(2)	0.0072(2)	0.0076(2)	-0.00012(2)	0.000	0.000
Ag5	0.00647(2)	0.0099(2)	0.00997(2)	0.00149(1)	-0.00022(1)	0.00075(1)
Ag6	0.0108(3)	0.0085(3)	0.0122(3)	-0.0001(2)	0.000	0.000
Ag7	0.00778(2)	0.00885(2)	0.00748(2)	0.00041(1)	-0.00129(1)	0.00032(1)
Ag8	0.0074(2)	0.0074(2)	0.0085(2)	0.00136(2)	0.000	0.000
Ag9	0.0061(2)	0.0071(2)	0.0097(2)	0.000	0.000	0.0009(2)
Ag10	0.00828(2)	0.00637(2)	0.00862(2)	-0.00076(1)	0.00009(1)	0.00046(1)
Ag11	0.0074(2)	0.0065(2)	0.0076(2)	0.000	0.000	0.0008(2)
Ag12	0.00641(2)	0.00750(2)	0.00977(2)	0.00021(1)	-0.00101(1)	0.00105(1)
Ag13	0.0081(3)	0.0090(2)	0.0085(2)	0.000	0.00143(2)	0.000
Ag14	0.0080(3)	0.0103(3)	0.0093(2)	0.000	0.0025(2)	0.000
Ag15	0.01035(2)	0.00757(2)	0.01135(2)	-0.00105(1)	0.00191(2)	0.00004(2)
Ag16	0.0091(3)	0.0087(3)	0.0107(3)	0.000	-0.0007(2)	0.000
Ag17	0.0085(5)	0.0088(5)	0.0105(5)	0.0003(3)	0.000	0.000
Ag18	0.0165(6)	0.0128(5)	0.0093(5)	0.000	0.000	0.000
Ag19	0.0137(1)	0.015(1)	0.0139(2)	-0.0031(9)	0.000	0.000
Ag20	0.067(4)	0.040(3)	0.042(4)	0.004(2)	0.000	0.000
Ag21	0.0053(8)	0.0050(7)	0.0055(7)	0.000	0.000	0.000
Ag22	0.0176(3)	0.0130(3)	0.0147(3)	0.000	-0.0062(2)	0.000
Ag26	0.0256(1)	0.098(4)	0.100(4)	0.080(3)	-0.0284(2)	-0.0341(2)
Ag27	0.103(9)	0.062(4)	0.054(5)	-0.036(4)	0.038(5)	-0.049(5)
Ag28	0.029(5)	0.021(5)	0.024(5)	0.000	0.000	0.000
M29	0.01329(2)	0.01302(2)	0.01094(2)	-0.00227(2)	-0.00077(2)	0.00015(2)
M30	0.0082(3)	0.0162(3)	0.0084(3)	-0.0020(2)	0.000	0.000
M31	0.0132(3)	0.0092(3)	0.0243(4)	-0.0003(2)	0.000	0.000
M32	0.0112(3)	0.0162(3)	0.0101(3)	-0.0022(2)	0.000	0.000
M33	0.0081(3)	0.0076(3)	0.0083(3)	0.000	0.0003(2)	0.000
M34	0.0123(2)	0.0097(2)	0.0100(2)	-0.00113(1)	-0.00184(1)	0.00203(1)
M35	0.0114(3)	0.0115(3)	0.0089(3)	0.00045(2)	0.000	0.000
M36	0.0105(2)	0.0107(2)	0.0103(2)	-0.00158(2)	-0.00166(2)	-0.00036(1)
N37	0.0195(1)	0.0113(1)	0.0097(1)	0.000	0.000	0.000
N38	0.0121(5)	0.0097(5)	0.0119(5)	0.000	0.000	0.0002(3)
N39	0.018(2)	0.024(2)	0.057(3)	0.000	0.000	0.000
Na1	0.0128(2)	0.0118(2)	0.0107(2)	0.0004(1)	0.000	0.000
Na2	0.0129(2)	0.0159(2)	0.0130(2)	0.0016(1)	0.000	0.000
Na3	0.011(2)	0.013(2)	0.013(2)	0.000	0.000	0.000
Na4	0.0137(2)	0.0115(2)	0.0101(1)	0.0013(1)	0.000	0.000
Na5	0.0110(1)	0.0118(1)	0.0135(1)	0.0012(9)	-0.0012(9)	0.0006(9)
Na6	0.0161(1)	0.0149(1)	0.0099(1)	0.0010(8)	0.0003(9)	-0.0056(9)
Na7	0.0113(2)	0.0130(2)	0.0121(2)	0.0008(1)	0.000	0.000
Na8	0.0113(2)	0.0133(2)	0.0112(1)	0.000	0.000	0.0004(1)
Na9	0.0132(2)	0.0188(2)	0.0112(2)	-0.0012(1)	0.000	0.000
Na10	0.0134(2)	0.0085(1)	0.0153(2)	0.000	0.0044(1)	0.000
Na11	0.0115(1)	0.0108(1)	0.0155(1)	-0.0020(8)	-0.0019(9)	-0.0013(8)
Na12	0.0095(2)	0.0120(2)	0.0105(2)	0.000	0.000	-0.0004(1)
Na13	0.0221(2)	0.0094(2)	0.0191(2)	0.000	-0.0018(2)	0.000
Na14	0.0130(1)	0.0163(1)	0.0139(1)	0.0007(9)	0.0036(9)	-0.0022(1)

Na15	0.0171(2)	0.0160(2)	0.0144(2)	0.000	-0.0032(1)	0.000
Na16	0.0107(1)	0.0167(1)	0.0163(1)	-0.0013(9)	-0.0013(9)	-0.0027(9)
Na17	0.009(2)	0.013(2)	0.015(2)	0.000	0.000	0.000
Na18	0.0084(1)	0.0089(1)	0.0124(1)	0.0022(8)	0.0002(8)	-0.0017(8)
Na19	0.011(2)	0.014(2)	0.009(2)	0.000	0.000	0.000
Na20	0.0159(1)	0.0171(1)	0.0120(1)	0.0026(9)	0.0014(9)	0.0015(1)
Na21	0.0145(1)	0.0132(1)	0.0145(1)	-0.0017(9)	0.0017(9)	-0.0019(9)

Compounds in the ternary system Na-Ag-Sn tend to contain a different type of disorder: defect positions and statistical mixtures of the atoms of different sorts. Both compounds $\text{Na}_{13}\text{Ag}_{5.5(5)}\text{Sn}_{21.2(5)}$ and $\text{Na}_{230.45(4)}\text{Ag}_{274(3)}\text{Sn}_{136(3)}$ are no exceptions. As in was discussed for the $\text{Na}_{29}\text{Ag}_{21}\text{Sn}_{39}$, lack of electron density in Sn positions could be interpreted as defect Sn position or Sn/Ag statistical mixture (labeled as *M*). Similarly, lack of electron density in Ag positions could indicate either defect positions or Ag/Na statistical mixture (labeled as *N*). One criteria to figure out what exactly is happening in the structure could be interatomic distances: homoatomic Sn-Sn are longer then heteroatomic Sn-Ag distances ($d_{\text{Sn-Sn}} = 3.115\text{-}3.350 \text{ \AA}$ ^[80] in $\beta\text{-Sn}$, $d_{\text{Sn-Ag}} = 2.949\text{-}3.016 \text{ \AA}$ ^[81] in Ag_3Sn); Ag-Na distances are usually above 3 \AA ($d_{\text{Ag-Na}} = 3.285 \text{ \AA}$ in NaAg_2 ^[88]). It showed that the formation of the Sn-Ag statistical mixture is more favorable then defects in Sn positions and the possibility of formation Ag-Na statistical mixture along with vacancies in Ag positions.

As it is shown in Table 3.12, for $\text{Na}_{13}\text{Ag}_{5.5}\text{Sn}_{21.2}$, a statistical mixture of Ag and Sn was observed in two atom sites Sn2/Ag2 and Sn3/Ag3, labeled as *M2* and *M3*, respectively. Compound $\text{Na}_{230.45}\text{Ag}_{274}\text{Sn}_{136}$ is a lot more complicated: formation of statistical mixtures of Sn and Ag in eight atomic positions (*M29-M26*) as well as Ag and Na in three atomic positions (*N37-N39*) was observed. Positional and atomic displacement parameters (ADPs) for Ag and Sn were set to be equal at the respective atom sites. The refinement of the occupancy parameters led to Sn/Ag ratio of 0.86/0.14(3) for *M2* (48*h*) and 0.81/0.19(3) for *M3* (24*g*) in $\text{Na}_{13}\text{Ag}_{5.5}\text{Sn}_{21.2}$ and to Sn/Ag ratio of 0.387/0.613(3), 0.21/0.79(4), 0.56/0.44(4), 0.35/0.65(4), 0.14/0.86(4), 0.29/0.71(3), 0.38/0.62(4), 0.26/0.74(3) for *M29* (16*o*), *M30* (8*l*), *M31* (8*l*), *M32* (8*l*), *M33* (8*m*), *M34* (16*o*), *M35* (8*l*), *M36* (16*o*) as well as Ag/Na ratio of 0.259/0.741(6), 0.528/0.472(4), 0.073/0.928(2) in *N37*(4*g*), *N38* (8*n*), *N39* (4*i*) in $\text{Na}_{230.45}\text{Ag}_{274}\text{Sn}_{136}$.

Additionally, defect positions of Ag atoms for both compounds were revealed during the refinement. For $\text{Na}_{13}\text{Ag}_{5.5}\text{Sn}_{21.2}$ it is just one atomic position – Ag4 (12*e*) with site occupancy factor of 0.886(3). In case of $\text{Na}_{230.45}\text{Ag}_{274}\text{Sn}_{136}$ thirteen Ag positions are partially occupied: Ag16 (8*m*), Ag17 (8*l*), Ag18 (4*g*), Ag21 (2*b*), Ag25 (8*m*), Ag28 (4*i*) with site occupancy factor

of 0.928(2), 0.613(3), 0.839(5), 0.764(6), 0.069(4), 0.116(5), respectively. Positions Ag19 (8*l*) and Ag20 (8*l*), as well as Ag26 (16*o*) and Ag27 (16*o*) resulted after splitted silver positions, both pairs are mutually excluding with partial Ag occupancy of 0.256(4), 0.195(5), 0.292(7) and 0.141(7) for Ag19, Ag20, Ag26, and Ag27, respectively. Two other positions, Ag23 (8*m*) and Ag24 (4*i*) both with occupancy of 0.073(2) together exclude the occurrence of Ag22 (8*m*) (occupancy 0.928(2)) and vice versa, For the defect Ag positions a possibility of forming statistical mixture Ag/Na was considered, but because of unusually short Na-*M* distances partial occupancy for these sites was preferred (see detailed discussion below).

No significant residual peaks were observed in the difference electron-density map for both compounds. Refined compositions of the new compounds are Na₁₃Ag_{5.5(5)}Sn_{21.2(5)} and Na_{230.45(4)}Ag₂₇₄₍₃₎Sn₁₃₆₍₃₎.

After single-crystal XRD analysis for both crystals from the samples 'Na₁₃Ag₆Sn₂₃' and 'Na₅AgSn' EDX analysis was performed. To transfer the crystals into the JSM 7500F scanning electron microscope they were shortly exposed to the air for around 2 seconds. It was enough to oxidize the surface of the crystal from the sample 'Na₅AgSn'. The atomic ratios of Na:Ag:Sn (Table 3.14) determined from at least three measurements are 34:12:51 and 80:13:7 for the compounds Na₁₃Ag_{5.5}Sn_{21.2} and Na_{230.45}Ag₂₇₄Sn₁₃₆, respectively.

Table 3.14 Comparison of the results EDX analysis of the crystal with the refined composition Na₁₃Ag_{5.5}Sn_{21.2} from the sample 'Na₁₃Ag₆Sn₂₃' and Na_{230.45}Ag₂₇₄Sn₁₃₆ from the sample 'Na₅AgSn'.

	Na (at. %)	Ag, (at. %)	Sn (at. %)	O (at. %)
EDX	34(5)	12(4)	51(4)	-
Na ₁₃ Ag _{5.5} Sn _{21.2}	32.7	13.9	53.4	-
EDX	36(8)	6(2)	3(2)	55(2)
Na _{230.45} Ag ₂₇₄ Sn ₁₃₆	36.0	42.8	21.2	-

Magnetic Properties of the Sample 'Na₁₃Ag₆Sn₂₃'

The results of the magnetic properties measurement for the 22.66 mg of 'Na₁₃Ag₆Sn₂₃' are shown in Figure 3.17. Obtained raw magnetization data were converted into molar magnetic susceptibilities (χ_{mol}) and subsequently corrected for the sample holder and diamagnetic contribution of the core electrons using Pascal's constants (for Na⁺, Ag⁺ and Sn^{IV}[49]). The form of the susceptibility curve at the temperatures below 20 K indicates the presence of paramagnetic impurities in an otherwise diamagnetic sample.

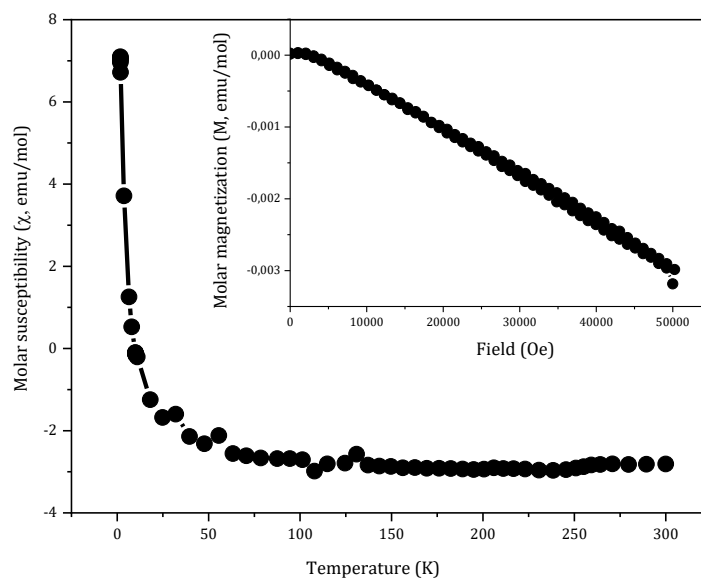


Figure 3.17 Molar magnetic susceptibility as a function of temperature at applied field of 10000 Oe and field-dependent magnetization measured at 300K (inset) for the sample 'Na₁₃Ag₆Sn₂₃'.

Crystal Structure of the Compound Na₁₃Ag_{5.5}Sn_{21.2}

The phase Na₁₃Ag_{3-x+y}Sn_{24-y}, which crystallizes in the space group $Im\bar{3}$, was first reported by A. Henze [79] with higher silver content compared to the title compound. The composition according to the earlier work is Na₁₃Ag_{2.7}Sn₂₄ and lattice parameter $a = 15.333(1)$ Å (smaller than $a = 15.495(1)$ Å for the Na₁₃Ag_{5.5}Sn_{21.2}). In Na₁₃Ag_{2.7}Sn₂₄ all three Sn positions (two in Wyckoff position 24*g* and one 48*h*) are fully occupied, on the contrast to Na₁₃Ag_{5.5}Sn_{21.2}, where tin-rich Sn/Ag statistical mixtures are forming in the positions *M2* and *M3* (48*h* and 24*g*). In both compounds the silver position (12*e*) is defect with occupancy of 0.90(1) and 0.886(3) in Na₁₃Ag_{2.7}Sn₂₄ and Na₁₃Ag_{5.5}Sn_{21.2}, respectively. The refined composition for the title compound is in a good agreement with the results of the EDX analysis, confirming higher content of silver, achieved by the formation of the statistical mixture. For the Na₁₃Ag_{2.7}Sn₂₄ no confirmation of the composition of the crystal was obtained.

The compound Na₁₃Ag_{5.5}Sn_{21.2} is a rather complex intermetallic phase, isomorphous to the Mg₃₂(Zn,Al)₄₉ Bergman phase [89] (Figure 3.18, a).

There is no unique way to classify, describe and visualize the crystal structure of a complex intermetallic compound. To reduce the degree of complexity and to understand the packing principles for both phases discussed in this Chapter a multi-shell cluster approach was used. Visualization of a crystal structure in terms of clusters (in the meaning of structural building blocks) or structure modules can be quite arbitrary. Furthermore, according to Walter Steuer [90]: “even if one finds atologically elucidating cluster-based description, this does not mean that it is supported from a crystal-chemical point of view”. It leads to the fact the chemical bonds between atoms within a cluster can differ from those outside a cluster.

Na₁₃Ag_{5.5}Sn_{21.2} can be described as bcc packing of endohedral fullerenes (Figure 3.19, a – cluster A) – Bergman-type clusters shown in violet, interconnected via sharing hexagonal faces and Ag₄-Ag₄ edges as it is shown in Figure 3.19, b. The space between the fullerenes is filled by 11-atomic Na₁-centered polyhedra, Na@Ag₃M₈ (yellow in Figure 3.18, b and Figure 3.20), sharing hexagonal and pentagonal faces with the clusters A. This type of polyhedron can be understood as a truncated tetrahedra shown in Figure 3.20, c, similar to the classical 12-atom Friauf polyhedra. It has two regular hexagonal faces, two pentagonal (instead of four hexagonal faces in Friauf polyhedron) and four triangle faces. This way the compact packing of the clusters within the structure of the Na₁₃Ag_{5.5}Sn_{21.2} is insured.

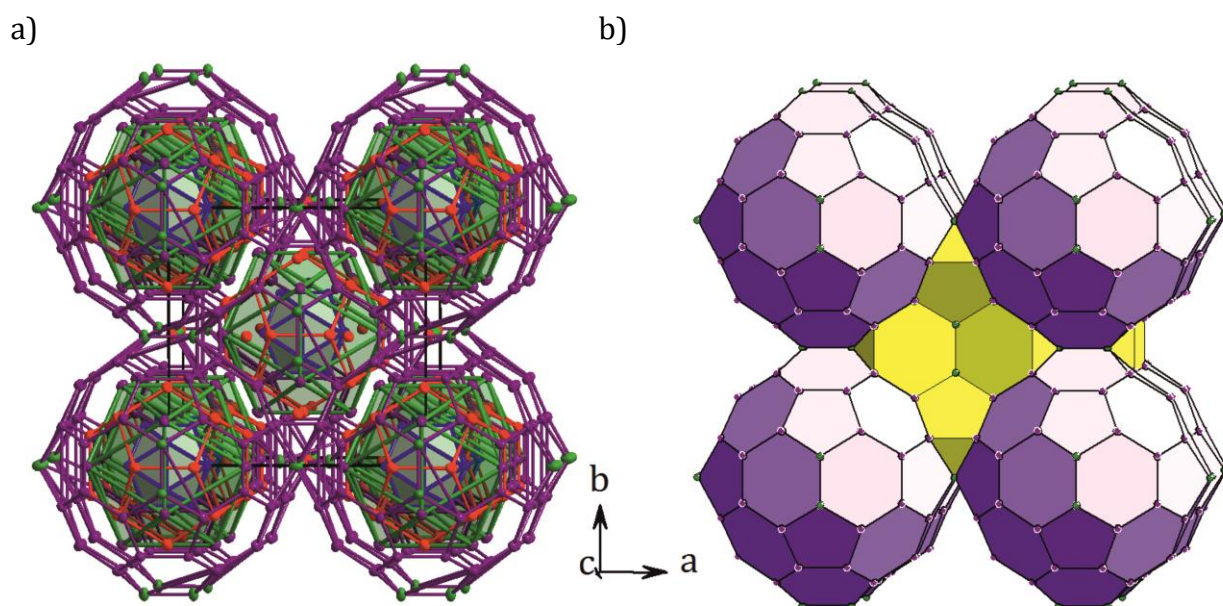


Figure 3.18 Unit cell of the compound $\text{Na}_{13}\text{Ag}_{5.5}\text{Sn}_{21.2}$: unit cell build of clusters with concentric shells (a) and packing of the Bergman-type clusters (violet polyhedra, cluster A) with Na-centered space fillers (yellow polyhedra). Na atoms are shown in red, Ag – green, Sn – blue and atoms of Sn/Ag statistical mixture – in violet. The displacement ellipsoids are drawn with 90 % probability level (a).

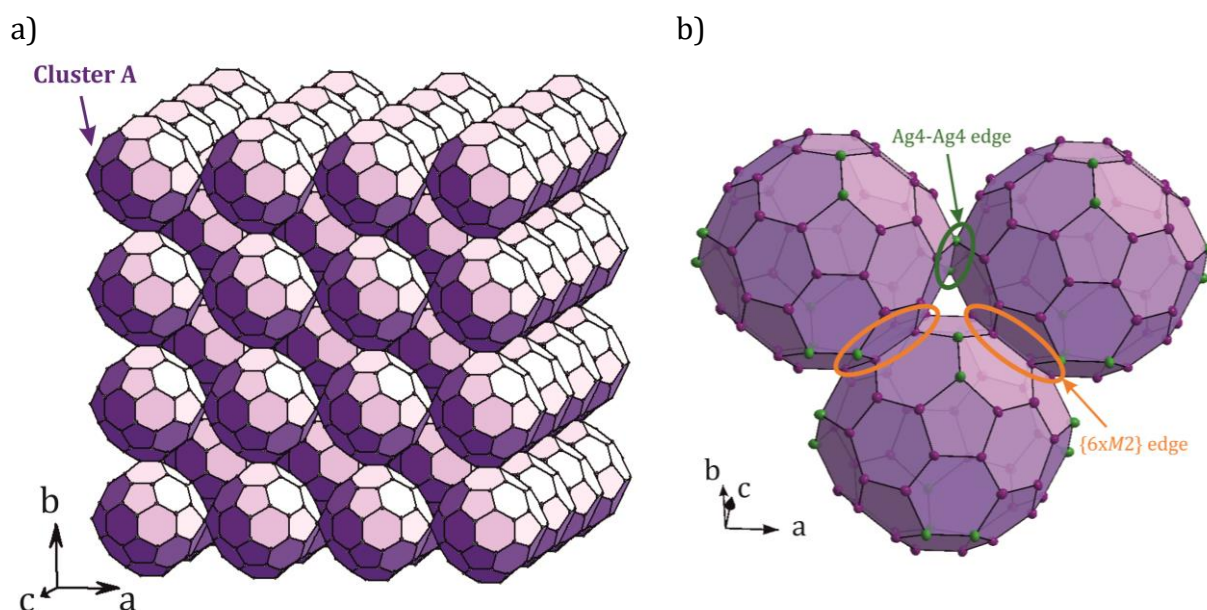


Figure 3.19 Bcc-packing of the endohedral fullerane clusters in $3 \times 3 \times 3$ unit cell of $\text{Na}_{13}\text{Ag}_{5.5}\text{Sn}_{21.2}$ (a). The clusters are connected via sharing hexagonal faces and Ag4-Ag4 dumbbells. Ag atoms are shown in green, atoms of Sn/Ag statistical mixture – in violet.

The Bergman-type cluster in $\text{Na}_{13}\text{Ag}_{5.5}\text{Sn}_{21.2}$ (cluster A) can be peeled, revealing four shells, shown in Figure 3.21. The first out of four shells of the cluster is an unfilled exo-bonded icosahedron, formed by Sn1-atoms ($24g$) around $2a$ Wyckoff position in the unit cell, with

$d_{\text{Sn1-Sn1}} = 2.933 \text{ \AA}$. The dual polyhedron – pentagonal dodecahedron in the second shell is defined by 8 Na2 (16*f*) and 12 Na3 (24*g*) atoms. Pentagonal faces of dodecahedron are capped with twelve atoms of the mixed M3 (24*g*) position that form a bigger icosahedron as the third shell. Atoms M3 of the bigger icosahedron are not interconnected, but form 12 exobonds to the Sn1-atoms of the inner icosahedron, with Sn1-M3 distances of 2.778 Å. Each of these bonds is perpendicular and points to the center of the pentagons of the fourth shell, a truncated icosahedron – buckminsterfullerene or Samson polyhedra. It is formed by 12 Ag4 (12*e*) and 48 mixed M2 (48*h*) atoms. Position Ag4, partially occupied by Ag (88.6 %) was checked regarding the possibility of forming statistical mixture Ag/Na, but the unusually short for Ag-Na distance of 2.988 Å to the neighboring Ag4 position shows that defect in this case is more realistic. Ag4 atoms within this cluster form dumbbells with Ag4-Ag4 distances of which matches very well with Ag-Ag distances in Ag₃Sn between 2.928 and 2.984 Å [81]. M2 atoms form hexagonal and, together with Ag4 atoms, pentagonal faces, M2-M2 distance is 2.970 Å and Ag4-M2 – 3.174 Å, which makes Ag₂ dumbbell to appear quite isolated.

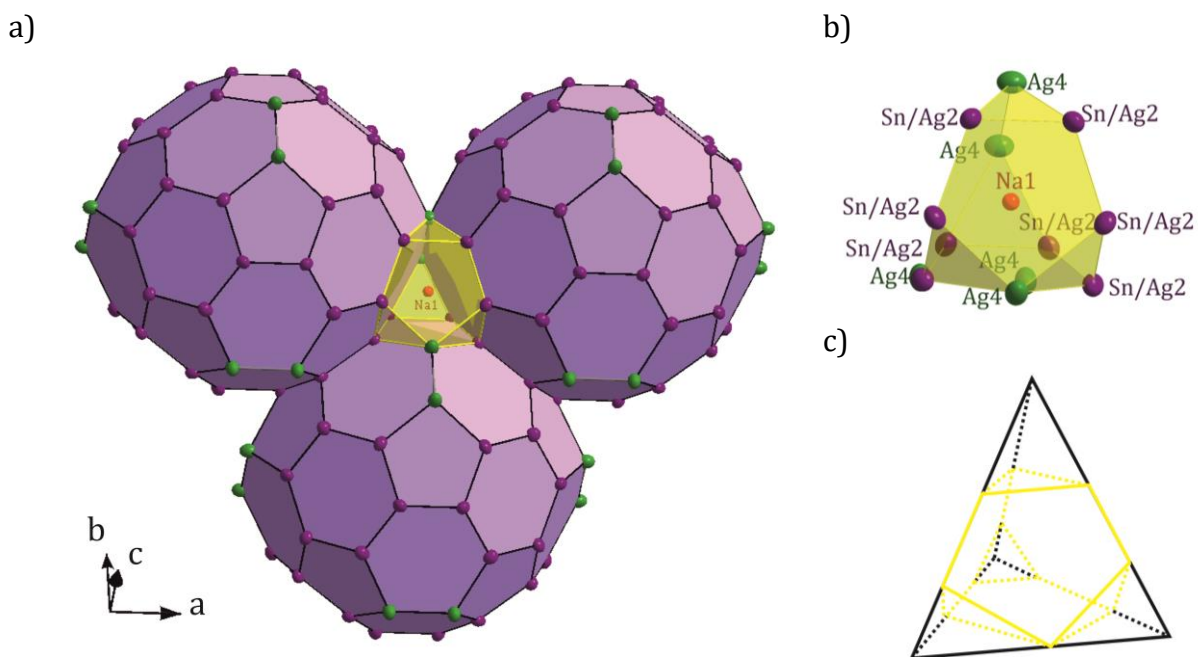


Figure 3.20 Position of the Na-centered space filler (yellow) in the structure of the compound Na₁₃Ag_{5.5}Sn_{21.2} surrounded by Bergman-clusters (violet) and sharing hexagonal and pentagonal faces with them (a). The new eleven atom polyhedra (b), represented as a truncated tetrahedron (c) with two hexagonal, one pentagonal and four triangle faces. Na atoms are shown in red, Ag – green, Sn – blue and atoms of Sn/Ag statistical mixture – in violet. The displacement ellipsoids are drawn at a 90 % probability level.

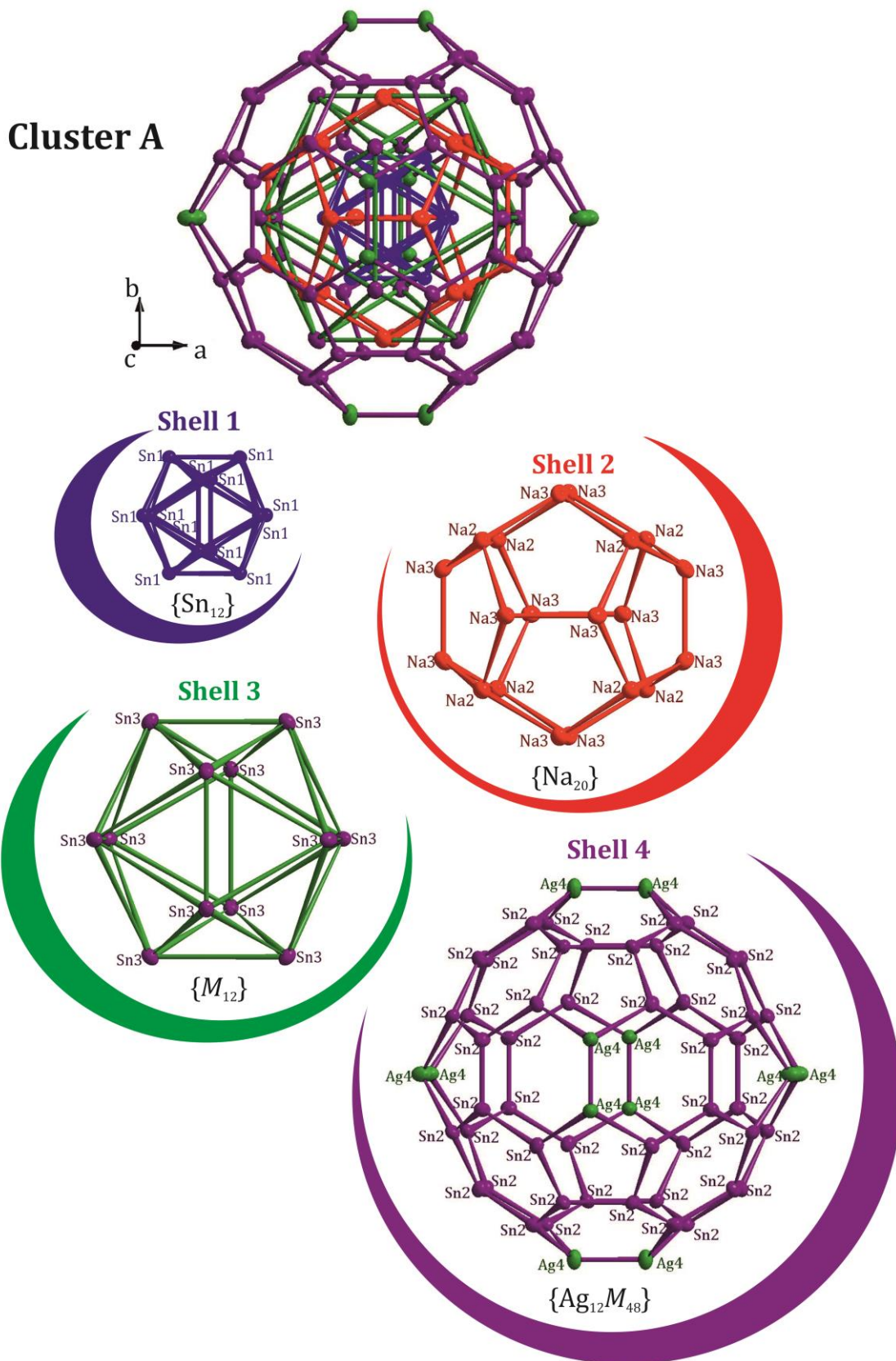


Figure 3.21 Concentric shells of the Bergman-type clusters in $\text{Na}_{13}\text{Ag}_{5.5}\text{Sn}_{21.2}$: (1) empty $\{\text{Sn}_{12}\}$ icosahedra; (2) $\{\text{Na}_{20}\}$ dual pentagonal dodecahedron; (3) $\{M_{12}\}$ icosahedra; (4) $\{\text{Ag}_{12}M_{48}\}$ buckminsterfullerene. Na atoms are shown in red, Ag – green, Sn – blue and atoms of Sn/Ag statistical mixture – in violet. The displacement ellipsoids are drawn at a 90 % probability level.

Table 3.15 Selected interatomic distances in the compound Na₂₉Ag₂₁Sn₃₉. For the details see Table 6.2 (Appendix)

Atom types		Distance range(Å)	Atom types		Distance range(Å)
Sn	-Sn	2.9128(5)-2.9331(3)	Na	-Sn	3.308(2)-3.332(2)
Sn	-M	2.7784(5)	Na	-M	3.309(1)-3.564(2)
M	-M	2.8407(4)-2.9704(5)	Na	-Ag	3.188(3)-3.410(2)
Ag	-M	3.1739(5)-3.2305(4)	Na	-Na	3.266(3)-3.618(2)
Ag	-Ag	2.9875(9)			

Crystal Structure of the Compound $\text{Na}_{230.45}\text{Ag}_{274}\text{Sn}_{136}$

Compound $\text{Na}_{230.45}\text{Ag}_{274}\text{Sn}_{136}$ with orthorhombic space group *Immm* and cell parameters $a = 15.1995(2)$, $b = 24.7063(3)$ and $c = 40.2152(6)$ Å crystallizes in its own structure type and have a rather complicated structure with two types of fullerene-type clusters. As it is shown in Figure 3.22, the unit cell of $\text{Na}_{230.45}\text{Ag}_{274}\text{Sn}_{136}$ contains two types of endohedral fullerene clusters (cluster A', shown in violet and B, shown in blue) in ratio 1:2. The outer shells of both clusters are resembling C_{60} (cluster A') and C_{80} (cluster B) fullerene structures.

The packing of these clusters is shown in Figure 3.23. As is it shown in Figure 3.23, b, clusters A' are interconnected with each other through Ag18-Ag18 dumbbells (edge sharing) and with clusters B via sharing pentagonal faces. Additionally, clusters B are sharing hexagonal faces with each other.

The space between the clusters A' and B are filling different types of the Na- and Ag-centered polyhedra –Figure 3.24, a-b. Deformed Na-centered Friauf polyhedra are built around Na1, Na2, Na5, Na7 and Na8 ($\{\text{Na1@Ag}_6\text{M}_3\text{Sn}_3\}$, $\{\text{Na2@Ag}_4\text{M}_3\text{Sn}_3\text{N}_2\}$, $\{\text{Na5@Ag}_6\text{M}_3\text{Sn}_3\}$, $\{\text{Na7@Ag}_4\text{M}_3\text{Sn}_3\text{N}_2\}$ and $\{\text{Na8@Ag}_9\text{M}_3\text{Sn}_3\}$ – shown in yellow in Figure 3.24, c-g) and contain four hexagonal and four triangle faces. Twelve-atom polyhedra around Na3 ($\{\text{Na3@Ag}_{10}\text{Sn}_2\}$ –in light green in Figure 3.24, h) have only three hexagonal faces and eight triangle. Coordination environment around Na19 is very similar to Na3, with the only difference: additional Ag atom centering one of the hexagonal faces, resulting in $\{\text{Na19@Ag}_9\text{Sn}_2\text{N}_2\}$ (orange polyhedra in Figure 3.24, i). Ag-centered space fillers are icosahedra $\{\text{Ag1@Ag}_8\text{Sn}_2\text{N}_2\}$ and $\{\text{Ag17@Sn}_3\text{M}_9\}$ (bright green in Figure 3.24, j-k).

Detailed structures of both clusters A' and B are presented in Figure 3.25 and Figure 3.26, respectively. Cluster A' resembles Bergman-type cluster A in $\text{Na}_{13}\text{Ag}_{5.5}\text{Sn}_{21.2}$, but unlike its analog cluster A' is centered by partially occupied Ag21 (76.4 %), with the distances between the Ag21 and the atoms of the inner shell (Table 3.16) between 2.7438(8) and 2.7734(6) Å – Ag-Ag and Ag-M bonds.

The first, inner shell of the cluster A' consists of eight Ag atoms (Ag4 and Ag11, four of each) and four atoms of the Sn/Ag statistical mixture (M33) forming an icosahedron (Shell 1 in Figure 3.25). Interatomic distances within the first shell are between 2.8934(6) and 2.9198(7) Å – Table 3.16.

The second shell is similar as in $\text{Na}_{13}\text{Ag}_{5.5}\text{Sn}_{21.2}$, a dual polyhedron $\{\text{Na}_{20}\}$ pentagonal dodecahedron (Na4, Na10, Na12 – four of each and eight Na18 – Shell 2 in Figure 3.25) with Na-Na distances in the range 3.541(3)-3.567(3) Å.

The third shell is an icosahedron built by twelve Sn atoms (Sn4, Sn6 and Sn11, four of each – Shell 3 in Figure 3.25), which are not bonded to each other, but forming exo-bonds of the atoms of the first shell (2.7148(8)-2.7361(8) Å) as well as with the atoms of the hexagonal or pentagonal faces of the shell 4 (2.7698(8)-3.2166(7) Å).

Finally, the fourth shell consists of sixty Ag atoms (Ag2, Ag3, Ag5, Ag7, Ag8, Ag10, Ag12, Ag13 and Ag18 – Shell 4 in Figure 3.25) forming a buckminsterfullerene. Atoms site Ag18 is partially occupied by 83.9 % Ag, Ag-Ag distance of 2.929 Å (Ag18-Ag18), excluding the possibility of formation Ag/Na statistical mixture at this site. The distances between the atoms of the fourth shell are 2.8733(6)-3.1084(8) Å, which shows quite strong interactions.

The second cluster, cluster B in Figure 3.26, is a lot more complicated. It also contains four shells, like cluster A'. Cluster B is centered by defect Ag28 atom (11.6 % Ag), with the shortest Ag28-Ag27 distance of 2.191 Å, which is possible due to the partial occupancy of both sites. In contrast to the cluster A', the inner polyhedra is formed by Ag, Na and atoms of the statistical mixture with a significant disorder, which results in quite long interatomic distances within the shell: 2.756(1)-3.47(1) Å. It can be summarized as $\{\text{Ag}_{28}@\text{Ag}_x\text{M}_2\text{Na}_2\}$, resembling icosahedral form. As it is shown in Figure 3.27, the inner shell of the cluster B can be splitted into two mutually exclusive polyhedra, both containing two Na atoms (position Na15), two atoms of the Sn/Ag statistical mixture (M31). The first one include additionally 2×Ag20 (19.5 % Ag), 2×Ag23 (7.3 %), 4×Ag24 (7.3 %) and Ag26 (29.2 %), which results in distorted 13 atom cluster $\{\text{Ag}@\text{Ag}_9\text{M}_2\text{Na}_2\}$ (Cluster I in Figure 3.26). The second one in addition to 2×Na15 and 2×M31 contain Ag19 (25.6 %), Ag22 (92.8 %), Ag25 (6.9 %) and Ag27 (14.1 %) atoms, forming distorted 14 atom cluster $\{\text{Ag}@\text{Ag}_{10}\text{M}_2\text{Na}_2\}$ (Cluster II in Figure 3.26).

This disorder, because of the volume increase of the cluster in the first shell induces enlargement of all the following shells (see the comparison of the distances from the center of the cluster to the atoms of the respective shell in cluster A, A' and B – Figure 3.28). The second shell is built by 29 Na atoms (Na6, Na9, Na11, Na13, Na14, Na16, Na17, Na20 and Na21) and one atom of the Ag/Na statistical mixture N39 (Ag:Na ratio of 0.073:0.928), forming icosidodecahedron with distances between the Na-Na atoms 3.542(3)-3.710(4) Å.

The third shell, formed by four Ag atoms ($2 \times \text{Ag6}$ and $2 \times \text{Ag16}$) and eight Sn atoms (Sn2, Sn6, Sn10 and Sn12, two of each), remains icosahedral shape, but significantly larger. Lack of the electron density in Ag16 position (92.8 % Ag) cannot be compensated by Ag/Na statistical mixture due to the short interatomic distance $d_{\text{Ag16-Ag22}} = 2.756 \text{ \AA}$. Atoms within the third shell are not bonded with each other, but forming bonds with atoms of the first and fourth shell with distances of 2.7518(8)-3.16(2) and 2.865(1)- 3.003(1) \AA , respectively.

Eighty atoms form the last, fourth shell of the cluster B: 30 Ag atoms (Ag5, Ag7, Ag8, Ag9, Ag10, Ag12, Ag13, Ag14 and Ag15), together with 30 atoms of Sn/Ag statistical mixture ($M29, M30, M32, M34, M35, M36$) and 20 Sn atoms (Sn1, Sn3, Sn5, Sn7, Sn8 and Sn9) with distances between 2.7336(8) and 2.982(1) \AA .

All the interatomic distances are listed in Table 6.3 (Appendix), whereas the summary is condensed in Table 3.17. The analysis of the interatomic distances within each shell is shown in Table 3.16.

There are interesting differences between all three types of endohedral fullerane clusters (A, A' and B) in $\text{Na}_{13}\text{Ag}_{5.5}\text{Sn}_{21.2}$ and $\text{Na}_{230.45}\text{Ag}_{274}\text{Sn}_{136}$. The main difference between the cluster A ($\text{Na}_{13}\text{Ag}_{5.5}\text{Sn}_{21.2}$) and cluster A' ($\text{Na}_{230.45}\text{Ag}_{274}\text{Sn}_{136}$) is the occupancy of the inner icosahedra: empty in the first case, in contrast to Ag-centered for the second one. Apparently, strong covalent interactions between the center and the atoms of the icosahedral shell leads to compression of the whole system, as it is shown in Figure 3.28, the distances from the center of the cluster to elements, building the respective shell for the endohedral cluster A of $\text{Na}_{13}\text{Ag}_{5.5}\text{Sn}_{21.2}$ are slightly larger compared to the empty analog cluster A' in $\text{Na}_{230.45}\text{Ag}_{274}\text{Sn}_{136}$. The disorder in the inner shell of the cluster B (also filled with Ag-atoms), as well as and Na atoms within it requires enlargement of the inner shell, which causes the enlargement of the shells 2-3 and 4th shell with eighty atoms instead of sixty in the cluster A (Figure 3.28).

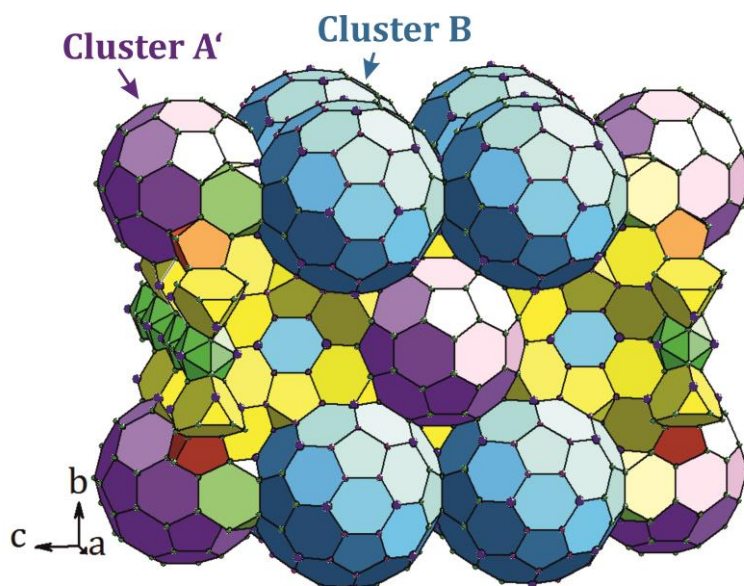


Figure 3.22 Unit cell of the compound $\text{Na}_{230.45}\text{Ag}_{274}\text{Sn}_{136}$ with two types of endohedral fullerene clusters: 60 atom clusters A (violet polyhedra) and 80 atom clusters B (blue). Na-centered space fillers are shown in yellow. Na atoms are shown in red, Ag – green, Sn – blue, atoms of statistical mixture Sn/Ag – in violet and Ag/Na – in brown. The displacement ellipsoids are drawn at a 90 % probability level.

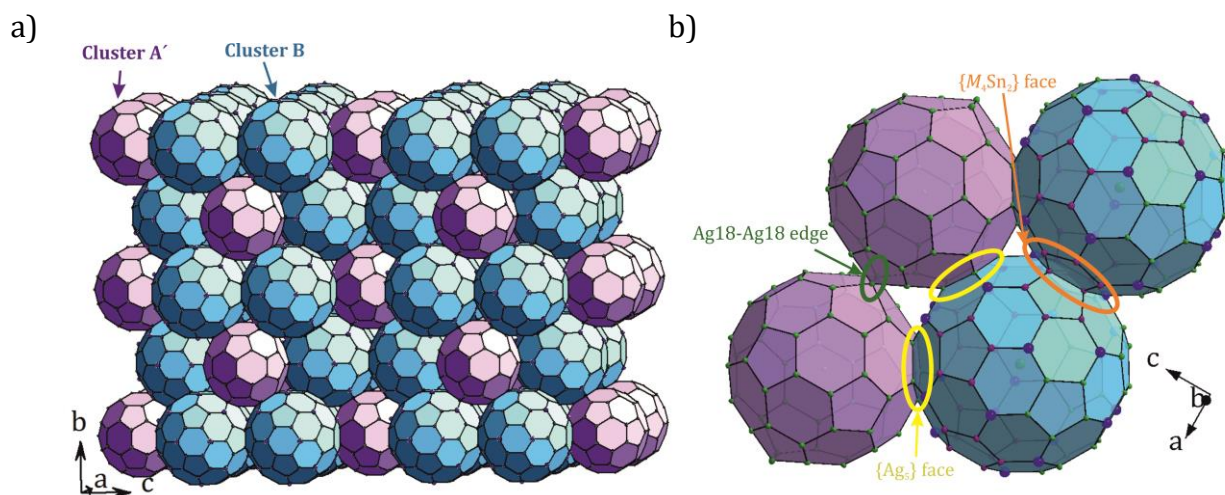
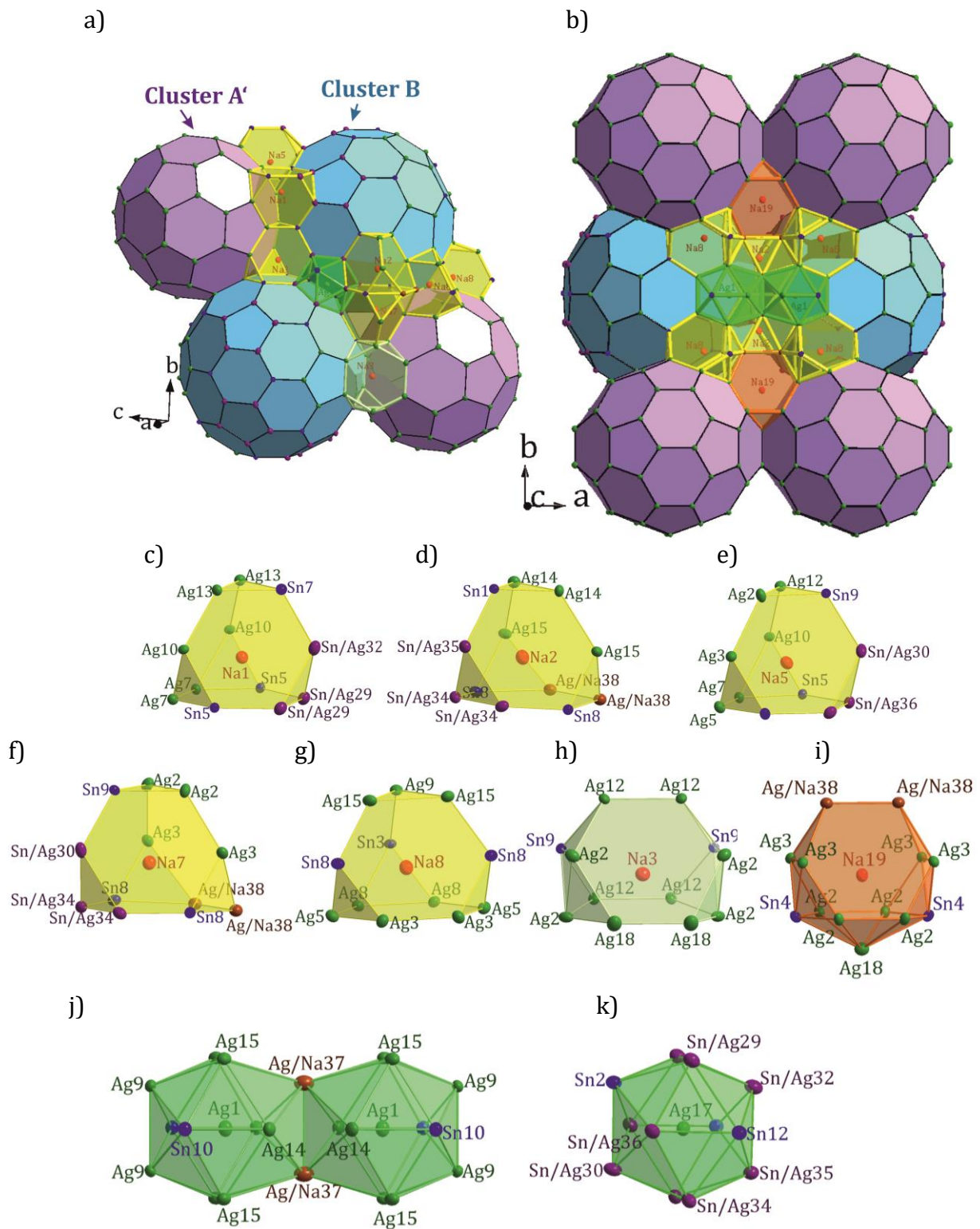


Figure 3.23 Packing of the two types endohedral fullerene clusters (A' and B) in the $2 \times 2 \times 2$ cell of $\text{Na}_{230.45}\text{Ag}_{274}\text{Sn}_{136}$ (a). The clusters A', interconnected with each other through sharing Ag18-Ag18 dumbbells – marked with green ellipse, and with clusters B via sharing pentagonal faces – marked with yellow ellipses; clusters B are sharing hexagonal faces with each other – marked with orange ellipse (b). Ag atoms are shown in green, atoms of Sn/Ag statistical mixture – in violet and Sn – in blue.



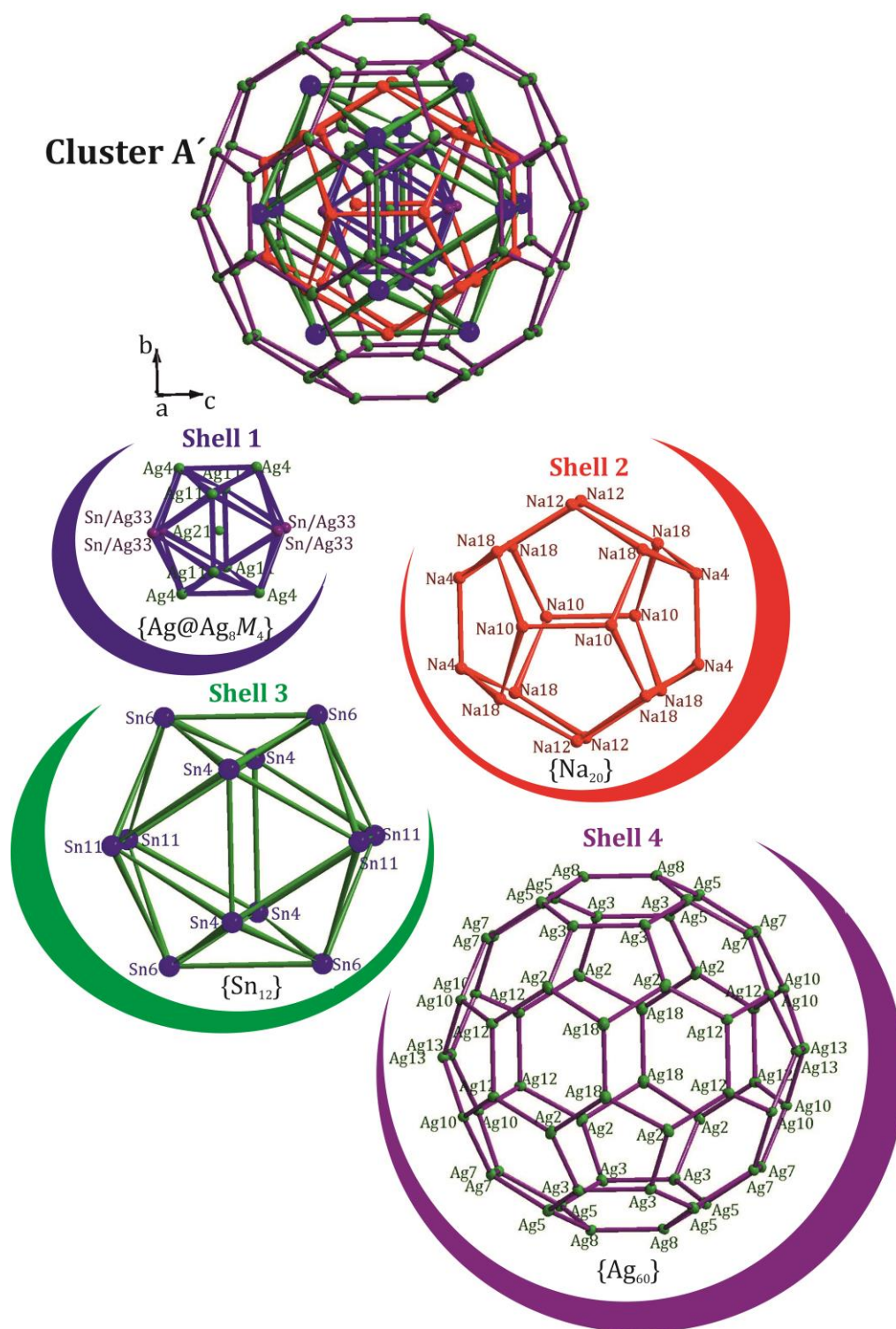


Figure 3.25 The first type of endohedral fullerene clusters in $Na_{230.45}Ag_{274}Sn_{136}$ (cluster A'), formed around Ag_{21} , containing four shells: (1) $\{Ag_{21}@Ag_8M_4\}$ icosahedra; (2) $\{Na_{20}\}$ dual pentagonal dodecahedron; (3) $\{Sn_{12}\}$ icosahedra and (4) $\{Ag_{60}\}$ buckminsterfullerene. Na atoms are shown in red, Ag – green, Sn – blue, atoms of statistical mixture Sn/Ag – in violet and Ag/Na – in brown. The displacement ellipsoids are drawn at a 90 % probability level.

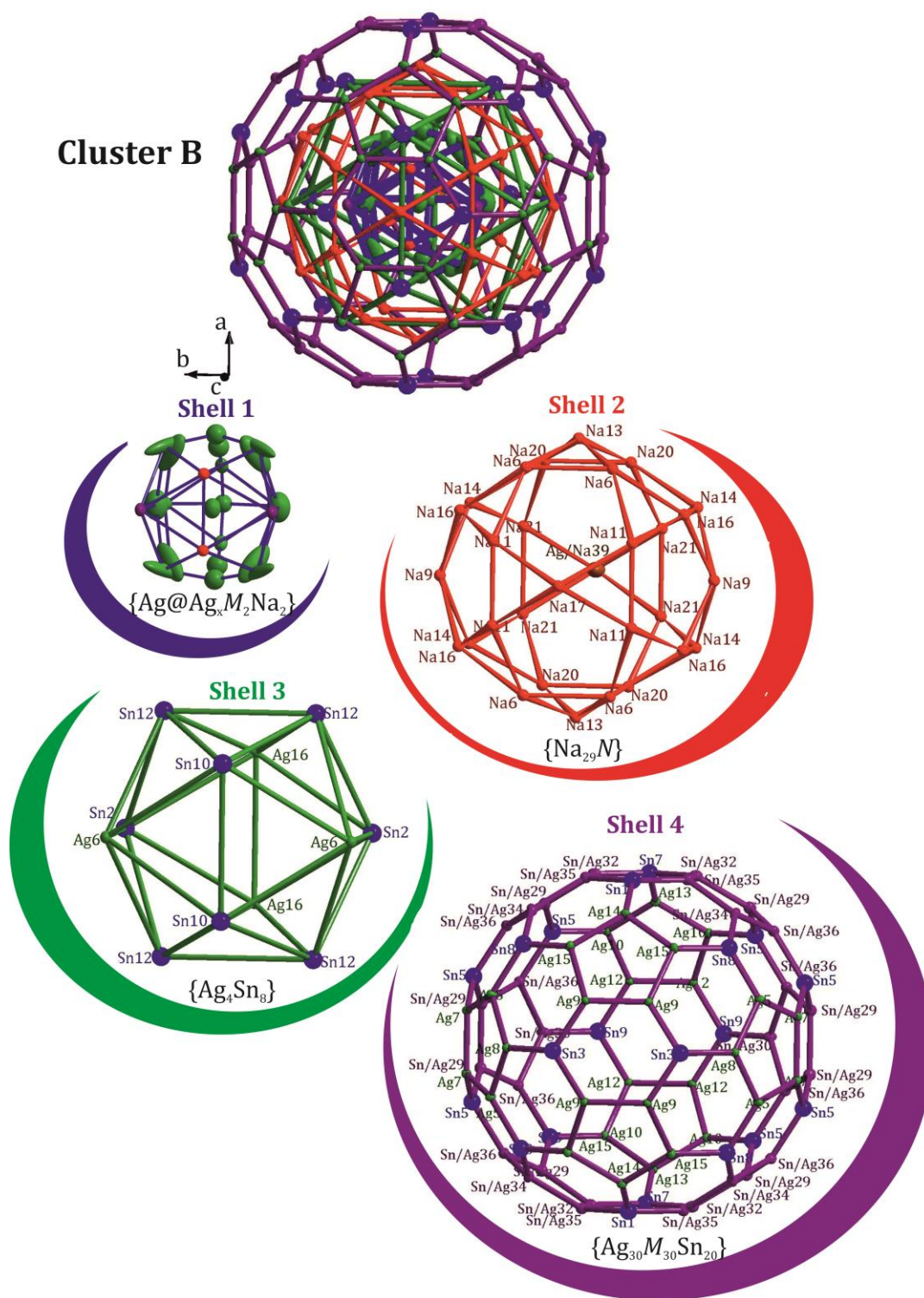


Figure 3.26 The second type of endohedral fullerene clusters in $Na_{230.45}Ag_{274}Sn_{136}$ (cluster B), containing shells: (1) disordered icosahedra around $Ag_{28} - \{Ag_{28}@Ag_xM_2Na_2\}$; (2) $\{Na_{29}N\}$ icosidodecahedron; (3) $\{Ag_4Sn_8\}$ icosahedra; $\{Ag_{30}M_{30}Sn_{20}\} - 80$ -atom fourth shell. Na atoms are shown in red, Ag – green, Sn – blue, atoms of statistical mixture Sn/Ag – in violet and Ag/Na – in brown. The displacement ellipsoids are drawn at a 90 % probability level.

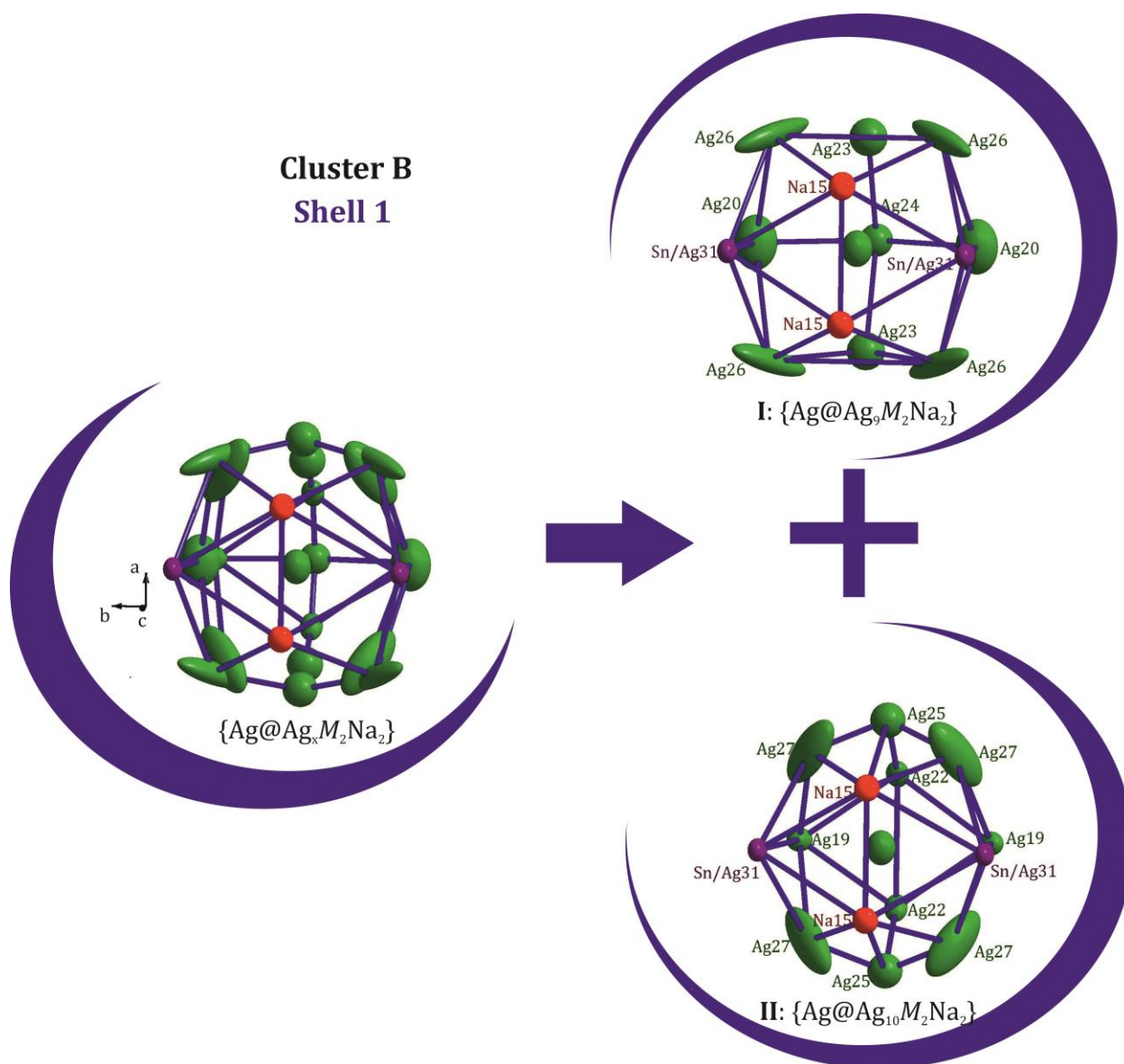


Figure 3.27 Disordered icosahedra around the atomic position Ag28: $\{\text{Ag}28@\text{Ag}_x\text{M}_2\text{Na}_2\}$. Na atoms are shown in red, Ag – green, atoms of statistical mixture Sn/Ag – in violet. The displacement ellipsoids are drawn at a 90 % probability level.

Table 3.16 Interatomic distances between the atoms of the respective shells in cluster A' and B in the compound $\text{Na}_{230.45}\text{Ag}_{274}\text{Sn}_{136}$

Atom types		Distance range(Å)	
		Cluster A'	Cluster B
Central atom	–Shell 1	2.7438(8)-2.7734(6)	2.92(1)-3.523(6)
Shell 1	–Shell 1	2.8934(6)-2.9198(7)	2.756(1)-3.47(1)
Shell 2	–Shell 2	3.541(3)-3.567(3)	3.542(3)-3.710(4)
Shell 3	–Shell 1	2.7148(8)-2.7361(8)	2.7518(8)-3.16(2)
Shell 3	–Shell 4	2.7698(8)-3.2166(7)	2.865(1)- 3.003(1)
Shell 4	–Shell 4	2.8733(6)-3.1084(8)	2.7336(8)-2.982(1)

Table 3.17 Selected interatomic distances in the compound $\text{Na}_{230.45}\text{Ag}_{274}\text{Sn}_{136}$. For the details see Table 6.3 (Appendix).

Atom types		Distance range(Å)	Atom types		Distance range(Å)
Sn	-Ag	2.7148(8)-3.2166(7)	Na	-Sn	3.071(3)-3.473(2)
Sn	-M	2.716(1)-3.003(1)	Na	-Ag	3.00(1)- 3.65(1)
Sn	-N	3.2253(8)-3.378(3)	Na	-M	3.196(3)-3.459(3)
M	-M	2.8861(9)-2.9773(8)	Na	-N	3.469(5)-3.942(3)
N	-N	3.106(3)-3.453(2)	Na	-Na	3.541(3)-3.710(4)
Ag	-M	2.7438(8)-3.23(1)			
Ag	-N	2.993(1)-3.444(5)			
Ag	-Ag	2.756(1)-3.21(1)			

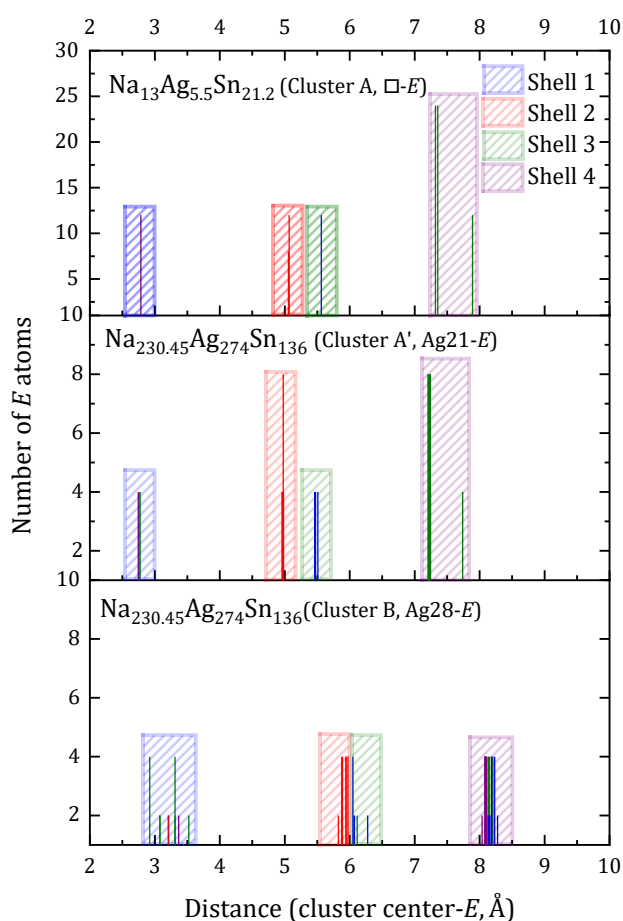


Figure 3.28 Comparison of the distances from the center of the cluster to elements, building the respective shell (E) for the $\text{Na}_{13}\text{Ag}_{5.5}\text{Sn}_{21.2}$ (center of the cluster is empty, site $2e$) and both clusters in $\text{Na}_{230.45}\text{Ag}_{274}\text{Sn}_{136}$ (center of the clusters: Ag21 and Ag28, sites $2b$ and $4i$, respectively). E -Ag distances are shown with a green line, E -M – violet, E -Sn – blue, E -N – brown, E -Na – red.

Discussion

Defining isomorphous to the $\text{Mg}_{32}(\text{Zn,Al})_{49}$ (first representative of the Bergman phases [89]), compounds as fullerane-like metal cages filled with smaller units – ‘shells’ was suggested by Sevov and Corbett in 1993 after obtaining ternary compounds $\text{Na}_{96}\text{In}_{97}\text{Z}_2$ ($Z = \text{Ni, Pd, Pt}$) [91] and $\text{Na}_{172}\text{In}_{197}\text{Z}_2$ ($Z = \text{Ni, Pd, Pt}$) [92]. This gave a start to a rapidly developing class of carbon-free condensed structures in solid-state intermetallic compounds. Later, in 1994, the term “fullercages” or “fulleranes” was introduced by Nesper [93].

Such clustering is very often observed in binary alkali (alkali earth) metal compounds with group 13 and 14 elements and ternary compounds of mentioned elements with transition metal as the third component. The detailed analysis of this group of compounds allows to classify several cluster types, as it is suggested in Table 3.18 and visualized in Figure 3.29. Examples of phases that contain such clusters are listed in Table 3.19.

The first and the most common class of the endohedral fullerane clusters are featuring empty inner icosahedron (shell 1), encapsulated in dual pentagonal dodecahedron of alkali metal atoms (shell 2). Atoms of the inner icosahedron form exo-bonds to the atoms of the shell 3, a larger icosahedron. Finally, a 60-atom polyhedron form shell 4. As a result, the type I polyhedron can be represented as $\{\square @M_{12}@A_{20}@M_{12}@M_{60}\}$ ($M =$ group 13/14 elements and/or transition metal, $A =$ alkali/alkali earth metal). Such a structure is formed by quite diverse ternary compounds: cubic phases $\text{Li}_{13}\text{Zn}_{6.5}\text{Al}_{20.5}$ [94] $\text{Li}_8\text{Mg}_5\text{Zn}_{10.5}\text{Al}_{16.5}$ [94] $\text{Li}_{12.21}\text{Cu}_{4.21}\text{Al}_{23.58}$ [95] $\text{Na}_{26}\text{Au}_{19.53}\text{Ga}_{34.47}$ [70] $\text{Na}_{13}(\text{Cd}_{0.7}\text{Tl}_{0.3})_{27}$ [96] $\text{Li}_{13}(\text{Cu}_{0.53}\text{Si}_{0.47})_{27}$ [71] $\text{Na}_{13}\text{Cd}_{20}\text{E}_7$ ($E = \text{Sn, Pb}$) [97]; hexagonal $\text{Na}_7\text{Ga}_{13}$ [98] and related compounds $\text{Na}_{17}\text{Zn}_{12}\text{Ga}_{40.5}$ [85], $\text{K}_{34}\text{Zn}_{13.07}\text{In}_{89.95}$ [99], $\text{Na}_{34}\text{Zn}_{66}\text{Sn}_{38}$ [75], $\text{Na}_{17}\text{Cu}_6\text{Ga}_{46.5}$ [86] and $\text{K}_{34}\text{Au}_{8.81}\text{In}_{96.19}$ [99]; orthorhombic isostructural $\text{Na}_{22}\text{Ga}_{39}$ [100] and $\text{Na}_{22}\text{Zn}_{20}\text{Sn}_{19}$ [75], as well as $\text{Na}_{16}\text{Zn}_{13.54}\text{Sn}_{13.46}$ [75] and $\text{Na}_{128}\text{Au}_{81}\text{Ga}_{275}$ [101]. To this group belongs also the new Cluster A in the $\text{Na}_{13}\text{Ag}_{5.5}\text{Sn}_{21.2}$.

A second class comprises an endohedrally filled icosahedron as inner shell and thus can be described as $\{M @M_{12}@A_{20}@M_{12}@M_{60}\}$ ($M =$ group 13/14 elements and/or transition metal, $A =$ alkali/alkali earth metal) and occurs in the first representative, $\text{Mg}_{32}(\text{Al,Zn})_{49}$ [89]. It is also present in gold compounds with group 14 elements: $\text{Na}_{52}\text{Au}_{80}\text{Ge}_{30}$ [102], $\text{Na}_{26}\text{Au}_{40}\text{Ge}_{15}$ [70], $\text{Na}_{30}\text{Au}_{39}\text{Sn}_{12}$ [102], $\text{Na}_{26}\text{Au}_{39.83}\text{Sn}_{15.17}$ [70]. The number of compounds containing this type of clusters is limited because in general, it is not common for the inner icosahedron to be centered. Cluster A' in $\text{Na}_{230.45}\text{Ag}_{274}\text{Sn}_{136}$ expands this class including for the first time element silver.

The third type of clusters appears in compounds $\text{Na}_{4.8}\text{Mg}_{8.2}\text{Zn}_{17}\text{Al}_{10}$ ^[103], $\text{Li}_{13}\text{Cu}_6\text{Ga}_{21}$ ^[104] and $\text{Li}_{13}\text{Ni}_9\text{Si}_{18}$ ^[71], where the icosahedron $\{M_{12}\}$ is centered by an octahedron $\{M_6\}$, instead of the single atom in the cluster type II, and the whole cluster can be described as $\{M_6@M_{12}@A_{20}@M_{12}@M_{48}\}$, M = group 13/14 elements and/or transition metal, A = alkali/alkali earth metal.

In type IV cluster the inner shell is formed by the 18-atom core (18-atom deltahedron), encapsulated in a cage of 32 alkali metal atoms (shell 2) and the elongated icosahedron (shell 3). The outer shell of the cluster is an 84-atom fullerene, resulting in $\{A@M_{18}@A_{32}@M_{12}@M_{84}\}$, where M = group 13/14 elements and/or transition metal, A = alkali/alkali earth metal. Together with the cluster type I it appears in the structure of $\text{Na}_{49}\text{Cd}_{58.34}\text{Sn}_{37.69}$ ^[76].

In compound $\text{K}_{21.33}\text{In}_{39.67}$ ^[105] an In-centered cluster $\{E@M_{16}@A_{28}@M_{16}@M_{84}\}$ (M = group 13/14 elements and/or transition metal, A = alkali/alkali earth metal, E = any of the three elements) with the inner shell containing 16 In atoms (Frank-Kasper polyhedron, shell 1), encapsulated in 28 alkali metal atoms (shell 2) and with the exo-bonds forming 16 atom shell 3. The outer shell contains 84 atoms. The same polyhedra, $\{E@M_{16}@A_{28}@M_{16}@M_{84}\}$, together with the type I polyhedra form isostructural $\text{K}_{17}\text{In}_{41}$ ^[106] and $\text{Na}_{17}\text{In}_{12}\text{Ga}_{29}$ ^[107], as well as $\text{Na}_{35}\text{Cd}_{24}\text{Ga}_{56}$ ^[108], $\text{Na}_{36}\text{Ag}_7\text{Ga}_{73}$ ^[84], $\text{Li}_{58}\text{Cd}_{16}\text{Ga}_{128}$ ^[109] and $\text{K}_{39}\text{In}_{80}$ ^[110].

Since atoms in complex intermetallic phases are frequently disordered and/or show defects, their structures have often deviations from the ideal shape of the polyhedra. The last two clusters: type VI $\{A@M_{16}@A_{24}@M_{16}@M_{73}\}$ and type VII $\{A@M_{16}@A_{30}@M_{14}@M_{76}\}$ (M = group 13 elements and/or transition metal, A = alkali metal), both are slightly distorted deviations of the cluster type V, and, together with the cluster type I, appear in $\text{Li}_{68}\text{Zn}_{16}\text{Ga}_{133}$ ^[111] and $\text{Na}_{15}\text{In}_{27.4}$ ^[112], respectively.

Table 3.18 Classification of the endohedral fullerene clusters according to their composition (A = s -metal, M = p - or d - metal, E = s - or p -metal).

Cluster Type	Cluster composition
Type I	$\square@M_{12}@A_{20}@M_{12}@M_{60}$
Type II	$M@M_{12}@A_{20}@M_{12}@M_{60}$
Type III	$M_6@M_{12}@A_{20}@M_{12}@M_{48}$
Type IV	$A@M_{18}@A_{32}@M_{12}@M_{84}$
Type V	$E@M_{16}@A_{28}@M_{16}@M_{84}$
Type VI	$A@M_{16}@A_{24}@M_{16}@M_{73}$
Type VII	$A@M_{16}@A_{30}@M_{14}@M_{76}$

Table 3.19 Intermetallic compounds, the structure of which can be presented as endohedral fullerene clusters.

Compound	Pearson's Symbol	Space Group	Site (cluster center)	Cluster	Ref .
Mg ₃₂ (Al,Zn) ₄₉ Na ₅₂ Au ₈₀ Ge ₃₀ Na ₃₀ Au ₃₉ Sn ₁₂ Na ₂₆ Au ₄₀ Ge ₁₅ Na ₂₆ Au _{39.83} Sn _{15.17}	<i>cI162</i>			Type II	[89] [102] [102] [70] [70]
Li ₁₃ Zn _{6.5} Al _{20.5} Na ₂₆ Au _{19.53} Ga _{34.47}					[94] [70]
Li ₁₃ (Cu _{0.53} Si _{0.47}) ₂₇ Li _{12.21} Cu _{4.21} Al _{23.58} Na ₁₃ Cd ₂₀ E ₇ (E – Sn, Pb) Li ₈ Mg ₅ Zn _{10.5} Al _{16.5} Na ₁₃ (Cd _{0.7} Tl _{0.3}) ₂₇ Li ₁₃ Cu ₆ Ga ₂₁ Na _{4.8} Mg _{8.2} Zn ₁₇ Al ₁₀ Li ₁₃ Ni ₉ Si ₁₈	<i>cI160</i>	<i>Im</i> $\bar{3}$	<i>2a</i>	Type I	[71] [95] [97] [94] [96]
K ₁₇ In ₄₁ Na ₁₇ In ₁₂ Ga ₂₉ Na ₃₅ Cd ₂₄ Ga ₅₆ Na ₃₆ Ag ₇ Ga ₇₃					[104] [103] [71]
K ₁₇ In ₄₁ Na ₁₇ In ₁₂ Ga ₂₉ Na ₃₅ Cd ₂₄ Ga ₅₆ Na ₃₆ Ag ₇ Ga ₇₃	<i>cF464</i>	<i>Fd</i> 3- <i>m</i>	<i>8a</i> <i>16d</i>	Type V Type I	[106] [107] [108] [84]
Li ₅₈ Cd ₁₆ Ga ₁₂₈					[109]
Li ₆₈ Zn ₁₆ Ga ₁₃₃	<i>hP</i> (212-2)	<i>P</i> $\bar{3}$ 1 <i>c</i>	<i>2b</i> <i>4f</i>	Type I Type VI	[111]
K ₃₉ In ₈₀	<i>hP</i> 238	<i>P</i> 3- <i>m</i> 1	<i>1a</i> <i>1b</i> <i>2d</i>	Type I Type I Type V	[110]
K _{21.33} In _{39.67} Na ₇ Ga ₁₃					[105] [98]
K ₃₄ Au _{8.81} In _{96.19} K ₃₄ Zn _{13.07} In _{89.95} Na ₃₄ Zn ₆₆ Sn ₃₈ Na ₁₇ Cu ₆ Ga _{46.5} Na ₁₇ Zn ₁₂ Ga _{40.5}	<i>hR</i> 417	<i>R</i> $\bar{3}$ <i>m</i>	<i>3b</i>	Type I	[99] [99] [75] [86] [85]
Na ₄₉ Cd _{58.34} Sn _{37.69}					[76]
Na ₂₂ Ga ₃₉ Na ₂₂ Zn ₂₀ Sn ₁₉	<i>oP</i> 244	<i>Pnma</i>	<i>4a</i> <i>4c</i>	Type I	[100] [75]
Na ₁₅ In _{27.4}					[112]
Na ₁₆ Zn _{13.54} Sn _{13.46} Na ₁₂₈ Au ₈₁ Ga ₂₇₅	<i>oI</i> 344 <i>oF</i> 968	<i>Ibam</i> <i>Fmmm</i>	<i>4c</i> <i>4b</i>	Type I Type I	[75] [101]

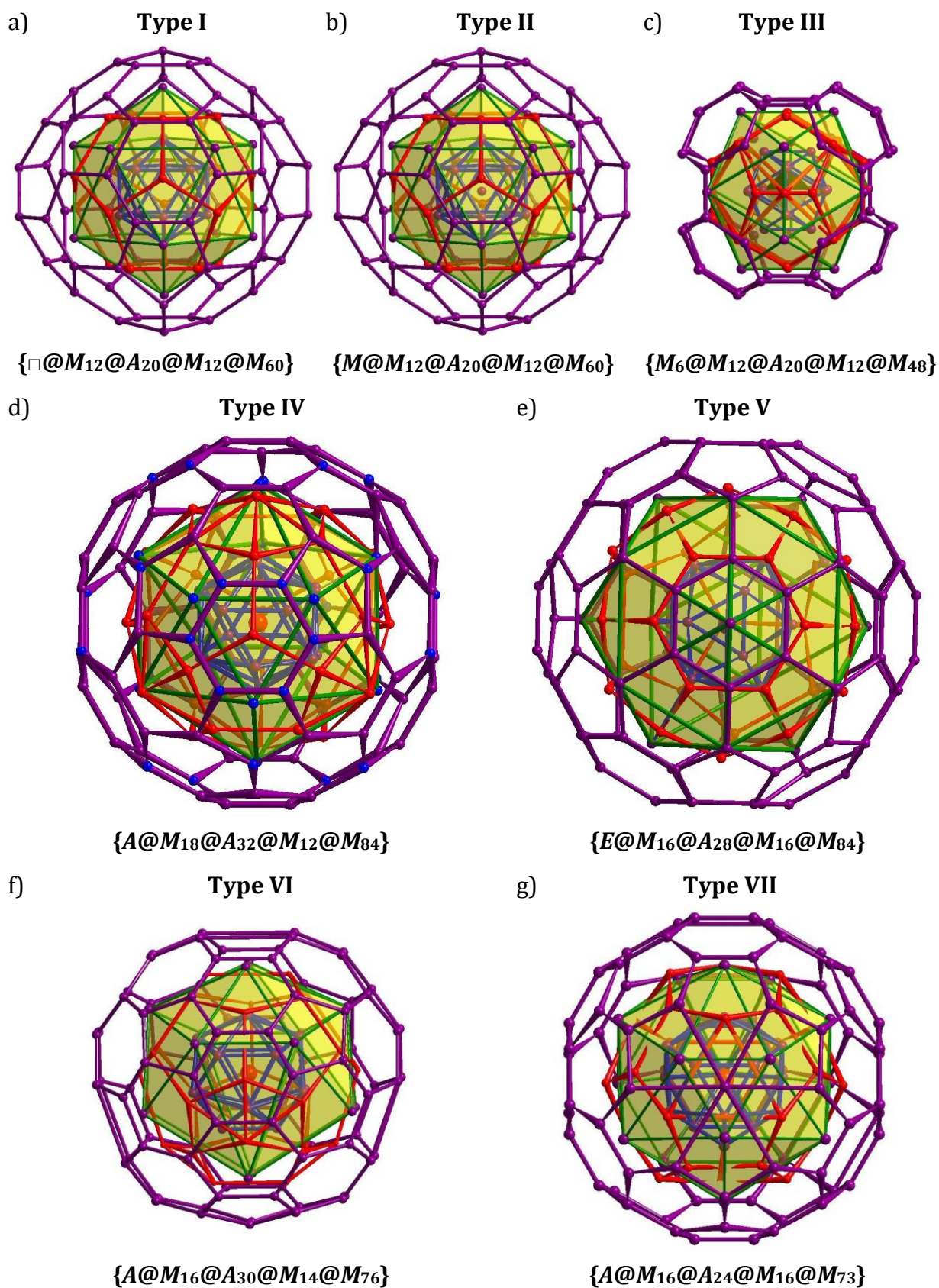


Figure 3.29 Seven types of the endohedral clusters in binary and ternary phases in the systems $A-Tr$, $A-M-Tr$ and $A-M-Tt$ ($A = Li, Na, K$; $Tr = Al, Ga, In$; $Tt = Si, Ge, Sn$; $M = Ni, Cu, Ag, Au, Zn, Cd$).

Cluster B in $\text{Na}_{230.45}\text{Ag}_{274}\text{Sn}_{136}$ described as $\{M@E_{4+x}@E_{30}@M_{12}@M_{80}\}$ is the first representative of a new type of fullerene clusters. It introduces a possibility of formation of the 80 atom polyhedra, along with 48-atom (type III), 60-atom (type I and II), 84 atom (type IV and V) as ordered outer shell. Another feature of this cluster, namely the of ability silver atoms to form statistical mixtures with both tin and sodium atoms is unique in $\text{Na}_{230.45}\text{Ag}_{274}\text{Sn}_{136}$. It is very common that transition metal in the compounds with fullerene clusters forms statistical mixtures with the *p*-block elements (Table 3.20), but mixing between alkali and *d*-metals were observed up to now only in $\text{Na}_{30}\text{Au}_{39}\text{Sn}_{12}$ [70].

Table 3.20 Formation of the statistical mixtures between *d*-metals and *p*-elements.

Atoms	Compound	Ref.
Ni/Si	$\text{Li}_{13}\text{Ni}_9\text{Si}_{18}$	[71]
Cu/Al	$\text{Li}_{12.21}\text{Cu}_{4.21}\text{Al}_{23.58}$	[95]
Cu/Ga	$\text{Li}_{13}\text{Cu}_6\text{Ga}_{21}$	[104]
	$\text{Na}_{17}\text{Cu}_6\text{Ga}_{46.5}$	[86]
Cu/Si	$\text{Li}_{13}(\text{Cu}_{0.53}\text{Si}_{0.47})_{27}$	[71]
Zn/Al	$\text{Li}_{13}\text{Zn}_{6.5}\text{Al}_{20.5}$	[94]
	$\text{Na}_{4.8}\text{Mg}_{8.2}\text{Zn}_{17}\text{Al}_{10}$	[103]
Zn/Ga	$\text{Li}_{68}\text{Zn}_{16}\text{Ga}_{133}$	[111]
	$\text{Na}_{17}\text{Zn}_{12}\text{Ga}_{40.5}$	[85]
Zn-In	$\text{K}_{34}\text{Zn}_{13.07}\text{In}_{89.95}$	[99]
Zn-Sn	$\text{Na}_{34}\text{Zn}_{66}\text{Sn}_{38}$	[75]
	$\text{Na}_{22}\text{Zn}_{20}\text{Sn}_{19}$	
	$\text{Na}_{16}\text{Zn}_{13.54}\text{Sn}_{13.46}$	
Ag/Ga	$\text{Na}_{36}\text{Ag}_7\text{Ga}_{73}$	[84]
Cd/Ga	$\text{Na}_{35}\text{Cd}_{24}\text{Ga}_{56}$	[108]
	$\text{Li}_{58}\text{Cd}_{16}\text{Ga}_{128}$	[109]
Cd/Sn	$\text{Na}_{49}\text{Cd}_{58.34}\text{Sn}_{37.69}$	[76]
Cd/Tl	$\text{Na}_{13}(\text{Cd}_{0.7}\text{Tl}_{0.3})_{27}$	[96]
Au/Ga	$\text{Na}_{26}\text{Au}_{19.53}\text{Ga}_{34.47}$	[70]
	$\text{Na}_{128}\text{Au}_{81}\text{Ga}_{275}$	[101]
Au/In	$\text{K}_{34}\text{Au}_{8.81}\text{In}_{96.19}$	[99]
Au/Ge	$\text{Na}_{26}\text{Au}_{40.93}\text{Ge}_{14.07}$	[70]
	$\text{Na}_{52}\text{Au}_{80}\text{Ge}_{30}$	[102]
Au/Sn	$\text{Na}_{26}\text{Au}_{39.83}\text{Sn}_{15.17}$	[102]
Au/Na	$\text{Na}_{30}\text{Au}_{39}\text{Sn}_{12}$	[70]
	$(\text{Na}_{60}\text{Au}_{78}\text{Sn}_{24})$	

3.1.3 Na₅Ag_{3.74}Sn_{8.26}: a Compound with an Open Sn/Ag Anionic Framework

Synthesis and Characterization

Sample with the composition 'Na₅Ag₄Sn₈' was prepared in two steps: (1) pre-melting 144.2 mg of Ag and 317.4 mg of Sn into a 'Ag₄Sn₈' reguli and (2) temperature treatment of the binary reguli together with 38.4 mg of elemental Na in a sealed niobium ampoule. Applied temperature program: heating up to 800°C and tempered for 12 hours; cooling with rate of 0.1 °C/min to 450 °C and tempering for another 64 hours; finally, cooling down to room temperature with a cooling rate of 1 °C/min. After the synthesis ampoule was opened in an argon atmosphere. The obtained product was a lustrous silver powder, sensitive to air and moisture. PXRD analysis of the sample (Figure 3.30) showed the presence of the new orthorhombic phase together with Na₂₉Ag₂₁Sn₃₉. Single crystals, picked from the sample 'Na₅Ag₄Sn₈' were measured using a Stoe Stadivari diffractometer. Corrections of the raw data for background, polarization, and Lorentz effects were applied. Due to a Gaussian-shaped primary X-ray beam profile a scaling procedure within LANA was applied along with the numerical absorption correction using X-Red and X-Shape software [43-44]. Due to the pseudo tetragonality ($a \approx c$) the crystal was systematically twinned and the corresponding twin law was considered in the structure refinement. The starting atomic parameters for the Na₅Ag_{2+x}Sn_{10-x} were obtained by Direct Method with the SHELXS-2014[45]. The structure was refined using SHELXL-2014 (full-matrix least-squares on F_o^2)[77] with anisotropic atomic displacement parameters for all atoms. In order to check the composition, the occupancy parameters were refined in separate least-squares cycles.

Due to the tendency of silver atoms to form statistical atom mixtures with tin in Na-Ag-Sn ternary compounds, the occupancy of the Sn positions was checked and the refinement revealed partial substitution of Sn with Ag in all five Sn sites in the compound Na₅Ag_{2+x}Sn_{10-x} (Wyckoff positions 8*d*). Particular free variables with an overall occupancy of 1 were applied to determine the occupation ratio at these positions. Positional and atomic displacement parameters (ADPs) for Ag and Sn were set to be equal at the respective atom sites. The refinement resulted in the ratio 0.82/0.18(6) for Sn1/Ag1 (*M1*) and Sn2/Ag2 (*M2*); 0.86/0.14(6) for Sn3/Ag3 (*M3*) and Sn4/Ag4 (*M4*); 0.76/0.24(6) for Sn5/Ag5 (*M5*), leading to the composition Na₅Ag_{3.7(4)}Sn_{8.2(4)}. No significant residual peaks were observed in the difference electron-density map. The crystallographic data and the structural refinement information are summarized in Table 3.21 and the atomic positions and equivalent isotropic

displacement parameters are listed in Table 3.22 and Table 3.23, respectively. Interatomic distances for $\text{Na}_5\text{Ag}_{3.7(4)}\text{Sn}_{8.2(4)}$ are listed in Table 6.4 (Appendix).

The results of the EDX analysis of the crystal, analyzed by the SCXRD from the sample 'Na₅Ag₄Sn₈' (Table 3.24) reveal the atomic ratio of Na:Ag:Sn is 35:25:40, which is in good agreement with the refined composition of the crystal ($\text{Na}_5\text{Ag}_{3.7}\text{Sn}_{8.2}$) and the sample composition used for the synthesis. The results were obtained from three measurements: two spot and one surface scan.

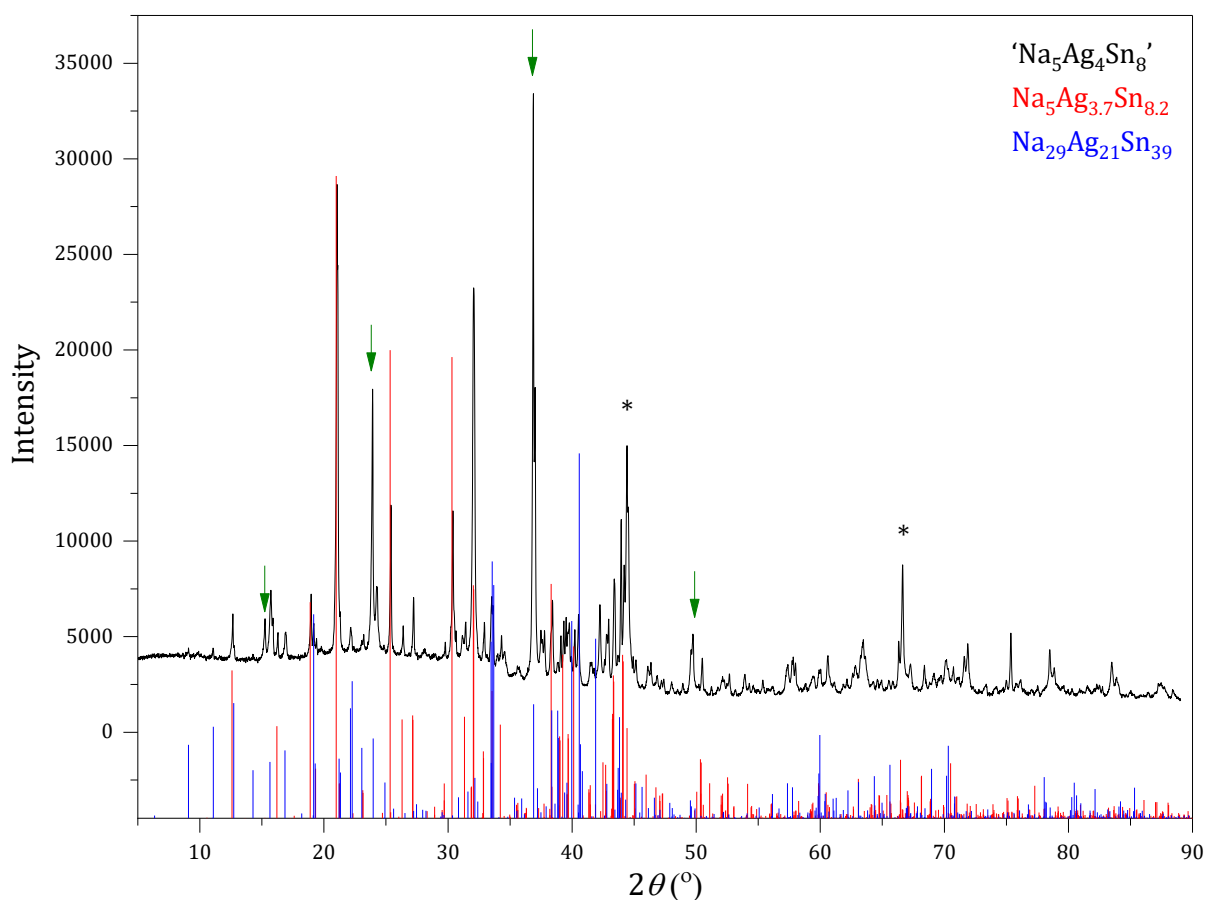


Figure 3.30 Experimental X-ray powder diffractogram of sample 'Na₅Ag₄Sn₈' (black) with the theoretical pattern of $\text{Na}_5\text{Ag}_{3.7(4)}\text{Sn}_{8.2(4)}$ (red) and $\text{Na}_{29}\text{Ag}_{21}\text{Sn}_{39}$ (blue). Diamond (*) as internal standard. With green arrows are marked unindexed reflexes.

Table 3.21 Crystallographic data and data and selected details of structure refinement for the compound $\text{Na}_5\text{Ag}_{3.7(4)}\text{Sn}_{8.2(4)}$.

Formula	$\text{Na}_5\text{Ag}_{3.7(4)}\text{Sn}_{8.2(4)}$
Formula weight ($\text{g}\cdot\text{mol}^{-1}$)	1498.93
Space group	<i>Pbcn</i> (no. 60)
<i>Z</i>	4
Unit cell parameters (\AA)	<i>a</i> = 12.972(1) <i>b</i> = 10.927(1) <i>c</i> = 12.985(1)
Volume (\AA^3)	1840.6(3)
$D_{\text{calcd.}}$ ($\text{g}\cdot\text{cm}^{-3}$)	5.409
Abs. Coeff. (mm^{-1})	14.967
$F(000)$ (e)	37260
Crystal shape/color	block/silver
Temperature (K)	150
θ range (deg)	2.899 – 25.242
Range in <i>hkl</i>	$\pm 18 \pm 15 -17 \div 18$
Reflections collected	37260 ($R_6 = 0.0493$)
Unique reflections	2849 ($R_{\text{int}} = 0.0916$)
Data / parameter	2849/85
GOF on F2	0.936
R_1, wR_2 ($I > 2 \sigma(I)$)	0.0328, 0.0507
R_1, wR_2 (all data)	0.0551, 0.0547
Largest diff. peak/hole ($\text{e}\ \text{\AA}^{-3}$)	1.209 and -1.213

Table 3.22 Atom coordinates and equivalent isotropic displacement parameters (\AA^2) for the compound $\text{Na}_5\text{Ag}_{3.7(4)}\text{Sn}_{8.2(4)}$; *M* = statistical mixture of Sn and Ag.

Atom	Wyck.	S.O.F.	<i>x</i>	<i>y</i>	<i>z</i>	U_{eq}
<i>M1</i>	8 <i>d</i>	0.82/0.18(6)	0.27263(5)	0.23221(5)	0.24968(6)	0.0192(2)
<i>M2</i>	8 <i>d</i>	0.82/0.18(6)	0.41701(6)	0.40980(5)	0.32773(5)	0.0199(2)
<i>M3</i>	8 <i>d</i>	0.86/0.14(6)	0.41963(6)	0.06195(5)	0.16426(5)	0.0203(2)
<i>M4</i>	8 <i>d</i>	0.86/0.14(6)	0.18598(5)	0.35017(5)	0.06710(5)	0.0213(2)
<i>M5</i>	8 <i>d</i>	0.76/0.24(6)	0.49711(6)	0.24450(5)	0.02284(5)	0.0190(2)
Ag6	8 <i>d</i>	1	0.15463(6)	0.13389(5)	0.40864(5)	0.0203(2)
Na1	8 <i>d</i>	1	0.1288(4)	0.0397(4)	0.0969(4)	0.034(1)
Na2	8 <i>d</i>	1	0.1633(4)	0.4433(4)	0.3944(4)	0.037(1)
Na3	4 <i>c</i>	1	0	0.2547(6)	1/4	0.038(1)

Table 3.23 Anisotropic displacement parameters (\AA^2) for $\text{Na}_5\text{Ag}_{3.7(4)}\text{Sn}_{8.2(4)}$. M = statistical mixture of Sn and Ag.

Atom	U_{11}	U_{22}	U_{33}	U_{12}	U_{13}	U_{23}
$M1$	0.0194(4)	0.0197(3)	0.0187(3)	-0.0011(3)	0.0004(3)	0.0006(2)
$M2$	0.0180(3)	0.0231(3)	0.0187(3)	0.0017(2)	-0.0011(2)	-0.0016(3)
$M3$	0.0204(4)	0.0225(3)	0.0180(3)	0.0006(2)	0.0002(2)	0.0015(3)
$M4$	0.0221(4)	0.0198(3)	0.0220(4)	0.0027(2)	-0.0028(2)	-0.0026(3)
$M5$	0.0189(4)	0.0200(3)	0.0183(3)	-0.0004(2)	-0.0006(3)	-0.0006(3)
Ag6	0.0221(4)	0.0198(3)	0.0220(4)	0.0027(2)	-0.0028(2)	-0.0026(3)
Na1	0.034(3)	0.0314(2)	0.037(2)	0.0000(2)	0.008(2)	0.0075(2)
Na2	0.032(3)	0.044(2)	0.036(2)	-0.0119(2)	0.001(2)	-0.006(2)
Na3	0.030(4)	0.049(3)	0.034(4)	0.000	0.005(3)	0.000

Table 3.24 Comparison of the results EDX analysis of the crystal with the refined composition of the compound $\text{Na}_5\text{Ag}_{3.7}\text{Sn}_{8.2}$ from the sample 'Na₅Ag₄Sn₈'.

	Na (at. %)	Ag (at. %)	Sn (at. %)
EDX	35(6)	25(5)	40(5)
$\text{Na}_5\text{Ag}_{3.7}\text{Sn}_{8.2}$	29.6	21.9	48.5

Crystal Structure of the $\text{Na}_5\text{Ag}_{3.74}\text{Sn}_{8.26}$

The compound $\text{Na}_5\text{Ag}_{3.74}\text{Sn}_{8.26}$ is isostructural to the known $\text{Na}_5T_{2+x}\text{Sn}_{10-x}$ ($T = \text{Zn}, \text{Hg}$)^[74] phases and crystallizes in an orthorhombic unit cell with the space group $Pbcn$ with cell parameters $a = 12.972(1)$, $b = 10.927(1)$, and $c = 12.985(1)$ Å. It has a 3-D open framework of Sn and Ag atoms with Na cations located in the voids (Figure 3.31). Selected interatomic distances within the structure of the $\text{Na}_5\text{Ag}_{3.74}\text{Sn}_{8.26}$ are listed in Table 3.25 (all of the distances –Table 6.4, Appendix).

It was shown earlier in this work (Chapter 3.1.2.1 and 3.1.2.2), that in the Na-Ag-Sn ternary system silver is often building statistical mixtures, partially substituting tin in its positions. $\text{Na}_5\text{Ag}_{3.74}\text{Sn}_{8.26}$ is an extreme example of this effect: five out of nine crystallographically independent atomic positions in the structures are occupied by a statistical mixture of tin and silver atoms (positions $M1$, $M2$, $M3$, $M4$ and $M5$), see Table 3.22.

The anionic Ag-Sn framework of $\text{Na}_5\text{Ag}_{3.74}\text{Sn}_{8.26}$ contains covalently bonded Sn and Ag atoms with distorted tetrahedral coordination environments (Figure 3.32, a). This sub-lattice contains two fundamental structural features: a realgarlike $\{M_8\}$ unit and a dimeric fragment $\{M\text{-Ag}\}$. The $\{M_8\}$ unit is built of eight atoms in $8d$ Wyckoff positions: $M1$ $M2$ $M3$ and $M5$, with M - M interatomic distances between 2.876 ($M3$ - $M5$) and 3.051 Å ($M3$ - $M3$). In $\text{Na}_5\text{Zn}_{2.28}\text{Sn}_{9.72}$ Sn-Sn distances within realgarlike units are slightly shorter (2.838-2.987 Å), compared to

Na₅Ag_{3.74}Sn_{8.26}. It can be explained by larger (20 %) covalent radii for Ag compared to Zn and higher content of transition metal in the respective compound.

Dimeric fragment {*M*-Ag} contains *M*₄ and the only fully occupied with Ag₆ silver atoms, with $d_{M_4-Ag_6} = 2.922 \text{ \AA}$. Both units are interconnected in the [101] direction to form a sheet with a {*M*-Ag}: {*M*₈} ratio of 2:1, as shown in Figure 3.33 c and distances of 2.905 and 2.785 Å for *M*₄-*M*₅ and *M*₁-Ag₆ respectively.

The stacking of the anionic sheets with the shift of 1/2 along the [101] direction in Na₅Ag_{3.74}Sn_{8.26} allows further connections along the [010] direction through the *M*₃-*M*₄ and *M*₂-Ag₆ bonds with distances of 2.970 and 2.822 Å, respectively. This results in a 3-D framework, with direct connections between cages and dimers, but no interaction within the fragments of the same sort. A related structure has the Zintl phase NaSn₂ [59], Figure 3.34, where realgar-type {Sn₈} units are forming a two-dimensional network, with layers separated by sodium atoms.

The anionic substructure of the Na₅Ag_{3.74}Sn_{8.26} can be constructed by connecting the {*M*-Ag} fragments between the {Sn₈} units of the NaSn₂ and increasing the dimensionality of the structure to a three-dimensional network, which is expected while introducing electron-poor Ag to the Na-Sn binary system.

The sodium atoms in three crystallographically independent positions are, as expected, occupying the voids of the anionic sub-structure and forming cationic sub-lattice of Na₅Ag_{3.74}Sn_{8.26} (Figure 3.32, b). Na₁ and Na₂ atoms (both in position 8*d*) are forming {Na₄} tetrahedra around Na₄ atom (4*c*) interconnected through Na₁-Na₂ bonds and result in a two-dimensional network (Figure 3.33, b, d).

Table 3.25 Selected interatomic distances in the compound Na₅Ag_{3.74}Sn_{8.26}. For the details, see Table 6.4 (Appendix).

Atom types		Distance range(Å)	Atom types		Distance range(Å)
<i>M</i>	- <i>M</i>	2.8755(9)-3.051(1)	Na	- <i>M</i>	3.195(5)-3.494(5)
Ag	- <i>M</i>	2.785(1)-2.922(1)	Na	-Ag	3.112(5)-3.388(4)
			Na	-Na	3.500(6)-3.503(6)

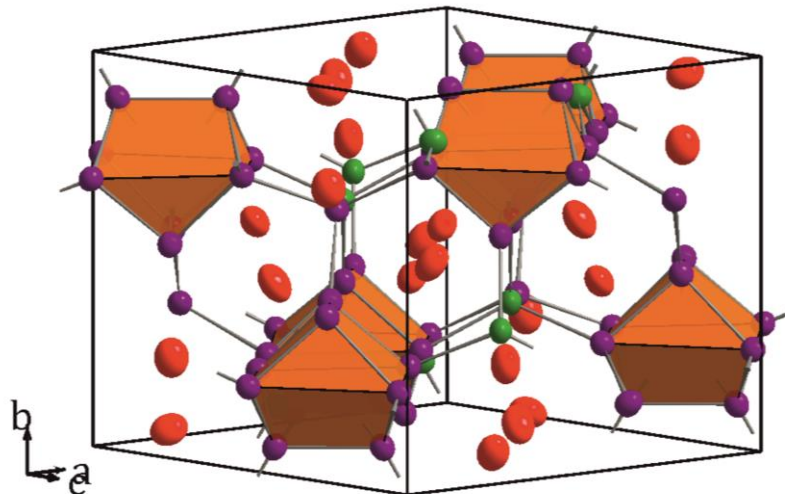


Figure 3.31 Crystal structure of the compound $\text{Na}_5\text{Ag}_{3.74}\text{Sn}_{8.26}$ within one unit cell. Na atoms are shown in red, Ag – green, atoms of statistical mixture Sn/Ag – in violet. The thermal ellipsoids are shown with the 90 % probability level.

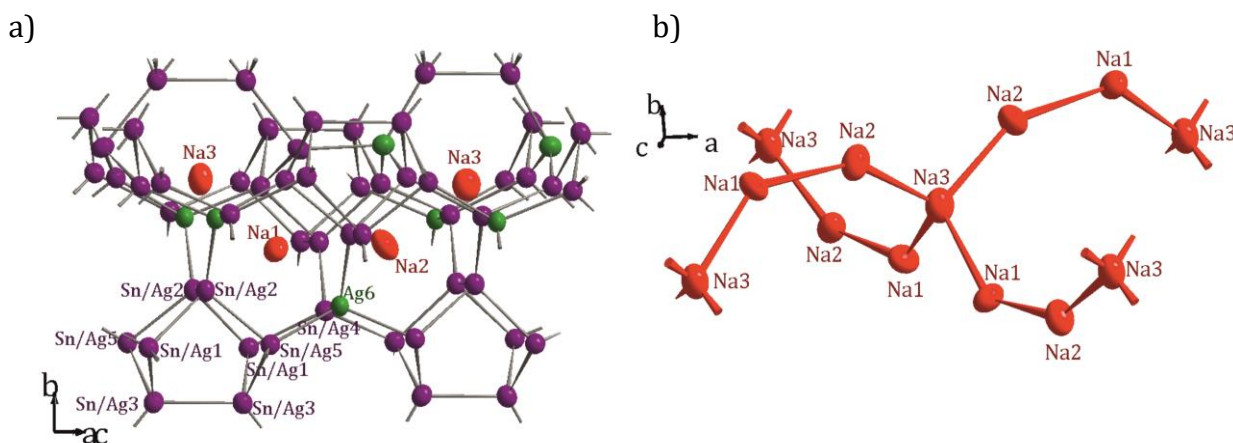


Figure 3.32 Structural fragment of anionic (a) and cationic (b) and sub-lattice in $\text{Na}_5\text{Ag}_{3.74}\text{Sn}_{8.26}$. Na4-centered $\{\text{Na}_4\}$ tetrahedra interconnected through Na1-Na2 bonds. Na atoms are shown in red, Ag – green, atoms of statistical mixture Sn/Ag – in violet. The thermal ellipsoids are shown with the 90 % probability level.

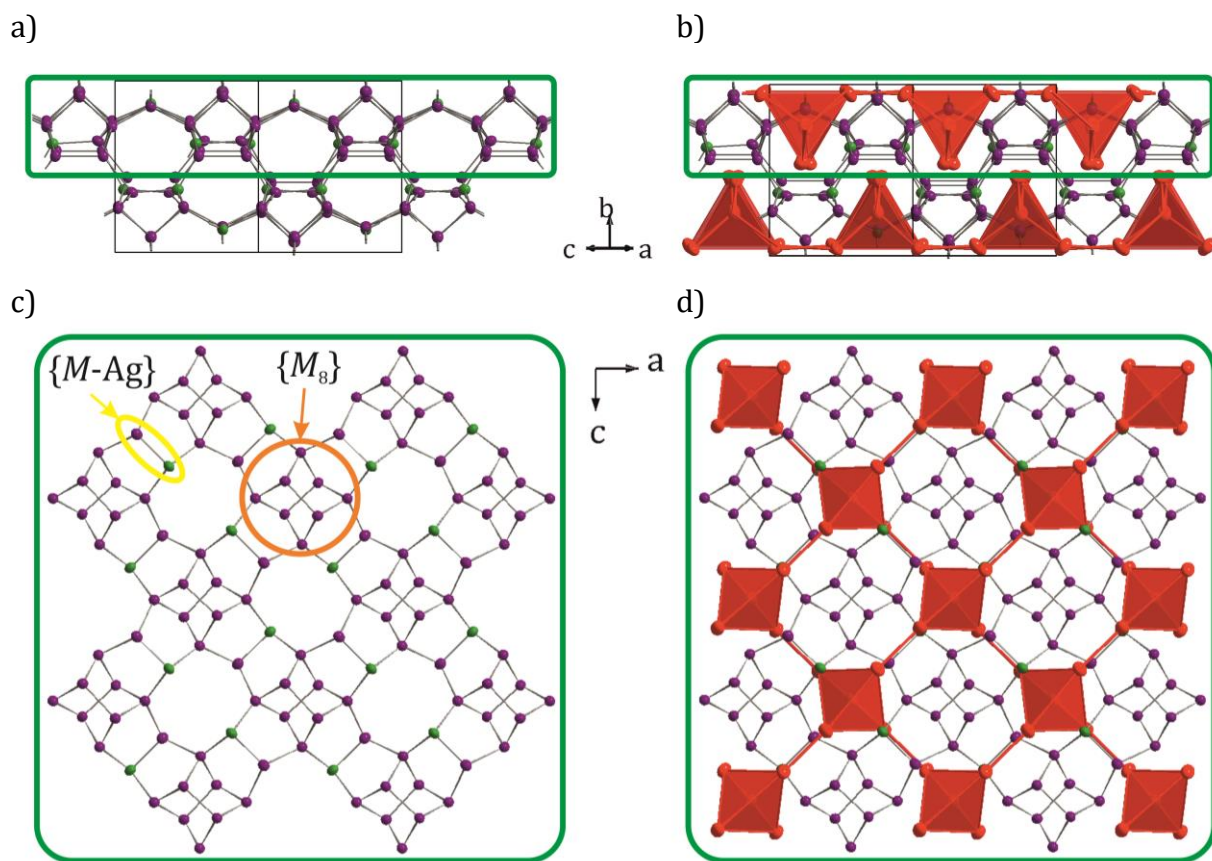


Figure 3.33 Two-dimensional structural fragment of the anionic network in $\text{Na}_5\text{Ag}_{3.74}\text{Sn}_{8.26}$ (a, c) and interplay of cationic and anionic frameworks (b, d). Realgarlike $\{M_8\}$ unit is marked with orange circle, dimeric fragment $\{M\text{-Ag}\}$ – yellow ellipse, $\{\text{Na}@Na_4\}$ tetrahedra are shown in red. Color coding of the atom types: Na – red, Ag – green, Sn/Ag – violet.

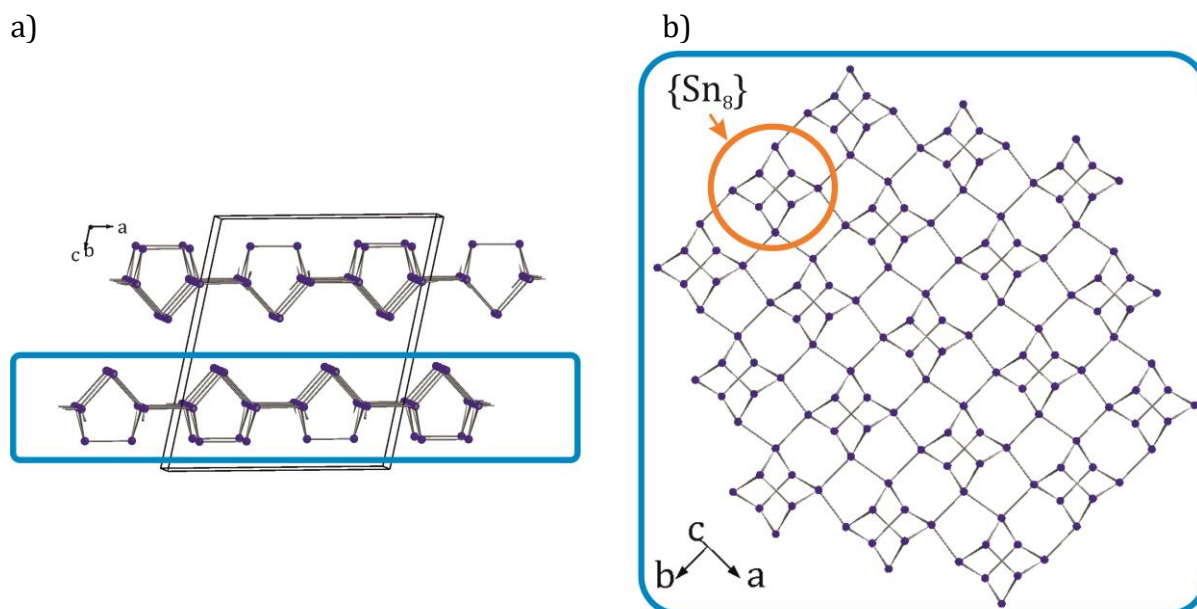


Figure 3.34 Anionic structure of the binary compound NaSn_2 [59] (a) with the layers containing realgarlike $\{\text{Sn}_8\}$ fragments (marked with orange circle). Sn atoms are shown in blue.

Electronic Structure

The electronic structure calculations were performed on the structural model based on the single crystal data refinement with the TB-LMTO-ASA method [51]. Because in the crystal structure of the $\text{Na}_5\text{Ag}_{3.74}\text{Sn}_{8.26}$ five Wyckoff positions are occupied by the statistical mixture of the Sn and Ag atoms, the calculations had to be performed for the hypothetical, fully ordered model, ' $\text{Na}_5\text{Ag}_2\text{Sn}_{10}$ ' where all the positions of the statistical mixture $M1$ - $M5$ are fully occupied only by Sn-atoms (Table 3.26), as it was done in the case of the compound $\text{Na}_{29}\text{Ag}_{21}\text{Sn}_{39}$. This model was chosen because the Ag content in all five positions is below 25%.

Table 3.26 Comparison of the compound $\text{Na}_5\text{Ag}_{3.74}\text{Sn}_{8.26}$ with five positions with Sn/Ag statistical mixture ($M1$ - $M5$) and a hypothetical fully ordered model ' $\text{Na}_5\text{Ag}_2\text{Sn}_{10}$ ' used for the LMTO calculations.

Wyck.	$\text{Na}_5\text{Ag}_{3.74}\text{Sn}_{8.26}$		' $\text{Na}_5\text{Ag}_2\text{Sn}_{10}$ '	
	Atom	S.O.F.	Atom	S.O.F.
8d	$M1$	0.82/0.18(6)	Sn1	1
8d	$M2$	0.82/0.18(6)	Sn2	1
8d	$M3$	0.86/0.14(6)	Sn3	1
8d	$M4$	0.86/0.14(6)	Sn4	1
8d	$M5$	0.76/0.24(6)	Sn5	1

The band structures as well as the density of states (DOS) plot are represented in Figure 3.35. The compound is metallic, although the Fermi level (E_F) for the model compound ' $\text{Na}_5\text{Ag}_2\text{Sn}_{10}$ ' is very close to a deep minimum (pseudo-gap) in the DOS ($273e^-$), which would correspond to the higher Ag content in the $\text{Na}_5\text{Ag}_{2+x}\text{Sn}_{10-x}$ ($x = 0.07$). However, refined by single crystal method composition $\text{Na}_5\text{Ag}_{3.74}\text{Sn}_{8.26}$ ($x = 1.74$) with $317e^-$ lies above the pseudo-gap, which does not help to understand the reason under the formation of the statistical mixtures of Ag and Sn in five atom sites. It seems to be quite similar to the band structures of metallic ' $\text{Na}_{29}\text{Ag}_{14}\text{Sn}_{48}$ ' and ' $\text{Na}_{29}\text{Ag}_{14}\text{Sn}_{48}$ ' (see Figure 3.13, Figure 3.14) with no gaps at Fermi level. Similar to these models, in ' $\text{Na}_5\text{Ag}_2\text{Sn}_{10}$ ' the low-lying bands between -12 and -4 eV predominantly correspond to the Sn s -orbitals. The main contribution to the DOS comes from the d orbitals of Ag, between -6 and -4 eV. Their overlap with p -orbitals of Sn indicates covalent contributions of the Ag-Sn interactions to the stabilization of the structure. The bands (generally Sn- p) cross the Fermi level underlying metallic character for this structural model.

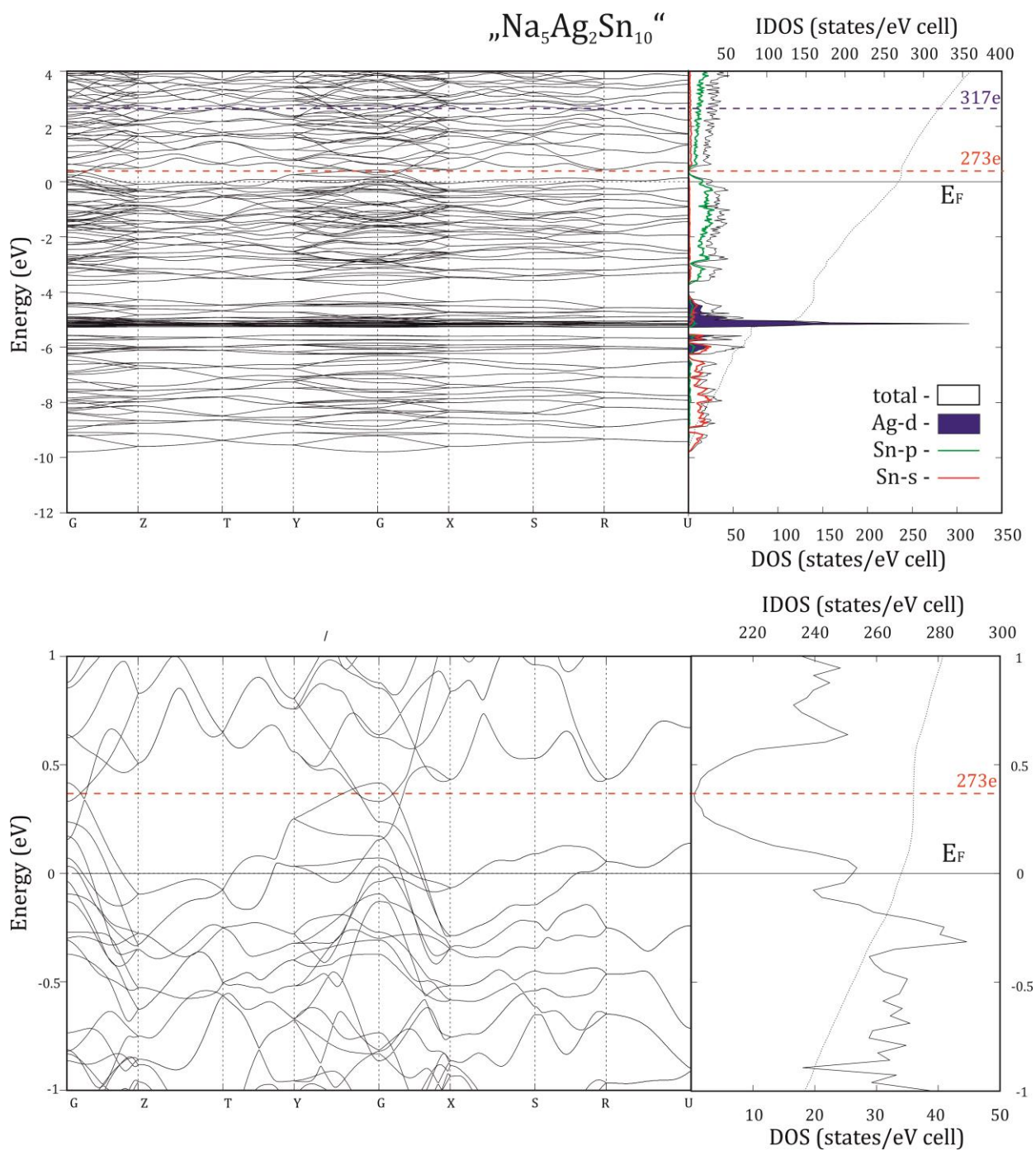


Figure 3.35 The band structures as well as the total Density of States (DOS) with orbital projected DOS calculated for the hypothetical, fully ordered model 'Na₅Ag₂Sn₁₀' (positions M1-M5, 8d are fully occupied by Sn-atoms).

Discussion and Comparison of the Na₅Ag_{3.74}Sn_{8.26} and Isostructural Phases Na₅T_{2+x}Sn_{10-x} (T = Zn, Hg)

All three compounds Na₅Ag_{3.7}Sn_{8.2}, Na₅Zn_{2.28}Sn_{9.72} and Na₅Hg_{2.39}Sn_{9.61} [74] belong to the same structure type. The cell parameters of these phases are compared in Table 3.27. It shows 4 % volume increase of the Ag compound compared to Zn, almost equal to that for the compound with Hg substituting Sn atoms, despite the fact that the measurements were performed at different temperatures (150K for the Na₅Ag_{3.7}Sn_{8.2} and 273 K for both Na₅Zn_{2.28}Sn_{9.72} and Na₅Hg_{2.39}Sn_{9.61}).

Table 3.27 Comparison of the cell parameters of the Na₅Ag_{3.74}Sn_{8.26} (measured at 150 K) with isostructural compounds Na₅T_{2+x}Sn_{10-x} (T = Zn, Hg) [74] (measured at 293 K).

Formula	Na ₅ Ag _{3.7(4)} Sn _{8.2(4)}	Na ₅ Zn _{2.28} Sn _{9.72(2)}	Na ₅ Hg _{2.39} Sn _{9.61(1)}
Unit cell parameters (Å)	<i>a</i> = 12.972(1) <i>b</i> = 10.927(1) <i>c</i> = 12.985(1)	<i>a</i> = 12.722(1) <i>b</i> = 10.804(1) <i>c</i> = 12.777(1)	<i>a</i> = 12.958(1) <i>b</i> = 10.987(1) <i>c</i> = 12.960(1)
Volume (Å ³)	1840.6(3)	1763.1(2)	1844.5(2)

In contrast to Na₅Ag_{3.74}Sn_{8.26}, where silver atoms are forming statistical mixtures with tin in all five positions, in both Na₅Zn_{2.28}Sn_{9.72} and Na₅Hg_{2.39}Sn_{9.61} only one out of five tin positions is partially substituted by T (T = Zn, Hg) atoms (see Table 3.28), which leads to overall lower *d*-metal content in Zn and Hg substituted phases.

Table 3.28 Comparison of the occupancies of the atomic sites within the polyanionic network in Na₅Ag_{3.74}Sn_{8.26} with the respective sites in Na₅T_{2+x}Sn_{10-x} (T = Zn, Hg) [74].

Wyck.	Na ₅ Ag _{3.7(4)} Sn _{8.2(4)}		Na ₅ Zn _{2.28} Sn _{9.72(2)}		Na ₅ Hg _{2.39} Sn _{9.61(1)}	
	Atom	S.O.F.	Atom	S.O.F.	Atom	S.O.F.
8 <i>d</i>	M1	0.82/0.18(6)	Sn1	1	Sn1	1
8 <i>d</i>	M2	0.82/0.18(6)	M2	0.86/0.14(1)	M2	0.805/0.195(5)
8 <i>d</i>	M3	0.86/0.14(6)	Sn3	1	Sn3	1
8 <i>d</i>	M4	0.86/0.14(6)	Sn4	1	Sn4	1
8 <i>d</i>	M5	0.76/0.24(6)	Sn5	1	Sn5	1

According to [74] with the formal charge of 2- of the T atoms (T = Zn, Hg) compound Na₅T_{2+x}Sn_{10-x} can be described as (Na⁺)₅[(4b-Sn⁰)_{10-x}(4b-T²⁻)_{2+x}], and with x = 0.5 the compound would be an electron balanced Zintl phase. This approach is very formal because the charge -2 does not make chemical sense.

With the formal charge of 2+ of the Zn/Hg atoms and x = 0 the electron count is (Na⁺)₅(T²⁺)₂[(3b-Sn⁻)₈(4b-Sn⁰)₂], the structure an excess of one electron. The formation of

the statistical mixture of T/Sn atoms would increase the positive charge through the amount $(T^{2+})_{2+x}$ ions (for Zn $x = 0.28$, for Hg $x = 0.39$) as well as increase negative charge creating additionally 3-bonded Sn^- and 2-bonded Sn^{2-} . Two of the Sn_3 atoms and two of Sn_4 atoms would stay unchanged, with the formal charge 0 and 3-: $(4b-Sn_3^0)$ and $(3b-Sn_4^-)$, whereas Sn_1 and Sn_5 , bonded to Sn_2 could be 3-bonded or 2-bonded: for Zn $(2b-Sn_1/5^{2-})_{0.28}(3b-Sn_1/5^-)_{1.72}$, for Hg $(2b-Sn_1/5^{2-})_{0.39}(3b-Sn_1/5^-)_{1.61}$. Atoms of the M_2 are as well 3- or 2-bonded: for Zn $(2b-Sn_2^{2-})_{1.48}(3b-Sn_2^-)_{0.24}$, for Hg $(2b-Sn_2^{2-})_{1.30}(3b-Sn_2^-)_{0.31}$.

This results in $(Na^+)_5(Zn^{2+})_{2.28}[(2b-Sn^{2-})_{1.76}(3b-Sn^-)_{3.96}(4b-Sn^0)_2]$ for $Na_5Zn_{2.28}Sn_{9.72}$ and $(Na^+)_5(Hg^{2+})_{2.39}[(2b-Sn^{2-})_{1.87}(3b-Sn^-)_{3.85}(4b-Sn^0)_2]$ for $Na_5Hg_{2.39}Sn_{9.61}$. The charge compensation through substituting Sn by Zn or Hg is sufficient to reduce the electron excess in both compounds.

Similarly, for the ordered 'Na₅Ag₂Sn₁₀' with the Ag charge of +1: $(Na^+)_5(Ag^+)_2[(3b-Sn^-)_8(4b-Sn^0)_2]$ ·the structure has an excess of the negative charge of one electron. Because all in all 5 Sn positions statistical mixture is formed the electron count is a lot more complex. It is guided by the same principle, which states that the substitution of Sn by Ag leads to increase of the positive charge through Ag^+ ions, as well as negative charge creating additional not only 3-bonded Sn^- and 2-bonded Sn^{2-} atoms, but also 1- and 0-bonded Sn^{3-} and Sn^{4-} .

3.1.4 Substitution of Sn by Bi in the Na-Sn Binary System

The opposite effect to the substitution Sn in Na-Sn binary phases with electron poor Ag can be performed by introducing electron-rich Bi. Ternary system Na-Sn-Bi is of particular interest because till now there are no evidence in the literature of the existence of ternary phases. It is known, that Bi can stabilize electron deficient compounds, as it was observed in case of the chiral clathrate $K_{6+x}Sn_{25}$, stabilized by Bi in $K_6Sn_{23}Bi_2$ [113].

To get a better understanding of how elements group 15 interact with Na-Sn, compounds in Na-Sn-*Pn* ternary systems were analyzed (Table 3.29, visualized in Figure 3.36). There are only seven compounds known with *Pn* = P, As and Sb. Three-dimensional structures have compounds Na_2SnAs_2 and Na_5SnSb_3 (Figure 3.36, highlighted with green rectangles): in Na_2SnAs_2 [114] tetrahedrally coordinated Sn atoms from $\{Sn_4As_{10}\}$ adamantine-like units, whereas in Na_5SnSb_3 [115] main structural elements can be described as $\{Sn@Sb_4\}$ tetrahedra, interconnected through vertices. Two other compounds, $NaSnP$ [116] and $NaSn_2As_2$ [117] (Figure 3.36, in blue rectangles) have both layered structures, featuring two-dimensional layers, similar to As layers in grey As. Finally, in $Na_{10}Sn_2Pn_6$ [118] (*Pn* = P, As; shown in red rectangles in Figure 3.36) dimeric $\{Sn_2As_6\}^{10-}$ anions are isolated by Na atoms.

Table 3.29 Ternary compounds in the Na-Sn-*Pn* system (*Pn* = P, As, Sb, Bi).

Compound	Space group	Cell parameters			V (Å ³)	Ref.
		<i>a</i> (Å)	<i>b</i> (Å)	<i>c</i> (Å)		
Na_8SnSb_4	$Fd\bar{3}m$	14.816	-	-	3252.32	[115]
$Na_{10}Sn_2P_6$	$P2_1/n$	13.400	7.456	8.289	828.15	[118a]
$Na_{10}Sn_2As_6$	$P2_1/n$	13.716	7.642	8.527	893.77	[118b]
Na_5SnSb_3	$P2_1/c$	18.5940	9.181	12.493	2110.36	[115]
Na_2SnAs_2	$I4_1/acd$	14.166	14.166	21.191	4252.52	[114]
$NaSnP$	$P6_3mc$	3.880	-	11.667	152.11	[116]
$NaSn_2As_2$	$R\bar{3}m$	4.006	-	27.5810	383.32	[117]

As it was shown for the Na-Ag-Sn ternary system (Chapter 3.1.2), tuning the VEC in the compounds of Na-Sn binary system through including the third component (*d*-block metal) can drastically influence the atomic properties, structure and bonding, leading to the smooth transition from Zintl to polar intermetallic phases. It initiates a radical change of the structure and bonding principles, leading to complex structures.

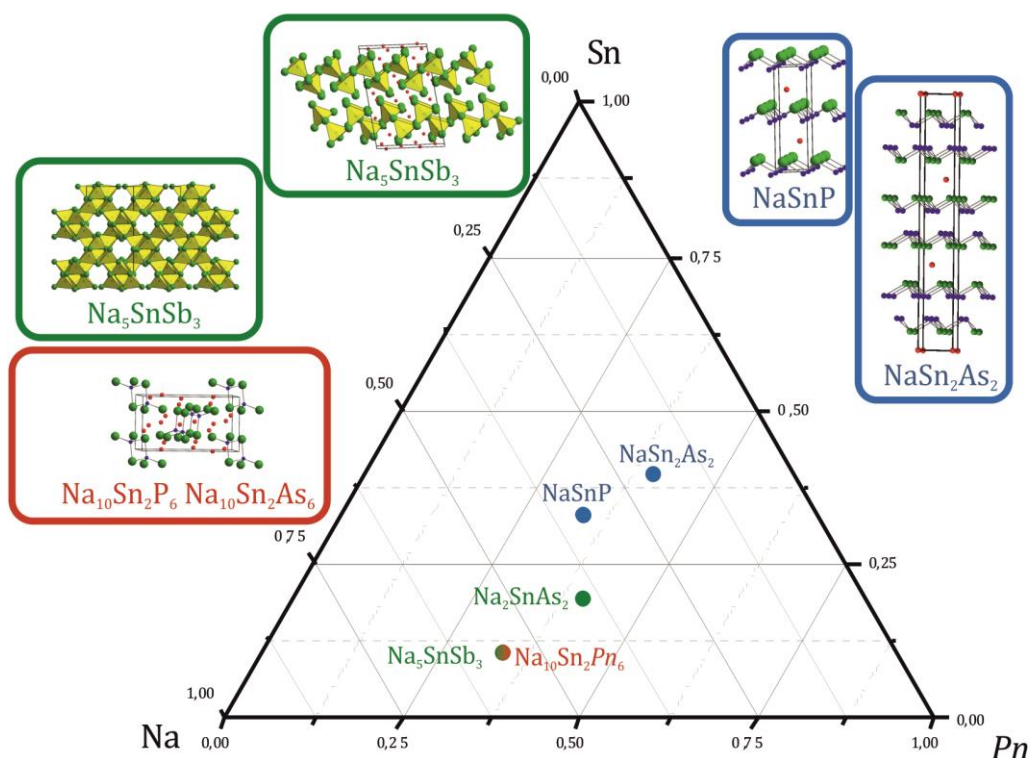


Figure 3.36 Crystal structures of the compounds in the Na-Sn-*Pn* (*Pn* = P, As, Sb, Bi) ternary systems. In red rectangles are phases with isolated fragments, blue – with two-dimensional nets, green – three-dimensional networks built by tetrahedrally coordinated Sn atoms.

In this Chapter the results of the investigation of the influence of the change in VEC in Zintl phases at the border to intermetallics, via the partial substitution of Sn by electron richer Bi to show how dominant the electron count factor is. Because all known compounds are either *Pn*-rich or have Sn:*Pn* ratio 1:1 (Figure 3.36), this work presents the results of the explorational synthesis of the Sn-rich compounds.

As the starting points in this search were chosen binary Zintl phases of the Na-Sn system while trying to dope them with the relatively small amount of Bi. The results, presented below (Chapter 3.1.4.1 and 3.1.4.2) are based on the modification of the $\text{Na}_5\text{Sn}_{13}$ ^[60] and $\text{Na}_7\text{Sn}_{12}$ ^[58], both featuring anionic networks where tin atoms are 2-, 3- and 4-bonded.

3.1.4.1 A Zintl Phase $\text{Na}_{13}\text{Sn}_{25.73}\text{Bi}_{1.27}$ Featuring Isolated Bi Atoms Encapsulated in 3-D Tin Network

Doping the Zintl phase $\text{Na}_5\text{Sn}_{13}$ [60], where Sn atoms are either 3- or 4-bonded, with electron rich Bi atoms results in the formation of the compound with multicenter bonding $\text{Na}_{12.73}\text{Sn}_{25.73}\text{Bi}_{1.27}$ [119]. In this Chapter the results of the attempt to reproduce and to characterize this phase more precisely are presented.

Synthesis and Characterization

Sample of the nominal composition 'Na₅Sn₁₂Bi₂' was synthesized from the elements (32.9 mg Na, 407.4 mg Sn and 59.8 mg Bi) in Ta ampoule using a two-step temperature program: (1) heating up to 650°C with the rate of 2°C/min and holding the temperature for 12 hours and (2) slowly cooling down to 270°C (rate 0,1°C/min) and dwelling the sample for 240 hours. The sample was cooled down to room temperature by switching off the oven. The PXRD analysis revealed along the presence of the $\text{Na}_{13}\text{Sn}_{26}\text{Bi}$, unreacted elemental Sn (Figure 3.37).

A block-shaped single crystal very dark, almost black in color was measured using Stoe Stadivari diffractometer. Corrections of the raw data for background, polarization, and Lorentz effects were applied. Due to a Gaussian-shaped primary X-ray beam profile a scaling procedure within LANA was applied along with the numerical absorption correction, extremely important because of the high absorption of Bi atoms, using X-Red and X-Shape software [43-44]. The starting atomic parameters for the $\text{Na}_{13}\text{Sn}_{25.73(2)}\text{Bi}_{1.27(2)}$ were obtained by Direct Method with the SHELXS-2014 [45] in the triclinic space group $P\bar{1}$. The structure was refined using SHELXL-2014 (full-matrix least-squares on F_o^2) [77] – Table 3.30. Atomic coordinated for twenty one crystallographically independent atoms are listed in Table 3.31 and anisotropic displacement parameters for all atoms – in Table 3.32.

Residual electron density at the Sn2 position suggested formation of the statistical mixture of Sn and Bi. The refinement showed the Sn/Bi ratio of 0.864/0.136(8), position M2. Another disorder was found in Bi1 position, which because of the high ADPs was splitted into two 2i positions, refined to the occupancy of 0.5 (Table 3.31). The correlation between occupancy of Na positions and partial occupancy of the position M2 was checked revealing to significant defects in Na positions.

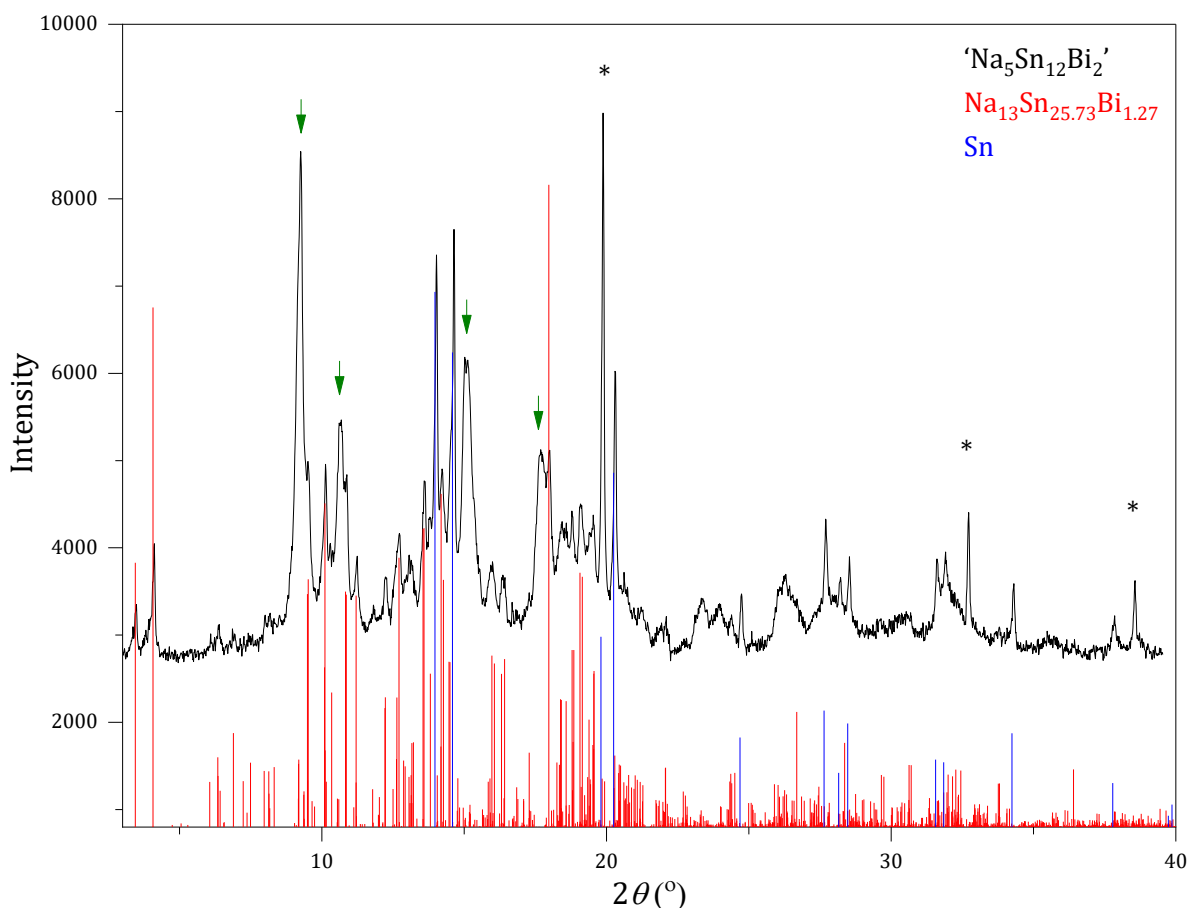


Figure 3.37 Experimental X-ray powder diffractogram of the sample 'Na₅Sn₁₂Bi₂' (black) with the theoretical pattern (red) of Na₁₃Sn_{25.73}Bi_{1.27} end elemental Sn (blue). Diamond (*) was used as internal standard. Unindexed reflections are marked with green arrows.

Table 3.30 Crystallographic data and data and selected details of structure refinement for the compound Na₁₃Sn_{25.73(2)}Bi_{1.27(2)}.

Formula	Na₁₃Sn_{25.73(2)}Bi_{1.27(2)}
Formula weight (g·mol ⁻¹)	3618.17
Space group	<i>P</i> $\bar{1}$ (No. 2)
<i>Z</i>	1
Unit cell parameters (Å)	<i>a</i> = 9.0826(4) <i>b</i> = 11.2527(5) <i>c</i> = 13.2278(6) α = 112.114(4) [°] β = 99.818(4) [°] γ = 101.379(4) [°]
Volume (Å ³)	1182.4(1)
<i>D</i> _{calcd.} (g·cm ⁻³)	5.081
Abs. coeff. (mm ⁻¹)	18.128
<i>F</i> (000) (e)	1535
Crystal shape/color	block/black
Temperature (K)	150
θ range (deg)	3.038–27.498
Range in <i>hkl</i>	±11 ±14 ±17

Reflections collected	42179 ($R_6 = 0.0217$)
Unique reflections	5426 ($R_{\text{int}} = 0.0306$)
Data / parameter	5426/189
GOF on F2	1.303
$R_1, wR_2 (I > 2 \sigma(I))$	0.0379, 0.0913
$R_1, wR_2 (\text{all data})$	0.0482, 0.0936
Largest diff. peak/hole ($e \text{ \AA}^{-3}$)	2.906 and -2.568

Table 3.31 Atom coordinates and equivalent isotropic displacement parameters (\AA^2) for the compound $\text{Na}_{13}\text{Sn}_{25.73(2)}\text{Bi}_{1.27(2)}$, M = statistical mixture of Sn and Bi.

Atom	Wyck.	S.O.F.	x	y	z	U_{eq}
Sn1	2i	1	0.44093(9)	0.43226(8)	0.0090(2)	0.0162(9)
Bi1	2i	0.5	0.5118(1)	0.0132(6)	0.0162(9)	0.0090(2)
$M2$	2i	0.864/0.136(8)	0.36986(8)	0.18593(7)	0.0095(3)	0.0095(3)
Sn3	2i	1	0.5403(1)	0.20270(9)	0.45310(7)	0.0080(2)
Sn4	2i	1	0.2026(1)	0.85338(9)	0.43784(8)	0.0091(2)
Sn5	2i	1	0.0342(1)	0.19197(9)	0.45582(7)	0.0079(2)
Sn6	2i	1	0.3007(1)	0.13760(9)	0.55179(8)	0.0086(2)
Sn7	2i	1	0.5875(1)	0.45092(9)	0.42016(8)	0.0101(2)
Sn8	2i	1	0.1261(1)	0.79320(9)	0.20159(8)	0.0097(2)
Sn9	2i	1	0.5746(1)	0.02976(9)	0.76238(7)	0.0083(2)
Sn10	2i	1	0.9075(1)	0.07131(9)	0.06880(8)	0.0087(2)
Sn11	2i	1	0.3719(1)	0.19887(9)	0.78769(8)	0.0090(2)
Sn12	2i	1	0.0706(1)	0.03159(9)	0.76016(7)	0.0082(2)
Sn13	2i	1	0.4097(1)	0.07286(9)	0.06582(8)	0.0094(2)
Na1	2i	1	0.3649(8)	0.5802(7)	0.2658(6)	0.031(2)
Na2	2i	1	0.2322(7)	0.2782(6)	0.0180(5)	0.021(1)
Na3	2i	1	0.2555(7)	0.2194(7)	0.2680(5)	0.018(1)
Na4	2i	1	0.6676(7)	0.2748(6)	0.0160(5)	0.018(1)
Na5	2i	1	0.7390(7)	0.2216(7)	0.2687(5)	0.019(1)
Na6	2i	1	0.1972(9)	0.4216(7)	0.7357(6)	0.032(2)
Na7	1c	1	0	1/2	0	0.037(3)

Table 3.32 Anisotropic displacement parameters (\AA^2) for the compound $\text{Na}_{13}\text{Sn}_{25.73(2)}\text{Bi}_{1.27(2)}$.

Atom	U_{11}	U_{22}	U_{33}	U_{12}	U_{13}	U_{23}
Bi1	0.0171(2)	0.020(3)	0.020(3)	0.015(2)	0.008(2)	0.008(2)
Sn1	0.0077(4)	0.0081(4)	0.0109(4)	0.0037(3)	0.0025(3)	0.0021(3)
$M2$	0.0084(4)	0.0104(5)	0.0112(5)	0.0059(3)	0.0028(3)	0.0028(3)
Sn3	0.0076(4)	0.0084(4)	0.0080(4)	0.0035(3)	0.0021(3)	0.0023(3)
Sn4	0.0084(4)	0.0123(4)	0.0100(4)	0.0070(4)	0.0035(3)	0.0044(3)
Sn5	0.0079(4)	0.0080(4)	0.0080(4)	0.0038(3)	0.0023(3)	0.0021(3)
Sn6	0.0075(4)	0.0115(4)	0.0086(4)	0.0054(3)	0.0029(3)	0.0034(3)
Sn7	0.0093(4)	0.0091(4)	0.0120(4)	0.0051(4)	0.0024(3)	0.0021(3)
Sn8	0.0094(4)	0.0100(4)	0.0095(4)	0.0035(3)	0.0030(3)	0.0033(3)
Sn9	0.0083(4)	0.0094(4)	0.0064(4)	0.0026(3)	0.0019(3)	0.0026(3)
Sn10	0.0080(4)	0.0092(4)	0.0093(4)	0.0043(3)	0.0025(3)	0.0026(3)
Sn11	0.0092(4)	0.0096(4)	0.0091(4)	0.0048(3)	0.0028(3)	0.0029(3)
Sn12	0.0083(4)	0.0087(4)	0.0066(4)	0.0026(3)	0.0014(3)	0.0022(3)
Sn13	0.0085(4)	0.0102(4)	0.0090(4)	0.0041(3)	0.0019(3)	0.0021(3)

Na1	0.026(4)	0.032(4)	0.021(3)	0.003(3)	0.001(3)	0.004(3)
Na2	0.022(3)	0.019(3)	0.025(3)	0.011(3)	0.009(3)	0.006(3)
Na3	0.010(3)	0.036(4)	0.018(3)	0.015(3)	0.008(2)	0.014(3)
Na4	0.017(3)	0.016(3)	0.022(3)	0.013(3)	-0.001(2)	0.003(2)
Na5	0.010(3)	0.034(4)	0.017(3)	0.015(3)	0.008(2)	0.007(3)
Na6	0.033(4)	0.031(4)	0.025(4)	0.002(3)	0.010(3)	0.011(3)
Na7	0.072(8)	0.017(5)	0.007(4)	-0.001(4)	-0.005(5)	0.004(5)
Bi1	0.0171(2)	0.020(3)	0.020(3)	0.015(2)	0.008(2)	0.008(2)
Sn1	0.0077(4)	0.0081(4)	0.0109(4)	0.0037(3)	0.0025(3)	0.0021(3)
Sn2	0.0084(4)	0.0104(5)	0.0112(5)	0.0059(3)	0.0028(3)	0.0028(3)
Bi2	0.0084(4)	0.0104(5)	0.0112(5)	0.0059(3)	0.0028(3)	0.0028(3)
Sn3	0.0076(4)	0.0084(4)	0.0080(4)	0.0035(3)	0.0021(3)	0.0023(3)
Sn4	0.0084(4)	0.0123(4)	0.0100(4)	0.0070(4)	0.0035(3)	0.0044(3)
Sn5	0.0079(4)	0.0080(4)	0.0080(4)	0.0038(3)	0.0023(3)	0.0021(3)
Sn6	0.0075(4)	0.0115(4)	0.0086(4)	0.0054(3)	0.0029(3)	0.0034(3)
Sn7	0.0093(4)	0.0091(4)	0.0120(4)	0.0051(4)	0.0024(3)	0.0021(3)
Sn8	0.0094(4)	0.0100(4)	0.0095(4)	0.0035(3)	0.0030(3)	0.0033(3)
Sn9	0.0083(4)	0.0094(4)	0.0064(4)	0.0026(3)	0.0019(3)	0.0026(3)
Sn10	0.0080(4)	0.0092(4)	0.0093(4)	0.0043(3)	0.0025(3)	0.0026(3)
Sn11	0.0092(4)	0.0096(4)	0.0091(4)	0.0048(3)	0.0028(3)	0.0029(3)
Sn12	0.0083(4)	0.0087(4)	0.0066(4)	0.0026(3)	0.0014(3)	0.0022(3)
Sn13	0.0085(4)	0.0102(4)	0.0090(4)	0.0041(3)	0.0019(3)	0.0021(3)
Na1	0.026(4)	0.032(4)	0.021(3)	0.003(3)	0.001(3)	0.004(3)
Na2	0.022(3)	0.019(3)	0.025(3)	0.011(3)	0.009(3)	0.006(3)
Na3	0.010(3)	0.036(4)	0.018(3)	0.015(3)	0.008(2)	0.014(3)
Na4	0.017(3)	0.016(3)	0.022(3)	0.013(3)	-0.001(2)	0.003(2)
Na5	0.010(3)	0.034(4)	0.017(3)	0.015(3)	0.008(2)	0.007(3)
Na6	0.033(4)	0.031(4)	0.025(4)	0.002(3)	0.010(3)	0.011(3)
Na7	0.072(8)	0.017(5)	0.007(4)	-0.001(4)	-0.005(5)	0.004(5)
Bi1	0.0171(2)	0.020(3)	0.020(3)	0.015(2)	0.008(2)	0.008(2)
Sn1	0.0077(4)	0.0081(4)	0.0109(4)	0.0037(3)	0.0025(3)	0.0021(3)

Presence of Bi, along with Na and Sn in the new compound was confirmed by EDX analysis (Table 3.33). Significant deviation of the composition according to the EDX results is occurring due to oxidation of the crystal.

Table 3.33 Results of the EDX analysis of the crystal with the refined composition $\text{Na}_{13}\text{Sn}_{25.73}\text{Bi}_{1.27}$ from the sample ' $\text{Na}_5\text{Sn}_{12}\text{Bi}_2$ '.

	Na (at. %)	Sn (at. %)	Bi (at. %)
EDX	39(12)	46(6)	15(6)
$\text{Na}_{13}\text{Sn}_{25.73}\text{Bi}_{1.27}$	32.5	64.3	3.2

Crystal Structure of the $\text{Na}_{13}\text{Sn}_{25.73}\text{Bi}_{1.27}$

$\text{Na}_{13-x}\text{Sn}_{26-x}\text{Bi}_{1+x}$ was firstly described in the PhD thesis of Simeon Ponou [119]. It was and still is the first and only representative of the Na-Sn-Bi ternary system. Its structure, shown in Figure 3.38, is related to the binary phase $\text{Na}_5\text{Sn}_{13}$ [55]. Twelve tin atoms (position Sn2-Sn13) together with atoms of the Sn/Bi statistical mixture ($M2$) are forming complex network (Figure 3.39), containing two major fragments (A – yellow frame and B – orange frame) with three types of cages: smaller cage I and II forming fragment B and bigger cage III around Bi1 atoms in fragment A. Cages II and III are encapsulating Na atoms as in is shown in Figure 3.38: Na3 and Na5 are inside of the cage II, whereas all the remaining Na atoms (Na1, Na2, Na4, Na5, Na6 and Na7) are located in the cage III.

Homoatomic Sn-Sn distances within the network of the $\text{Na}_{13}\text{Sn}_{25.73}\text{Bi}_{1.27}$ are between 2.822 and 2.947 Å (Table 3.34), which suggests strong covalent interactions: Sn7, Sn8 and Sn13 are two-bonded, Sn1, Sn3, Sn4, Sn5, Sn6, Sn9, Sn10 and Sn12 – four bonded. The atoms of the statistical mixture Sn/Bi ($M2$) are two bonded with $d_{\text{Sn1}-M2} = 2.965$ Å and $d_{\text{Sn11}-M2} = 2.985$ Å. The atom Bi1 is encapsulated in a cage marked in a yellow frame (fragment A) in Figure 3.39. Bi1 is rather isolated with the shortest distance to a neighboring Sn11 of 3.145 Å, which is significantly larger than the sum of covalent radii of single-bonded Bi (1.51 Å [120]) and Sn (1.40 Å [120]).

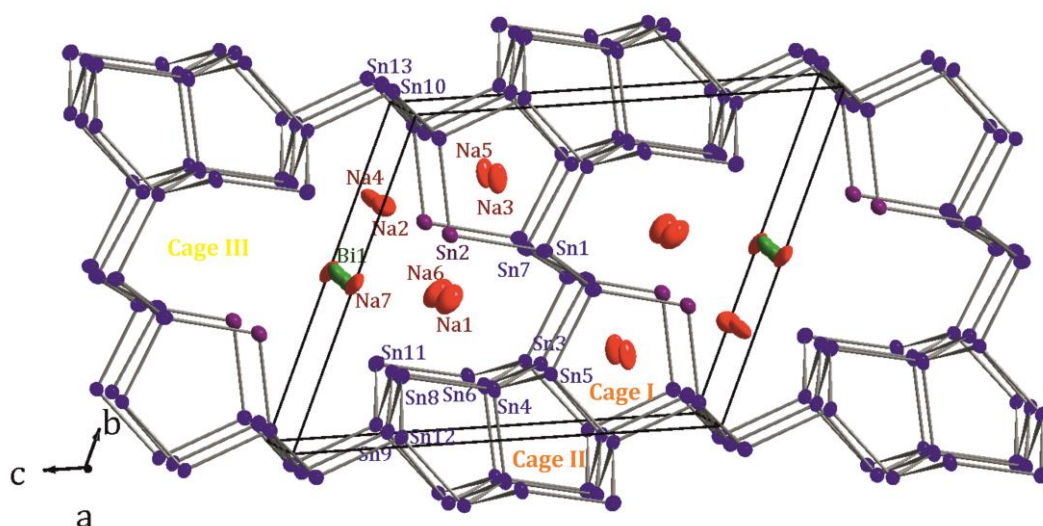


Figure 3.38 Structure of the compound $\text{Na}_{13}\text{Sn}_{25.73}\text{Bi}_{1.27}$. Na atoms are shown in red, Sn – in blue, Bi – in green, atoms of statistical mixture Sn/Bi – violet. The thermal ellipsoids are drawn with 90 % probability level.

Table 3.34 Selected interatomic distances in the compound $\text{Na}_{13}\text{Sn}_{25.73}\text{Bi}_{1.27}$. For the detail see Table 6.5 (Appendix).

Atom types		Distance range(Å)	Atom types		Distance range(Å)
Sn	-Bi	3.145(8)-3.456(8)	Na	-Bi	3.22(3)-3.86(1)
Sn	-M	2.965(1)-2.985(1)	Na	-M	3.243(7)-3.302(8)
Sn	-Sn	2.822(1)-2.947(2)	Na	-Sn	3.186(8)-3.925(6)
			Na	-Na	3.521(8)-4.080(9)

Electron Count

For the ordered variant of the compound $\text{Na}_{13}\text{Sn}_{25.73}\text{Bi}_{1.27}$, where *M2* position is occupied only by Sn atoms the electron count results in complete charge compensation $(\text{Na}^+)_{13}[(0\text{-b Bi}^{3-})_1(2\text{-b Sn}^{2-})_2(3\text{-b Sn}^-)_6(4\text{-b Sn}^0)_{16}]$ (0-b – isolated atom, 2-b – two-bonded and 4-b – four bonded atoms), showing that the compound $\text{Na}_{13}\text{Sn}_{26}\text{Bi}$ is an electron balanced Zintl phase, considering that Bi1 atoms are indeed isolated and have charge 3-.

For the composition obtained as a result of the SCXRD, $\text{Na}_{13}\text{Sn}_{25.73}\text{Bi}_{1.27}$ electron count is $(\text{Na}^+)_{13}[(0\text{-b Bi}^{3-})_1[(2\text{-b Bi}^-)_{0.272}(2\text{-b Sn}^{2-})_{1.728}(3\text{-b Sn}^-)_6(4\text{-b Sn}^0)_{16}]$, where additionally 2-bonded Bi^- anions appear, generating more 2-bonded Sn^{2-} instead of 3-bonded Sn^- and reducing the negative charge. Substituting one out of two Sn atoms in the *M2* position reduces the negative charge by 1, requiring 12 Na atoms: $(\text{Na}^+)_{12}[(0\text{-b Bi}^{3-})_1(2\text{-b Bi}^-)_1(2\text{-b Sn}^{2-})_1(3\text{-b Sn}^-)_6(4\text{-b Sn}^0)_{16}]$. It suggests that partial substitution of the Sn atoms by Bi in the *M2* atomic site results in electron deficiency. However, no defects in the Na positions in the structure of the $\text{Na}_{13}\text{Sn}_{25.73}\text{Bi}_{1.27}$ was observed.

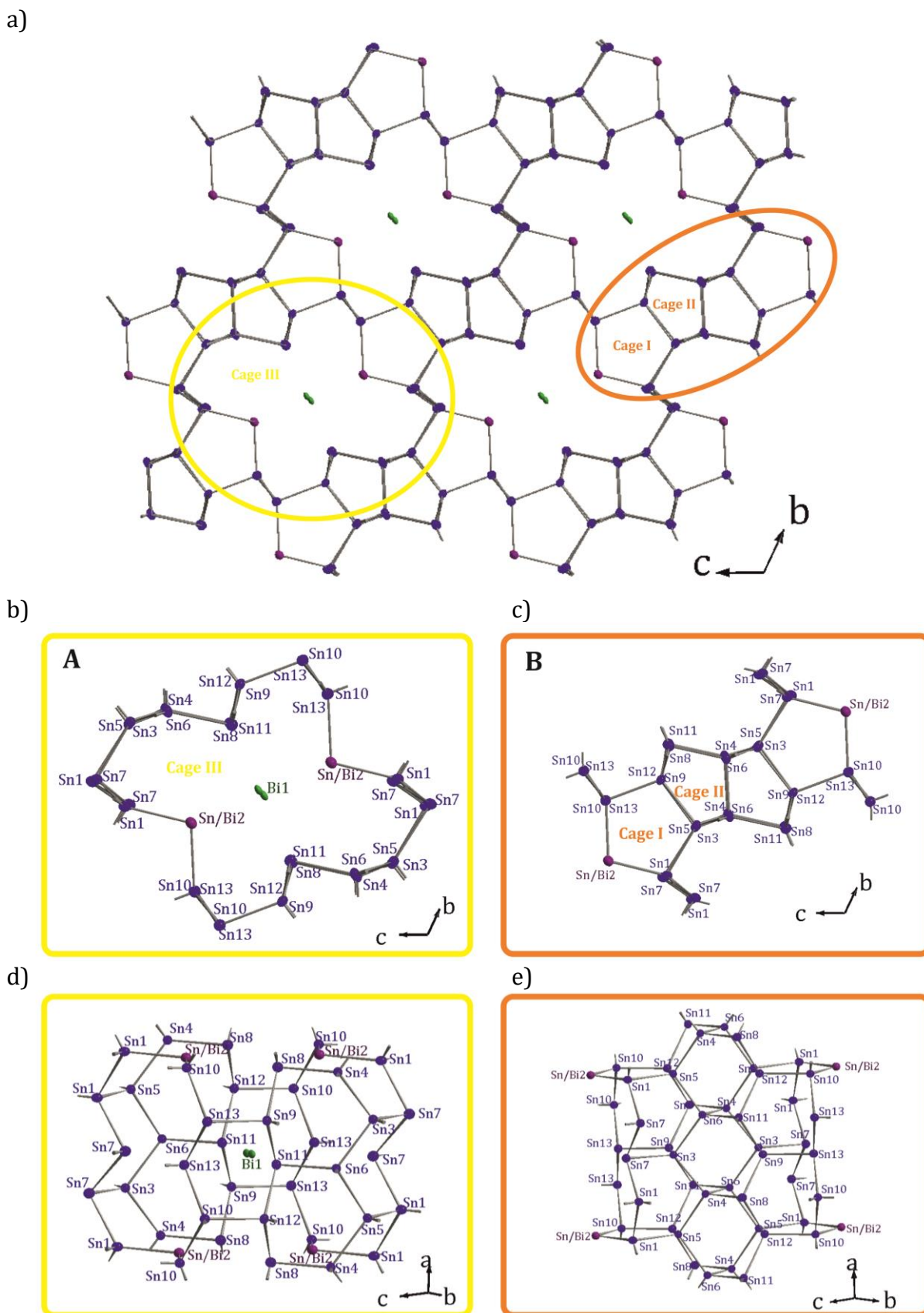


Figure 3.39 Anionic structure of the compound $\text{Na}_{13}\text{Sn}_{25.73}\text{Bi}_{1.27}$ (a), featuring two types of structural fragments: fragment A (b, d, yellow frames) with cage III around Bi1 atom, and fragment B (c, d, orange frames), featuring the network of Sn pentagons, forming the cage I and II. Sn atoms are shown – in blue, Bi – in green, atoms of statistical mixture Sn/Bi – violet.

Comparison to the Na_{12.73}Sn_{25.73}Bi_{1.27} and Discussion

According to Table 3.35, the cell parameters for both Na₁₃Sn_{25.73}Bi_{1.27} and Na_{12.73}Sn_{25.73}Bi_{1.27} [119] is quite similar, despite of the significant difference in the temperature of the measurement. The crystal quality and the data set of the Na₁₃Sn_{25.73}Bi_{1.27} is better to compared compound [119] in terms of R_{int} and R_6 , but in general, refinement turned out to be quite reproducible. There are two main differences in the models of the structure solution. The first one is split Bi1 position (2i) in Na₁₃Sn_{25.73}Bi_{1.27} with occupancy of 0.5, compared to not splitted 1f Bi position in Na_{12.73}Sn_{25.73}Bi_{1.27} (Table 3.36). This leads to a significant decrease of the isotropic displacement parameters in the first model. The second difference is the defects in the two Na positions (2i) with the occupancy of 0.935 in previously described structure.

Table 3.35 Comparison of the cell parameters and refinement details of the Na₁₃Sn_{25.73}Bi_{1.27} (measured at 150 K) and Na_{12.73}Sn_{25.73}Bi_{1.27} [119] (measured at 293 K).

Formula	Na ₁₃ Sn _{25.73} (2)Bi _{1.27} (2)	Na _{12.73} Sn _{25.73} Bi _{1.27}
Unit cell parameters (Å)	$a = 9.0826(4)$ $b = 11.2527(5)$ $c = 13.2278(6)$ $\alpha = 112.114(4)^\circ$ $\beta = 99.818(4)^\circ$ $\gamma = 101.379(4)^\circ$	$a = 9.0942(1)$ $b = 11.2637(2)$ $c = 13.2573(2)$ $\alpha = 112.008(1)^\circ$ $\beta = 99.793(1)^\circ$ $\gamma = 101.455(1)^\circ$
Volume (Å ³)	1182.4(1)	1188.46(3)
R_6	0.0217	0.035
R_{int}	0.0306	0.188
GOF on F2	1.303	1.060
$R_1, wR_2 (I > 2 \sigma(I))$	0.0379, 0.0913	0.033, 0.073
$R_1, wR_2 (all\ data)$	0.0482, 0.0936	0.040, 0.076
Largest diff. peak/hole (e Å ⁻³)	2.906 and -2.568	4.07 and -3.05

Compound Na₁₃Sn_{25.73}Bi_{1.27} (Figure 3.40, a) is structurally related to the binary phases Na₇Sn₁₂ [58] (Figure 3.40, b) and Na₅Sn₁₃ [55] (Figure 3.40, c). All three compounds contain cages type I and II, constructed by Sn-pentagons: in Na₁₃Sn_{25.73}Bi_{1.27} they are condensed in tetramers I-II-II-I (orange ellipse in Figure 3.40, a), and, together with cage III are forming three-dimensional network; in Na₅Sn₁₃ the cages are condensed in trimers II-I-II (red ellipse in Figure 3.40, c), forming together with additional fragments 3-D network as well, whereas in Na₅Sn₁₃ – dimers I-II (green ellipse in Figure 3.40, b), interconnected in a -direction and forming layers.

Na₁₃Sn_{25.73}Bi_{1.27} shows the tendency of Bi in Sn-rich Na-Sn-Bi compounds to form either isolated atoms (Bi³⁻) or substitute Sn in positions, forming two bonds to the neighboring atoms, preserving the integrity of the Sn network.

Table 3.36 Comparison of the occupancies of the atomic sites in Na₁₃Sn_{25.73}Bi_{1.27} with the respective sites in Na_{12.73}Sn_{25.73}Bi_{1.27} [119].

Atom	Na ₁₃ Sn _{25.73(2)} Bi _{1.27(2)}			Na _{12.73} Sn _{25.73} Bi _{1.27}		
	Wyck.	S.O.F.	<i>U</i> _{eq}	Wyck.	S.O.F.	<i>U</i> _{eq}
Sn1	2 <i>i</i>	1	0.0162(9)	2 <i>i</i>	1	0.0161(2)
Bi1	2<i>i</i>	0.5	0.0090(2)	1<i>f</i>	1	0.0438(2)
<i>M2</i>	2 <i>i</i>	0.864/0.136(8)	0.0095(3)	2 <i>i</i>	0.863/0.137(5)	0.0147(3)
Sn3	2 <i>i</i>	1	0.0080(2)	2 <i>i</i>	1	0.0140(2)
Sn4	2 <i>i</i>	1	0.0091(2)	2 <i>i</i>	1	0.0122(2)
Sn5	2 <i>i</i>	1	0.0079(2)	2 <i>i</i>	1	0.0137(2)
Sn6	2 <i>i</i>	1	0.0086(2)	2 <i>i</i>	1	0.0111(2)
Sn7	2 <i>i</i>	1	0.0101(2)	2 <i>i</i>	1	0.0112(2)
Sn8	2 <i>i</i>	1	0.0097(2)	2 <i>i</i>	1	0.0105(2)
Sn9	2 <i>i</i>	1	0.0083(2)	2 <i>i</i>	1	0.0122(2)
Sn10	2 <i>i</i>	1	0.0087(2)	2 <i>i</i>	1	0.0117(2)
Sn11	2 <i>i</i>	1	0.0090(2)	2 <i>i</i>	1	0.0133(2)
Sn12	2 <i>i</i>	1	0.0082(2)	2 <i>i</i>	1	0.0111(2)
Sn13	2 <i>i</i>	1	0.0094(2)	2 <i>i</i>	1	0.0120(2)
Na1	2<i>i</i>	1	0.031(2)	2<i>i</i>	0.935(5)	0.046(2)
Na2	2 <i>i</i>	1	0.021(1)	2 <i>i</i>	1	0.035(1)
Na3	2 <i>i</i>	1	0.018(1)	2 <i>i</i>	1	0.033(1)
Na4	2 <i>i</i>	1	0.018(1)	2 <i>i</i>	1	0.028(1)
Na5	2 <i>i</i>	1	0.019(1)	2 <i>i</i>	1	0.030(1)
Na6	2<i>i</i>	1	0.032(2)	2<i>i</i>	0.935(5)	0.049(2)
Na7	1 <i>c</i>	1	0.037(3)	1 <i>b</i>	1	0.034(2)

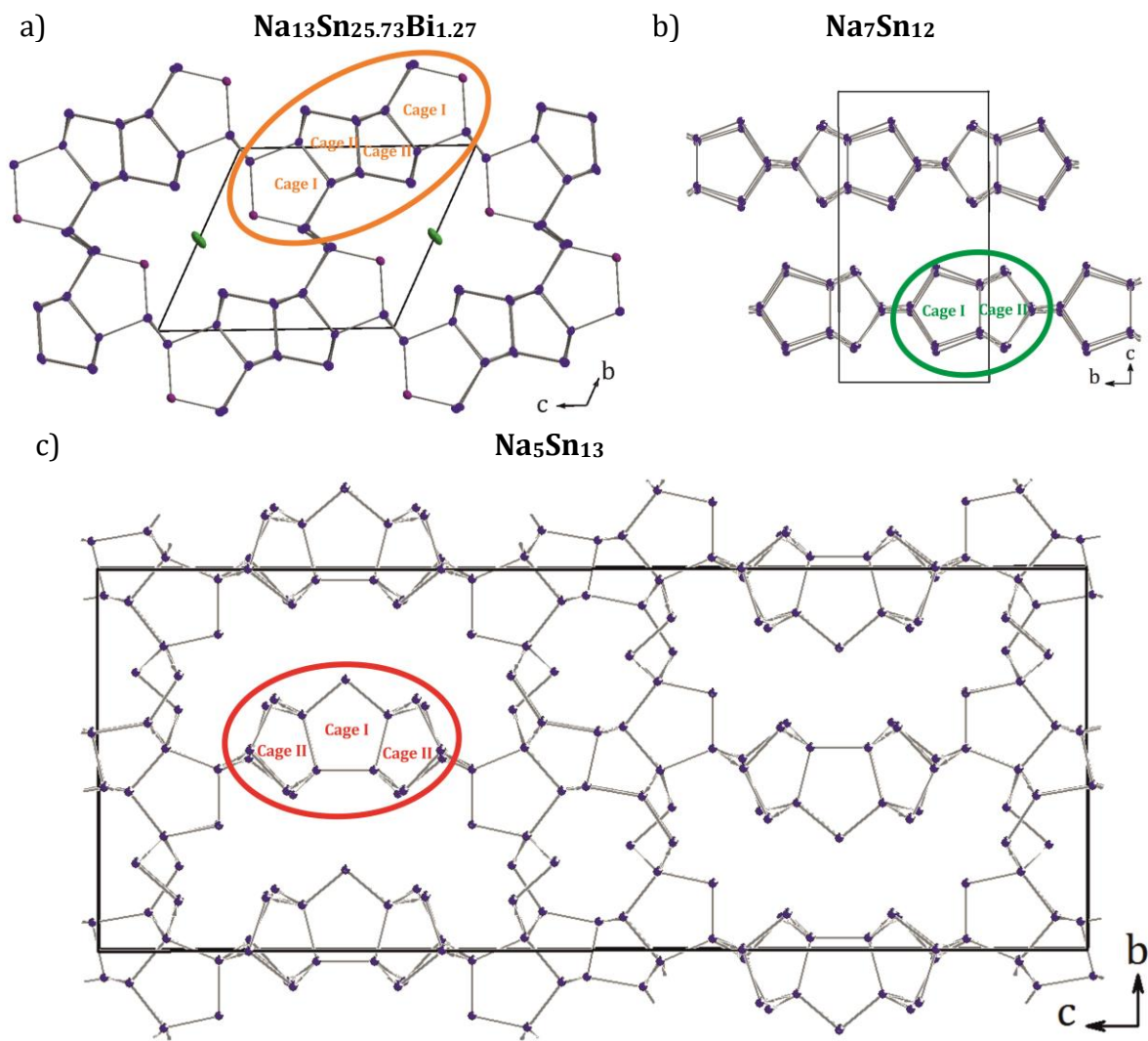


Figure 3.40 Structural relation of the Na₁₃Sn_{25.73}Bi_{1.27} (a) to the binary phases Na₇Sn₁₂ (b) and Na₅Sn₁₃ (c).

3.1.4.2 Partial Substitution of Sn by Bi in the Binary $\text{Na}_7\text{Sn}_{12}$: $\text{Na}_{27}\text{Sn}_{47.33}\text{Bi}_{0.57}$

Continuing doping the binary Na-Sn phases with small amounts of Bi showed it possible to partially substitute Sn atoms in the $\text{Na}_7\text{Sn}_{12}$ ^[58].

Synthesis and Characterization

Sample with the composition 'Na₇Sn₁₁Bi' was synthesized from the elements (48.0 mg Na, 389.6 mg Sn and 62.4 mg Bi) in Ta ampoule using a two-step temperature program: (1) heating up to 600°C with the rate of 4 °C/min and holding the temperature for 12 hours and (2) slowly cooling down to 250°C (rate 0,1°C/min) and dwelling the sample for 168 hours. The sample was cooled down to room temperature by switching off the oven. The PXRD analysis revealed along with the presence of the compound, similar to $\text{Na}_7\text{Sn}_{12}$, unreacted elemental Sn and binary phase Na₃Bi. The EDX analysis (Table 3.40) showed the presence of a small amount of bismuth along with tin and sodium.

Selected single crystals were tested for the singularity and measured on the StadiVari single crystal diffractometer. Obtained reflexes were indexed in the monoclinic space group $P2/n$ with the cell parameter $a = 13.3476(4)$ $b = 9.3094(2)$ $c = 17.9260(5)$ Å and $\beta = 90.331(2)^\circ$. The solution of the crystal showed a statistical mixture of Sn and Bi in $M1$ atomic position with the ratio Sn/Bi of 0.858/0.142(6), which is in agreement with the results of the EDX analysis. Partial defects were tested for all Na positions, giving significantly lower occupation factor (34 %) for only one position (Na₈), suggesting a correlation with the Bi/Sn mixed occupied position. The details of structure refinement for the compound with the refined composition $\text{Na}_{27.4(2)}\text{Sn}_{47.33(2)}\text{Bi}_{0.57(2)}$ are listed in Table 3.37, atom coordinates and equivalent isotropic and anisotropic displacement parameters – in Table 3.38 and Table 3.39, respectively.

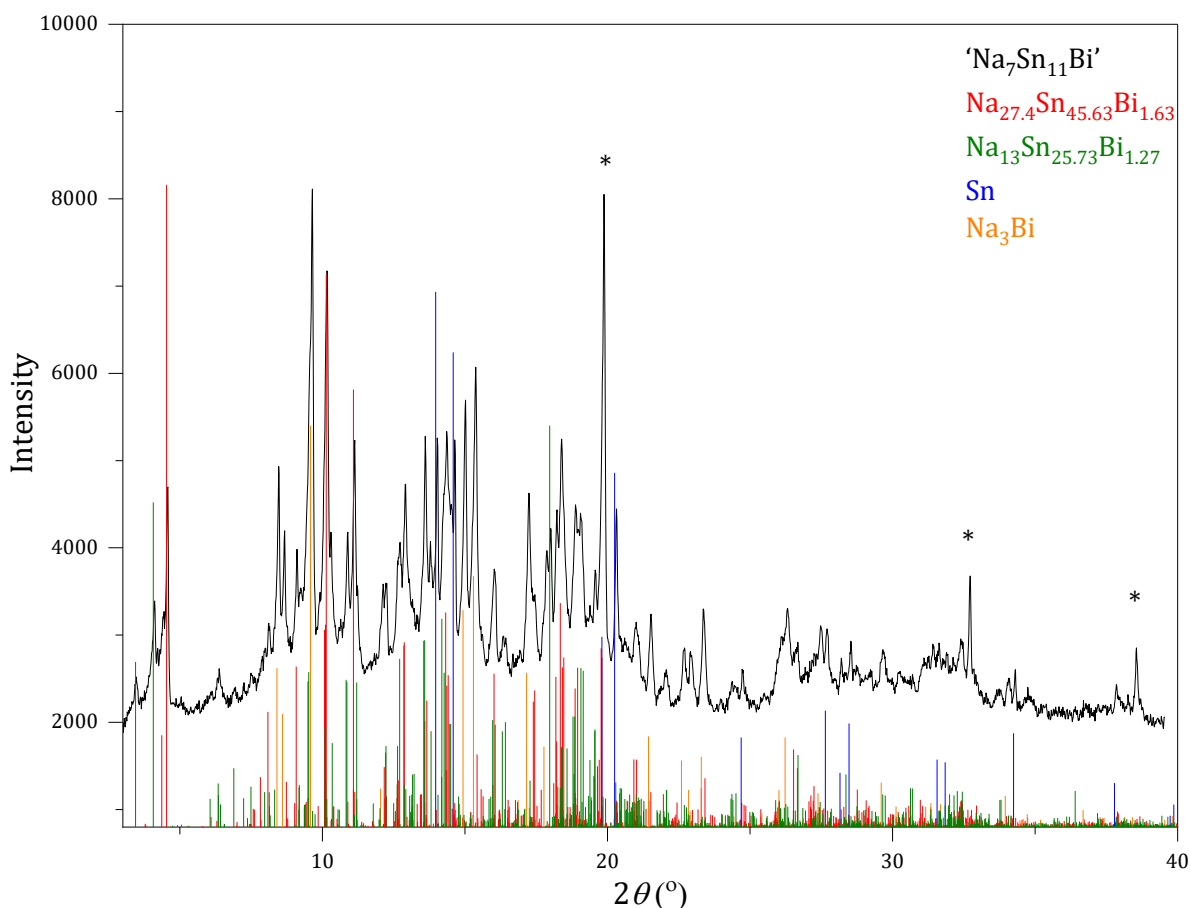


Figure 3.41 Experimental X-ray powder diffractogram of the sample 'Na₇Sn₁₁Bi' (black) with the theoretical pattern of the Na_{27.4(2)}Sn_{45.63(2)}Bi_{1.63(2)} (red), Na₁₃Sn_{25.73}Bi_{1.27} (green), elemental Sn (blue) and binary phase Na₃Bi (orange). Diamond (*) was used as internal standard.

Table 3.37 Crystallographic data and data and selected details of structure refinement for the compound Na_{27.4(2)}Sn_{47.33(2)}Bi_{0.57(2)}.

Formula	Na_{27.4(2)}Sn_{47.33(2)}Bi_{0.57(2)}
Formula weight (g·mol ⁻¹)	6385.47
Space group	<i>P2₁/n</i> (No. 13)
<i>Z</i>	1
Unit cell parameters (Å)	<i>a</i> = 13.3476(4) <i>b</i> = 9.3094(2) <i>c</i> = 17.9260(5) <i>β</i> = 90.331(2)°
Volume (Å ³)	2227.4(1)
<i>D</i> _{calcd.} (g·cm ⁻³)	4.760
Abs. Coeff. (mm ⁻¹)	15.864
<i>F</i> (000) (e)	2718
Crystal shape/color	block/black
Temperature (K)	150
<i>θ</i> range (deg)	2.896–32.499
Range in <i>hkl</i>	±20 ±14 ±27

Reflections collected	112070 ($R_6 = 0.0276$)
Unique reflections	8059 ($R_{\text{int}} = 0.0694$)
Data / parameter	8059/181
GOF on F2	1.198
$R_1, wR_2 (I > 2 \sigma(I))$	0.0477, 0.1081
$R_1, wR_2 (\text{all data})$	0.0580, 0.1111
Largest diff. peak/hole ($e \text{ \AA}^{-3}$)	4.457 and -3.719

Table 3.38 Atom coordinates and equivalent isotropic displacement parameters (\AA^2) for the compound $\text{Na}_{27.4(2)}\text{Sn}_{47.43(2)}\text{Bi}_{0.57(2)}$, M = statistical mixture of Sn and Bi.

Atom	Wyck.	S.O.F.	x	y	z	U_{eq}
M1	4g	0.858/0.142(6)	0.41271(4)	0.85219(6)	0.10108(3)	0.01234(2)
Sn2	4g	1	0.42052(4)	0.02537(6)	0.23769(4)	0.01085(1)
Sn3	4g	1	0.58460(4)	0.22015(6)	0.23971(3)	0.01035(1)
Sn4	4g	1	0.58239(4)	0.37803(7)	0.37420(3)	0.01205(1)
Sn5	4g	1	0.25820(4)	0.39500(6)	0.37826(3)	0.01089(1)
Sn6	4g	1	0.42507(4)	0.56273(7)	0.32367(4)	0.01251(1)
Sn7	4g	1	0.08441(4)	0.55796(6)	0.34030(4)	0.01100(1)
Sn8	4g	1	0.74071(4)	0.56418(6)	0.33216(4)	0.01132(1)
Sn9	4g	1	0.69546(4)	0.86065(7)	0.38205(4)	0.01288(1)
Sn10	4g	1	0.58997(4)	0.40146(6)	0.11134(4)	0.01136(1)
Sn11	4g	1	0.46516(5)	0.85793(7)	0.37277(4)	0.01530(1)
Sn12	2e	1	1/4	0.21363(9)	1/4	0.01065(2)
Sn13	2f	1	3/4	0.02757(9)	1/4	0.01040(2)
Na1	2e	1	1/4	0.7710(7)	1/4	0.01234(2)
Na2	4g	1	0.9118(3)	0.7682(5)	0.2792(2)	0.0167(7)
Na3	4g	1	0.6036(3)	0.0571(4)	0.0750(3)	0.0183(8)
Na4	4g	1	0.5963(4)	0.6844(5)	0.0117(3)	0.0228(9)
Na5	4g	1	0.2201(4)	0.0563(5)	0.0775(3)	0.0258(1)
Na6	4g	1	0.2284(4)	0.6855(6)	0.0200(3)	0.0312(1)
Na7	4g	1	0.5795(4)	0.6486(6)	0.4911(3)	0.0305(1)
Na8	4g	0.34(2)	0.557(1)	0.088(1)	0.4544(8)	0.019(4)

Table 3.39 Anisotropic displacement parameters (\AA^2) for the compound $\text{Na}_{27.4(2)}\text{Sn}_{47.33(2)}\text{Bi}_{0.57(2)}$, M = statistical mixture of Sn and Bi.

Atom	U_{11}	U_{22}	U_{33}	U_{12}	U_{13}	U_{23}
M1	0.0109(3)	0.0114(3)	0.0147(3)	0.00108(2)	-0.00113(2)	-0.00028(2)
Sn2	0.0072(2)	0.0094(2)	0.0160(3)	0.00087(2)	-0.00024(2)	0.00024(2)
Sn3	0.0082(2)	0.0087(2)	0.0141(3)	-0.00025(2)	-0.00041(2)	0.00026(2)
Sn4	0.0097(2)	0.0145(3)	0.0119(3)	0.0002(2)	-0.00015(2)	-0.00165(2)
Sn5	0.0082(2)	0.0110(2)	0.0134(3)	0.00084(2)	0.00035(2)	0.00070(2)
Sn6	0.0087(2)	0.0127(2)	0.0162(3)	0.0019(2)	0.0008(2)	-0.00027(2)
Sn7	0.0068(2)	0.0107(2)	0.0155(3)	0.00083(2)	-0.00025(2)	0.00078(2)
Sn8	0.0069(2)	0.0107(2)	0.0163(3)	0.0006(2)	0.00069(2)	0.00016(2)
Sn9	0.0094(2)	0.0132(3)	0.0160(3)	0.0014(2)	-0.00058(2)	-0.00118(2)
Sn10	0.0100(2)	0.0098(2)	0.0143(3)	0.00013(2)	0.00040(2)	-0.00062(2)
Sn11	0.0107(2)	0.0172(3)	0.0181(3)	0.0041(2)	0.0036(2)	0.0042(2)
Sn12	0.0087(3)	0.0092(3)	0.0141(4)	0.000	0.0008(3)	0.000
Sn13	0.0072(3)	0.0084(3)	0.0157(4)	0.000	0.0012(3)	0.000

Na1	0.0109(3)	0.0114(3)	0.0147(3)	0.00108(2)	-0.00113(2)	-0.00028(2)
Na2	0.010(2)	0.018(2)	0.023(2)	0.0013(2)	-0.0023(1)	0.0006(2)
Na3	0.018(2)	0.015(2)	0.022(2)	0.0007(2)	0.0011(2)	-0.0009(2)
Na4	0.025(2)	0.021(2)	0.023(2)	0.0007(2)	0.0039(2)	0.0031(2)
Na5	0.022(2)	0.017(2)	0.039(3)	-0.0004(2)	0.0066(2)	0.0005(2)
Na6	0.028(2)	0.035(3)	0.030(3)	0.000(2)	-0.004(2)	-0.014(2)
Na7	0.022(2)	0.044(3)	0.026(2)	0.012(2)	-0.0038(2)	-0.014(2)
Na8	0.023(7)	0.010(6)	0.024(7)	-0.007(4)	0.000(5)	-0.003(4)

Table 3.40 Comparison of the results EDX analysis of the crystal with the refined composition $\text{Na}_{27.4}\text{Sn}_{47.33}\text{Bi}_{0.57}$ from the sample 'Na₇Sn₁₁Bi'.

	Na (at. %)	Sn (at. %)	Bi (at. %)
EDX	48(9)	50(9)	2(1)
$\text{Na}_{27.4}\text{Sn}_{47.33}\text{Bi}_{0.57}$	36.7	61.1	2.2

Crystal Structure of the Na_{27.4}Sn_{47.33}Bi_{0.57}

Na_{27.4}Sn_{47.33}Bi_{0.57} is a ternary substitution variant of the binary Zintl Phase Na₇Sn₁₂ [58] with 14% bismuth in site *M1* (4*g*). The crystal structure of the Na_{27.4}Sn_{47.33}Bi_{0.57}, same as in Na₇Sn₁₂: it contains layers of the {Sn_{12-x}Bi_x}^{(7-x)-} - Figure 3.42, a. It is formed by the atoms of tin in 13 atomic positions. The layer of the Na_{27.4}Sn_{47.33}Bi_{1.63}, shown in Figure 3.42, c contains four types of cages. The bigger cages I and I' are formed by thirteen atoms (cage I: 2×*M1*, 2×Sn2, 2×Sn5, 2×Sn6, 2×Sn7, 2×Sn11, and Sn12; cage I': *M1*, Sn2, Sn3, Sn4, Sn6, Sn7, 2×Sn8, 2×Sn9, Sn10, Sn11 and Sn13) and are encapsulating Na1 (cage I) and Na2 (cage I') atoms. Two other cages are very similar (cage II: Sn2, Sn3, Sn4, 2×Sn5, Sn6, Sn7, Sn10 and Sn12; cage II': 2×Sn3, 2×Sn4, 2×Sn10, 2×Sn8 and Sn13), both formed by nine atoms and sharing three of them (Sn2, Sn4, Sn10) and are stacked along [100] direction. Sn-Sn distances within the layer are between 2.824 and 3.078 Å (Table 3.41). Extremely short Na-Sn distance of 2.87 Å is between sodium atoms in the partially occupied position Na8 (34 % Na) and Sn11.

With the partial substitution of Sn atoms by Bi atoms with 8 % bigger covalent radius, it would be expected to observe cell parameter increase for Na_{27.4}Sn_{47.33}Bi_{0.57} compared to Na₇Sn₁₂ [58]. However, Table 3.42 shows the opposite effect. It should be noted, that the SCXRD measurements were performed at 150 K, which should explain this fact. Moreover, a lower content of Na atoms (defective Na8 position) can lead to compression of the unknit cell. A comparison of the interatomic distances in both compounds (Table 3.41) confirmed no major change. Apparently, the amount of Bi, substituting Sn in Na_{27.4}Sn_{47.33}Bi_{0.57} (14 % in position *M1*) is low enough to preserve the original structure of the binary Na₇Sn₁₂, not changing the Sn framework significantly.

Table 3.41 Selected interatomic distances in the compound Na_{27.4}Sn_{47.33}Bi_{0.57}, compared to those in Na₇Sn₁₂ [58]. For the detail see Table 6.6 (Appendix).

Atom types		Na _{27.4} Sn _{47.33} Bi _{0.57}	Na ₇ Sn ₁₂
		Distance range(Å)	Distance range(Å)
Sn	- <i>M</i>	2.9333(9)-2.9339(8)	-
Sn	-Sn	2.8239(8)-3.0776(9)	2.8266-3.0878
Na	- <i>M</i>	3.219(4)-3.325(5)	-
Na	-Sn	2.87(1)-3.924(5)	2.9097-3.9326
Na	-Na	3.37(1)-4.094(7)	2.0759-3.9730

Correlation between the bismuth content in the compound and partial occupancy of the sodium site (Na8) allows Na_{27.4}Sn_{47.33}Bi_{0.57}, to remain electron precise compound: (Na⁺)_{27.4}[(2-b Sn²⁻)_{3.4}(2-b Bi)_{0.6}(3-b Sn⁻)₂₀(4-b Sn⁰)₂₄] (2b – two-bonded atoms, 3b – three-

bonded and 4b – four bonded). For comparison, electron count for the Zintl phase $\text{Na}_7\text{Sn}_{12}$ ^[58]: $(\text{Na}^+)_7[(2\text{-b Sn}^{2-})_1(3\text{-b Sn}^-)_5(4\text{-b Sn}^0)_6]$.

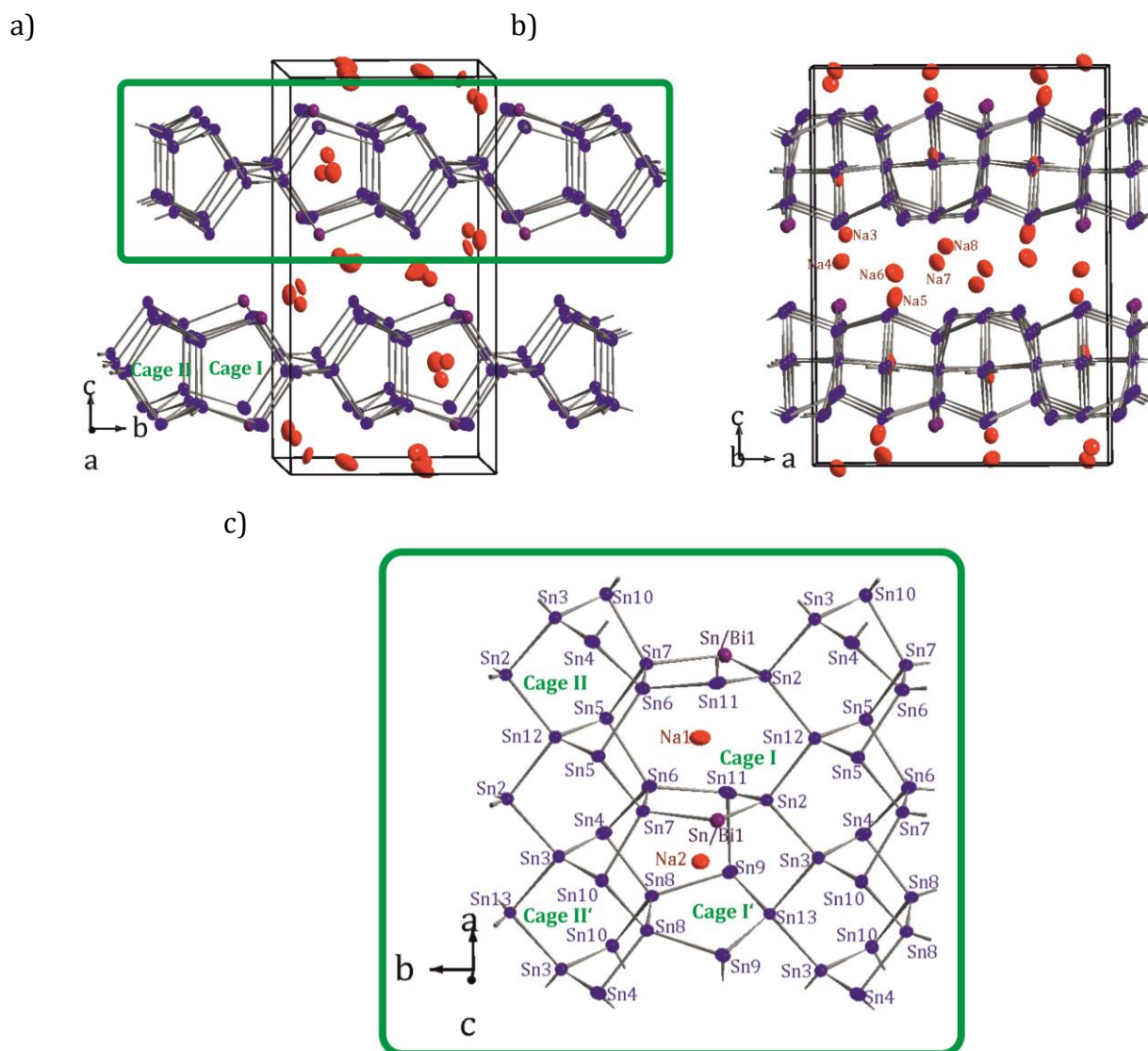


Figure 3.42 Crystal structure of the layered compound $\text{Na}_{27.4}\text{Sn}_{47.33}\text{Bi}_{0.57}$: unit cell (a, b) and a fragment of one layer (c).

Table 3.42 Cell parameters of the $\text{Na}_{27.4}\text{Sn}_{47.33}\text{Bi}_{0.57}$ (measured at 150 K) and $\text{Na}_7\text{Sn}_{12}$ ^[58] (293 K).

Formula	$\text{Na}_{27.4(2)}\text{Sn}_{47.33(2)}\text{Bi}_{0.57(2)}$	$\text{Na}_7\text{Sn}_{12}$
Z	1	4
Unit cell parameters (Å)	$a = 13.3476(4)$ $b = 9.3094(2)$ $c = 17.9260(5)$ $\beta = 90.331(2)^\circ$	$a = 13.375(3)$ $b = 9.329(2)$ $c = 22.376(4)$ $\beta = 126.55(8)^\circ$
Volume (Å ³)	2227.4(1)	2243.0(8)

3.2 Solid-state Synthesis of the Endohedrally Filled Clusters with Transition Metals

3.2.1 Introduction

The phase diagram of the K-Sn [121] (Figure 6.1, b) suggests the existence of four binary phases: K_2Sn , KSn , KSn_2 and KSn_4 . In the last few decades, this knowledge was extended, showing more various compounds between the two elements (Table 3.43). Unlike Na-Sn, for K-Sn binary system (Figure 3.43, a) no structures of K-rich phases are known. Most compounds have either isolated $\{Sn_4\}^{4-}$ (in K_4Sn_4), $\{Sn_9\}^{4-}$ (in K_4Sn_9), both $\{Sn_4\}^{4-}$ and $\{Sn_9\}^{4-}$ (in $K_{12}Sn_{17}$ and $K_{51}Sn_{82}$) or three types of isolated clusters: $\{Sn_4\}^{4-}$, $\{Sn_9\}^{4-}$ along with $\{Sn_5\}^{2-}$ clusters ($K_{70}Sn_{103}$ [72]) or have clathrate structure with K-centered condensed pentagonal dodecahedra of Sn atoms (in $K_{7.4}Sn_{25}$, K_6Sn_{25} and K_8Sn_{46}). The only exception is KSn_2 with the $MgZn_2$ -type structure which shows superconductivity at 3.2K [122].

It seems that the atomic radii increase for potassium compared to sodium plays a crucial role in defining the structures of the binary phases, insuring tendency of the formation of isolated clusters or clathrates in K-Sn in contrast to condensed anionic networks in Na-Sn binary system. The variety of the compounds with isolated clusters in K-Sn opens an opportunity to use them as a matrix for the intercalation of *d*-elements in the clusters.

Table 3.43 Binary compounds in the K-Sn binary system.

Compound	Space group	Cell parameters				Ref.
		<i>a</i> (Å)	<i>b</i> (Å)	<i>c</i> (Å)	<i>V</i> (Å ³)	
K_4Sn_4	<i>I4₁/acd</i>	11.409	11.409	18.649	2427.45	[31]
$K_{12}Sn_{17}$	<i>P2₁/c</i>	25.71	14.770	48.19	18292	[32]
$K_{70}Sn_{103}$	<i>Pbca</i>	24.471	29.652	77.261	56063	[72]
$K_{51}Sn_{82}$	<i>P2₁/c</i>	25.618	14.792	55.653	20834	[123]
KSn_2	<i>P6₃/mmc</i>	6.427	6.427	10.43	373.11	[122]
K_4Sn_9	<i>P2₁/c</i>	14.238	8.3554	16.487	1953.1	[33]
$K_{7.4}Sn_{25}$	<i>P4₁32</i>	16.294	16.294	16.294	4325.97	[124]
K_6Sn_{25}	<i>P4₃32</i>	16.202	16.202	16.202	4253.1	[113]
K_8Sn_{46}	<i>Pm-3n</i>	12.03	12.03	12.03	1740.99	[125]

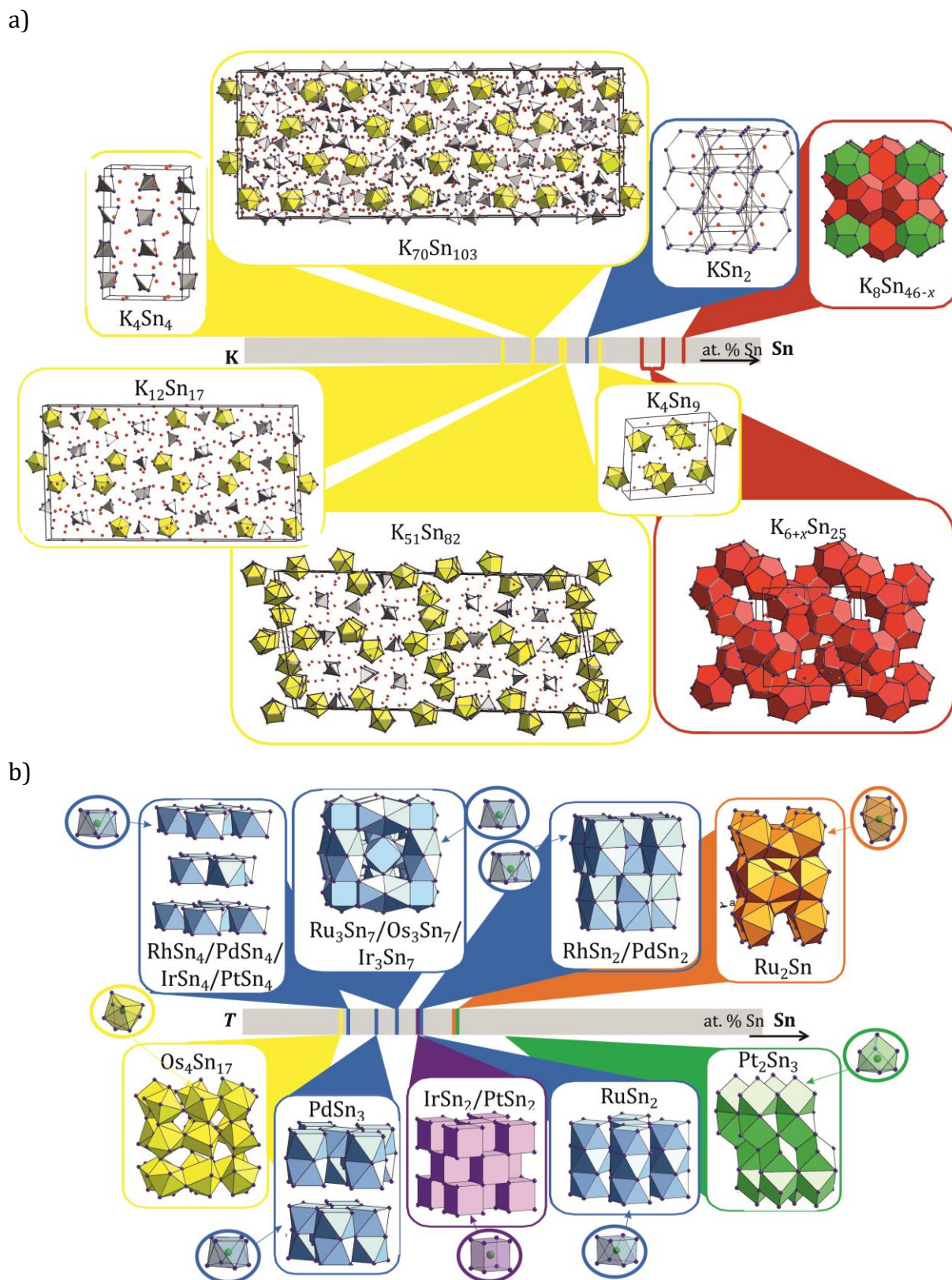


Figure 3.43 Binary compounds in the K-Sn system, color-coded according to dimensionality of the Sn anionic frameworks: three-dimensional Sn-network – blue rectangles; isolated clusters – yellow; clathrate structures – red (a). Sn-rich binary T -Sn (T – element of the Pt-group) phases are featuring T metal encapsulated in $\{Sn_n\}$ -cages: $\{Sn_6\}$ octahedron – green, $\{Sn_8\}$ antiprism – blue, $\{Sn_8\}$ cube – violet, deformed $\{Sn_8\}$ cage – orange, $\{Sn_9\}$ – yellow (b).

In the Sn-rich compounds of the T -Sn (T - Ru, Rh, Pd, Os, Ir, Pt) binary systems transition metals are encapsulated in the cages of tin atoms $\{T@Sn_n\}$ ($n = 6$ – octahedra; $n = 8$ – cubes, antiprisms; $n = 9$ – nine atom clusters), as it is shown in Figure 3.43, b. Compounds differ by the way of packing of the cages of tin atoms, built around transition metals. Such $\{Pt@Sn_6\}$ octahedra, $\{T@Sn_8\}$ antiprisms or cubes or $\{Os@Sn_9\}$ clusters can theoretically be reduced by alkali metals, functioning as ‘metallic scissors’ to obtain isolated clusters.

There are plenty of known clusters formed by group 14 elements (Tt) and d -block metals (T) of formula $\{T@Tt_n\}$ ($n = 9, 10, 12$) fragments: both as building blocks in intermetallic phases, or quasi-discrete units in salt-like crystals. Most of the known filled 9-atom clusters were synthesized by the reaction of dissolved K_4Tr_9 with organometallic compounds of transition metals in the presence of cryptands (e.g. [2.2.2]crypt), for example, Cu^+ centered $\{Cu@Sn_9\}^{3-}$ and $\{Cu@Pb_9\}^{3-}$ clusters as a result [126].

In comparison to a large number of the known endohedral clusters formed in solution, there are only a few examples of discrete clusters formed by solid-state synthesis. A remarkable example of these are mentioned earlier $A_{12}Cu_{12}Sn_{21}$ [36] and $Na_{2.8}Cu_5Sn_{5.6}$ [65] compounds with Cu-centered units: isolated $\{Sn@Cu_{12}@Sn_{20}\}^{12-}$ clusters and $\frac{1}{\infty}\{Sn_{0.6}@Cu_5@Sn_5\}$ rods respectively. The $\{Sn@Cu_{12}@Sn_{20}\}^{12-}$ anion, in contrast to isosteric $\{As@Ni_{12}@As_{20}\}^{3-}$ and $\{Sb@Pd_{12}@Sb_{20}\}^{3-/4}$, exists only in the solid-state and is not soluble. There were several successful attempts to synthesize via solid-state approach endohedrally filled 9-atom clusters: $\{Co@Sn_9\}^{5-}$ in $K_{5-x}Co_{1-x}Sn_9$ [127] and $K_{13}CoSn_{17}$ [66] as well as $\{Ni@Sn_9\}^{4-}$ in $K_{12}Ni_{1-x}Sn_{17}$ [66]. These results together with great potential for application in catalysis [128] inspired us to look into the possibility of forming $\{T@Sn_9\}^{n-}$ clusters with platinum group metals.

All obtained endohedrally filled compounds showed a rather good solubility in the liquid ammonia with crown ether (18-crown-6). The solubility was checked by M. Sc. Benedikt Witzel. Bringing the clusters, already formed in the solid-state, to the solution opens another synthetic approach for this type of material. In this Chapter the possibility of forming $[T@Sn_9]^{n-}$ clusters in neat solids using controlled high temperature reactions were explored.

3.2.2 Ternary Phase $K_{12}Pd_{0.47}Sn_{17}$ Featuring $\{Pd@Sn_9\}^{4-}$ Clusters

Synthesis and Characterization

Ternary sample was prepared using the high temperature reaction of elemental potassium with binary Pd-Sn precursor (Pd:Sn ratio of 1:9, see Chapter 2.1.2.1) with the total ratio K:Pd:Sn of 5:1:9 (5.87 mg of K, 40.0 mg Pd and 401.3 mg of Sn). The sample was sealed in Ta ampoule and hold at 1000 and 600°C for 12 and 48 hours, respectively, with slowly cooling (0.1°C/min) in-between two steps and finally rapidly cooled by quenching to the room temperature. Powder X-ray phase analysis (Figure 3.44) showed that the main phase was the cluster containing a compound very similar to the binary $K_{12}Sn_{17}$ along with binary side phase $PdSn_2$ and some unindexed reflexes. However, EDX analysis (Table 3.47) showed the presence up to 5 at. % Pd in selected crystals of the new phase, indicating Pd filling the Sn_9 clusters.

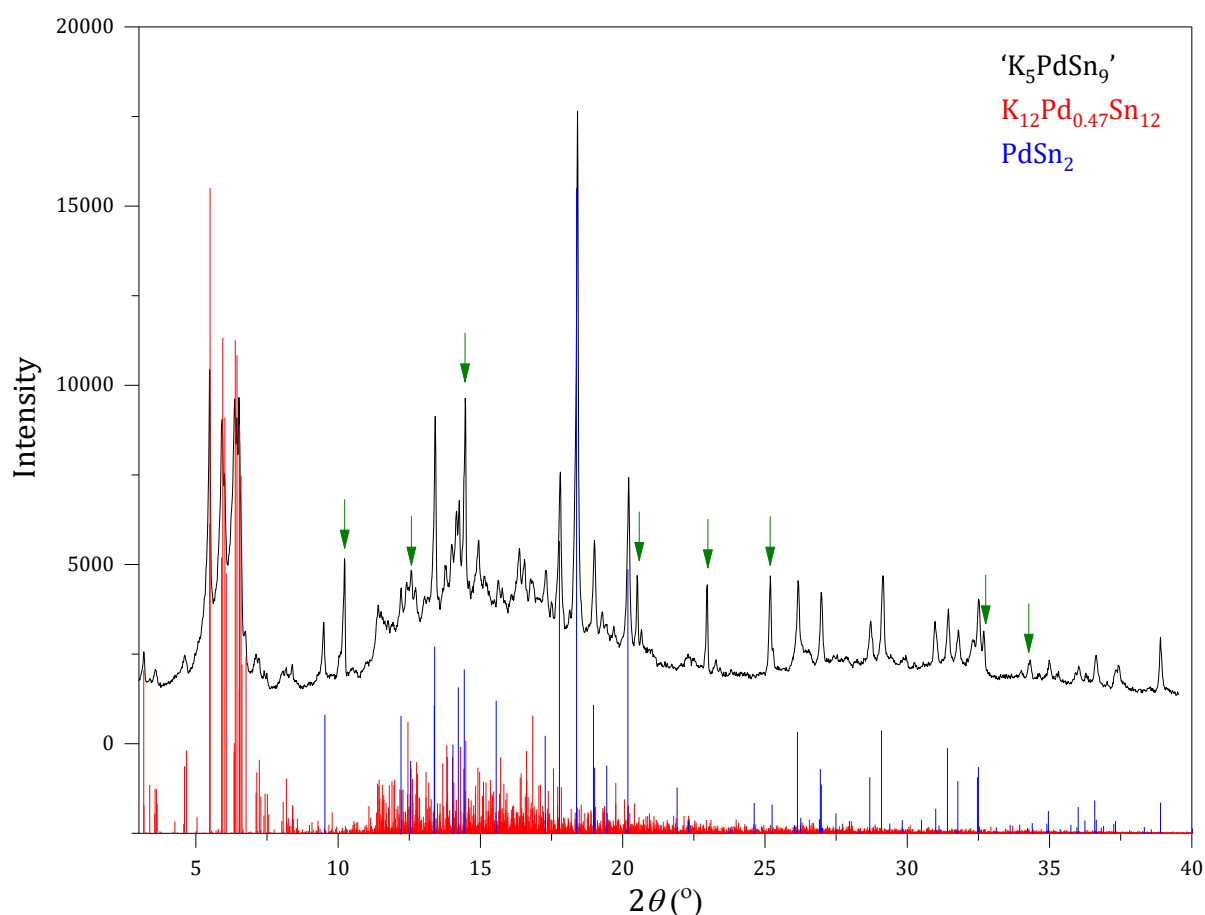


Figure 3.44, Experimental X-ray powder diffractogram of the sample 'K₅PdSn₉' (black) with the theoretical pattern of the $K_{12}Pd_{0.47}Sn_{17}$ (red) obtained from single crystal diffraction data. Main side phase, binary $PdSn_2$, is shown in blue, unindexed reflexes – with green arrows.

Single crystals were picked and measured at Bruker D8 QUEST single-crystal X-ray diffractometer with PHOTON II CMOS Detector and I μ S 3.0 Microfocus X-ray source (Mo-K α) at 130K. The frames were integrated with the Bruker SAINT software package [129] using a narrow-frame algorithm. Initially the data set was indexed in the hexagonal symmetry, however, no acceptable structure solution could be implemented. A closer look into the diffraction pattern showed that the studied crystal has multiple (triple) twinning: three domains were rotated by about 60° with respect to each other with a rotational axis along direction [001]. Integration of the diffraction data was performed with three orientation matrices with a ratio of 0.33:0.33:0.33 in a monoclinic unit cell with the final cell constants of $a = 25.606(3)$ Å, $b = 14.815(2)$ Å, $c = 48.100(5)$ Å, $\beta = 91.678(2)$ and volume $V = 18238.68(4)$ Å³. Adsorption correction was performed using SADABS [130]. The structure was solved and refined using the SHELXTL Software Package [131] with monoclinic space group $P2_1/c$, with $Z = 16$ for the formula unit $K_{12}Pd_{0.47}Sn_{17}$ and refined composition $K_{12.04(2)}Pd_{0.47(1)}Sn_{17}$. The title compound diffracts poorly on account of large unit-cell parameters and poor crystal quality, which explains relatively high R factors (Table 3.44).

Table 3.44 Crystallographic data and data and selected details of structure refinement for the compound $K_{12.04(2)}Pd_{0.47(1)}Sn_{17}$.

Formula	$K_{12.04(2)}Pd_{0.47(1)}Sn_{17}$
Formula weight (g·mol ⁻¹)	41224.1
Space group	$P2_1/c$ (No. 14)
Z	16
Unit cell parameters (Å)	$a = 25.606(3)$ $b = 14.815(2)$ $c = 48.100(5)$ $\beta = 91.678(2)^\circ$
Volume (Å ³)	18238.68(4)
$D_{\text{calcd.}}$ (g·cm ⁻³)	3.697
Abs. Coeff. (mm ⁻¹)	10.399
$F(000)$ (e)	17602
Crystal shape/color	block/black
Temperature (K)	130
θ range (deg)	1.789–25.086
Range in hkl	± 30 0 \div 17 0 \div 57
Reflections collected	27536 ($R_\theta = 0.0554$)
Unique reflections	21710 (triple twinning)
Data / parameter	27536/1179
GOF on F ²	1.065
R_1, wR_2 ($I > 2 \sigma(I)$)	0.0758, 0.2026
R_1, wR_2 (all data)	0.1007, 0.2153
Largest diff. peak/hole (e Å ⁻³)	4.495 and -2.977

Significant disorder with split Sn positions within tetrahedral clusters (positions Sn29-Sn36) and nine atom clusters (positions Sn68-Sn77) as well as defect K positions with the partial occupancy of potassium (K46-K51) was found during the refinement. Positions of all four crystallographically independent Pd atoms, filling the nine atom clusters are also partially occupied. Table 3.44 shows relevant crystallographic data and conditions for the data collections and refinement procedure, Table 3.45 and Table 3.46– atomic parameters and anisotropic displacement parameters respectively. No significant residual peaks were observed in the difference electron-density map. In Table 6.7 (Appendix). are presented all the interatomic distances in the compound $K_{12}Pd_{0.47}Sn_{17}$.

Table 3.45 Atom coordinates and equivalent isotropic displacement parameters (\AA^2) for the compound $K_{12.04(2)}Pd_{0.47(1)}Sn_{17}$.

Atom	Wyck.	Occ.	<i>x</i>	<i>y</i>	<i>z</i>	<i>U_{eq}</i>
Sn1	4 <i>e</i>	1	0.4383(1)	0.7997(2)	0.09381(5)	0.0229(6)
Sn2	4 <i>e</i>	1	0.3536(1)	0.7396(2)	0.13096(5)	0.0231(6)
Sn3	4 <i>e</i>	1	0.4480(1)	0.6314(2)	0.12652(5)	0.0222(6)
Sn4	4 <i>e</i>	1	0.4526(1)	0.8086(2)	0.15434(5)	0.0237(6)
Sn5	4 <i>e</i>	1	0.3232(1)	0.4041(2)	0.39479(5)	0.0202(5)
Sn6	4 <i>e</i>	1	0.3846(1)	0.4620(2)	0.34739(5)	0.0202(6)
Sn7	4 <i>e</i>	1	0.3716(1)	0.5820(2)	0.39538(5)	0.0218(6)
Sn8	4 <i>e</i>	1	0.2829(1)	0.5450(2)	0.35711(5)	0.0207(6)
Sn9	4 <i>e</i>	1	0.2340(1)	0.8704(2)	0.23494(5)	0.0229(6)
Sn10	4 <i>e</i>	1	0.2581(1)	0.7651(2)	0.28524(5)	0.0206(5)
Sn11	4 <i>e</i>	1	0.2990(1)	0.7085(2)	0.23164(5)	0.0246(6)
Sn12	4 <i>e</i>	1	0.1879(1)	0.6893(2)	0.24176(5)	0.0233(6)
Sn13	4 <i>e</i>	1	0.2889(1)	0.9563(2)	0.40219(5)	0.0206(5)
Sn14	4 <i>e</i>	1	0.3120(1)	0.0979(2)	0.36208(5)	0.0225(6)
Sn15	4 <i>e</i>	1	0.3942(1)	0.0319(2)	0.40054(5)	0.0210(5)
Sn16	4 <i>e</i>	1	0.3556(1)	0.9179(2)	0.35469(5)	0.0225(6)
Sn17	4 <i>e</i>	1	0.0162(1)	0.7361(2)	0.38757(5)	0.0225(6)
Sn18	4 <i>e</i>	1	0.1153(1)	0.8327(2)	0.39735(5)	0.0238(6)
Sn19	4 <i>e</i>	1	0.1149(1)	0.6451(2)	0.37796(5)	0.0272(6)
Sn20	4 <i>e</i>	1	0.0785(1)	0.7875(2)	0.34039(5)	0.0274(6)
Sn21	4 <i>e</i>	1	0.1851(1)	0.4609(2)	0.59556(5)	0.0250(6)
Sn22	4 <i>e</i>	1	0.1255(1)	0.4203(2)	0.64534(5)	0.0261(6)
Sn23	4 <i>e</i>	1	0.2179(1)	0.5375(2)	0.64961(6)	0.0266(6)
Sn24	4 <i>e</i>	1	0.1226(1)	0.5991(2)	0.62056(6)	0.0333(7)
Sn25	4 <i>e</i>	1	0.2704(1)	0.6423(2)	0.52728(6)	0.0274(6)
Sn26	4 <i>e</i>	1	0.3057(1)	0.7578(2)	0.48231(6)	0.0281(6)
Sn27	4 <i>e</i>	1	0.2271(1)	0.8250(2)	0.52097(6)	0.0379(8)
Sn28	4 <i>e</i>	1	0.1996(1)	0.6849(2)	0.48072(7)	0.0404(8)
Sn29	4 <i>e</i>	0.897(5)	0.1289(1)	0.9660(3)	0.65337(6)	0.0225(8)
Sn30	4 <i>e</i>	0.897(5)	0.1913(1)	0.9133(2)	0.60565(6)	0.0244(8)
Sn31	4 <i>e</i>	0.897(5)	0.1963(1)	0.0980(2)	0.62610(6)	0.0239(8)
Sn32	4 <i>e</i>	0.897(5)	0.1020(1)	0.0320(3)	0.59686(6)	0.0227(7)
Sn33	4 <i>e</i>	0.103(5)	0.133(1)	0.910(2)	0.6526(5)	0.017(6)
Sn34	4 <i>e</i>	0.103(5)	0.126(1)	0.104(2)	0.6509(5)	0.023(7)
Sn35	4 <i>e</i>	0.103(5)	0.215(1)	0.015(2)	0.6268(6)	0.030(7)
Sn36	4 <i>e</i>	0.103(5)	0.114(1)	0.995(2)	0.5984(6)	0.012(7)
Sn37	4 <i>e</i>	1	0.3622(1)	0.3956(2)	0.23158(6)	0.0334(7)
Sn38	4 <i>e</i>	1	0.3750(1)	0.2342(2)	0.26896(6)	0.0342(7)

Sn39	4e	1	0.4743(1)	0.3853(2)	0.21412(5)	0.0235(6)
Sn40	4e	1	0.4904(1)	0.2184(2)	0.25289(6)	0.0280(6)
Sn41	4e	1	0.3853(1)	0.1339(2)	0.17315(6)	0.0318(7)
Sn42	4e	1	0.3834(1)	0.3347(2)	0.17373(6)	0.0337(7)
Sn43	4e	1	0.4916(1)	0.1986(2)	0.19066(6)	0.0323(7)
Sn44	4e	1	0.3123(1)	0.2155(2)	0.21476(6)	0.0324(7)
Sn45	4e	1	0.4103(1)	0.0799(2)	0.23274(7)	0.0389(8)
Sn46	4e	1	0.3724(1)	0.3809(2)	0.50326(6)	0.0290(6)
Sn47	4e	1	0.4592(1)	0.2209(2)	0.57815(6)	0.0381(7)
Sn48	4e	1	0.4882(1)	0.3435(2)	0.52207(7)	0.0375(7)
Sn49	4e	1	0.3165(1)	0.2007(2)	0.50896(5)	0.0235(6)
Sn50	4e	1	0.421(1)	0.2185(2)	0.47959(6)	0.0322(7)
Sn51	4e	1	0.409(1)	0.3966(2)	0.56319(6)	0.0385(8)
Sn52	4e	1	0.4946(1)	0.1409(2)	0.52326(6)	0.0382(8)
Sn53	4e	1	0.3377(1)	0.2360(2)	0.57137(6)	0.0395(8)
Sn54	4e	1	0.3887(1)	0.0808(2)	0.54529(8)	0.0463(9)
Sn55	4e	1	0.1414(1)	0.2512(2)	0.51133(6)	0.0383(7)
Sn56	4e	1	0.1751(1)	0.3553(3)	0.46287(6)	0.0446(9)
Sn57	4e	1	0.0756(1)	0.0946(2)	0.49115(7)	0.0413(8)
Sn58	4e	1	0.0512(1)	0.1345(2)	0.43143(6)	0.0391(8)
Sn59	4e	1	0.0240(1)	0.2647(3)	0.51047(7)	0.0474(9)
Sn60	4e	1	0.1611(1)	0.1588(3)	0.45449(8)	0.0482(9)
Sn61	4e	1	0.9925(1)	0.3000(2)	0.45122(8)	0.0490(9)
Sn62	4e	1	0.0907(2)	0.3150(3)	0.42072(8)	0.0609(1)
Sn63	4e	1	0.0711(2)	0.4158(3)	0.48080(9)	0.0612(1)
Sn64	4e	1	0.0702(1)	0.1161(2)	0.25540(6)	0.0354(7)
Sn65	4e	1	0.0016(1)	0.2823(3)	0.26011(9)	0.0581(1)
Sn66	4e	1	0.1049(2)	0.2973(2)	0.23274(7)	0.0534(1)
Sn67	4e	1	0.1356(1)	0.3009(3)	0.33145(7)	0.0498(1)
Sn68	4e	0.425(7)	0.0544(3)	0.1495(6)	0.3185(2)	0.038(2)
Sn69	4e	0.425(7)	0.1630(3)	0.1386(6)	0.2964(2)	0.038(2)
Sn70	4e	0.425(7)	0.1865(3)	0.3232(8)	0.2715(2)	0.043(3)
Sn71	4e	0.425(7)	0.0861(5)	0.4294(6)	0.2783(2)	0.047(3)
Sn72	4e	0.425(7)	0.0284(3)	0.3430(5)	0.3237(2)	0.034(2)
Sn73	4e	0.575(7)	0.0942(5)	0.1077(5)	0.3145(1)	0.081(4)
Sn74	4e	0.575(7)	0.1792(3)	0.1815(6)	0.2802(2)	0.055(2)
Sn75	4e	0.575(7)	0.1722(3)	0.3816(5)	0.2809(1)	0.049(2)
Sn76	4e	0.575(7)	0.0605(3)	0.4215(5)	0.2926(3)	0.080(3)
Sn77	4e	0.575(7)	0.0159(2)	0.2575(7)	0.3200(1)	0.069(3)
Pd1	4e	0.56(1)	0.4111(2)	0.2461(4)	0.2181(1)	0.015(2)
Pd2	4e	0.54(1)	0.4076(2)	0.2461(4)	0.5325(1)	0.013(2)
Pd3	4e	0.26(1)	0.0841(4)	0.2552(8)	0.4684(2)	0.013(4)
Pd4	4e	0.50(1)	0.0919(2)	0.2600(4)	0.2846(1)	0.017(2)
K1	4e	1	0.0694(4)	0.938(1)	0.7200(2)	0.062(4)
K2	4e	1	0.2164(4)	0.852(1)	0.3468(2)	0.081(5)
K3	4e	1	0.5010(3)	0.0957(6)	0.6362(2)	0.026(2)
K4	4e	1	0.3362(3)	0.9079(6)	0.1864(2)	0.024(2)
K5	4e	1	0.1816(3)	0.4405(6)	0.3892(2)	0.029(2)
K6	4e	1	0.3716(3)	-0.2990(6)	0.3314(2)	0.026(2)
K7	4e	1	0.2456(3)	0.7140(6)	0.4087(2)	0.029(2)
K8	4e	1	0.9885(3)	0.0918(6)	0.5567(2)	0.029(2)
K9	4e	1	0.2971(3)	0.2001(6)	0.4312(2)	0.027(2)
K10	4e	1	0.4046(3)	0.6182(6)	0.1977(2)	0.027(2)
K11	4e	1	0.3951(3)	0.7922(6)	0.4239(2)	0.026(2)
K12	4e	1	0.5117(3)	0.5415(7)	0.3727(2)	0.030(2)
K13	4e	1	0.2902(4)	0.5170(6)	0.4586(2)	0.030(2)
K14	4e	1	0.2844(3)	0.3012(6)	0.3287(2)	0.025(2)
K15	4e	1	0.5061(3)	0.0820(6)	0.4410(2)	0.026(2)
K16	4e	1	0.1158(3)	0.8788(7)	0.2772(2)	0.032(2)
K17	4e	1	0.2851(4)	0.0282(6)	0.2892(2)	0.032(2)

K18	4e	1	0.1932(3)	-0.0805(6)	0.4547(2)	0.031(2)
K19	4e	1	0.2462(4)	0.4033(6)	0.5344(2)	0.033(2)
K20	4e	1	0.0176(4)	0.9832(7)	0.3651(2)	0.036(2)
K21	4e	1	0.3898(4)	0.8501(7)	0.2670(2)	0.040(2)
K22	4e	1	0.4059(3)	0.6195(6)	0.5228(2)	0.031(2)
K23	4e	1	0.2257(4)	0.7194(6)	0.1670(2)	0.034(2)
K24	4e	1	0.3585(4)	0.9796(6)	0.474(2)	0.036(2)
K25	4e	1	0.1653(3)	0.6011(7)	0.3126(2)	0.031(2)
K26	4e	1	0.2948(3)	0.5267(6)	0.2809(2)	0.027(2)
K27	4e	1	0.2171(4)	0.0656(6)	0.5479(2)	0.033(2)
K28	4e	1	0.4722(3)	0.4356(6)	0.2915(2)	0.030(2)
K29	4e	1	0.3289(4)	0.4854(7)	0.1208(2)	0.038(2)
K30	4e	1	0.2592(4)	0.3012(7)	0.6366(2)	0.036(2)
K31	4e	1	0.3427(4)	0.8402(6)	0.5590(2)	0.038(2)
K32	4e	1	0.4282(3)	0.2578(6)	0.3833(2)	0.036(2)
K33	4e	1	0.1089(4)	0.2684(7)	0.5835(2)	0.040(2)
K34	4e	1	0.2288(4)	0.7019(7)	0.5919(2)	0.040(2)
K35	4e	1	0.4501(4)	0.4466(7)	0.4416(2)	0.037(2)
K36	4e	1	0.0815(4)	0.6427(7)	0.4491(2)	0.041(2)
K37	4e	1	0.2249(4)	0.0469(7)	0.7042(2)	0.038(2)
K38	4e	1	0.0942(4)	0.8833(7)	0.5338(2)	0.041(2)
K39	4e	1	0.0569(4)	0.7981(6)	0.6167(2)	0.042(3)
K40	4e	1	0.1924(4)	0.0936(7)	0.2130(2)	0.044(3)
K41	4e	1	0.4385(4)	0.1020(8)	0.3224(2)	0.044(3)
K42	4e	1	0.1676(4)	0.0891(9)	0.3798(2)	0.050(3)
K43	4e	1	0.3316(4)	0.5344(8)	0.6037(3)	0.060(3)
K44	4e	1	0.1094(4)	0.632(1)	0.6930(2)	0.064(4)
K45	4e	1	0.1264(5)	0.5829(9)	0.5363(2)	0.067(4)
K46	4e	0.897(5)	0.9964(5)	0.616(1)	0.3131(3)	0.060(4)
K47	4e	0.897(5)	0.0871(4)	0.1928(7)	0.6589(2)	0.030(2)
K48	4e	0.103(5)	0.043(3)	0.269(4)	0.681(1)	0.01(1)
K49	4e	0.26(2)	0.979(2)	0.530(4)	0.637(1)	0.07(2)
K50	4e	0.74(2)	0.9967(6)	0.515(1)	0.6120(5)	0.067(7)
K51	4e	0.26(2)	0.042(1)	0.453(2)	0.5706(7)	0.024(9)

Table 3.46 Anisotropic displacement parameters (\AA^2) for the compound $\text{K}_{12.04(2)}\text{Pd}_{0.47(1)}\text{Sn}_{17}$.

Atom	U_{11}	U_{22}	U_{33}	U_{12}	U_{13}	U_{23}
Sn1	0.021(1)	0.028(2)	0.020(1)	0.004(1)	0.002(1)	0.000(1)
Sn2	0.015(1)	0.027(2)	0.027(1)	0.002(1)	0.001(1)	-0.002(1)
Sn3	0.024(1)	0.020(1)	0.023(1)	0.001(1)	0.004(1)	0.002(1)
Sn4	0.021(1)	0.028(2)	0.022(1)	-0.004(1)	0.000(1)	-0.004(1)
Sn5	0.022(1)	0.020(1)	0.018(1)	0.002(1)	0.001(1)	-0.001(1)
Sn6	0.019(1)	0.022(2)	0.020(1)	-0.001(1)	0.006(1)	-0.000(1)
Sn7	0.024(1)	0.021(1)	0.020(1)	-0.002(1)	-0.000(1)	-0.002(1)
Sn8	0.016(1)	0.026(1)	0.020(1)	0.003(1)	0.001(1)	0.001(1)
Sn9	0.024(1)	0.022(1)	0.022(1)	0.003(1)	0.002(1)	0.002(1)
Sn10	0.021(1)	0.025(1)	0.016(1)	0.001(1)	-0.001(1)	0.000(1)
Sn11	0.023(1)	0.027(2)	0.024(1)	0.003(1)	0.010(1)	0.003(1)
Sn12	0.022(1)	0.028(2)	0.019(1)	-0.001(1)	-0.001(1)	-0.006(1)
Sn13	0.018(1)	0.023(1)	0.021(1)	0.005(1)	0.002(1)	-0.002(1)
Sn14	0.024(1)	0.021(1)	0.022(1)	0.004(1)	0.001(1)	0.004(1)
Sn15	0.017(1)	0.022(1)	0.024(1)	-0.001(1)	-0.003(1)	-0.001(1)
Sn16	0.021(1)	0.023(1)	0.023(1)	-0.005(1)	0.002(1)	0.002(1)
Sn17	0.016(1)	0.031(2)	0.021(1)	-0.001(1)	0.002(1)	-0.001(1)
Sn18	0.017(1)	0.032(2)	0.023(1)	0.001(1)	0.001(1)	-0.001(1)
Sn19	0.027(2)	0.029(2)	0.026(1)	0.003(1)	0.008(1)	0.007(1)
Sn20	0.026(2)	0.038(2)	0.018(1)	0.003(1)	0.003(1)	0.003(1)
Sn21	0.024(1)	0.028(2)	0.024(1)	-0.002(1)	0.006(1)	-0.003(1)
Sn22	0.022(1)	0.033(2)	0.024(1)	-0.001(1)	0.004(1)	-0.003(1)

Sn23	0.019(1)	0.032(2)	0.028(1)	-0.006(1)	0.001(1)	-0.000(1)
Sn24	0.025(2)	0.031(2)	0.044(2)	-0.001(1)	0.000(1)	0.009(1)
Sn25	0.026(2)	0.029(2)	0.028(1)	0.008(1)	-0.001(1)	-0.002(1)
Sn26	0.026(2)	0.028(2)	0.031(2)	0.006(1)	0.006(1)	0.001(1)
Sn27	0.044(2)	0.043(2)	0.027(2)	-0.006(1)	-0.001(1)	0.024(2)
Sn28	0.034(2)	0.045(2)	0.042(2)	0.006(2)	-0.015(1)	-0.008(2)
Sn29	0.022(2)	0.028(2)	0.017(2)	0.004(2)	-0.001(1)	0.001(2)
Sn30	0.027(2)	0.022(2)	0.025(2)	0.003(1)	0.003(1)	0.004(1)
Sn31	0.020(2)	0.024(2)	0.028(2)	-0.004(1)	-0.001(1)	-0.004(1)
Sn32	0.020(2)	0.026(2)	0.021(2)	0.003(1)	-0.004(1)	0.000(2)
Sn33	0.013(1)	0.018(2)	0.019(1)	0.012(1)	-0.003(9)	0.006(1)
Sn34	0.033(2)	0.009(1)	0.028(1)	0.000(1)	0.010(1)	0.012(1)
Sn35	0.021(1)	0.031(2)	0.038(2)	0.008(1)	0.003(1)	-0.007(1)
Sn37	0.029(2)	0.028(2)	0.045(2)	-0.006(1)	0.013(1)	0.0061(1)
Sn38	0.031(2)	0.050(2)	0.021(1)	0.007(1)	0.005(1)	0.002(2)
Sn39	0.020(1)	0.024(1)	0.026(1)	-0.000(1)	-0.002(1)	-0.002(1)
Sn40	0.022(1)	0.035(2)	0.027(1)	0.008(1)	-0.003(1)	-0.004(1)
Sn41	0.027(2)	0.037(2)	0.031(2)	-0.012(1)	-0.001(1)	-0.003(1)
Sn42	0.035(2)	0.038(2)	0.027(2)	0.012(1)	-0.006(1)	-0.011(1)
Sn43	0.027(2)	0.035(2)	0.035(2)	-0.012(1)	0.009(1)	-0.001(1)
Sn44	0.023(2)	0.042(2)	0.032(2)	-0.003(1)	-0.003(1)	-0.006(1)
Sn45	0.040(2)	0.025(2)	0.051(2)	-0.003(1)	-0.011(2)	-0.002(1)
Sn46	0.027(2)	0.027(2)	0.033(2)	0.004(1)	-0.001(1)	0.003(1)
Sn47	0.030(2)	0.048(2)	0.035(2)	0.005(2)	-0.009(1)	0.007(2)
Sn48	0.030(2)	0.039(2)	0.044(2)	0.007(2)	0.002(1)	-0.009(1)
Sn49	0.020(1)	0.026(1)	0.024(1)	-0.002(1)	0.001(1)	-0.002(1)
Sn50	0.027(2)	0.041(2)	0.029(2)	-0.016(1)	0.003(1)	0.003(1)
Sn51	0.064(2)	0.028(2)	0.023(2)	-0.005(1)	-0.002(1)	0.005(2)
Sn52	0.041(2)	0.040(2)	0.035(2)	0.005(1)	0.009(1)	0.021(2)
Sn53	0.037(2)	0.057(2)	0.025(2)	-0.003(2)	0.0064(1)	-0.004(2)
Sn54	0.048(2)	0.024(2)	0.066(2)	-0.005(2)	-0.023(2)	0.006(2)
Sn55	0.037(2)	0.050(2)	0.028(2)	0.011(1)	-0.002(1)	-0.006(2)
Sn56	0.039(2)	0.063(2)	0.031(2)	0.014(1)	-0.002(1)	-0.032(2)
Sn57	0.054(2)	0.028(2)	0.042(2)	0.008(1)	0.005(2)	-0.007(2)
Sn58	0.034(2)	0.048(2)	0.035(2)	-0.005(2)	-0.006(3)	-0.009(2)
Sn59	0.039(2)	0.060(2)	0.045(2)	0.007(2)	0.021(2)	0.002(2)
Sn60	0.033(2)	0.056(2)	0.056(2)	-0.020(2)	0.012(2)	0.004(2)
Sn61	0.028(2)	0.048(2)	0.071(2)	0.005(2)	-0.009(2)	0.005(2)
Sn62	0.051(2)	0.084(3)	0.047(2)	0.034(2)	-0.009(2)	-0.038(2)
Sn63	0.065(3)	0.037(2)	0.082(3)	0.002(2)	-0.002(2)	-0.016(2)
Sn64	0.034(2)	0.029(2)	0.043(2)	-0.006(1)	-0.013(1)	0.002(1)
Sn65	0.027(2)	0.049(2)	0.098(3)	-0.021(2)	-0.015(2)	0.012(2)
Sn66	0.094(3)	0.039(2)	0.028(2)	0.010(2)	0.012(2)	-0.002(2)
Sn67	0.049(2)	0.060(2)	0.0396(2)	-0.019(2)	-0.020(2)	0.015(2)
Sn68	0.054(5)	0.033(5)	0.026(4)	0.005(3)	0.009(3)	-0.007(4)
Sn69	0.032(4)	0.039(5)	0.042(5)	-0.006(4)	-0.010(4)	0.017(4)
Sn70	0.020(4)	0.086(8)	0.022(4)	0.016(4)	-0.002(3)	-0.019(4)
Sn71	0.069(7)	0.034(5)	0.038(5)	-0.015(4)	-0.005(4)	0.001(5)
Sn72	0.026(4)	0.039(5)	0.037(4)	-0.004(3)	0.005(3)	0.009(3)
Sn73	0.184(1)	0.032(4)	0.028(3)	0.005(3)	0.002(5)	-0.020(5)
Sn74	0.047(4)	0.061(5)	0.054(5)	-0.031(4)	-0.028(4)	0.033(4)
Sn75	0.049(4)	0.047(4)	0.051(4)	-0.004(3)	0.018(3)	-0.024(3)
Sn76	0.054(5)	0.035(4)	0.15(1)	-0.026(6)	-0.028(6)	0.010(4)
Sn77	0.026(3)	0.149(9)	0.032(3)	0.007(4)	0.007(3)	-0.018(4)
Pd1	0.014(3)	0.016(3)	0.013(3)	-0.001(2)	-0.001(2)	0.003(2)
Pd2	0.013(3)	0.019(3)	0.007(3)	0.001(2)	0.001(2)	-0.001(2)
Pd3	0.011(6)	0.023(7)	0.006(5)	0.008(4)	-0.002(4)	-0.003(5)
Pd4	0.018(4)	0.021(4)	0.012(3)	0.004(2)	0.000(2)	-0.002(3)
K1	0.043(7)	0.09(1)	0.052(7)	0.034(7)	0.016(5)	0.015(6)
K2	0.031(6)	0.17(2)	0.043(6)	-0.052(8)	0.011(5)	-0.045(8)

K3	0.026(4)	0.031(5)	0.020(4)	0.004(4)	0.000(3)	0.001(4)
K4	0.026(4)	0.027(5)	0.019(4)	-0.002(3)	0.004(3)	0.002(4)
K5	0.020(4)	0.039(5)	0.029(5)	0.011(4)	0.006(4)	-0.002(4)
K6	0.029(5)	0.023(4)	0.028(4)	0.006(4)	0.003(4)	-0.006(4)
K7	0.028(5)	0.023(5)	0.036(5)	-0.004(4)	-0.002(4)	0.006(4)
K8	0.025(5)	0.034(5)	0.029(5)	0.000(4)	0.005(4)	-0.003(4)
K9	0.031(5)	0.025(5)	0.023(4)	0.004(4)	0.001(4)	-0.001(4)
K10	0.022(4)	0.034(5)	0.026(4)	0.003(4)	0.008(3)	0.007(4)
K11	0.022(4)	0.026(5)	0.031(4)	0.001(4)	0.003(4)	-0.002(4)
K12	0.019(4)	0.042(6)	0.028(5)	0.007(4)	0.002(3)	-0.003(4)
K13	0.042(5)	0.020(4)	0.030(5)	-0.001(4)	0.002(4)	0.000(4)
K14	0.025(4)	0.019(4)	0.031(4)	-0.002(4)	-0.007(4)	0.002(4)
K15	0.020(4)	0.030(5)	0.029(4)	0.004(4)	0.004(3)	0.005(4)
K16	0.028(5)	0.042(6)	0.025(4)	0.006(4)	0.007(4)	0.004(4)
K17	0.030(5)	0.031(5)	0.036(5)	-0.004(4)	-0.009(4)	0.002(4)
K18	0.028(5)	0.038(5)	0.028(5)	0.005(4)	0.002(4)	0.000(4)
K19	0.035(5)	0.034(5)	0.030(5)	-0.003(4)	0.015(4)	-0.005(4)
K20	0.032(5)	0.038(6)	0.039(5)	0.007(4)	0.003(4)	0.009(4)
K21	0.023(5)	0.035(5)	0.062(7)	0.014(5)	-0.004(4)	-0.003(4)
K22	0.030(5)	0.034(5)	0.029(5)	-0.004(4)	-0.006(4)	0.002(4)
K23	0.052(6)	0.027(5)	0.023(4)	0.002(4)	0.002(4)	-0.009(4)
K24	0.063(7)	0.025(5)	0.019(4)	-0.003(4)	0.009(4)	-0.006(5)
K25	0.025(5)	0.044(6)	0.024(4)	0.006(4)	0.009(4)	-0.003(4)
K26	0.035(5)	0.027(5)	0.020(4)	-0.002(4)	0.003(4)	0.007(4)
K27	0.033(5)	0.031(5)	0.036(5)	0.008(4)	0.006(4)	0.001(4)
K28	0.025(5)	0.041(6)	0.025(4)	-0.004(4)	-0.002(4)	0.003(4)
K29	0.044(6)	0.034(6)	0.036(5)	0.010(4)	-0.010(4)	-0.011(5)
K30	0.031(5)	0.042(6)	0.036(5)	-0.004(4)	-0.005(4)	0.006(4)
K31	0.037(5)	0.026(5)	0.050(6)	0.001(4)	-0.015(5)	-0.001(4)
K32	0.016(4)	0.023(5)	0.071(7)	0.005(5)	0.006(4)	0.003(4)
K33	0.028(5)	0.059(7)	0.034(5)	-0.011(5)	0.001(4)	-0.014(5)
K34	0.044(6)	0.046(6)	0.031(5)	-0.004(4)	0.007(4)	-0.004(5)
K35	0.035(5)	0.043(6)	0.031(5)	0.008(4)	-0.001(4)	0.001(4)
K36	0.050(6)	0.052(6)	0.020(4)	0.005(4)	0.002(4)	-0.005(5)
K37	0.032(5)	0.051(6)	0.029(5)	-0.007(4)	-0.007(4)	-0.001(5)
K38	0.041(6)	0.044(6)	0.038(5)	-0.004(5)	0.010(4)	-0.001(5)
K39	0.061(7)	0.022(5)	0.042(6)	0.004(4)	-0.012(5)	0.010(5)
K40	0.033(5)	0.044(6)	0.054(6)	0.019(5)	-0.011(5)	-0.004(5)
K41	0.030(5)	0.060(7)	0.042(6)	0.026(5)	-0.011(4)	-0.012(5)
K42	0.025(5)	0.083(9)	0.042(6)	0.010(6)	0.007(4)	0.004(5)
K43	0.033(6)	0.062(8)	0.086(9)	-0.027(7)	0.027(6)	-0.013(5)
K44	0.035(6)	0.11(1)	0.043(6)	-0.037(7)	-0.014(5)	0.028(7)
K45	0.067(8)	0.081(9)	0.052(7)	-0.009(7)	-0.020(6)	0.044(7)
K46	0.029(6)	0.09(1)	0.058(8)	-0.030(8)	0.005(6)	-0.011(7)
K47	0.029(5)	0.03(6)	0.030(5)	-0.001(4)	-0.007(4)	0.008(4)
K50	0.033(9)	0.05(1)	0.12(2)	0.02(1)	-0.03(1)	-0.016(7)
K51	0.011(2)	0.03(2)	0.03(2)	0.00(1)	0.01(1)	0.00(1)

Table 3.47 Results of the EDX analysis of the crystal of the compound $K_{12}Pd_{0.47}Sn_{17}$ from the sample 'K₅PdSn₉' (average of the four measurements: two spots and two surface scans from the same crystal).

	K (at. %)	Pd (at. %)	Sn (at. %)
EDX	44(8)	1.2(9)	55(6)
$K_{12}Pd_{0.47}Sn_{17}$	40.7	1.6	57.7

Crystal Structure of the $K_{12}Pd_{0.47}Sn_{17}$

The compound $K_{12}Pd_{1-x}Sn_{17}$ was obtained for the first time by Hanpeng Jin as a part of his Master thesis [132]. However, poor quality of the crystals did not allow to sufficiently solve the crystal structure. It was reinvestigated in order to obtain better structure solution, which was successfully achieved in this work.

Compound $K_{12}Pd_{0.47}Sn_{17}$ crystallizes in monoclinic space group $P2_1/c$, same as $K_{12}Sn_{17}$. It is remarkable that the unit cell parameter of the $K_{12}Pd_{0.46}Sn_{17}$ didn't increase compared to the binary $K_{12}Sn_{17}$ [123] (measured higher temperature – 193 K), on contrary, the cell volume got smaller by 1.2%. This was also observed for both $Na_{11.98(3)}Ni_{0.93(1)}Sn_{17}$ (30.5% volume decrease) and $K_{13}CoSn_{17}$. (10.3% volume decrease, Table 3.48). In case of $Na_{11.98(3)}Ni_{0.93(1)}Sn_{17}$ volume decrease compare to $K_{12}Sn_{17}$ is logical: sodium atoms are smaller than potassium, whereas for $K_{13}CoSn_{17}$, it is even more unusual because of the negative charge of the cobalt atoms centering the cluster. This remarkable fact was traced back to the degree of disorder of the empty clusters in $K_{12}Sn_{17}$. The volume of the unit cell increases as higher the disorder is.

The unit cell of the reported compound (shown in Figure 3.45) consists of eight tetrahedral clusters $\{Sn_4\}^{4-}$ (4A, 4B, 4C, 4D, 4E, 4F, 4G, and 4H; Figure 3.46) and four nine-atom clusters centered by Pd atoms $\{Pd@Sn_9\}^{4-}$ (9A, 9B, 9C, and 9D; Figure 3.47). The cluster packing pattern shows close relation to the hexagonal $MgZn_2$ -type, where $\{Pd@Sn_9\}^{4-}$ clusters are taking Mg position and $\{Sn_4\}^{4-}$ - both of Zn positions (Figure 3.49). All four crystallographically independent Pd atoms centering 9-atom Sn clusters are partially occupied with 56(1), 54(1), 26(1), 50(1) of Pd for Pd1, Pd2, Pd3, and Pd4 position respectively.

A special feature of $K_{12}Pd_{0.46}Sn_{17}$ is disorder observed in 4H tetrahedra and 9D nine-atom cluster. Both types of disorder within the structure are shown in Figure 3.48. The 4H tetrahedra can be represented as a combination of the $4H_1$ (formed by Sn29, Sn30, Sn31 and Sn32 atoms) and $4H_2$ (Sn33, Sn34, Sn35 and Sn36 atoms) tetrahedra that occur in the structure with the ratio of 0.897(5):0.103(5). The 9D cluster is a combination of $9D_1$ (Sn64, Sn65, Sn66, Sn67, Sn68, Sn69, Sn70, Sn71 and Sn72) and $9D_2$ (Sn64, Sn65, Sn66, Sn67, Sn73, Sn74, Sn75, Sn76 and Sn77) clusters that have four common atoms (Sn64, Sn65, Sn66 and Sn67) and ratio 42.6(7):57.4(7). On one hand, Pd1, Pd3 and Pd4 atoms are surrounded with nine Sn atoms (clusters 9A, 9C, $9D_2$ respectively) forming a polyhedron with one quadrangle

face and could be defined as slightly deformed monocapped square prism. On the other hand, Pd₂ and Pd₄ are encapsulated into tricapped trigonal prisms (9B, 9D₁ respectively) with only trigonal faces.

In Table 3.49 selected interatomic distances are shown. Sn-Sn distances are between 2.7870(8) and 3.5049(4) Å in the {Pd@Sn₉}⁴⁻ cluster which is on average longer in comparison to the empty {Sn₉}⁴⁻ clusters in K₄Sn₉ and K₁₂Sn₁₇. The Sn-Sn distances in the {Sn₄}⁴⁻ (2.8829(4) and 2.9859(4) Å) are in good correlation with those in K₁₂Sn₁₇ and K₄Sn₄. Despite the negligible cell parameter increase compare to the K₁₂Sn₁₇, filling clusters with transition metals, in our case with Palladium, has an effect on the cluster size: elongation of the Sn-Sn distances and cluster volume increase, calculated with VESTA^[133] (Table 3.50). The volume increase of the ordered 9-atom cluster {Pd@Sn₉}⁴⁻ compared to the empty {Sn₉}⁴⁻ is 11.1% for the clusters with approximate symmetry *C*_{4v} (13.8 % for those with *D*_{3h} symmetry), which is lower than for other known {*T*@Sn₉}ⁿ⁻ clusters – Table 3.50. This fact has to do with the relatively low occupancy of the Pd atom sites in the structure of the K₁₂Pd_{0.46}Sn₁₇, which is between 26 and 56 %, whereas occupancy of Co-centered {Co@Sn₉}⁵⁻ in K_{5-x}Co_{1-x}Sn₉ is between 76 and 82% and Co- and Ni-centered [(Ni/Co)@Sn₉]^{4-/5-} in K_{12/13}(Ni/Co)_{1-x}Sn₁₇ is more than 93%. Logically, the cluster volume increases because of incorporation atoms of the transition metal (Pd, Ni or Co) interatomic distances between *T* and Sn atoms increase in the raw Pd-Co-Ni, proportionate to the occupation of the *T*-positions in the respective structures.

Pd-Sn distances within the {Pd@Sn₉}⁴⁻ cluster are between 2.4650(1) and 2.8073(9) Å, which is a lot shorter than in the binary Pd-Sn compounds with high coordination number of Pd (2.788-2.837 Å for α-PdSn₂; 2.800-2.839 Å for β-PdSn₂; 2.805- 2.810 Å for PdSn₃; 2.750-2.814 Å for PdSn₄). This shows cluster effect forcing Sn atoms to form closer packing and a unique interaction between Pd and Sn atoms.

After dissolving the sample in liquid ammonia no filled clusters were found. However, the sample with the composition 'Na₁₂Pd₂Sn₁₇' showed the presence of {Pd@Sn₉}⁴⁻ anions. For the details, see PhD dissertation of M. Sc. B. Witzel (TUM, 2020).

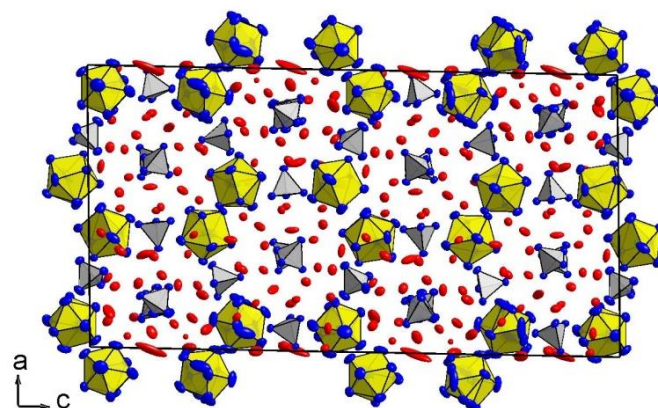


Figure 3.45 Crystal structure of the $K_{12}Pd_{1-x}Sn_{17}$. Potassium atoms are shown in red, tin – in blue and palladium – in green. Thermal ellipsoids are drawn with 90 % probability level.

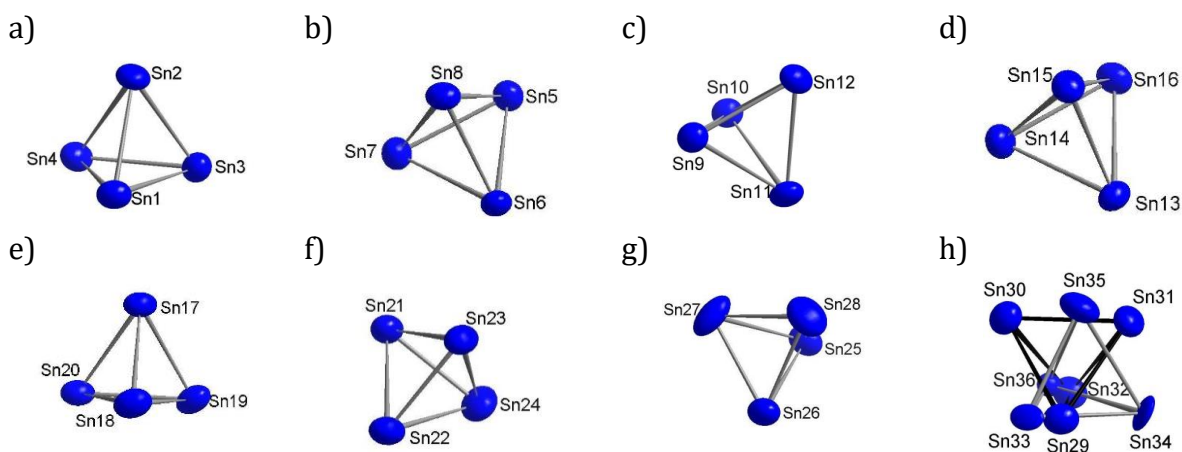


Figure 3.46 Tetrahedral $\{Sn_4\}$ clusters in $K_{12}Pd_{0.47}Sn_{17}$: seven ordered (a-g) and a disordered one (h).

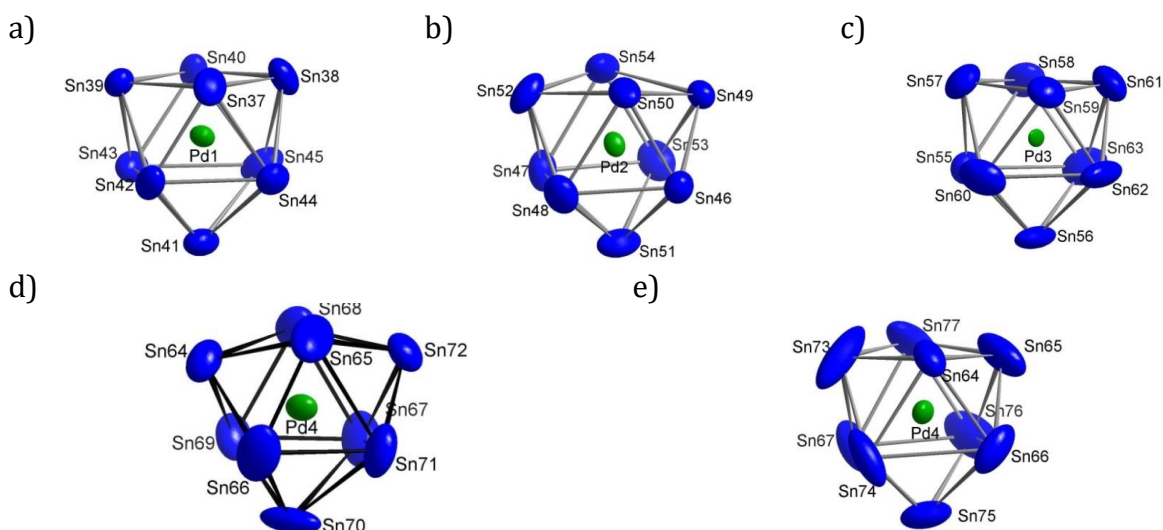
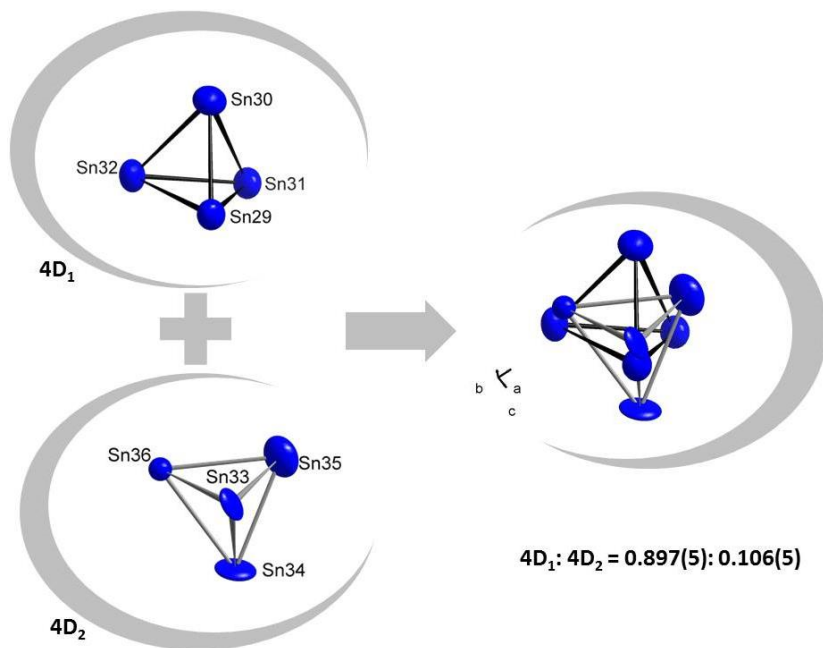


Figure 3.47 $\{Pd@Sn_9\}$ clusters in $K_{12}Pd_{0.47}Sn_{17}$: slightly deformed monocapped square prism with symmetry close to C_{4v} : $9A$ (a), $9C$ (c) and $9D_2$ (e) around Pd1 (54.2 % Pd); Pd3 (26.1 %); and Pd4 (50.2 %) atoms respectively; tricapped trigonal prism with approximate symmetry D_{3h} for Pd2 (b), (54.2 %) and Pd4 (d).

a)



b)

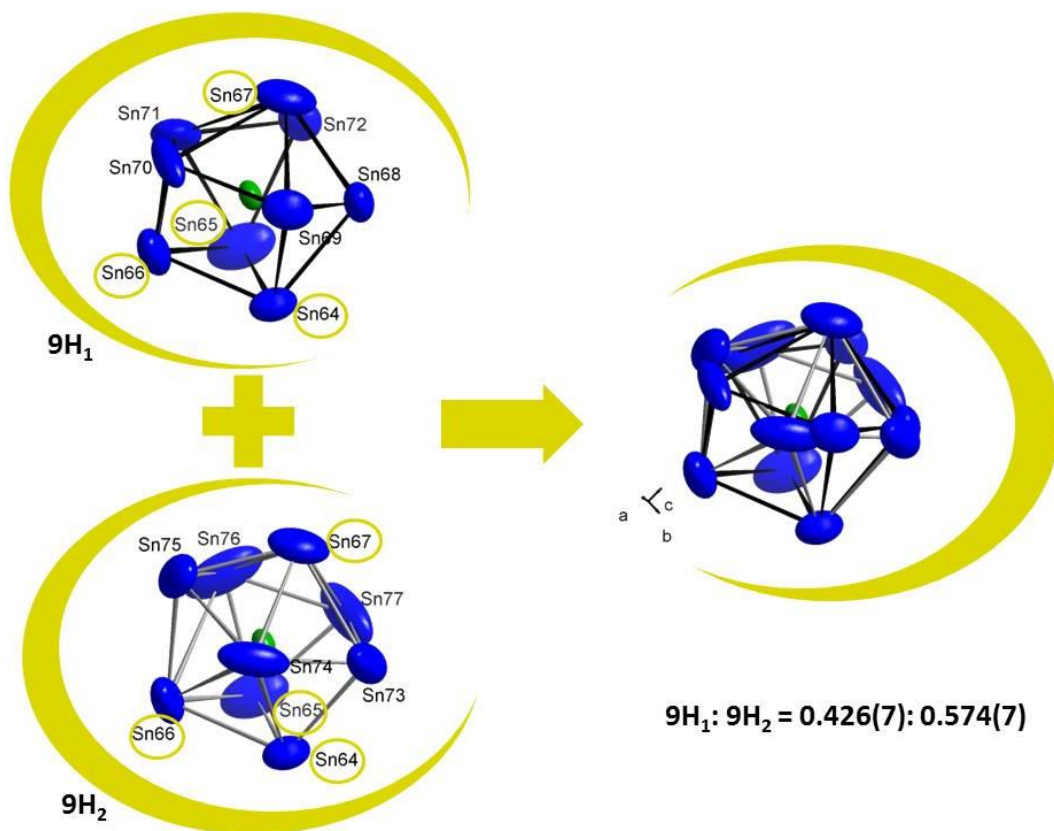


Figure 3.48 Two types of disordered polyhedra in the structure of the $K_{12}Pd_{0.47}Sn_{17}$: tetrahedra I and II with respected probability 90:10% and clusters around position Pd4 (50.2% Palladium occupancy) with probability 43:57%.

Table 3.48 Unit cell parameter for the binary cluster compound $K_{12}Sn_{17}$ and its ternary derivatives: compounds with $\{Sn_9\}$ clusters endohedrally filled with transition metal.

Formula	Space group	Z	Unit cell parameters (Å)			Volume (Å ³)	T (K)
			a	b	c		
$K_{12.063(4)}Pd_{0.47(2)}Sn_{17}$	$P2_1/c$	16	25.606(3)	14.815(2) $\beta = 91.68(0)^\circ$	48.100(5)	18238(4)	130
$Na_{11.98(3)}Ni_{0.93(1)}Sn_{17}$ ^[66]	$P2_1/c$	16	23.734(1)	13.680(1) $\beta = 91.527(4)^\circ$	44.620(2)	14482(1)	110
$K_{13}CoSn_{17}$ ^[66]	Pbca	16	26.1558(3)	23.9928(3)	29.7683(3)	18681.1(4)	150
$K_{12}Sn_{17}$ ^[123]	$P2_1/c$	16	25.618(7)	14.792(5) $\beta = 98.92(0)^\circ$	55.653(9)	20834.0(1)	193

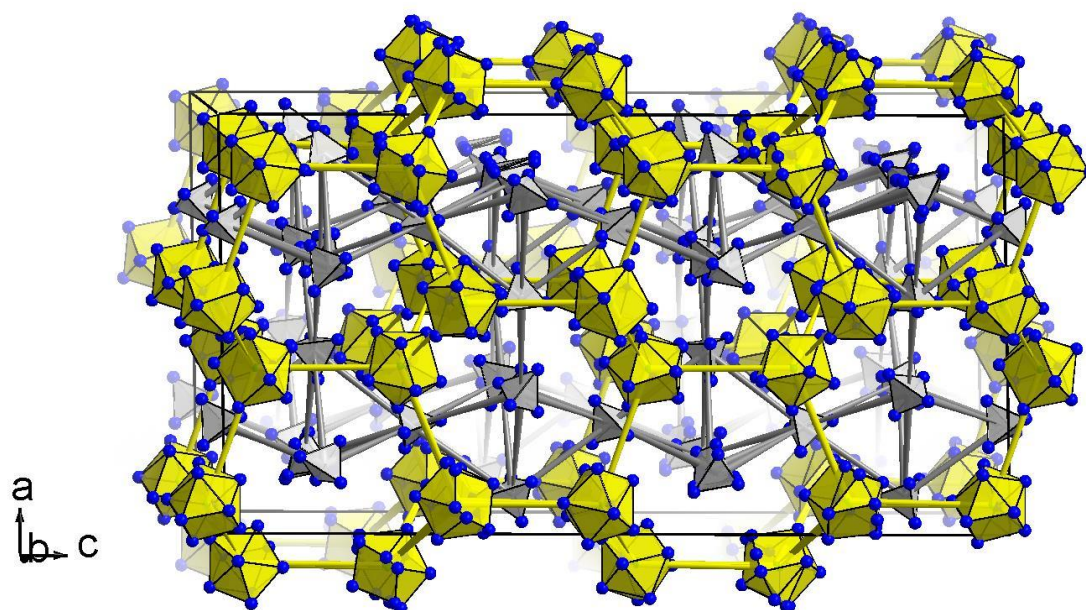
Table 3.49 Comparison of the Sn-Sn and Sn-T (T = transition metal) interatomic distances in empty and filled Sn_9 and Sn_4 clusters (in Å).

Compound	d_{Sn-Sn} in $[_@Sn_9]^{n-}$	d_{Sn-Sn} in $[Sn_4]^{4-}$	D_{T-Sn} in $[T@Sn_9]^{n-}$
K_4Sn_4 ^[31]	-	2.947-2.955	-
K_4Sn_9 ^[33]	2.9264-3.0163	-	-
$K_{51}Sn_{82}$ ^[123]	2.510-3.682	2.804-2.996	-
$K_{12}Ni_{1-x}Sn_{17}$ ^[66]	2.943-3.743	2.898-2.973	2.563-2.755
$K_{13}Co_{1-x}Sn_{17}$ ^[66]	2.964-3.457	2.893-2.951	2.563-2.680
$K_{12}Pd_{1-x}Sn_{17}$	2.787(8)- 3.505(4)	2.883(4) - 2.986(4)	2.4700(1)- 2.8073(9)

Table 3.50 Cluster volumes for various ordered $[T@Sn_9]^{n-}$ clusters calculated with VESTA^[134] and their relation to empty $[Sn_9]^{4-}$ cluster.

Compound	Cluster	Approximate symmetry	Average Cluster Volume (Å ³)	Volume increase (%)
K_4Sn_9 ^[33]	$\{Sn_9\}^{4-}$	C_{4v}	33.4	-
$K_{51}Sn_{82}$ ^[123]	$\{Sn_9\}^{4-}$	C_{4v}	31.5	-
	$\{Sn_9\}^{4-}$	D_{3h}	31.8	-
$K_{12}Ni_{1-x}Sn_{17}$ ^[66]	$\{Ni1@Sn_9\}^{4-}$	C_{4v}	36.1	14.6
	$\{Ni2@Sn_9\}^{4-}$	D_{3h}	36.2	13.8
$K_5Co_{1-x}Sn_9$ ^[127]	$\{Co2@Sn_9\}^{5-}$	C_{4v}	35.3	12.1
	$\{Co1@Sn_9\}^{5-}$	D_{3h}	35.4	11.3
	$\{Co3@Sn_9\}^{5-}$	D_{3h}	35.4	11.3
	$\{Co4@Sn_9\}^{5-}$	D_{3h}	35.4	11.3
$K_{13}Co_{1-x}Sn_{17}$ ^[66]	$\{Co@Sn_9\}^{5-}$	C_{4v}	36.1	14.6
$K_{12}Pd_{1-x}Sn_{17}$	$\{Pd1@Sn_9\}^{4-}$	C_{4v}	36.0	11.1
	$\{Pd3@Sn_9\}^{4-}$	C_{4v}	34.0	7.9
	$\{Pd2@Sn_9\}^{4-}$	D_{3h}	36.2	13.8

a)



b)

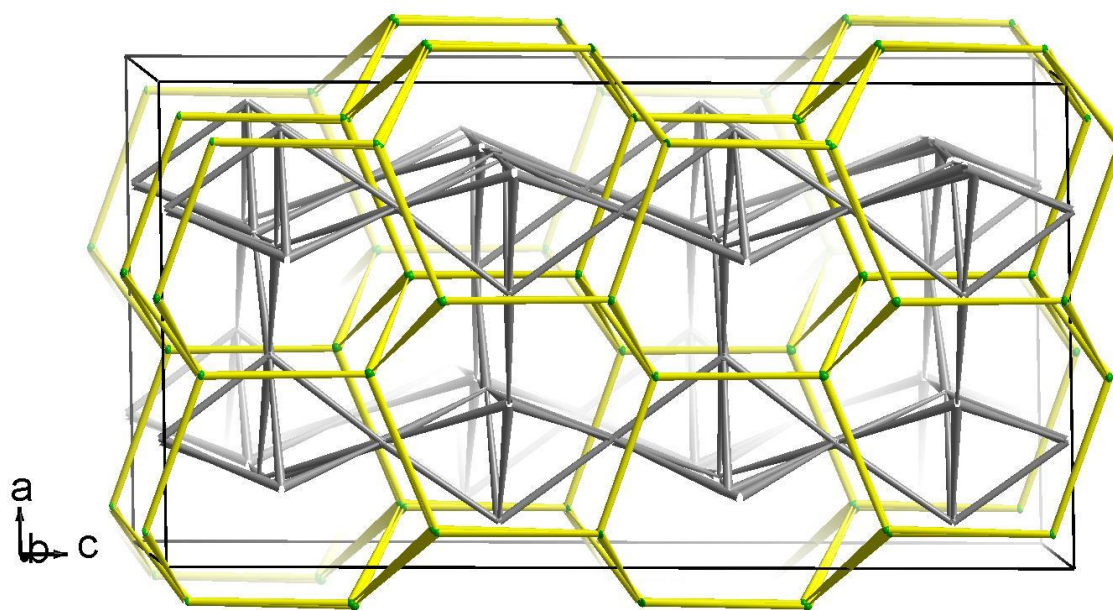


Figure 3.49 Representation of the anionic substructure within the structure of the $K_{12}Pd_{0.47}Sn_{17}$: $\{Pd@Sn_9\}$ clusters in yellow and $\{Sn_4\}$ in grey (a) and packing of the clusters showing relation to $MgZn_2$ -type (b).

3.2.3 Other {*T*@Sn₉} Clusters Obtained as Neat Solids

To investigate the possibility of obtaining endohedrally filled {Sn₉} clusters series of samples with different compositions in the systems *A-T-Sn*, where *A* is Na or K, *T* = Ru, Rh, Pd, Os, Ir, or Pt were prepared. Results of the powder X-ray phase analysis (Figure 3.3.3.1) showed that all the main phases for most of the samples are cluster compounds similar to the binary K₁₂Sn₁₇ (Na₁₂Sn₁₇), showing the fingerprint reflexes typical for such cluster packing in the low angle area (2θ interval 2-10° measured on powder diffractometer with Mo-K α radiation, $\lambda = 0.07932 \text{ \AA}$, or 5-18° measured on powder diffractometer with Cu-K α radiation, $\lambda = 1.54056 \text{ \AA}$). Side products are binary phases *T-Sn*. The only exception was in case of Iridium, when only binary K₄Sn₄ (Na₄Sn₄) and various Ir-Sn phases were obtained, independent from the temperature program or stoichiometry. EDX analysis showed the presence in the expected phases of *T*-metal between 2 and 5 at. %. This together with the results of Raman spectroscopy (see Chapter 3.2.4) confirms the hypothesis that atoms of transition elements are filling the clusters.

3.2.3.1 {Ru@Sn₉}⁶⁻: *Synthesis and Characterization of the K₁₂Ru_{1-x}Sn₁₇*

Ternary sample with a molar ratio K:Ru:Sn of 4:3:7 was prepared using the high temperature reaction of the pre-melted binary Ru-Sn reguli (117.5 mg Ru and 321.9 mg Sn) and elemental Potassium (60.6 mg K). The mixture was sealed in a tantalum ampoule, placed in an evacuated quartz glass tube and subsequently heated to 1000 °C at a rate of 6 °C/min and held for 6 h. The temperature was lowered to 600 °C at 0.1 °C/min, held for 120 h and then cooled to room temperature at 1 °C/min.

Powder X-ray phase analysis (Figure 3.50) showed that the main phase was the cluster containing a compound similar to the binary K₁₂Sn₁₇. EDX analysis showed the presence of Ru up to 2 at. %. This confirms the hypothesis that Ru atoms are filling the clusters. Binary side phases Ru₂Sn₃, Ru₃Sn₇ and RuSn₂ were identified as side products.

Single crystals from the sample were picked and tested for singularity. Monoclinic unit cell with parameters $a = 24.6532$, $b = 15.1389$, $c = 26.1786 \text{ \AA}$ and $\beta = 90.325^\circ$ was found. Unfortunately, the quality of the tested crystals did not allow to properly refine the structure. In order to get better crystallinity of the sample different temperature programs were used but it didn't bring better results. EDX analysis confirmed the presence of Ru atoms in the clusters (Table 3.51).

Dissolving of the sample in the liquid ammonia with 18-crown-6 by M. Sc. Benedikt Witzel and holding it at -42 °C for 2 months led to the crystallization of the $[K_7(OH)]RuSn_9 \cdot 10 NH_3$ [135]. Obtained $[Ru@Sn_9]^{6-}$ cluster is an extraordinary example with respect to the large size of the incorporated metal atoms (Ru), the stabilization of high negative charges of the transition metal (Ru^{2-}) and the so-far highest charge of -6 for an endohedrally filled cluster in the solution.

3.2.3.2 $\{Rh@Sn_9\}^{5-}$: *Synthesis and Characterization of the $Na_{13}Rh_{1-x}Sn_{17}$*

Ternary sample with a molar ratio Na:Rh:Sn of 13:1:17 was prepared using the high temperature reaction of the pre-melted binary Rh-Sn reguli (melted in arc melting furnace pallet of 4.08 mg Rh and 400.0 mg Sn-powder pressed together) and elemental Sodium (5.92 mg Na). The mixture was sealed in a niobium ampoule, placed in an evacuated quartz glass tube and subsequently heated to 1000 °C at a rate of 4 °C/min and held for 2 h. The temperature was lowered to 500°C at 0.1 °C/min, held for 120 h and then cooled to room temperature at 1 °C/min. Single crystals were picked from the sample, but the quality of those did not allow to obtain a model of the structure. EDX analysis (Table 3.51) confirmed the presence of Rh atoms along with Sn and atoms of alkali metals (Na or K). After dissolving both samples $Na_{13}RhSn_{17}$ and K_5RhSn_9 in liquid ammonia $\{Rh@Sn_9\}^{5-}$ cluster was also found crystallizing from the solution. For the details, see PhD dissertation of M. Sc. B. Witzel (TUM, 2020).

3.2.3.3 $\{Os@Sn_9\}^{6-}$ and $\{Pt@Sn_9\}^{4-}$

Samples with the ratio $A:T:Sn$ 6:1:9 (5:1:9) were synthesized using the reaction of 49.4 mg elemental Na (67.0 mg K) with the binary T -Sn precursor in sealed Ta ampoules with the following temperature programs: heating up to 1000° with 4°C/min and holding the temperature for 1 hour and slowly cooling (0.1°C/min) to 600°C, holding for 120 hours and in the last step cooling with 1°C/min to room temperature. Binary precursors were prepared by melting in arc melting oven pallets containing 68.1 mg Os and 382.5 mg Sn powder (66.9 mg Pt and 366.1 mg Sn powder). While testing single crystals for the sample ' K_6OsSn_9 ' a trigonal unit cell with the parameters $a = 29.5651(7)$ and $c = 165.200(6)$ Å was found, but the crystals were not suitable for precise measurement. For the ' Na_5PtSn_9 ' cell parameters were not possible to identify. Only according to Raman and XRPD stating that Pt is also forming endohedrally filled clusters is possible. EDX measurements were not conclusive

because of the rapid oxidation of the crystals during the short contact with air while inserting the sample in the device.

Table 3.51 EDX analysis of the crystal of the crystals 'K₁₄RuSn₁₇', 'Na₁₃RhSn₁₇' and K₁₃RhSn₁₇ from the samples 'K₄Ru₃Sn₇' 'Na₁₃RhSn₁₇' and 'K₅RhSn₉', respectively.

	A (at. %)	T (at. %)	Sn (at. %)
EDX 'K ₁₄ RuSn ₁₇ '	30(8)	2.3(7)	68(6)
'K ₁₄ RuSn ₁₇ '	43.7	3.1	53.1
EDX 'Na ₁₃ RhSn ₁₇ '	58(9)	2.1(3)	40(8)
'Na ₁₃ RhSn ₁₇ '	41.9	3.2	54.8
EDX 'K ₁₃ RhSn ₁₇ '	59(9)	2(3)	39(8)
'K ₁₃ RhSn ₁₇ '	41.9	3.2	54.8

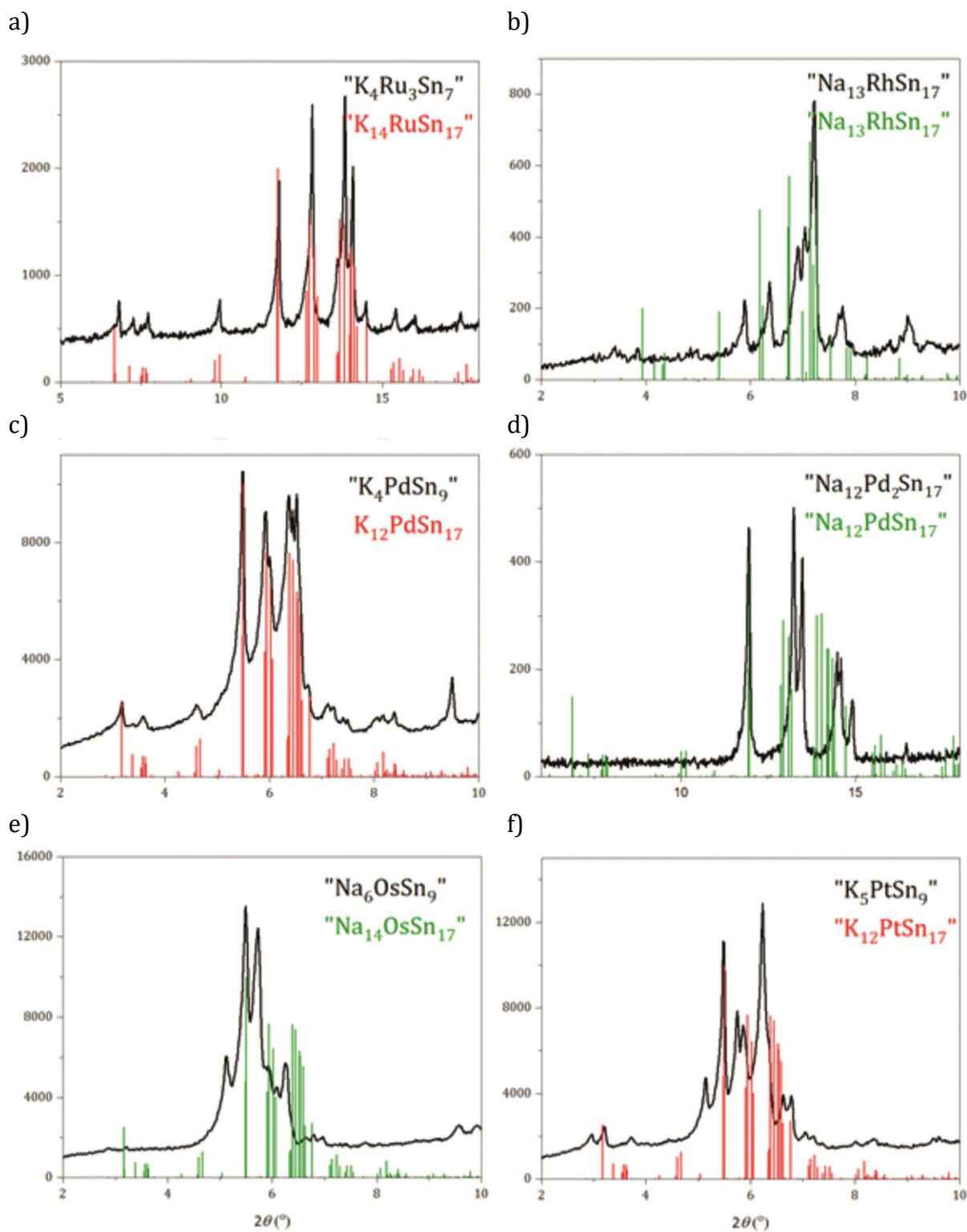


Figure 3.50 Experimental X-ray powder diffractogram in the low angles area of the samples $\text{K}_4\text{Ru}_3\text{Sn}_7$ (a), $\text{Na}_{13}\text{RhSn}_{17}$ (b), K_4PdSn_9 (c), $\text{Na}_{12}\text{Pd}_2\text{Sn}_{17}$ (d), Na_6OsSn_9 (e), K_5PtSn_9 (d). Theoretical patterns of the respective phases were obtained by optimizing known models: $\text{K}_{13}\text{RuSn}_{17}$ (obtained from $\text{K}_{13}\text{Co}_{1-x}\text{Sn}_{17}$ ^[66]); $\text{Na}_{12}\text{Pd}_2\text{Sn}_{17}$ (from $\text{Na}_{12}\text{Ni}_{1-x}\text{Sn}_{17}$ ^[66]); $\text{Na}_{12}\text{RhSn}_{17}$, $\text{Na}_{12}\text{OsSn}_{17}$ and $\text{K}_{12}\text{PtSn}_{17}$ (from $\text{K}_{12}\text{Pd}_{0.46}\text{Sn}_{17}$). Na compounds are shown in green, K – in red.

3.2.4 Raman Spectroscopy for the Characterization of the Endohedrally Filled Clusters

Another important evidence of the presence of the T ($T = \text{Ru}, \text{Rh}, \text{and Pd}$) atoms inside of the clusters are the results of Raman spectroscopy. Typical shifts for the $\text{K}_{12}\text{Sn}_{17}$ were reported by H.G. von Schnering and coauthors in 1997 [136]: 93, 110, 152 – highest intensity), and 190 cm^{-1} . The measurement was reproduced with the following shifts: 88, 109, 152 and 192 cm^{-1} (Figure 3.3.4.1, a).

Because of the lack of experimental data on Raman spectroscopy for the endohedrally filled clusters the calculation of the Raman frequencies for the clusters $\{T@Sn_9\}$ was performed by M. Sc. Jasmin Dums. Computational analyses was made using the Gaussian09 program package [137], with exchange correlation hybrid functional after Perdew, Burke and Ernzerhof (PBE0) and def2-TZVPP basis sets for all considered elements ($\text{Ru}^{[138]}$, $\text{Rh}^{[138]}$, $\text{Pd}^{[138]}$ and $\text{Sn}^{[138b, 139]}$). Structure parameters for single point calculations are taken from respective single crystal structures and the compensation of positive charges occurred using a solvation model (polarizable continuum model, PCM)[140]. Jmol[141], VESTA 3[133], IBOview[142] and OriginPro [48] are used for data processing and visualization. Calculated Raman shifts are subject to change using appropriate scale factors[143]. Three shifts for the $\{T@Sn_9\}$ clusters were obtained: (1) 141-148 (2) 174-175 – highest intensity and (3) 246-267 cm^{-1} – characteristic shift for the endohedral clusters.

Experimental results of the Raman spectroscopy measurements for the samples ‘ $\text{K}_4\text{Ru}_3\text{Sn}_7$ ’, ‘ $\text{Na}_{13}\text{RhSn}_{17}$ ’, ‘ K_5PdSn_9 ’ and ‘ $\text{Na}_{12}\text{Pd}_2\text{Sn}_{17}$ ’ are shown in Figure 3.51, b-e, respectively. It shows that in three out of four samples (‘ $\text{K}_4\text{Ru}_3\text{Sn}_7$ ’, ‘ $\text{Na}_{13}\text{RhSn}_{17}$ ’, and ‘ $\text{Na}_{12}\text{Pd}_2\text{Sn}_{17}$ ’) the main signals are coming from the endohedrally filled clusters, whereas in the fourth sample ‘ K_5PdSn_9 ’, endohedrally filled clusters exist along with empty ones.

For the sample ‘ $\text{K}_4\text{Ru}_3\text{Sn}_7$ ’ all the three shifts are observed, including the characteristic one at 258 cm^{-1} , although slightly deviating from the calculated signals. For ‘ $\text{Na}_{13}\text{RhSn}_{17}$ ’ ‘ $\text{Na}_{12}\text{Pd}_2\text{Sn}_{17}$ ’ and only major two shifts with the minimal deviation are observed. In ‘ K_5PdSn_9 ’ dominating signals are as those in $\text{K}_{12}\text{Sn}_{17}$. However, the shoulder at 171 cm^{-1} indicates the presence of the endohedrally filled clusters, along with the empty ones.

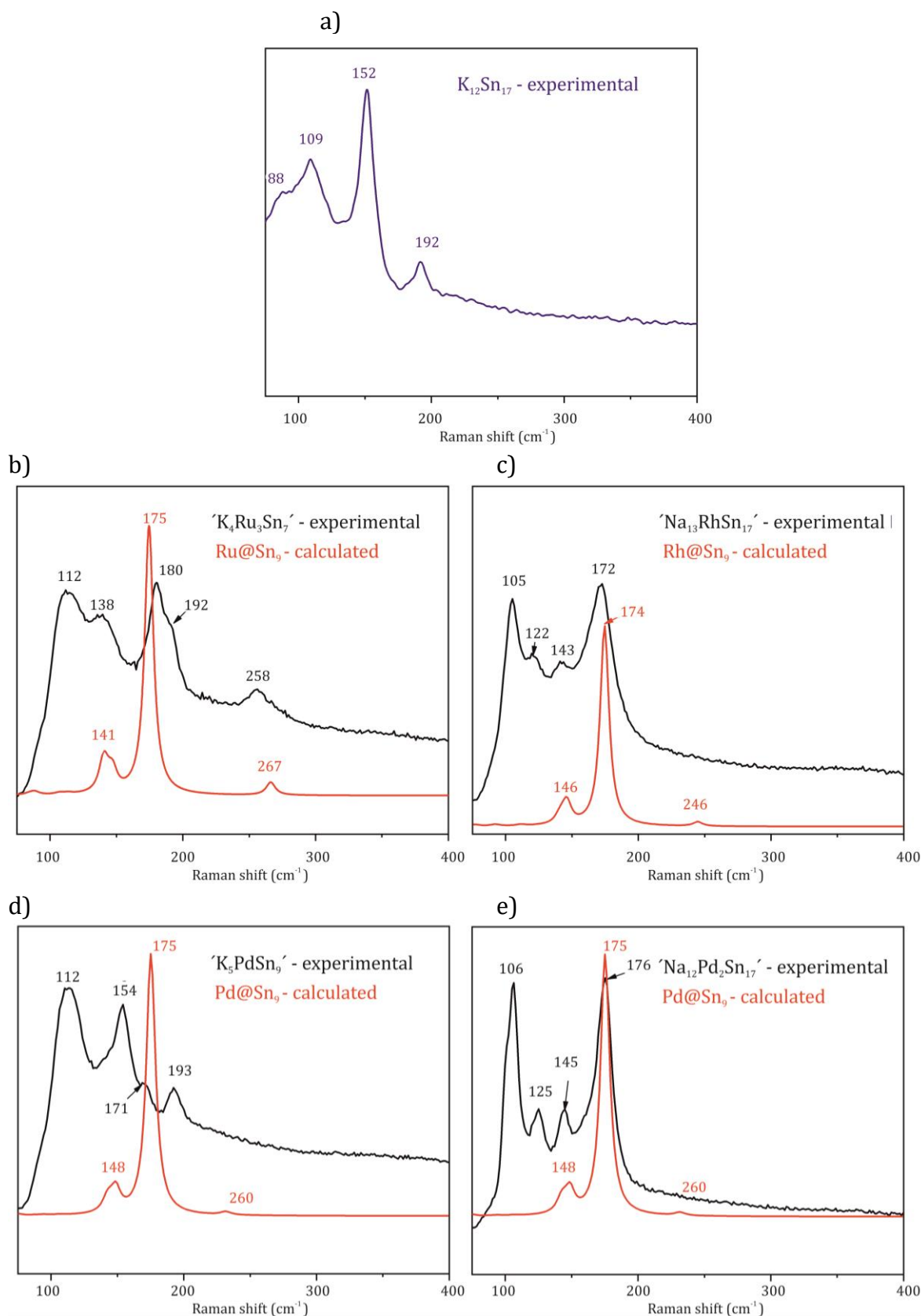


Figure 3.51 Experimental Raman spectra for $K_{12}Sn_{17}$ (a, blue) of the samples (black) $K_4Ru_3Sn_7$ (b), $Na_{13}RhSn_{17}$ (c), K_5PdSn_9 (d), $Na_{12}Pd_2Sn_{17}$ (e) and calculated Raman spectra for the respective $\{T@Sn_9\}$ clusters (red). Raman intensity in arbitrary units.

3.3 Ternary Compounds in *K-Tr-Pn* Systems (*Tr* = Ga, In; *Pn* = As, Bi)

3.3.1 Introduction

The elements of group 14 and the isoelectronic binaries of groups 13 and 15 attract much interest due to their semiconducting properties. They provide a variety of band gaps and properties that can be modified by extrinsic doping, temperature, pressure, etc. [144] For example, at higher pressures silicon adopts the metal-like structure of α -tin while the metallic InBi becomes superconducting [145]. Alternatively, the properties can be modified by changing the atomic charges, of course, and of particular interest to us has been the chemistry of the negatively charged early post-transition elements. Such oxidation states are obtained in compounds with the most electropositive elements in the periodic table, the alkali metals. [144]

In the last three decades, plenty of attempts in the exploratory synthesis of the alkali-metal-*Tr-Pn* compounds were undertaken, but no isolated heteroatomic clusters have been found so far. However, the *A*-In-Bi phases (*A* = Na, K, Rb), surprisingly, dissolve in ethylenediamine, and, in the presence of 2,2,2-crypt, compounds with exactly the proposed above deltahedral clusters of $\{\text{In}_4\text{Bi}_5\}^{3-}$ can be crystallized from the solution [146].

In this Chapter, our attention focuses on mixtures of group 13 and 15 elements, that are modified by alkali metals, similar to the binary *A-Sn* systems described earlier. The idea behind this is to look at the possibility of formation isoelectronic clusters made of elements of two different groups, heteroatomic clusters. For example, isoelectronic to $\{\text{Sn}_9\}^{4-}$ would be anions like $\{\text{Tr}_4\text{Pn}_5\}^{3-}$, $\{\text{Tr}_{4.5}\text{Pn}_{4.5}\}^{4-}$ or $\{\text{Tr}_5\text{Pn}_4\}^{5-}$. Theoretically, the formal charge can be varied by simply tuning the ratio between the atoms of *Tr* and *Pn*. This gives additional flexibility to the system since the oxidation numbers can be varied without changing the geometry of the cluster, something impossible in simple binary phases [147]. There are several pre-requisites that have to be considered before starting the experimental, as not just any combination of *Tr* and *Pn* elements will be appropriate in specific conditions to design such a heteroatomic cluster. First of all, the elements should be distinguishable by X-ray diffraction. Another point is that elements need to have similar sizes and similar electronegativities. All mentioned factors are narrowing our search group to the following combinations: *A*-In-Bi, *A*-In-As. Additionally, *A*-Ga-Bi attracts special interest because there are no phases characterized in this ternary system.

3.3.1.1 Binary Phases

Within A - Tr binary systems ($A = \text{Na, K, Rb, Cs}$; $Tr = \text{Ga, In}$), as it is shown in Figure 3.52, a wide variety of compounds can be found (Table 3.52), starting from structures with three-dimensional network of Tr -atoms with alkali metals in hexagonal channels in ATr_4 (NaGa_4 , KIn_4 and RbIn_4 [148] crystallizing in BaAl_4 structure type) or honeycombs of NaIn [21c] to isolated clusters or cluster networks. Na_2In [112] containing isolated In_4 tetrahedra can be compared to the $A_4\text{Sn}_4$ phases within the A - Sn binary systems, whereas isolated pentacapped trigonal prismatic Tr_{11} clusters, interconnected Tr_8 octahedra or Tr_8 interconnected clusters are unique features of the A_8Tr_{11} [35, 149], A_2Tr_3 [150] and ATr_3 [151] respectively.

Separate group of compounds contain icosahedral phases, featuring complicated networks of interconnected Tr_{12} icosahedra: both modifications of $\text{Na}_7\text{Ga}_{13}$ [98, 152], $\text{Na}_{22}\text{Ga}_{39}$ [100], K_3Ga_{13} [153] and $A\text{Ga}_7$ [151a, 154] ($A = \text{Rb, Cs}$) in A - Ga (Figure 3.52, a) as well as $\text{K}_{21.33}\text{In}_{39.67}$ [105], $\text{Na}_7\text{In}_{11.8}$ [155], $\text{Na}_{15}\text{In}_{27.4}$ [112], $\text{K}_{39}\text{In}_{80}$ [110] and $\text{K}_{17}\text{In}_{41}$ [106] in A - In (Figure 3.52, b) binary systems.

$A\text{Ga}_7$ [151a, 154] ($A = \text{Rb, Cs}$) can be described as packing of Ga_{12} icosahedra around inversion centers in a sheet with non-compact netting leaving the channels where A atoms are located. In $\text{Na}_7\text{Ga}_{13}$ [98, 152] Ga -atoms form Ga_{12} icosahedra and Ga_{15} -clusters interconnected to a 3-D network. The centers of gravity of these clusters correspond to the atomic positions of the MgCu_2 structure – Ga_{12} -clusters in positions of Cu atoms, Ga_{15} -clusters – larger Mg atoms of MgCu_2 . $\text{Na}_{22}\text{Ga}_{39}$ [100] features also a non-compact framework of icosahedra directly linked to each other through exo-bonds and a few satellite Ga atoms. Related structure to the $\text{Na}_7\text{Ga}_{13}$ and $\text{Na}_{22}\text{Ga}_{39}$ has $\text{K}_{21.33}\text{In}_{39.67}$ [105]: In atoms form icosahedra and In_{15} clusters, connected to a three-dimensional network. The arrangement of the clusters is related to MgCu_2 structure type.

In the other Ga -compound, K_3Ga_{13} [153] the Ga_{12} icosahedra and Ga_{11} polyhedra (icosahedra missing one atom) are linked to each other in a non-compact way, leaving voids for K atoms. Similarly, the tetragonal structure of $\text{Na}_7\text{In}_{11.8}$ [155] contains *closo*- In_{16} clusters and *nido*-icosahedra, connected through exo-bonds and four-bonded indium atoms in pairs of triangles. In the orthorhombic structure of $\text{Na}_{15}\text{In}_{27.4}$ [112], related to $\text{Na}_7\text{In}_{11.8}$, all three types of clusters are present: In_{16} , In_{12} icosahedra and In_{11} clusters. The structure of $\text{K}_{17}\text{In}_{41}$ [106] is featuring In_{12} icosahedra and In -centered truncated tetrahedra. In $\text{K}_{39}\text{In}_{80}$ [110] three-dimensional indium network is composed of empty In_{12} icosahedra with different exo-

bonding and symmetry, an In_{16} polyhedra, centered by a tetrahedral In atom, and a rather open K-centered In_{15} spacer.

Chemistry of $A\text{-}Pn$ ($A = \text{Na, K, Rb, Cs}$; $Pn = \text{As, Bi}$) binary systems is not as rich as $A\text{-}Tr$, but still is represented by various compounds (Table 3.52, Figure 3.53). In alkali metal rich area compounds with isolated Pn atoms are observed – hexagonal and cubic A_3Pn phases [156]. By increasing the content of Pn element compounds with $Pn\text{-}Pn$ dumbbells can be obtained: Cs_3Bi_2 [157] and A_5Pn_4 [158].

The alkaline monoarsenides and monobismuthides (Figure 3.53, a) can have quite diverse structures: some of the $A\text{-}As$ ($A = \text{Na, K, Rb}$) [159] compounds crystallize in tetragonal NaP structure type, forming chains of 2-bonded Pn atoms, same as in monoclinic Na_2As_2 [160] (LiAs structure type) and ABi ($A = \text{K, Rb, Cs}$) [161], whereas the crystal structure of hexagonal CsAs [159] contains three-membered rings. This row completes tetragonal NaBi [21b] with flat 4-boded Bi layers. In orthorhombic Rb_4As_6 and Cs_4As_6 [162] Pn atoms are building isolated flat six-membered rings.

In As-rich area of $A\text{-}As$ binary system (Figure 3.53, a) are located Zintl phases $A_3\text{As}_7$ ($A = \text{Na, K, Rb, Cs}$) [159, 163] and $A_3\text{As}_{11}$ ($A = \text{K, Rb, Cs}$) [164] with As atoms forming nortricyclene-analogous anions As_7^{3-} , in $A_3\text{As}_7$ and chiral ufosan-anions As_{11}^{3-} . The Bi-richest compounds (Figure 3.53, b) are ABi_2 [161] ($A = \text{K, Rb, Cs}$) with Bi atoms forming honeycombs, exactly as In atoms in NaIn [21c].

According to the phase diagram of the Bi-Ga binary system [165] a very small mutual solubility of the components in the solid-state exists, but the elements are not forming any binary compounds (Figure 6.3, e).

In In-As [166] binary system (see Figure 6.3, f) only one phase is known at normal pressure: cubic InAs [167] (Figure 3.54, a). It is formed by In-centered As_4 tetrahedra, sharing common vertexes. For the two high pressure modifications of InAs (Figure 3.54, b, c) In atoms (atoms of statistical mixture In/As in the tetragonal modification) have octahedral coordination, centering intercalated As_8 ($(\text{In}/\text{As})_8$ in the tetragonal modification) polyhedra.

Table 3.52 Compounds in the *A-Tr* and *A-Pn* (*A* = Na, K, Rb, Cs; *Tr* = Ga, In; *Pn* = As, Bi) as well as Ga-Bi, In-As and In-Bi binary systems.

Compound	Space group	Cell parameters			<i>V</i> (Å ³)	Ref.
		<i>a</i> (Å)	<i>b</i> (Å)	<i>c</i> (Å)		
A-Ga						
Cs ₈ Ga ₁₁	<i>R</i> $\bar{3}c$	9.9962	-	50.839	4399.44	[149a]
K ₂ Ga ₃	<i>I</i> 4/ <i>mmm</i>	6.1382	-	14.815	558.19	[150a]
Na ₇ Ga ₁₃	<i>R</i> $\bar{3}m$	14.965	-	38.93	7550.37	[98]
Na ₇ Ga ₁₃ II	<i>Pnma</i>	15.625	14.979	21.678	5073.67	[152]
Na ₂₂ Ga ₃₉	<i>Pnma</i>	15.585	14.984	21.632	5051.63	[100]
KGa ₃	<i>I</i> $\bar{4}m2$	6.271	-	14.81	582.41	[151a]
RbGa ₃	<i>I</i> $\bar{4}m2$	6.315	-	15.000	598.19	[151b]
CsGa ₃	<i>I</i> $\bar{4}m2$	6.393	-	15.829	646.94	[151a]
NaGa ₄	<i>I</i> 4/ <i>mmm</i>	4.223	-	11.19	199.56	[148]
K ₃ Ga ₁₃	<i>Cmcm</i>	6.441	16.143	28.404	2953.36	[153]
RbGa ₇	<i>R</i> $\bar{3}m$	6.600	-	28.563	1077.51	[151a]
RbGa ₇	<i>C</i> 2/ <i>m</i>	11.432	6.603	10.259	718.77	[154]
		$\beta = 111.85^\circ$				
CsGa ₇	<i>R</i> 3 <i>m</i>	6.620	-	29.045	1102.35	[151a]
A-In						
Na ₂ In	<i>Cmcm</i>	16.108	32.279	15.931	8283.33	[112]
NaIn	<i>F</i> \bar{d} $\bar{3}m$	7.312	-	-	390.94	[21c]
K ₈ In ₁₁	<i>R</i> $\bar{3}c$	10.021	-	50.891	4425.82	[35]
Rb ₈ In ₁₁	<i>R</i> $\bar{3}c$	10.301	-	52.367	4812.24	[149b]
Rb ₂ In ₃	<i>I</i> $\bar{4}m2$	6.883	-	15.913	753.89	[150b]
Cs ₂ In ₃	<i>I</i> $\bar{4}m2$	6.910	-	16.512	788.42	[150c]
K _{21.33} In _{39.67}	<i>R</i> $\bar{3}m$	17.214	-	44.612	11448.43	[105]
Na ₇ In _{11.8}	<i>P</i> 4 ₂ / <i>nmc</i>	16.093	-	23.384	6056.1	[155]
Na ₁₅ In _{27.4}	<i>C</i> 222 ₁	13.855	8.836	11.762	1439.94	[112]
K ₃₉ In ₈₀	<i>P</i> $\bar{3}m$ 1	17.211	-	28.888	7410.72	[110]
K ₁₇ In ₄₁	<i>F</i> \bar{d} $\bar{3}m$	24.241	-	-	14244.64	[106]
CsIn ₃	<i>I</i> $\bar{4}m2$	7.047	-	16.803	834.44	[151c]
KIn ₄	<i>I</i> 4/ <i>mmm</i>	4.835	-	12.71	297.12	[148]
RbIn ₄	<i>I</i> 4/ <i>mmm</i>	4.914	-	12.82	309.57	[148]
A-As						
Na ₃ As	<i>P</i> 6 ₃ <i>mmc</i>	4.874	-	8.515	175.18	[168]
HP-Na ₃ As	<i>F</i> \bar{m} $\bar{3}m$	6.835	-	-	319.31	[168]
K ₃ As	<i>P</i> 6 ₃ <i>mmc</i>	5.794	-	10.242	297.76	[156a]
Rb ₃ As	<i>P</i> 6 ₃ <i>mmc</i>	6.052	-	10.242	297.76	[156a]
Cs ₃ As	<i>P</i> 6 ₃ <i>cm</i>	10.783	-	10.73	340.35	[156a]
K ₅ As ₄	<i>C</i> 2/ <i>m</i>	11.592	5.2114	10.383	575.56	[158]
		$\beta = 113.421^\circ$				
NaAs	<i>P</i> 2 ₁ 2 ₁ 2 ₁	6.240	5.910	10.510	387.59	[159]
KAs	<i>P</i> 2 ₁ 2 ₁ 2 ₁	6.617	6.888	11.973	545.7	[159]
RbAs	<i>P</i> 2 ₁ 2 ₁ 2 ₁	6.581	6.916	12.047	548.31	[159]
CsAs	<i>P</i> $\bar{6}2m$	12.197	-	10.463	1348.01	[159]
Na ₂ As ₂	<i>P</i> 2 ₁ / <i>c</i>	6.242	5.849	11.55	375.39	[160]
		$\beta = 117.1^\circ$				

Rb ₄ As ₆	<i>Fmmm</i>	10.078	15.186	9.170	1577.67	[162]
Cs ₄ As ₆	<i>Fmmm</i>	10.373	15.577	9.764	1577.67	[162]
Na ₃ As ₇	<i>P2₁/c</i>	15.554	10.898	14.280	2178.73	[163]
		$\beta = 115.83^\circ$				
K ₃ As ₇	<i>Pbca</i>	12.919	25.441	15.377	5053.99	[159]
Rb ₃ As ₇	<i>P2₁/c</i>	7.573	13.102	26.927	2670.15	[159]
		$\beta = 91.972^\circ$				
Cs ₃ As ₇	<i>Pbca</i>	10.228	13.176	21.952	2958.34	[159]
K ₃ As ₁₁	<i>Pnab</i>	10.596	14.525	10.914	1679.74	[164]
Rb ₃ As ₁₁	<i>Pbcn</i>	11.082	15.335	10.601	1801.56	[164]
Cs ₃ As ₁₁	<i>C2/c</i>	13.245	15.245	19.372	3894.93	[164]
		$\beta = 95.291^\circ$				
A-Bi						
Na ₃ Bi	<i>P6₃mmc</i>	5.459	-	9.675	249.69	[156a]
α -K ₃ Bi	<i>P6₃cm</i>	10.649	-	10.940	1074.4	[156b]
β -K ₃ Bi	<i>Fm$\bar{3}$m</i>	8.805	-	-	682.63	[156d]
α -Rb ₃ Bi	<i>P6₃mmc</i>	6.49	-	11.49	419.12	[156c]
β -Rb ₃ Bi	<i>Fm$\bar{3}$m</i>	8.989	-	-	726.33	[156e]
Cs ₃ Bi	<i>Fm$\bar{3}$m</i>	9.31	-	-	806.95	[156e]
Cs ₃ Bi ₂	<i>C2/c</i>	10.078	10.3207	10.145	1018.24	[157]
		$\beta = 105.21^\circ$				
K ₅ Bi ₄	<i>C2/m</i>	12.517	5.5412	11.625	750.41	[158]
		$\beta = 111.46^\circ$				
Rb ₅ Bi ₄	<i>C2/m</i>	12.945	5.7851	12.018	829.8	[158]
		$\beta = 112.78^\circ$				
Cs ₅ Bi ₄	<i>C2/m</i>	12.8867	6.3232	12.6363	864.12	[158]
		$\beta = 122.942^\circ$				
NaBi	<i>P4/mmm</i>	3.46	-	4.8	57.46	[21b]
KBi	<i>P2₁/c</i>	14.223	7.248	13.420	1273.18	[161]
		$\beta = 113.03^\circ$				
RbBi	<i>P2₁/c</i>	14.742	7.502	13.921	1416.85	[161]
		$\beta = 113.033^\circ$				
CsBi	<i>P2₁/c</i>	15.237	7.737	14.399	1565.74	[161]
		$\beta = 112.722^\circ$				
KBi ₂	<i>Fd$\bar{3}$m</i>	9.521	-	-	863.07	[161]
RbBi ₂	<i>Fd$\bar{3}$m</i>	9.625	-	-	891.67	[161]
CsBi ₂	<i>Fd$\bar{3}$m</i>	9.720	-	-	891.67	[161]
Ga-Bi						
-						
In-As						
InAs	<i>F$\bar{4}$3m</i>	6.058	-	-	222.32	[167]
HP-InAs	<i>Fd$\bar{3}$m</i>	5.5005	-	-	166.42	[169]
HP-InAs	<i>I4₁/amd</i>	5.226	-	2.73	74.56	[169]

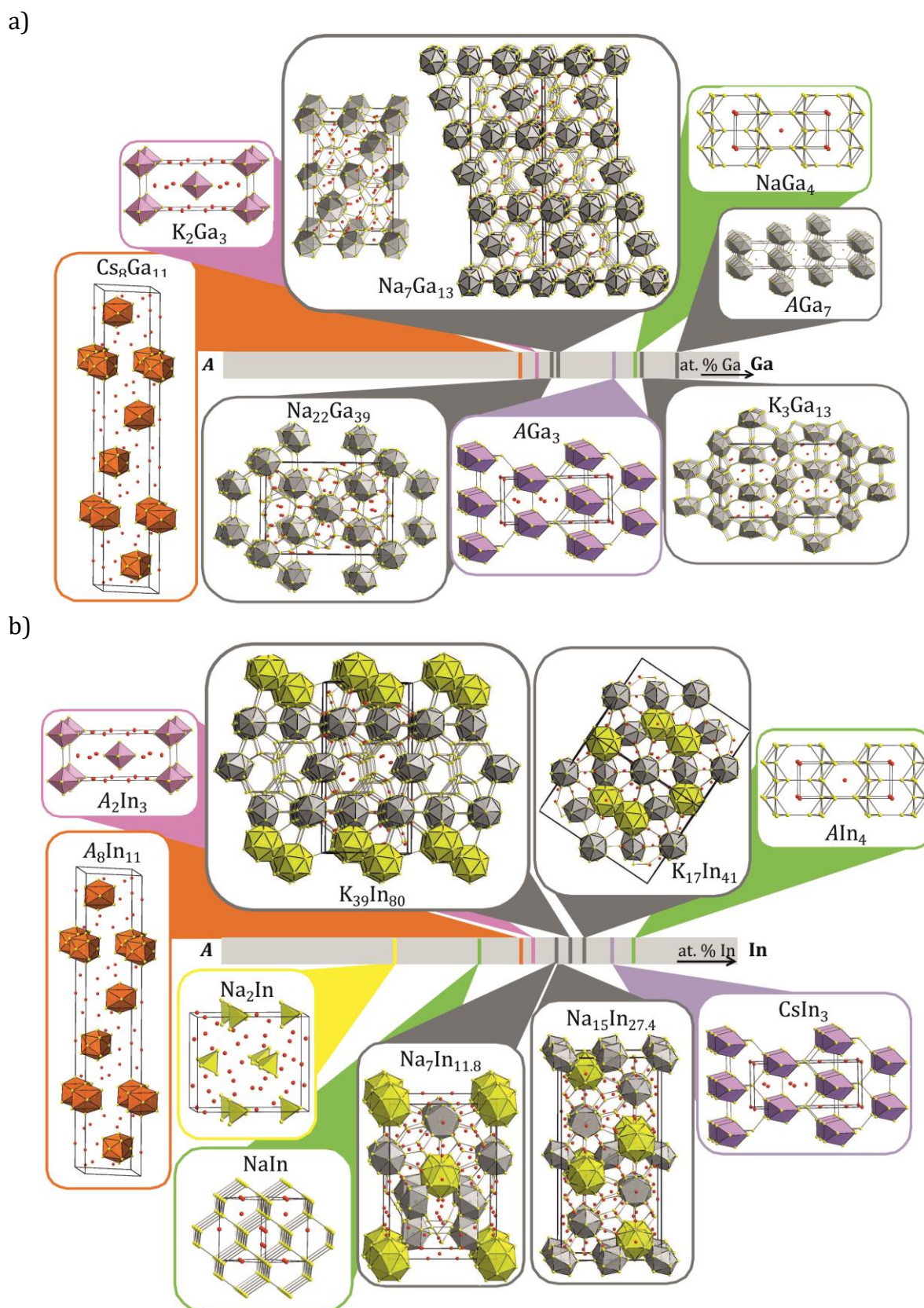


Figure 3.52 Crystal structure of the binary phases in A -Ga (a) and A -In (b) binary systems, where A = Na, K, Rb, Cs. Compounds with Tr_{12} icosahedra are marked in grey, with Tr_8 octahedra in pink, Tr_8 interconnected clusters – in violet, pentacapped trigonal prismatic Tr_{11} – in orange, In_4 isolated tetrahedra in yellow and three-dimensional Tr -network in green.

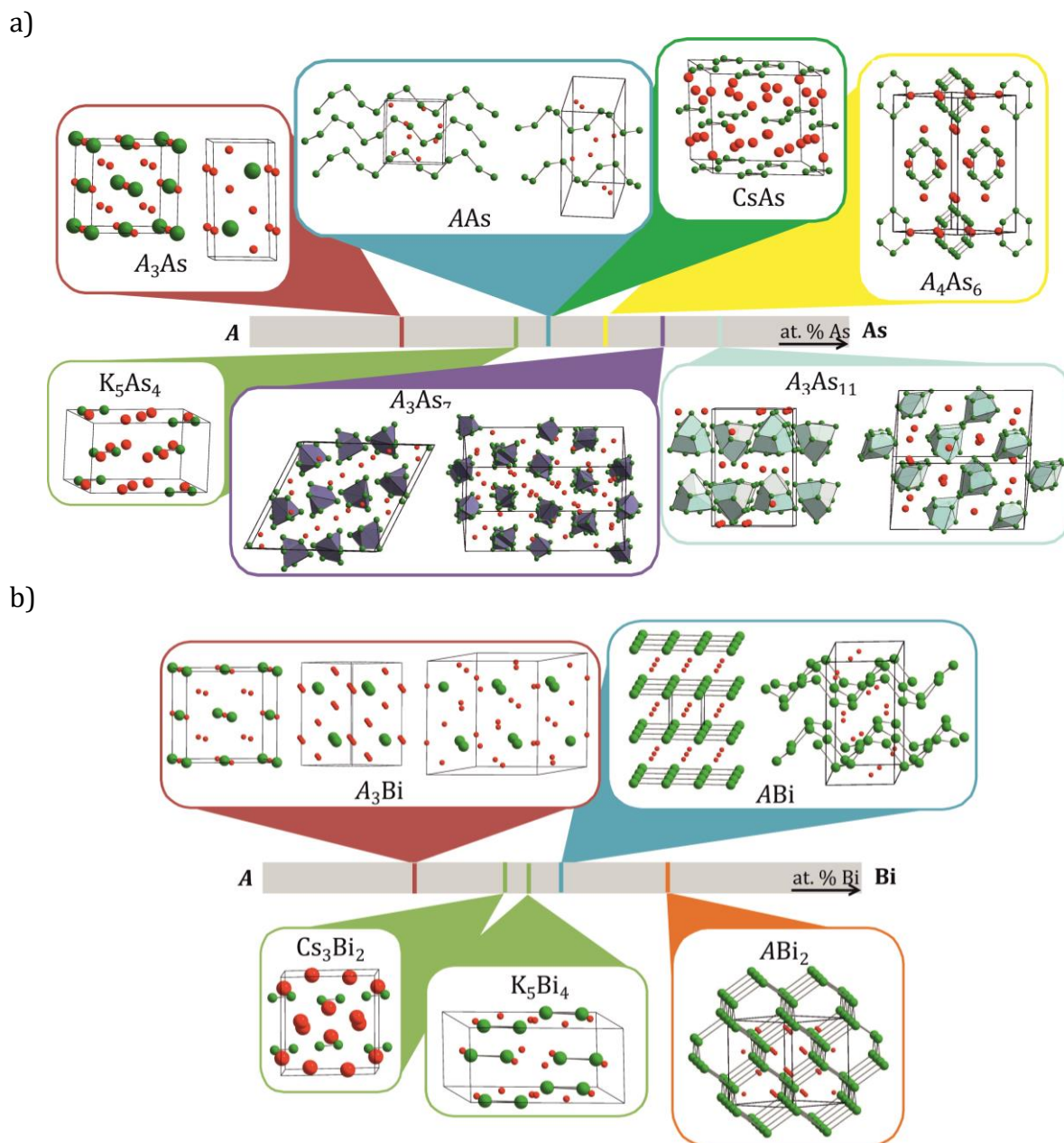


Figure 3.53 Crystal structure of the binary phases in A -As (a) and A -Bi (b) systems, where A = Na, K, Rb, Cs. Compounds with isolated Pn atoms are marked in red, isolated $Pn-Pn$ fragments in olive green, 1-D Pn -chains in aqua blue, As_3 triangles in green, As_6 rings in yellow, As_7 clusters in violet and As_{11} clusters in light blue and 3-D Bi-network in orange.

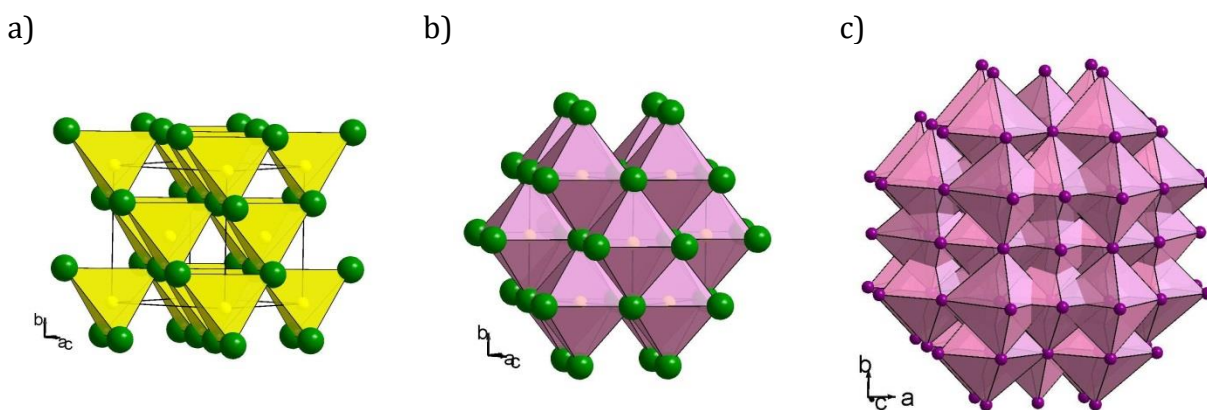


Figure 3.54 Crystal structure of the compound InAs (space group $F\bar{4}3m$, a) and its high pressure modifications: cubic and tetragonal (space groups $Fd\bar{3}m$, b and $I4_1/amdS$, c), respectively). In atoms are shown in yellow, As – in green, atoms of In/As statistical mixture – in violet.

3.3.1.2 Existing Ternary Phases in A-Tr-Pn Systems ($A = Na, K, Rb, Cs$; $Tr = Ga, In, Tl$ and $Pn = P, As, Sb, Bi$)

Heteroatomic anions $\{Tr_xPn_y\}^{z-}$ with different compositions, charges and bonding contain a large number of compounds (Table 3.53). Trigonal fragment $\{TrPn_3\}$ together with its dimers, trimers or condensed five-membered rings and $Tr@Pn_4$ as structural units, which are interconnected in different ways: sharing edges, faces, corners to build up structures in all dimensions. Among these structures, the nature of the anionic framework is collectively related to the number, size, and charge of the cations and, in turn, to the atomic ratio in the $\{Tr_xPn_y\}^{z-}$ anion and its valence electron count. Consequently, the less reduced general anionic compositions $\{Tr_xPn_y\}^{z-}$ exhibit one-, two-, or three-dimensional anionic frameworks [170].

Isolated polyanions in A-Tr-Pn Compounds

The first group of *A-Tr-Pn* compounds represents phases with isolated fragments, which happen to be in the alkali metal rich area of the ternary phase diagrams (Figure 3.55). Trigonal planar $\{TrPn_3\}^{6-}$ anion (isostructural to $B_3O_3^{3-}$) with the centering atom Ga or In is isolated by the cations in the structures of the compounds with the highest alkali metal content: Na_6GaPn_3 ($Pn = P, As$)^[171], K_6InPn_3 ($Pn = P, As$)^[172] and Cs_6GaSb_3 ^[173] (Figure 3.55, a). Compounds with heavier alkali metals $Cs_6Ga_2P_4$ ^[174], Rb_3GaP_2 ^[175] Cs_3GaAs_2 ^[176] contain isolated dimeric anions $\{Ga_2Pn_4\}^{6-}$ with slightly bent anionic units forming a butterfly-like structure (Figure 3.55, b). Other Ga-containing ternary phases $K_{20}Ga_6As_{12.66}$ and $K_{20}Ga_6Sb_{12.66}$ ^[177] consist of $\{Ga_3Tr_6\}^{9-}$ anions with trigonal planar coordination Ga-atoms linked through three As (Sb) atoms and forming slightly deformed hexagon (Figure 3.55, c).

1-D Polyanionic Chains in A-Tr-Pn Compounds

The second group of ternary compounds is built of one-dimensional infinite chains. Nearly planar five-membered rings, formed by two Ga atoms and three *Pn* atoms and are connected by terminal *Pn* atoms are present in compounds only with Ga: K_2GaP_2 ^[178], A_2GaAs_2 ($A = K, Rb$)^[179], A_2GaSb_2 ($A = K, Rb, Cs$)^[180] and where $\{GaP_2\}^{2-}$ structural fragment is isostructural to BS_2 (Figure 3.56, a). The only two known compounds in *A-Tl-Pn* systems both are formed by heteroatomic chains: in Na_6TlSb_4 ^[181] four-membered $\{TlSb_3\}$ rings interlinked by pairs of Sb_2 bridges generate swing-like units $\{Tl_2Sb_3\}$ that are further interlinked through external Tl–Tl bonds to form infinite one-dimensional chains (Figure 3.56, b). In contrast to the Zintl phase $K_6Tl_2Sb_3$ ^[170] with similar swing-like $\{Tl_4Sb_6\}^{12-}$ chains repeating units and Tl–Tl interlinkages (Figure 3.56, c), Na_6TlSb_4 has a more compact conformation of the chains and a notably smaller cell volume than expected.

Among tetrahedral phases there are also two examples of structures that could be described as one-dimensional chains: K_3InP_2 ^[182], isotypic to Na_3AlAs_2 , where InP_4 tetrahedra are connected by common edges to form wiggled chains of edge-sharing tetrahedra $\{InP_{4/2}\}^{3-}$ parallel to [110] (Figure 3.56, d) and compounds with the same stoichiometry $A_{12}In_4P_8$ ($A = Rb, Cs$)^[183] which combine chains $\{InP_{4/2}\}^{3-}$ and dimers $\{In_2P_6\}^{6-}$ with nearly trigonal planar coordinated In atoms (b), embedded in alkali-metal matrix. (Figure 3.56, e).

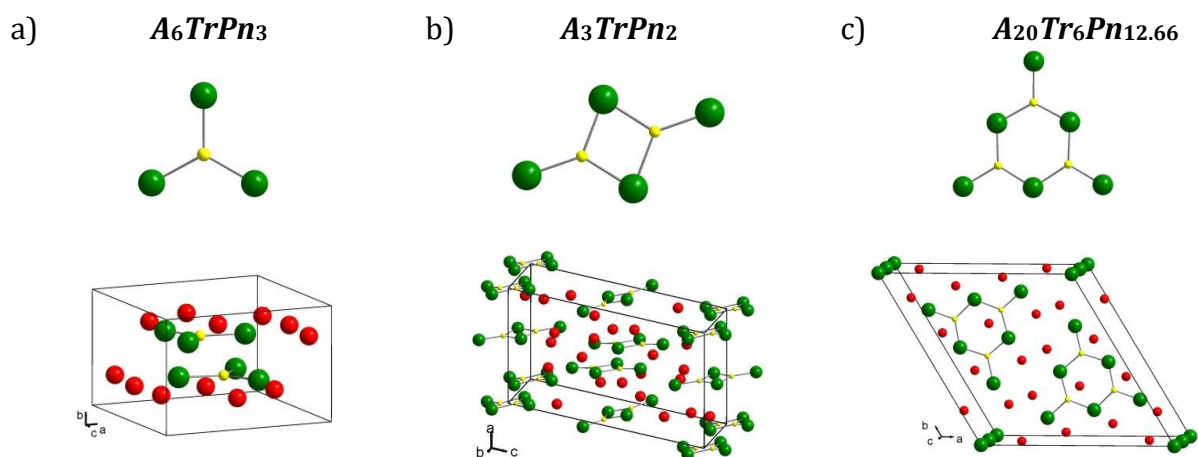


Figure 3.55 Alkali metal rich compounds with isolated fragments in $A-Tr-Pn$ ternary systems. Trigonal planar $\{TrPn_3\}^{6-}$ anion and the structure of the compounds with stoichiometry 6:1:3; (a), butterfly-like $\{Ga_2Pn_4\}^{6-}$ in Ga-compounds with stoichiometry 3:1:2 (b) and $\{Ga_2Pn_4\}^{6-}$ in $K_{20}Ga_6Pn_{12.66}$ (c). Top – isolated fragments, bottom – structures of the compounds. A atoms are shown in red, Tr – in yellow and Pn in green color.

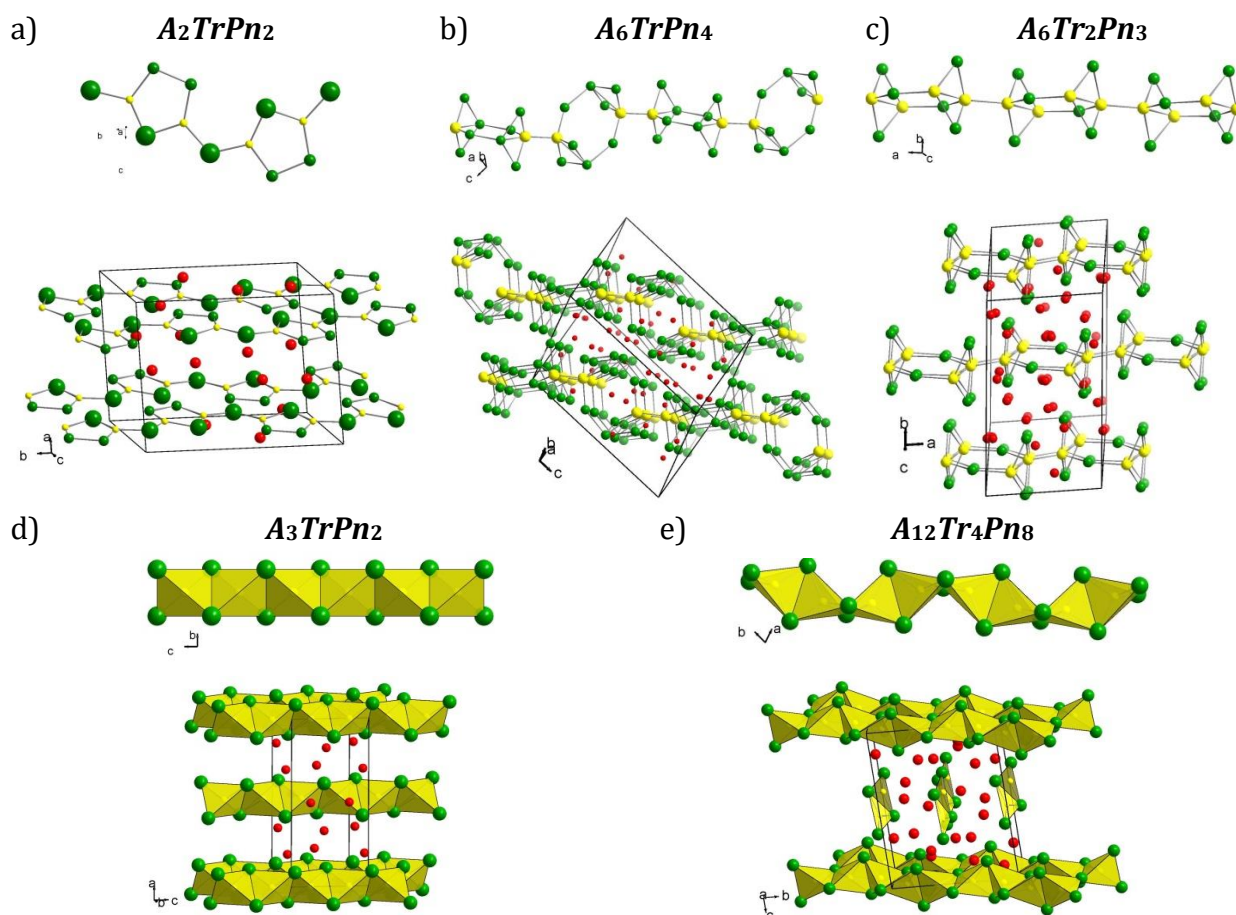


Figure 3.56 One-dimensional chains in $A-Tr-Pn$ compounds: heteroatomic five-membered rings bridged through Pn atom in 2:1:2 compounds (a), 'swings' of four-membered rings interlinked by pairs of Sb_2 bridges in Na_6TlSb_4 (b) and similar 'swings' of six-membered rings in $K_6Tl_2Sb_3$ (c); $\{InP_{4/2}\}^{3-}$ chains in K_3InP_2 (d) and $\{InP_{4/2}\}^{3-}$ chains with dimers $\{In_2P_6\}^{6-}$ in $Rb_{12}In_4P_8$ and $Cs_{12}In_4P_8$ (e). Top – fragments of the chains, bottom – structures of the compounds. A atoms are shown in red, Tr – in yellow and Pn in green color.

2-D Polyanionic Layers in A-Tr-Pn Compounds

The next group can be defined as two-dimensional layered compounds (Figure 3.57), where the layers consist of tetrahedra or defect cubanes (in case of $\text{Cs}_5\text{In}_3\text{As}_4$ ^[184]) with a different way of packing.

The anionic substructure of the quite unusual in the group of *A-Tr-Pn* compounds $\text{Cs}_5\text{In}_3\text{As}_4$ ^[184] (Figure 3.57, a) contains both chains and layers of interconnected defect cubanes of three indium and four arsenic atoms with exactly the same overall composition of $\{\text{In}_3\text{As}_4\}^{5-}$, and the compound can be considered as made of two coexisting polymorphic forms of itself. Similar structural fragments, a ‘cubane with a handle’ $\{(\text{In}_3\text{As}_4\text{Nb})-\text{As}\}^{7-}$ anions were found also in $\text{Cs}_7\text{NbIn}_3\text{As}_5$ ^[185], obtained as a result of the reaction of the mixture of elements with Nb (ampoule material).

For all the other compounds with layered structure *TrPn*₄ tetrahedra are connected by common edges, faces or corners, having additional bridging *Pn*-atoms, *Pn*₂ dumbbells and/or *Tr-Tr* bonds. These layers are typically separated by *A* atoms.

Compound $\text{K}_{10}\text{In}_5\text{Sb}_9$ ^[186] contains chains of InSb_4 tetrahedra connected by common edges and additional bridging Sb-atoms and layers formed by tetrahedra linked via In-In bonds connected by common edges and corners (Figure 3.57, b). In $\text{K}_3\text{In}_2\text{As}_3$ ^[187] edge sharing InAs_4 tetrahedra form four-membered and twelve membered rings which are connected to layers. (Figure 3.57, c). Another example of the layered structure is $\text{K}_3\text{Ga}_3\text{As}_4$ ^[188]: it is composed of covalently bonded sheets of $\{\text{Ga}_3\text{As}_4\}_\infty^{3-}$, alternating in the *b*-direction (Figure 3.57, d).

The most common structure type among *A-Tr-Pn* compounds is described for the stoichiometry 2:2:3 – $\text{Na}_2\text{Al}_2\text{Sb}_3$ -type with represented by seven compounds: $\text{Na}_2\text{Ga}_2\text{As}_3$ ^[189], $\text{K}_2\text{Ga}_2\text{As}_3$ ^[190], $\text{K}_2\text{Ga}_2\text{Sb}_3$ ^[191], $\text{K}_2\text{In}_2\text{As}_3$ ^[189], $\text{Na}_2\text{In}_2\text{Sb}_3$ ^[186], $\text{K}_2\text{In}_2\text{Sb}_3$ ^[186, 189b] and $\text{Cs}_2\text{In}_2\text{Sb}_3$ ^[192]. It can be described as *TrPn*₄ tetrahedra connected via common corners and *Pn*₂ dumbbells to two-dimensional nets (Figure 3.57, e).

In KGaSb_2 ^[193] GaSb_4 tetrahedra and three bonded Sb atoms form four-, five-, and six-membered rings, which are connected to layers (Figure 3.57, f). $\text{Na}_2\text{Ga}_3\text{Sb}_3$ ^[194] form more complicated wavelike hexagonal nets by Ga- and Sb-atoms form in alternative sequence. Three of them are connected to threefold sheets, which are stacked in the *a*-direction. (Figure 3.57, g).

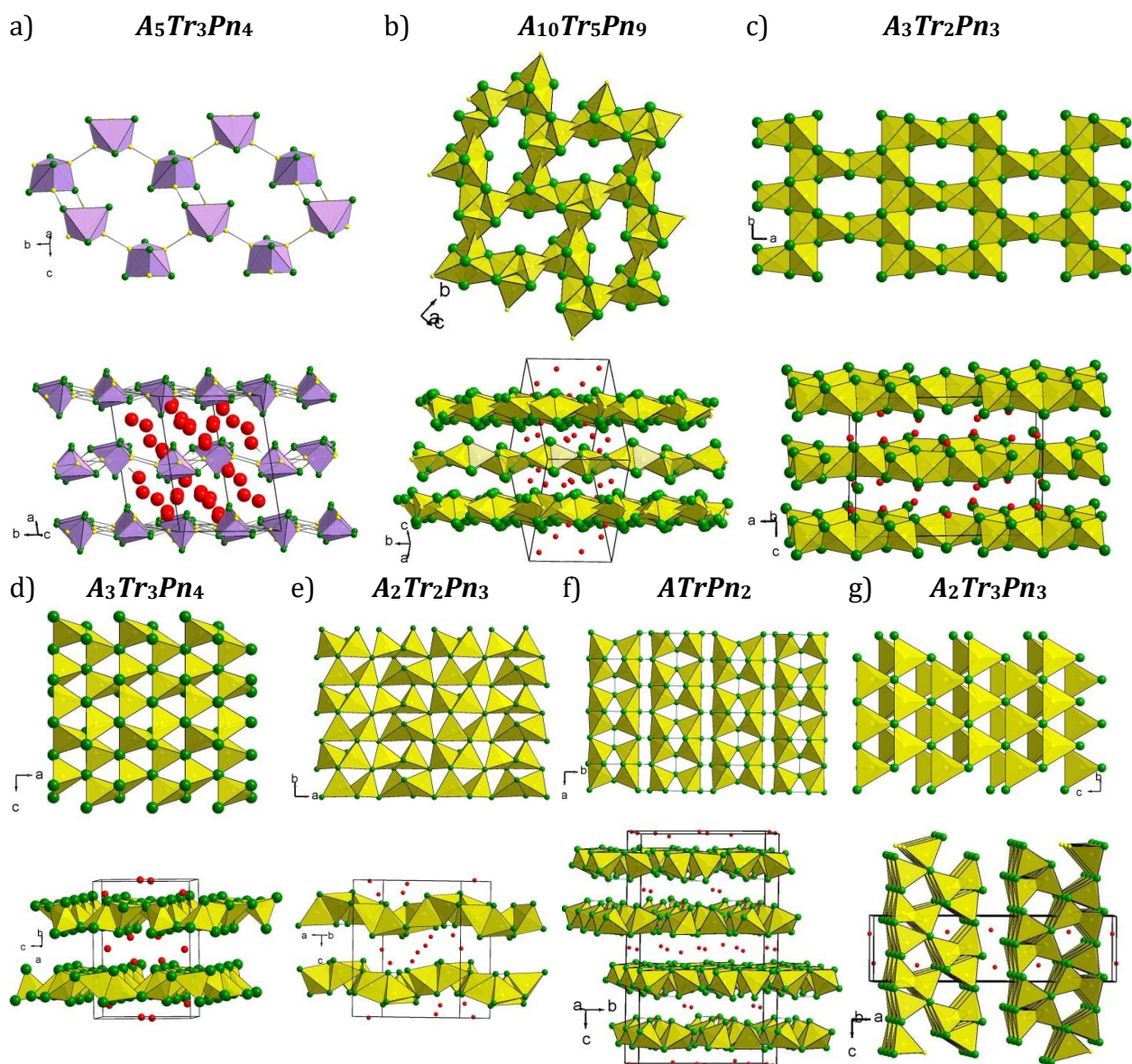


Figure 3.57 Layered structures with different packing type of tetrahedra in the $A-Tr-Pn$ ternary systems: compounds with the stoichiometry 5:3:4 (a), 10:5:9 (b), 3:2:3 (c), 3:3:4 (d), 2:2:3(e), 1:1:2 (f) and 2:3:3 (g). Top – fragment of the layers, bottom – structures of the compounds. A atoms are shown in red, Tr – in yellow and Pn in green color.

3-D Polyanionic Networks in A-Tr-Pn Compounds

There are four types of structures for In compounds with stoichiometry 3:1:2 which differ from those with Ga. The first two types are K_3InP_2 and $A_{12}In_4P_8$ ($A = Rb, Cs$) and were already discussed above. The other two types are Indium compounds, with smaller Na^+ cations, Na_3InPn_2 ($Pn = P, As, Sb$) [195] and $Na_9In_3Bi_6$ [147] have structures with tetrahedrally coordinated In atoms. The special features of Na_3InPn_2 ($Pn = P, As, Sb$) are channels formed by twelve membered rings (Figure 3.58, a). The $Na_9In_3Bi_6$ (Na_3InBi_2) on the other hand has a fairly complicated structure and is again built of indium-centered tetrahedra of bismuth, assembled in hexamers. The middle two tetrahedra of the hexamer share an edge (an inversion center) while the rest share corners. The hexamers are then interconnected as building bricks by sharing with each other all remaining corners (Figure 3.58, b).

Compound $K_{11}In_6Bi_9$ [147] has one of the most complicated structures among *A-Tr-Pn* compounds, which results in the low triclinic symmetry and the complicated connectivity between the $InBi_4$ tetrahedra. Two of the six indium atoms are tetrahedrally coordinated by three bismuth atoms and one other indium atom, creating In-In bonds. The structure can be viewed as made of bilayers of corner-sharing tetrahedra that are parallel to the *ac* plane. Neighboring layers are related to each other by inversion. (Figure 3.58, c). A similar structure with In-In bonds in a rather complicated three-dimensional network has $Cs_7In_4Bi_6$ [144, 147]. The structure can be explained as being carved out from the layered PbO-type structure of the parent group III-V compound of InBi by reduction of the latter (Figure 3.58, d).

$K_{4.67}In_{2.67}Bi_4$ ($K_7In_4Bi_6$) and $Rb_7In_4Bi_6$ [147] crystallize in a very rare chiral tetragonal space group $P4_3$. Compounds are not isostructural to $Cs_7In_4Bi_6$. Both structures contain chains of edge-sharing $InBi_4$ tetrahedra. However, the sequences of shared *trans* and *cis* edges are different for the two structures: simply alternating *cis* and *trans* modes – CTCTCTCT. It makes the chains helical, spiral-like (Figure 3.58, e).

The compound $NaIn_{0.67}Bi$ [147] ($Na_3In_2Bi_3$), unlike $K_3In_2As_3$, which has the same stoichiometry and the layered structure described above, forms a three-dimensional network with channels (Figure 3.58, f). The channels, made of eight-member rings of alternating indium and bismuth atoms, make it very reminiscent of the zeolite structures. The structure can be viewed also as made edge-sharing tetrahedra building chains along *b*-direction, which are then connected to each other by sharing the remaining vertices. Similar chains are observed in $Cs_7In_4Bi_6$.

The most *Pn*-rich compound is KGaSb_4 ^[196] with six distorted GaSb_4 tetrahedra and four additional Sb atoms forming 22-membered rings. These rings are connected by common Sb atoms to channels and form a framework by common Sb atoms (Figure 3.58, g).

A summary of all the ternary compounds in *A-Tr-Pn* ternary systems (*A* = Na, K, Rb, Cs; *Tr* = Ga, In, Tl; *Pn* = P, As, Sb, Bi) are shown in Figure 3.59. It shows that in general, the dimensionality of the compounds correlates with the alkali metal content and the size of the atoms: alkali metal rich compounds contain 0-D isolated fragments or have structures with one-dimensional chains while decreasing alkali metal content leads to 2-D layered structures or compounds with 3-D networks. It shows that alkali metals are playing the role of atomic scissors within those structures.

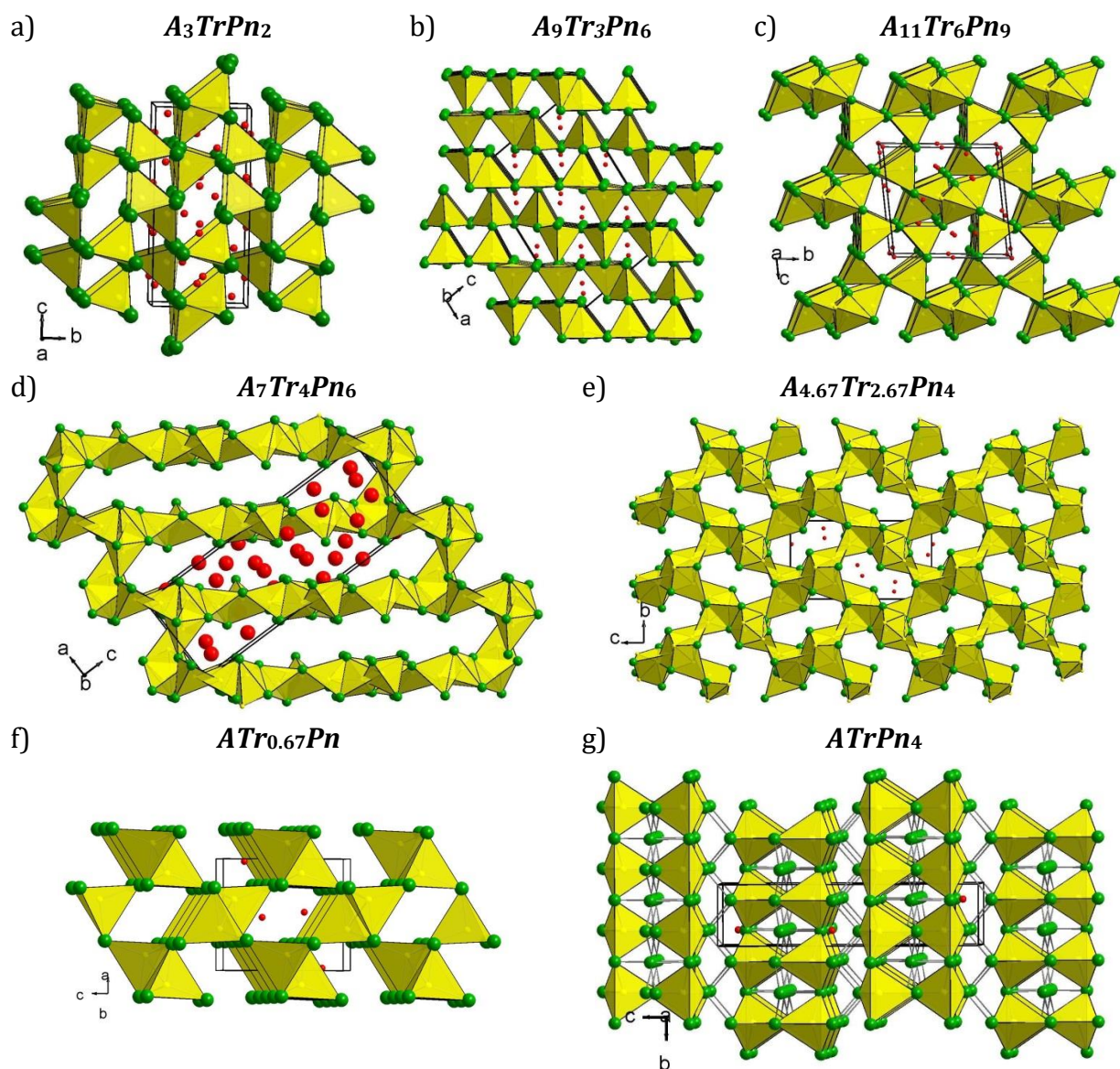


Figure 3.58 Compounds with three-dimensional packing of tetrahedra in the *A-Tr-Pn* systems and stoichiometry 3:1:2 (a, b), 11:6:9 (c) 7:4:6 (d, e), 3:2:3 (f) and 1:1:4 (g). *A* atoms are shown in red, *Tr* – in yellow and *Pn* in green color.

Table 3.53 Compounds in the *A-Tr-Pn* systems (*Tr* = Ga, In, Tl; *Pn* = P, As, Sb, Bi) ternary systems.

Compound	Space group	Cell parameters				Ref.
		<i>a</i> (Å)	<i>b</i> (Å)	<i>c</i> (Å)	<i>V</i> (Å ³)	
A-Ga-P						
K ₂ GaP ₂	<i>P2₁/n</i>	10.215	14.016	8.636	1166.46	[178]
			$\beta = 109.37^\circ$			
Rb ₃ GaP ₂	<i>Pbca</i>	14.6336	24.8932	9.1630	3337.87	[175]
Cs ₆ Ga ₂ P ₄	<i>P2₁/c</i>	11.1730	8.661	18.9390	1806.84	[174]
			$\beta = 99.64^\circ$			
Na ₆ GaP ₃	<i>P$\bar{1}$</i>	7.971	7.967	16.919	921.42	[171a]
		$\alpha = 94.13^\circ$	$\beta = 94.8^\circ$	$\gamma = 119.76^\circ$		
A-Ga-As						
Na ₂ Ga ₂ As ₃	<i>P2₁/c</i>	13.175	6.705	14.459	1277.28	[197]
			$\beta = 90.2^\circ$			
K ₂ Ga ₂ As ₃	<i>P2₁/c</i>	13.782	6.739	15.644	1452.93	[190]
			$\beta = 90.4^\circ$			
K ₃ Ga ₃ As ₄	<i>Pnna</i>	6.597	14.792	10.589	1033.3	[188]
K ₂ GaAs ₂	<i>P2₁/n</i>	10.476	14.393	8.884	1257.15	[179a]
			$\beta = 110.2^\circ$			
Rb ₂ GaAs ₂	<i>P2₁/n</i>	10.867	14.751	8.992	1367.72	[179b]
			$\beta = 108.4^\circ$			
Cs ₃ GaAs ₂	<i>P2₁/c</i>	11.3709	8.8574	19.4599	1934.59	[176]
			$\beta = 99.225^\circ$			
K ₂₀ Ga ₆ As _{12.66}	<i>P6₃/m</i>	16.780	-	5.245	1278.97	[177]
Na ₆ GaAs ₃	<i>P$\bar{1}$</i>	8.170	8.202	17.287	992.89	[171b]
		$\alpha = 94.25^\circ$	$\beta = 94.84^\circ$	$\gamma = 119.77^\circ$		
A-Ga-Sb						
KGaSb ₄	<i>Pnma</i>	10.348	4.203	17.823	775.17	[196]
Na ₂ Ga ₃ Sb ₃	<i>Pnma</i>	26.890	4.283	7.236	833.37	[194]
KGaSb ₂	<i>Cmca</i>	7.650	18.048	29.635	4091.62	[193]
K ₂ Ga ₂ Sb ₃	<i>P2₁/c</i>	14.743	7.185	16.584	1756.65	[191]
			$\beta = 90.5^\circ$			
K ₂ GaSb ₂	<i>Pnma</i>	15.062	10.373	9.145	1428.8	[180a]
Rb ₂ GaSb ₂	<i>Pnma</i>	15.408	10.776	9.302	1544.47	[180b]
Cs ₂ GaSb ₂	<i>Pnma</i>	18.060	11.167	8.358	1685.61	[180c]
K ₂₀ Ga ₆ Sb _{12.66}	<i>P6₃/m</i>	17.800	-	5.438	1492.14	[177]
Cs ₆ GaSb ₃	<i>P2₁/m</i>	10.858	6.490	12.729	880.15	[173]
			$\beta = 101.12^\circ$			
A-Ga-Bi						
-						
A-In-P						
Na ₃ InP ₂	<i>P2₁/c</i>	9.401	7.371	15.358	1063.3	[195a]
			$\beta = 92.39^\circ$			
K ₃ InP ₂	<i>Ibam</i>	14.489	7.658	6.816	756.28	[182]
K ₆ InP ₃	<i>P$\bar{1}$</i>	8.880	8.935	9.952	657.47	[172b]
		$\alpha = 82.03^\circ$	$\beta = 73.11^\circ$	$\gamma = 60.48^\circ$		
Rb ₁₂ In ₄ P ₈	<i>P$\bar{1}$</i>	9.397	12.500	15.927	1668.34	[183a]
		$\alpha = 97.16^\circ$	$\beta = 107.00^\circ$	$\gamma = 106.72^\circ$		
Cs ₁₂ In ₄ P ₈	<i>P$\bar{1}$</i>	9.662	12.884	15.840	1828.38	[183b]

$\alpha = 81.08^\circ \quad \beta = 81.55^\circ \quad \gamma = 70.66^\circ$						
A-In-As						
$K_2In_2As_3$	$P2_1/c$	14.344	7.112	15.850	1616.91	[189]
			$\beta = 90.3^\circ$			
$K_3In_2As_3$	$Cmca$	19.764	6.784	14.871	1993.89	[187]
Na_3InAs_2	$P2_1/c$	9.677	7.547	15.731	1147.69	[195b]
			$\beta = 92.6^\circ$			
K_6InAs_3	$P\bar{1}$	9.120	9.112	19.609	1398.6	[172a]
		$\alpha = 94.2^\circ$	$\beta = 94.5^\circ$	$\gamma = 119.9^\circ$		
Cs_6InAs_3	$P2_1/m$	10.469	6.356	12.208	796.67	[198]
			$\beta = 101.27^\circ$			
$Cs_5In_3As_4$	$P2_1/c$	17.0370	12.2533	18.105	3360.42	[184]
			$\beta = 117.24^\circ$			
A-In-Sb						
$Na_2In_2Sb_3$	$P2_1/c$	14.595	7.532	15.635	1718.75	[186]
			$\beta = 90.0^\circ$			
$K_2In_2Sb_3$	$P2_1/c$	15.254	7.534	16.798	1930.41	[186, 189b]
			$\beta = 90.5^\circ$			
$Rb_2In_2Sb_3$	$P2_1/c$	15.555	7.5692	17.362	2044.07	[192]
			$\beta = 90.598^\circ$			
$Cs_2In_2Sb_3$	$P2_1/c$	15.820	7.568	17.998	2154.66	[199]
			$\beta = 90.7^\circ$			
Na_3InSb_2	$P2_1/c$	10.285	7.963	16.652	1362.39	[195c]
			$\beta = 92.6^\circ$			
$K_{10}In_5Sb_9$	$P2_1/n$	16.744	12.558	17.691	3317.9	[186]
			$\beta = 116.9^\circ$			
Cs_6InSb_3	$P2_1/m$	10.858	6.490	12.729	880.2	[173]
			$\beta = 101.1^\circ$			
A-In-Bi						
$NaIn_{0.67}Bi$	$Pnma$	8.062	4.8684	9.2455	362.88	[147]
$Na_9In_3Bi_6$	$P2_1/c$	18.841	9.235	12.661	2177.8	[147]
			$\beta = 98.67^\circ$			
$K_{4.67}In_{2.67}Bi_4$	$P4_3$	9.703	-	17.519	1649.38	[147]
$Rb_7In_4Bi_6$	$P4_3$	9.915	-	17.870	1756.75	[147]
$Cs_7In_4Bi_6$	$P\bar{1}$	10.1851	10.2318	27.617	2868.34	[144, 147]
		$\alpha = 94.46^\circ$	$\beta = 91.46^\circ$	$\gamma = 90.21^\circ$		
$K_{11}In_6Bi_9$	$P\bar{1}$	12.012	13.380	13.695	1900.19	[147]
		$\alpha = 76.70^\circ$	$\beta = 64.14^\circ$	$\gamma = 75.68^\circ$		
A-Tl-P						
-						
A-Tl-As						
-						
A-Tl-Sb						
Na_6TlSb_4	$P2_1/c$	15.154	10.401	17.413	2515.61	[181]
			$\beta = 113.57^\circ$			
$K_6Tl_2Sb_3$	$P2_1/c$	9.951	17.137	19.640	3246.02	[170]
			$\beta = 104.26^\circ$			
A-Tl-Bi						
-						

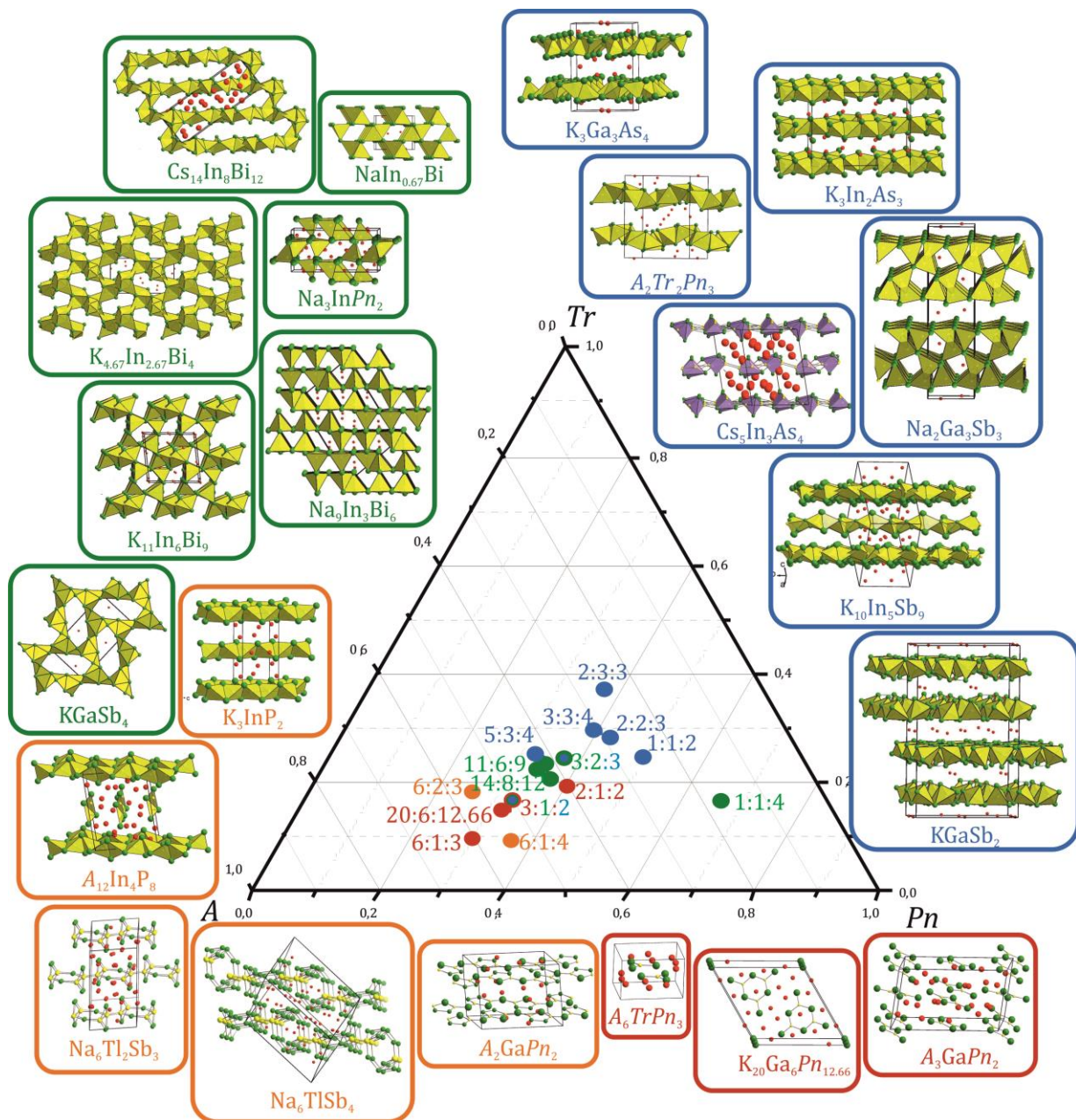


Figure 3.59 Ternary compounds in A - Tt - Pn ternary systems ($A = \text{Na, K, Rb, Cs}$; $Tr = \text{Ga, In, Tl}$; $Pn = \text{P, As, Sb, Bi}$) [144, 147, 170-184, 186-199]. In red are marked alkali metal rich compounds with isolated fragments; in orange structures with one-dimensional chains; in blue two-dimensional layered compounds and in green compounds with three-dimensional networks.

3.3.2 $K_{20}Ga_6Bi_{13.294}$ – the First Compound in the A-Ga-Bi Ternary System

Synthesis and Characterization

Compound $K_{20}Ga_6Bi_{13.294}$ was first obtained as one of the products, along with copper gallides, during an attempt to substitute Sn in $Na_{12}Cu_{12}Sn_{21}$ with the mixture of Ga and Bi. Later, it was reproduced by the high temperature reaction of the elements in ternary sample K, Bi and Ga with the ratio 10:3:6 using 210.9 mg K, 124.4 mg Ga and 676.2 mg Bi in Niobium ampoule. The sealed ampoule was heated to 500°C with rate of 4°/min and held at this temperature for 72 hours, then slowly cooled (with rate of 0.1°/min) to 400°C and quenched to room temperature. The PXRD analysis showed the presence of $K_{20}Ga_6Bi_{13.294}$ as the main phase with some residual binary KBi_2 – Figure 3.60. Because of the high Bi absorption the sample had to be significantly diluted by the diamond powder.

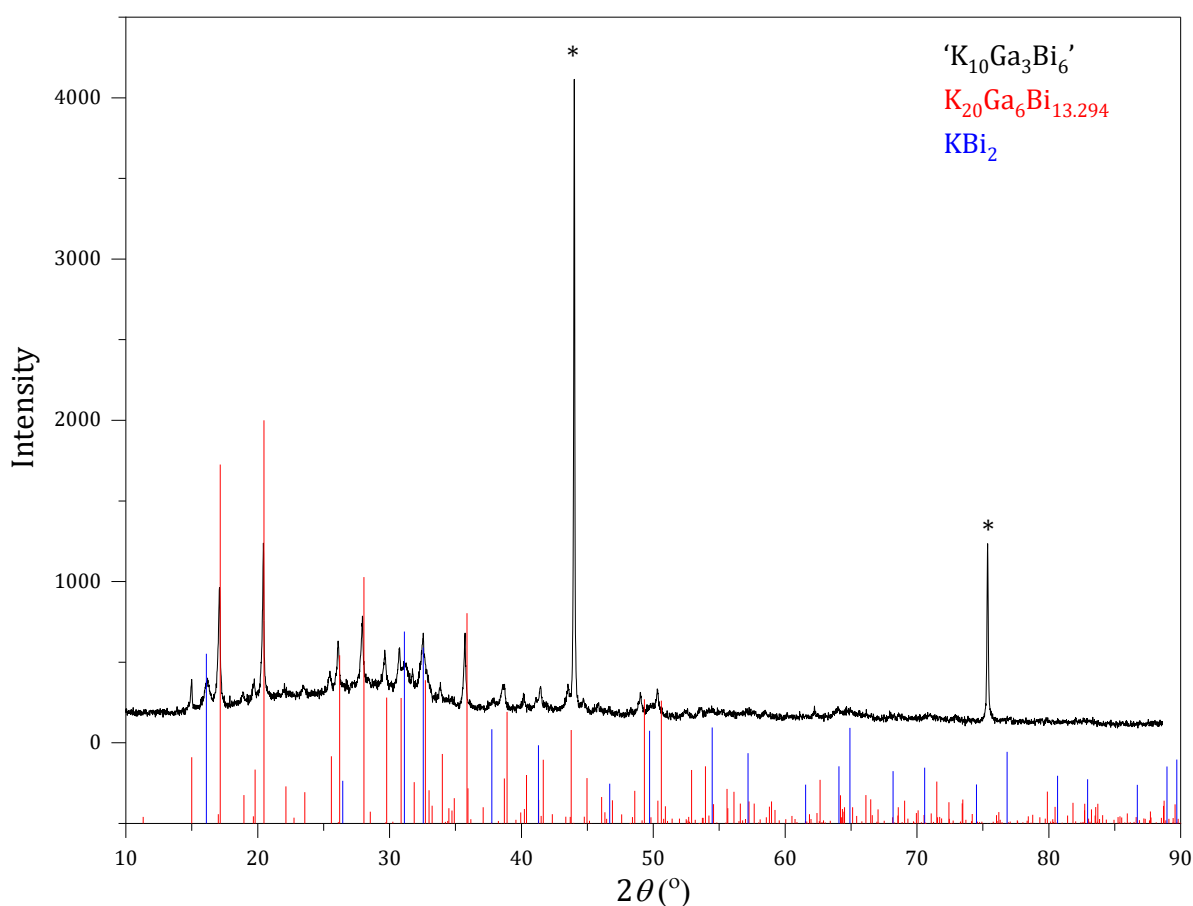


Figure 3.60 Experimental X-ray powder diffractogram of the sample ' $K_{10}Ga_3Bi_6$ ' (black) with the theoretical pattern of $K_{20}Ga_6Bi_{13.294}$ (8) (red), residual KBi_2 (blue) and diamond (*) as internal standard.

Single crystals were picked in the glovebox to characterize the structure of the compound and checked for singularity. The crystal of the best quality was used for the full data collection at the Stoe StadiVari diffractometer with the exposure time of 50 seconds and detector distance of 60 mm. The structure was successfully solved by direct methods in hexagonal space group $P6_3/m$. The numerical absorption correction was made using X-Red and X-Shape software [43-44] and showed high absorption coefficient of 41.729 mm^{-1} , which is consistent for compounds containing Bi. The refinement revealed three crystallographically independent Bi sites (two of which are in the Wyckoff position $6h$ and one in $2b$), one Ga ($6h$) and three K (all three in the Wyckoff position $6h$). The electron deficiency in the Bi3 position is most likely due to the defect, resulting in an occupancy of 64.7 %. Partial defects were tested for all K positions, giving lower occupation factors for Bi3 position, but no sufficient difference was observed, suggesting no significant correlation of the K content with the defect in Bi position. Crystallographic data and selected details of structure refinement for the compound with the refined composition $\text{K}_{20}\text{Ga}_6\text{Bi}_{13.294(8)}$ are listed in Table 3.54, atomic parameters and anisotropic displacement parameters in Table 3.55 and Table 3.56 respectively. In Table 6.8 (Appendix) are presented all the interatomic distances in the compound $\text{K}_{20}\text{Ga}_6\text{Bi}_{12.66}$.

Table 3.54 Crystallographic data and selected details of structure refinement for the compound $\text{K}_{20}\text{Ga}_6\text{Bi}_{13.294(8)}$.

Formula	$\text{K}_{20}\text{Ga}_6\text{Bi}_{13.294(8)}$
Formula weight ($\text{g}\cdot\text{mol}^{-1}$)	3979.75
Space group	$P6_3/m$ (no. 176)
Z	1
Unit cell parameters (\AA)	$a = 18.0393(9)$ $c = 5.4689(3)$
Volume (\AA^3)	1541.2(2)
$D_{\text{calcd.}}$ ($\text{g}\cdot\text{cm}^{-3}$)	4.288
Abs. Coeff. (mm^{-1})	41.729
$F(000)$ (e)	1670
Crystal shape/color	block/silver
Temperature (K)	150
θ range (deg)	3.450–30.000
Range in hkl	$\pm 25, \pm 25, -7 \div 5$
Reflections collected	18200 ($R_6 = 0.0307$)
Unique reflections	1653 ($R_{\text{int}} = 0.0648$)
Data / parameter	1653/43
GOF on F^2	1.061
R_1, wR_2 ($I > 2 \sigma(I)$)	0.0283, 0.0501
R_1, wR_2 (all data)	0.0463, 0.0542
Largest diff. peak/hole (e \AA^{-3})	1.969 and -2.386

Table 3.55 Atom coordinates and equivalent isotropic displacement parameters (\AA^2) for the compound $\text{K}_{20}\text{Ga}_6\text{Bi}_{13.294(8)}$.

Atom	Wyck.	S.O.F.	<i>x</i>	<i>y</i>	<i>z</i>	<i>U_{eq}</i>
Bi1	6 <i>h</i>	1	0.54902(2)	0.15899(2)	1/4	0.01337(9)
Bi2	6 <i>h</i>	1	0.33572(2)	0.22619(2)	1/4	0.01400(9)
Bi3	2 <i>b</i>	0.647(4)	0	0	0	0.145(2)
Ga	6 <i>h</i>	1	0.50165(6)	0.27951(6)	1/4	0.0138(2)
K1	2 <i>c</i>	1	1/3	2/3	1/4	0.0183(7)
K2	6 <i>h</i>	1	0.0049(1)	0.1898(2)	1/4	0.0277(5)
K3	6 <i>h</i>	1	0.0667(1)	0.4507(1)	1/4	0.0183(4)
K4	6 <i>h</i>	1	0.2723(1)	0.3938(1)	1/4	0.0187(4)

Table 3.56 Anisotropic displacement parameters (\AA^2) for $\text{K}_{20}\text{Ga}_6\text{Bi}_{13.294(8)}$.

Atom	<i>U₁₁</i>	<i>U₂₂</i>	<i>U₃₃</i>	<i>U₁₂</i>	<i>U₁₃</i>	<i>U₂₃</i>
Bi1	0.0113(1)	0.0112(1)	0.0172(1)	0.000	0.000	0.0054(1)
Bi2	0.0113(1)	0.0154(1)	0.0151(1)	0.000	0.000	0.0067(1)
Bi3	0.0198(6)	0.0198(6)	0.394(4)	0.000	0.000	0.0099(3)
Ga	0.0117(4)	0.0128(4)	0.0168(4)	0.000	0.000	0.0061(4)
K1	0.0197(1)	0.019(1)	0.0155(1)	0.000	0.000	0.0098(5)
K2	0.0190(1)	0.028(1)	0.0275(1)	0.000	0.000	0.0058(9)
K3	0.0168(9)	0.020(1)	0.0170(9)	0.000	0.000	0.0089(8)
K4	0.0221(1)	0.0180(9)	0.017(1)	0.000	0.000	0.0106(8)

EDX analysis of the measured crystal confirmed the presence of the all three elements in ratio K:Ga:Bi of 54:18:28 (27:9:14).

Table 3.57 Results of the EDX analysis of the crystal with the refined composition $\text{K}_{20}\text{Ga}_6\text{Bi}_{13.294}$ from the sample “ $\text{K}_{10}\text{Ga}_3\text{Bi}_6$ ”. The measured values were averaged from three point measurements of the same crystal.

	K (at. %)	Ga (at. %)	Bi (at. %)
EDX	54(4)	18(8)	28(7)
$\text{K}_{20}\text{Ga}_6\text{Bi}_{13.294}$	50.9	15.3	33.8

Crystal Structure and Discussion

The compound $\text{K}_{20}\text{Ga}_6\text{Bi}_{13.294}$ is the first representative of the *A*-Ga-Bi ternary system and crystallizes in the same hexagonal structure type as $\text{K}_{20}\text{Ga}_6\text{Sb}_{12.66}$ and $\text{K}_{20}\text{Ga}_6\text{Sb}_{12.66}$ [177], with the only difference in the higher occupation of the Bi3 (Sb in case of $\text{K}_{20}\text{Ga}_6\text{Sb}_{12.66}$ and $\text{K}_{20}\text{Ga}_6\text{Sb}_{12.66}$) atom site. Main structural fragments of the compound $\text{K}_{20}\text{Ga}_6\text{Bi}_{13.294}$ are $\{\text{Ga}_3\text{Bi}_6\}^{9-}$ fragments, that have a planar triangular coordinated Ga atom (analog to Boron in $\text{B}_3\text{O}_6^{6-}$ anion) and isolated Bi-Bi dumbbells. Alkali metal cations are counterbalancing the charges and filling the space among them (Figure 3.61).

Three $\{\text{GaBi}_3\}$ triangles (Figure 3.62, a) condensate to form a trimer, sharing 2 of 3 Bi atoms and building a slightly deformed hexagonal ring (with Bi-Ga-Bi angle of 125.47° and Ga-Bi-Ga 114.53°) within a structure of the flat $\{\text{Ga}_3\text{Bi}_6\}^{9-}$ anion, therefore Bi atoms attached to the ring are one-bonded, in the ring – two-bonded and all the Ga atoms are three-bonded. Bi-Ga distances are 2.710 and 2.647 Å within the hexagonal ring and exo-bond, respectively (Table 3.58). The bands are shorter than a sum of covalent radii of single-bonded Ga and Bi ($1.24+1.51=2.75$ Å [120]), but longer than the sum of double-bonded Ga and Bi ($1.17+1.41=2.58$ Å [120]), which indicates bond order of more than one and possibly π -bond character within the hexagonal ring. The occupancy almost 2/3 of Bi3 atoms, unlike 1/3 in isostructural $\text{K}_{20}\text{Ga}_6\text{As}_{12.66}$ and $\text{K}_{20}\text{Ga}_6\text{Sb}_{12.66}$, suggests formation of the $\{\text{Bi}_2\}$ dumbbells (Figure 3.62, b) with quite short distance of 2.734 Å, which is shorter than single bonded $\{\text{Bi}_2\}^{2-}$ ($1.51\times 2=3.02$ Å [120]) and is between double bonded $\{\text{Bi}_2\}^-$ ($1.41\times 2=2.82$ Å [120]) and $\{\text{Bi}_2\}^-$, with triple-bonded Bi atoms ($1.35\times 2=2.70$ Å [120]). In $\text{K}_{20}\text{Ga}_6\text{As}_{12.66}$ and $\text{K}_{20}\text{Ga}_6\text{Sb}_{12.66}$ As or Sb atoms in the position *2b* have occupancy factor of 1/3, which makes them isolated by potassium atoms (As-As and Sb-Sb distances of 2.623 and 2.719 Å does not exist in the structure because there are no direct contacts thanks to the low occupancy of the *2e* position). $\{\text{Bi}_2\}$ dumbbells exist in several *A*-Bi (*A* = K, Cs) binary phases, with Bi-Bi distances of 2.998 Å in K_5Bi_4 [158] or 2.975 Å in Cs_3Bi_2 [156e], which is longer than 2.734 Å $\text{K}_{20}\text{Ga}_6\text{Bi}_{13.294}$. In another binary compound formed by chains of two-bonded Bi atoms, KBi [161] Bi-Bi distances are over 3 Å.

Potassium atoms are building trigonal prisms oriented in [001] direction and are linked via sharing rectangular faces, each of the prisms is centered by $\{\text{Ga}_3\text{Bi}_6\}^{9-}$ atoms as it is shown in Figure 3.63, a. In the unit cell two of the $\{\text{Ga}_3\text{Bi}_6\}^{9-}$ fragments are shifted by $\frac{1}{2}$ in [001] direction so that vertexes of the prisms in one layer are capping the outer rectangular faces

of the prisms surrounding neighboring $\{\text{Ga}_3\text{Bi}_6\}^{9-}$ fragments. This way potassium atoms are forming octahedra (Figure 3.63, b), sharing trigonal faces along [001] direction. Those octahedra are encapsulating isolated Bi-Bi dumbbells in Bi1 position.

Table 3.58 Selected interatomic distances in $\text{K}_{20}\text{Ga}_6\text{Bi}_{13.294}$.

Atom types			Distance range(Å)			Atom types			Distance range(Å)		
Bi	-Bi	2.7345(2)	K	-Ga	3.689(2)-3.7940(7)	K	-Bi	3.606(1)-3.8992(3)	K	-K	4.261(4)-5.4689(3)
Ga	-Bi	2.647(1)-2.7096(9)									

$\text{K}_{20}\text{Ga}_6\text{As}_{12.66}$ and $\text{K}_{20}\text{Ga}_6\text{Sb}_{12.66}$ are electron balanced Zintl-phase, counting both Ga and As/Sb atoms as tri-valent species: $(\text{K}^+)_{20}(\text{Ga}^{3+})_6(\text{Pn}^{3-})_{12.66}$ ($\text{Pn} = \text{As}, \text{Sb}$); or based on the formal charge: $(\text{K}^+)_{20}\{\text{Ga}_3\text{Bi}_6\}^{9-2}(\text{Bi}^{3-})_{2/3}$.

The electronic situation within $\text{K}_{20}\text{Ga}_6\text{Bi}_{13.294}$ is different from the isostructural compounds $\text{K}_{20}\text{Ga}_6\text{As}_{12.66}$ and $\text{K}_{20}\text{Ga}_6\text{Sb}_{12.66}$. Because the higher occupancy of the $2e$ position Bi atoms are not isolated, but forming dumbbells in $\text{K}_{20}\text{Ga}_6\text{Bi}_{13.294}$. It has a direct influence on the negative charge in the compound with Bi^{2-} or Bi^- , depending on the bonding situation of the Bi3 atom. Electronic count for these two cases is $(\text{K}^+)_{20}\{\text{Ga}_3\text{Bi}_6\}^{9-2}(\text{Bi}^{2-})_{1.294}$ and $(\text{K}^+)_{20}\{\text{Ga}_3\text{Bi}_6\}^{9-2}(\text{Bi}^-)_{1.294}$. with the overall negative charge of 20.66 and 19.294, respectively, compensated by 20 potassium atoms.

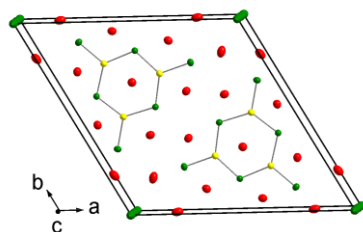


Figure 3.61 Unit cell of the $K_{20}Ga_6Bi_{13.294}$. Gallium atoms are shown in yellow, bismuth – in green and potassium – in red color, the thermal ellipsoids are drawn 90% probability level.

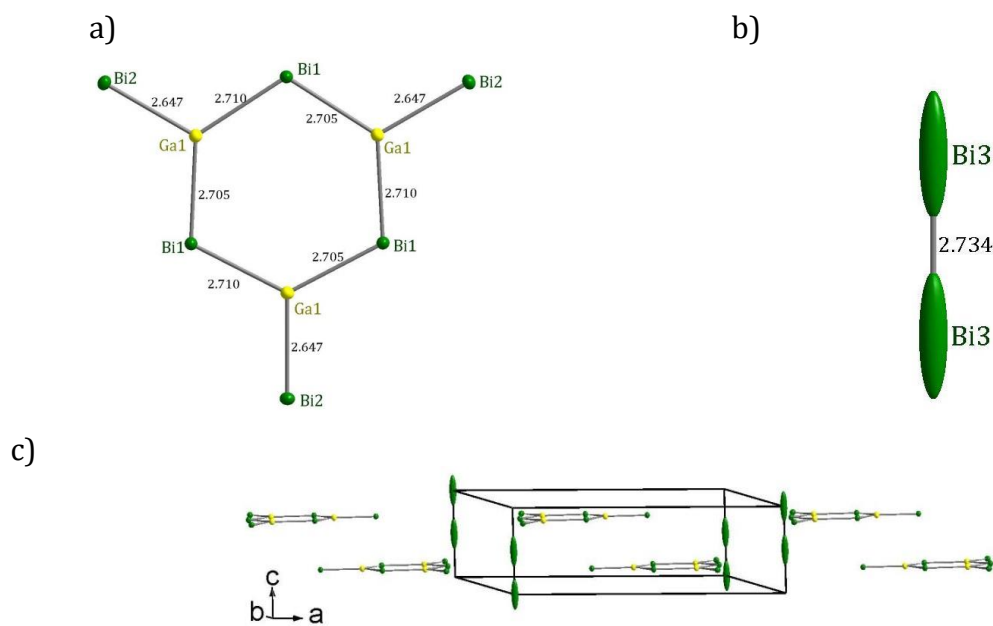


Figure 3.62 Anionic substructure of the $K_{20}Ga_6Bi_{13.294}$: trigonal planar coordination of Ga atoms in $\{Ga_3Bi_6\}^{9-}$ anion (a), $\{Bi_2\}$ dumbbells (b) and packing of the $\{Ga_3Bi_6\}^{9-}$ and $\{Bi_2\}$ fragments, in the crystal structure of the $K_{20}Ga_6Bi_{13.294}$. Thermal ellipsoids are drawn 50% probability level.

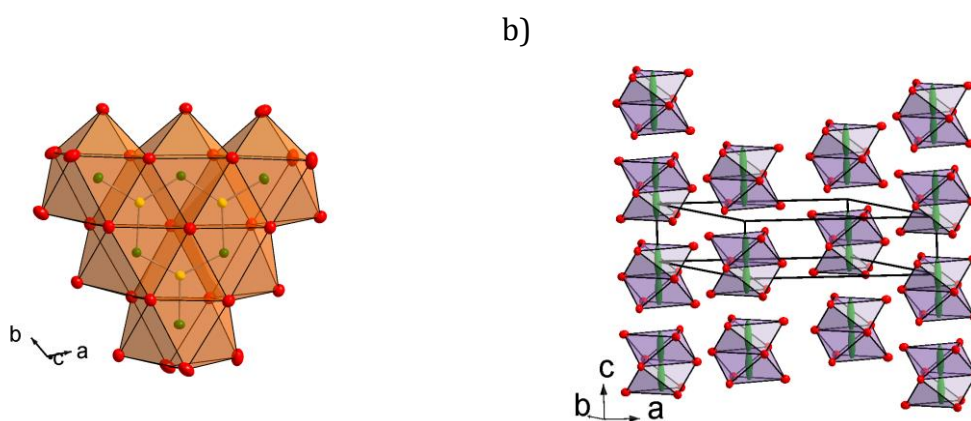


Figure 3.63 Packing of trigonal prisms of K atoms around $\{Ga_3Bi_6\}^{9-}$ fragments (a); and octahedra of K atoms sharing triangular faces and encapsulating isolated $\{Bi_2\}$ dumbbells (b). Thermal ellipsoids are drawn 90% probability level.

3.3.3 New Zintl Phase $K_7In_4As_6$

Synthesis and Characterization

Compound $K_7In_4As_6$, was obtained, similar to the compound $K_{20}Ga_6Bi_{13.294}$, first from the elements in quaternary sample K, Cu, In and As with the ratio 1:1:1.5:1.5 (6.12 mg K, 9.94 mg Cu, 163.6 mg In and 175.8 mg As). The aim of this synthesis was to obtain a compound, similar to $Na_{12}Cu_{12}Sn_{21}$, substituting Sn with the mixture of In and As. The elements were packed and sealed in Nb ampoule. A two stage temperature program was applied: the first stage was heating up to $800^{\circ}C$ with rate $5^{\circ}C/min$ and holding for 12 hours and the second stage was slowly ($0.1^{\circ}C/min$) cooling down to 500° and holding the temperature for 60 hours. PXRD analysis revealed the formation of the $K_7In_4As_6$ as the main product (Figure 3.64). An attempt to synthesize using stoichiometric amounts of the elements led to a new K_3InAs_2 as a main product and is described in Chapter 3.3.4.

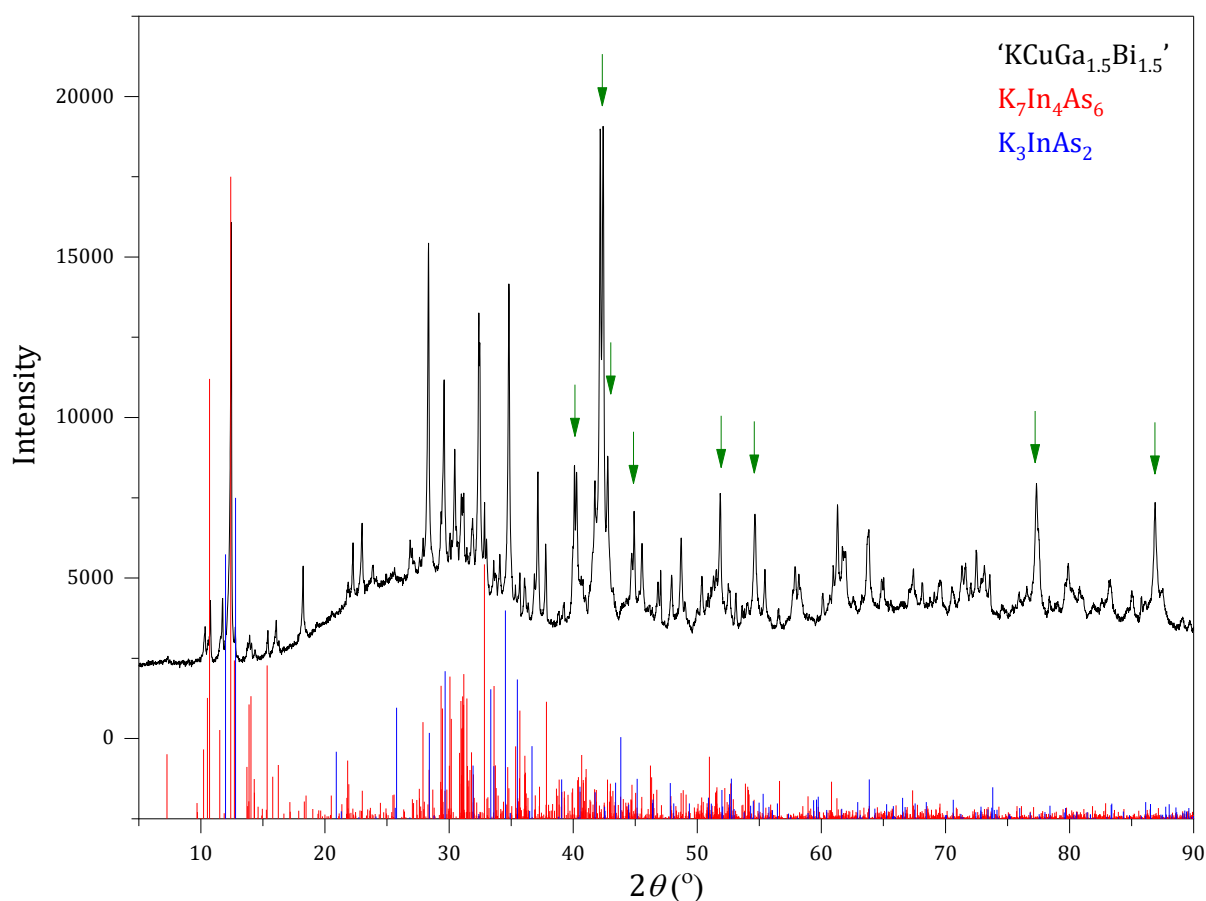


Figure 3.64 Experimental X-ray powder diffractogram (black) of the sample 'KCuGa_{1.5}Bi_{1.5}' with the theoretical pattern of $K_7In_4As_6$ (red), K_3InAs_2 (blue) and reflexes from the binary Cu_9Ga_4 and $CuGa_2$.

Table 3.59 Crystallographic data and data and selected details of structure refinement for the compound $K_7In_4As_6$.

Formula	$K_7In_4As_6$
Formula weight ($g \cdot mol^{-1}$)	1414.18
Space group	$P\bar{1}$ (no. 2)
Z	4
Unit cell parameters (\AA)	$a = 9.1098(3)$ $b = 9.1641(4)$ $c = 24.4564(9)$ $\alpha = 95.796(3)^\circ$ $\beta = 92.578(3)$ $\gamma = 90.013(3)^\circ$
Volume (\AA^3)	2029.2(1)
$D_{\text{calcd.}}$ ($g \cdot cm^{-3}$)	3.871
Abs. Coeff. (mm^{-1})	15.610
$F(000)$ (e)	2108
Crystal shape/color	block/dark grey
Temperature (K)	150
θ range (deg)	2.735–27.497
Range in hkl	$\pm 11 \pm 11 -30 \div 31$
Reflections collected	30084 ($R_e = 0.0307$)
Unique reflections	9316 ($R_{\text{int}} = 0.0648$)
Data / parameter	9316/308
GOF on F ²	1.037
R_1, wR_2 ($I > 2 \sigma(I)$)	0.0489, 0.1302
R_1, wR_2 (all data)	0.0665, 0.1621
Largest diff. peak/hole ($e \text{\AA}^{-3}$)	2.917 and -4.108

Shiny block-shaped crystals were picked and measured using a Stoe Stadivari diffractometer at the temperature 150K with detector distance 70 mm and exposure time 15 seconds. The unit cell of the new compound was indexed in the triclinic space group $P\bar{1}$. Crystallographic data and data and selected details of structure refinement for the compound $K_7In_4As_6$ are listed in Table 3.59. Atomic parameters, isotropic and anisotropic displacement parameters for all eight crystallographically independent indium, twelve arsenic and fourteen potassium atoms are listed in Table 3.60 and

Table 3.61 respectively. In Table 6.10 (Appendix) are presented all the interatomic distances in the compound $K_7In_4As_6$.

EDX analysis of the measured crystal confirmed the presence of the three elements (Table 3.62) in the ratio of K:In:As of 38:26;36 (19:13:18).

Table 3.60 Atom coordinates and equivalent isotropic displacement parameters (\AA^2) for the compound $K_7In_4As_6$.

Atom	Wyck.	S.O.F.	x	y	z	U_{eq}
In1	2i	1	0.00533(7)	0.10322(8)	0.20349(3)	0.0096(2)
In2	2i	1	0.63488(7)	0.03143(8)	0.45631(3)	0.0089(2)
In3	2i	1	0.09044(7)	0.10111(8)	0.70666(3)	0.0096(2)
In4	2i	1	0.40155(7)	0.46176(8)	0.03951(3)	0.0099(2)
In5	2i	1	0.53838(7)	0.38691(8)	0.45920(3)	0.0097(2)
In6	2i	1	0.74892(7)	0.22830(8)	0.36325(3)	0.0090(2)
In7	2i	1	0.04950(7)	0.36139(8)	0.04064(3)	0.0099(2)
In8	2i	1	0.28601(7)	0.24759(8)	0.13138(3)	0.0096(2)
As1	2i	1	0.1814(1)	0.7288(1)	0.52494(4)	0.0095(2)
As2	2i	1	0.9973(1)	0.3419(1)	0.14575(4)	0.0100(2)
As3	2i	1	0.2818(1)	0.1788(1)	0.01711(4)	0.0096(2)
As4	2i	1	0.3417(1)	0.0578(1)	0.64953(4)	0.0096(2)
As5	2i	1	0.0056(1)	0.7995(1)	0.68959(4)	0.0093(2)
As6	2i	1	0.4810(1)	0.4653(1)	0.14659(4)	0.0109(2)
As7	2i	1	0.3566(1)	0.1455(1)	0.46421(4)	0.0099(2)
As8	2i	1	0.1578(1)	0.6402(1)	0.03952(4)	0.0104(2)
As9	2i	1	0.1935(1)	0.1111(1)	0.81448(4)	0.0110(2)
As10	2i	1	0.5390(1)	0.4242(1)	0.35133(4)	0.0110(2)
As11	2i	1	0.1044(1)	0.7144(1)	0.32412(4)	0.0123(2)
As12	2i	1	0.2861(1)	0.0268(1)	0.19109(4)	0.0101(2)
K1	2i	1	0.7825(2)	0.6007(3)	0.09393(9)	0.0129(4)
K2	2i	1	0.6049(2)	0.2578(2)	0.59193(9)	0.0124(4)
K3	2i	1	0.0392(2)	0.9866(3)	0.42629(9)	0.0143(4)
K4	2i	1	0.0243(2)	0.9592(3)	0.07385(9)	0.0147(4)
K5	2i	1	0.1426(3)	0.4233(3)	0.4169(1)	0.0175(5)
K6	2i	1	0.2493(2)	0.4104(3)	0.26349(9)	0.0138(4)
K7	2i	1	0.6081(3)	0.1765(3)	0.2299(1)	0.0172(5)
K8	2i	1	0.1321(2)	0.6922(3)	0.17883(9)	0.0151(4)
K9	2i	1	0.3208(2)	0.0653(3)	0.32877(9)	0.0172(5)
K10	2i	1	0.5005(3)	0.2445(3)	0.7546(1)	0.0217(5)
K11	2i	1	0.1918(3)	0.3451(3)	0.5844(1)	0.0182(5)
K12	2i	1	0.1678(3)	0.4943(3)	0.7416(1)	0.0185(5)
K13	2i	1	0.4596(3)	0.8464(3)	0.0900(1)	0.0212(5)
K14	2i	1	0.6820(3)	0.1946(3)	0.0725(1)	0.0221(5)

Table 3.61 Anisotropic displacement parameters (\AA^2) for the compound $\text{K}_7\text{In}_4\text{As}_6$.

Atom	U_{11}	U_{22}	U_{33}	U_{12}	U_{13}	U_{23}
In1	0.0107(3)	0.0126(3)	0.0053(3)	0.0012(3)	-0.0011(2)	0.0012(3)
In2	0.0103(3)	0.0111(3)	0.0053(3)	0.0014(2)	-0.0011(2)	0.0010(3)
In3	0.0117(3)	0.0116(3)	0.0055(3)	0.0018(3)	-0.0019(2)	0.0019(3)
In4	0.0111(3)	0.0133(3)	0.0057(3)	0.0027(3)	-0.0014(2)	0.0002(3)
In5	0.0116(3)	0.0116(3)	0.0059(3)	0.0009(3)	-0.0008(2)	0.0025(3)
In6	0.0109(3)	0.0112(3)	0.0049(3)	0.0014(2)	-0.0012(2)	0.0018(3)
In7	0.0111(3)	0.0132(3)	0.0057(3)	0.0027(3)	-0.0015(2)	0.0015(3)
In8	0.0102(3)	0.0129(3)	0.0059(3)	0.0026(3)	-0.0017(2)	0.0006(3)
As9	0.0098(5)	0.0128(5)	0.0056(4)	0.0007(4)	-0.0018(3)	0.0013(4)
As10	0.0119(5)	0.0123(5)	0.0059(4)	0.0026(4)	-0.0010(3)	0.0024(4)
As11	0.0112(5)	0.0111(5)	0.0063(5)	0.0006(4)	-0.0012(3)	0.0009(4)
As12	0.0105(5)	0.0117(5)	0.0062(5)	0.0002(4)	-0.0008(3)	-0.0002(4)
As13	0.0105(5)	0.0124(5)	0.0050(4)	0.0004(4)	-0.0007(3)	0.0005(4)
As14	0.0127(5)	0.0145(5)	0.0054(5)	0.0013(4)	-0.0023(3)	-0.0004(4)
As15	0.0103(5)	0.0122(5)	0.0073(5)	0.0031(4)	-0.0017(3)	0.0008(4)
As16	0.0117(5)	0.0124(5)	0.0069(5)	0.0008(4)	-0.0029(3)	0.0017(4)
As17	0.0116(5)	0.0150(5)	0.0060(5)	-0.0004(4)	-0.0020(3)	0.0001(4)
As18	0.0135(5)	0.0131(5)	0.0061(5)	0.0013(4)	-0.0024(4)	0.0041(4)
As19	0.0145(5)	0.0135(5)	0.0084(5)	0.0002(4)	-0.0038(4)	0.0041(4)
As20	0.0109(5)	0.0123(5)	0.0072(5)	0.0030(4)	-0.0016(3)	0.0024(4)
K21	0.012(1)	0.017(1)	0.009(1)	0.0020(8)	-0.0023(7)	0.0022(8)
K22	0.014(1)	0.014(1)	0.009(1)	0.0013(8)	-0.0024(7)	0.0001(8)
K23	0.015(1)	0.017(1)	0.011(1)	-0.0013(8)	-0.0009(8)	0.0009(8)
K24	0.019(1)	0.016(1)	0.009(1)	0.0006(8)	-0.0013(8)	0.0026(9)
K25	0.018(1)	0.021(1)	0.014(1)	0.0024(9)	-0.0039(8)	0.0019(9)
K26	0.015(1)	0.016(1)	0.011(1)	0.0016(8)	-0.0020(8)	0.0005(8)
K27	0.016(1)	0.021(1)	0.014(1)	-0.0016(9)	-0.0044(8)	0.0020(9)
K28	0.016(1)	0.019(1)	0.010(1)	0.0029(9)	-0.0036(8)	0.0009(9)
K29	0.018(1)	0.026(1)	0.008(1)	0.0046(9)	0.0001(8)	0.0099(9)
K30	0.023(1)	0.023(1)	0.017(1)	-0.002(1)	-0.0081(9)	0.003(1)
K31	0.018(1)	0.018(1)	0.019(1)	0.0030(9)	-0.0013(9)	0.0021(9)
K32	0.017(1)	0.022(1)	0.017(1)	0.0025(9)	0.0007(8)	0.0011(9)
K33	0.019(1)	0.024(1)	0.020(1)	-0.005(1)	0.0044(9)	-0.001(1)
K34	0.020(1)	0.021(1)	0.026(1)	-0.001(1)	0.0029(9)	0.000(1)

Table 3.62 Results of the EDX analysis of the crystal with the refined composition $\text{K}_7\text{In}_4\text{As}_6$ from the sample 'KCuIn_{1.5}As_{1.5}'.

	K (at. %)	In (at. %)	As (at. %)
EDX	38(3)	26(2)	36(2)
$\text{K}_7\text{In}_4\text{As}_6$	41.2	23.5	35.3

Crystal Structure

The crystal structure of the triclinic $K_7In_4As_6$ is rather complex: the compound is isostructural to $Cs_7In_4Bi_6$ [144]. It shows rather typical tetrahedral coordination of In atoms by four As atoms, similar as in other compounds in *A-Tr-Pn* ternary systems. The structure of $K_7In_4As_6$ could be described as build of chains of In-centered tetrahedra sharing two out of six available edges –Figure 3.65, a). The low symmetry of the compound is quite unusual between *A-Tr-Pn* compounds and is a result of different sharing models between the tetrahedra that cause chains to twist and turn, which also results in quite long *c*-axis. The stacking of the In-centered tetrahedra within one layer from different perspectives is shown in Figure 3.65, b).

Six out of eight In atoms are encapsulated in tetrahedra, formed by four As-atoms, In-As distances are between 2.592 and 2.854 Å (Table 3.63). Two other In atoms, In4 and In5 are both surrounded by three As atoms and one ‘outer’ In atom, this way two In-centered tetrahedra {In4@As₃In4} ({In5@As₃In5}) are intercalating, so that Indium atom centering one tetrahedron is in the same time vertex of the other tetrahedra – Figure 3.66. It leads to elongation of both tetrahedra along In-In bond: $d_{In4-In4} = 2.833$ and $d_{In5-In5} = 2.838$ Å, which are nearly perpendicular to the chains and are responsible for interconnecting them.

Table 3.63 Selected interatomic distances in the compound $K_7In_4As_6$. For details see Table 6.10 (Appendix).

Atom types			Distance range(Å)			Atom types			Distance range(Å)		
In	-In	2.833(1)-3.475(1)	K	-In	3.321(2)-3.871(2)	K	-As	3.214(3)-3.938(3)	K	-K	3.603(4)-3.957(3)
In	-As	2.592(1)-2.854(1)									

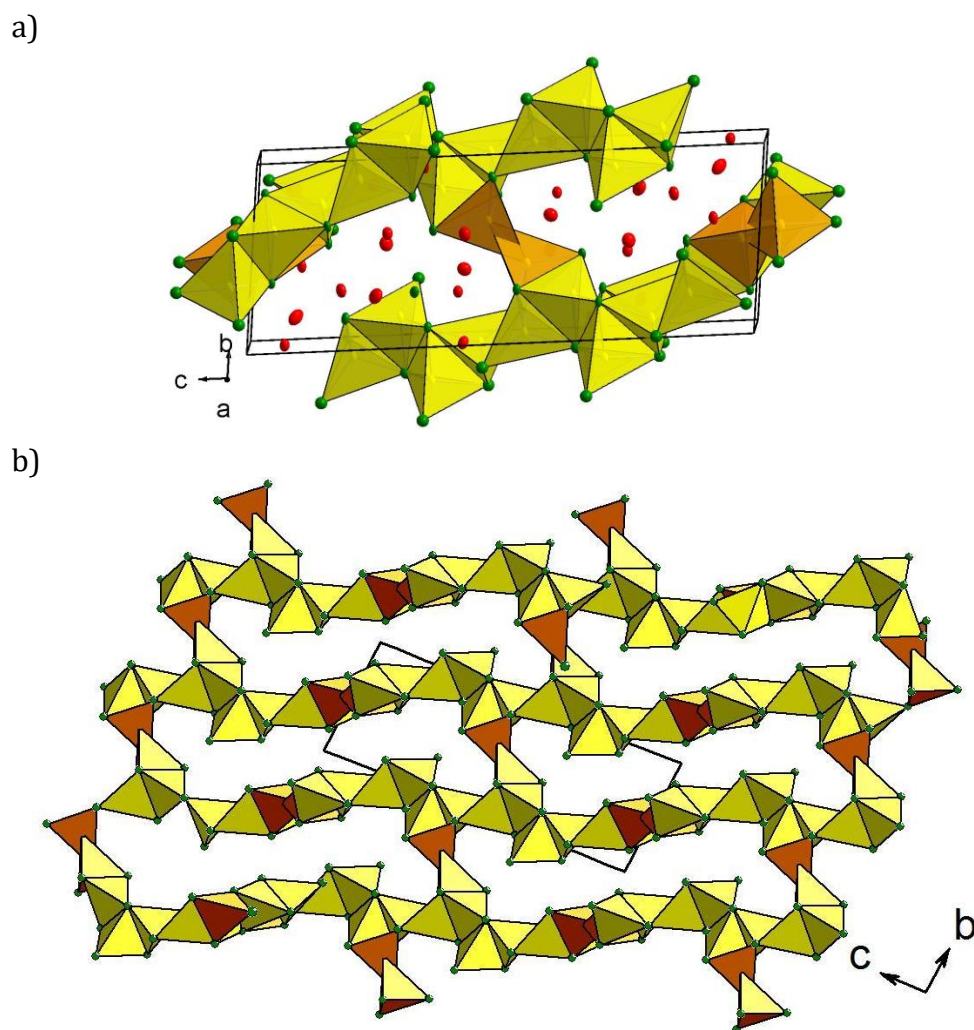


Figure 3.65 Structure of the compound $K_7In_4As_6$: unit cell (a) and stacking of the yellow $\{In@As_4\}$ and orange $\{In@As_3In\}$ tetrahedra within one layer along $[100]$ direction. In atoms are yellow, arsenic – green and potassium – red, the thermal ellipsoids are drawn with 90 % probability level.

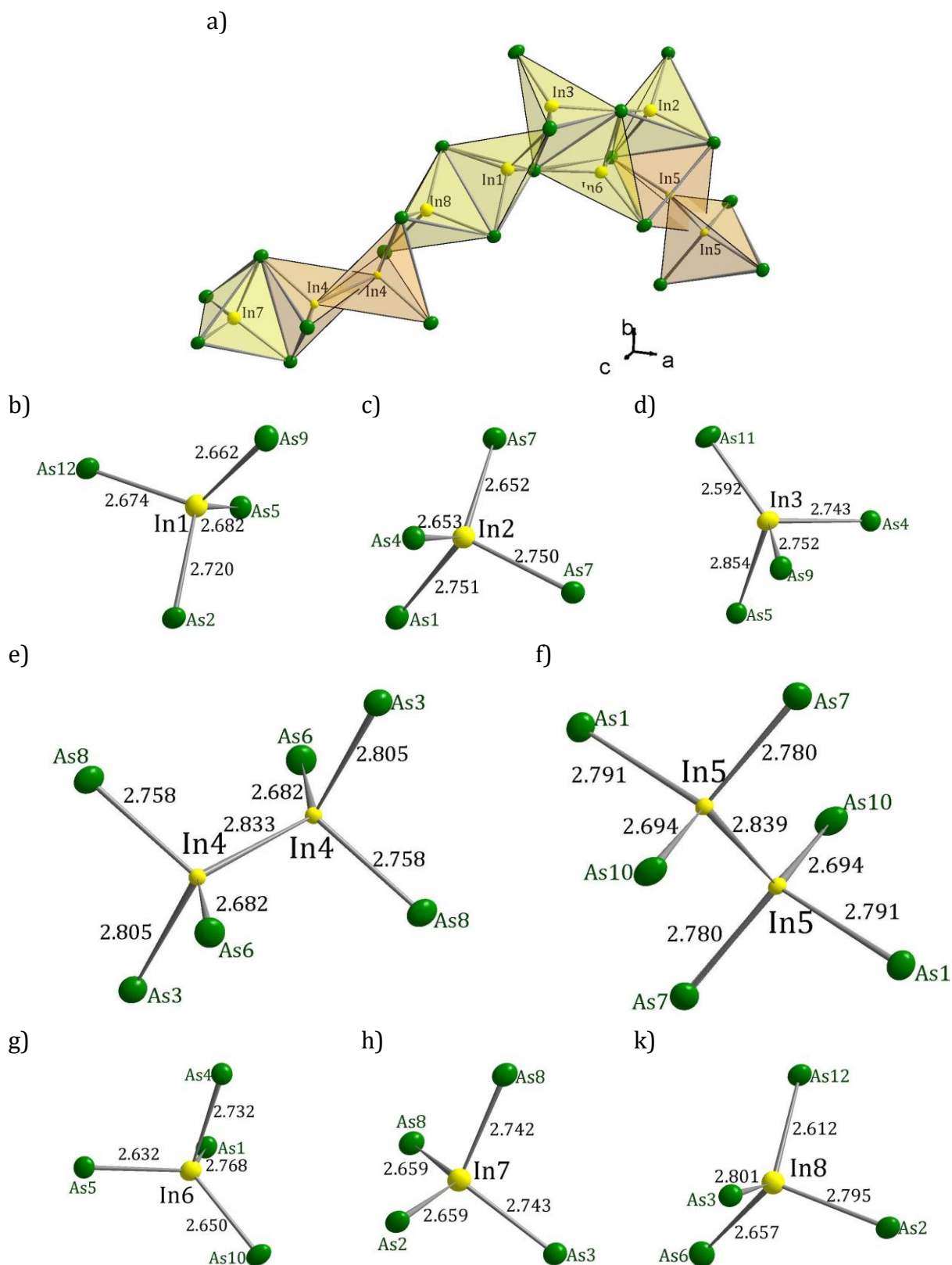


Figure 3.66 Repeated structural fragment is the structure of the $K_7In_4As_6$ (a) and the environment of the In-atoms: indium atoms (In1-In3, In6-In7) centering As_4 tetrahedra (b-d, g-k) and intercalated tetrahedra around In4 (d) and In5 (e) atoms.

Electronic Situation

LMTO calculations for the compound $K_7In_4As_6$ suggest it is a semiconductor with a band gap of 0.5 eV. The band structure and the total Density of States (DOS) with orbital projected DOS and the separate contributions from the constituting elements for the $K_7In_4As_6$ are represented in Figure 3.67. The choice of the lattice vectors was implemented path (X-G-Y-G-Z-G-U-V) was selected as it was suggested in [200] for the triclinic Brillouin zone of TRI_{1b} lattice using Bilbao Crystallographic Server [201].

The peak with the lowest energies in the valence region of DOS between -12 and -10 eV is mainly the arsenic *s*-orbitals with the small contributions of In and K *s*-orbitals. The continuous region (-6-0 eV) following the gap at -10 - -6 eV contains predominantly contributions from the *p*-orbitals of As with participation of the *s*-orbitals of potassium and *p*-orbitals of indium. In the conduction band after the Fermi level the main contributions are from As and In *p*-orbitals and K *s*-orbitals.

Compound $K_7In_4As_6$ is an electron balanced Zintl phase relatively simple with electron count: $(K^{+14})(In^{3+})_6(In^{2+})_2(As^{3-})_{12}$.

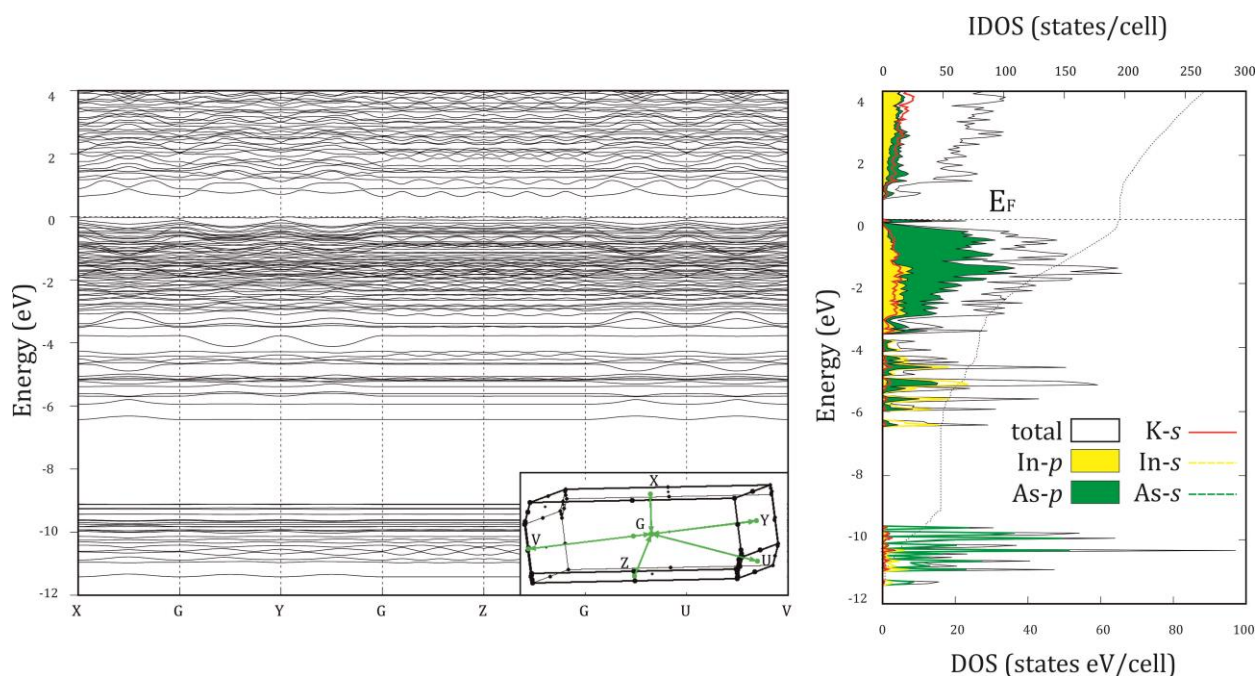


Figure 3.67 The band structure as well as the total Density of States (DOS) with orbital projected DOS calculated for the $K_7In_4As_6$.

3.3.4 An Electron Precise Zintl Phase K_3InAs_2

Synthesis and Characterization

The sample with K:In:As ratio of 7:4:6 was synthesized from pure elements (127.2 mg of K, 194.2 mg of In and 190.1 mg of As) in sealed niobium ampoule with the following temperature program: heating up with $5^\circ\text{C}/\text{min}$ to 600°C , holding the temperature for 200 hours and quenching to the room temperature. Phase analysis of the obtained sample showed the presence of two ternary phases: K_3InAs_2 and $K_7In_4As_6$ (Figure 3.68).

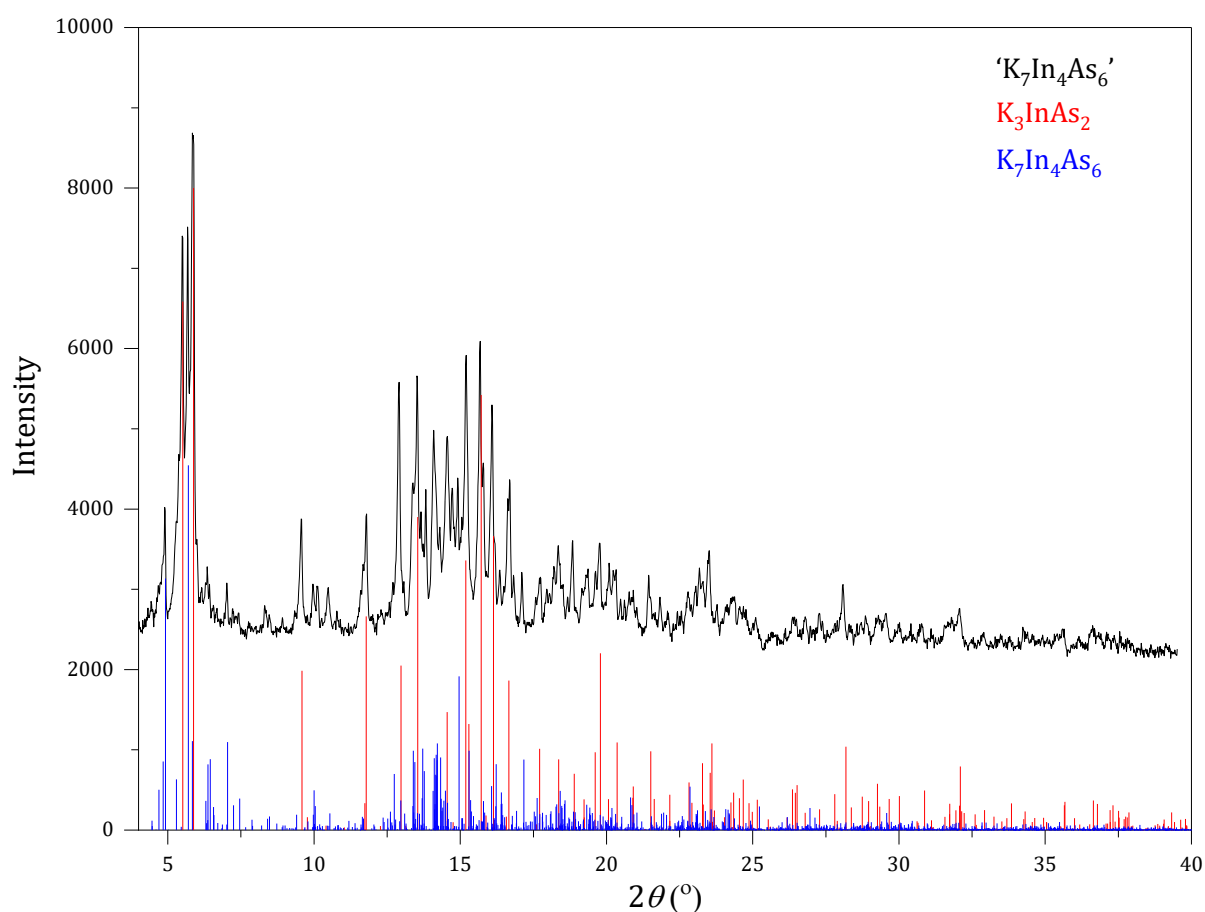


Figure 3.68 Experimental X-ray powder diffractogram (black) of the sample ' $K_7In_4As_6$ ', annealed at 600°C , with the theoretical pattern of the K_3InAs_2 (red) and $K_7In_4As_6$ (blue).

The structure solution of the K_3InAs_2 , which is isostructural to the K_3InP_2 [182], was straightforward and reveals the similarity of the two crystal structures. A shiny grey crystal was selected for the single crystal X-ray diffraction analysis and was measured on Stoe StadiVari diffractometer. The unit cell of the new compound was indexed in the orthorhombic space group $Ibam$ and cell parameters $a = 7.821(2)$, $b = 14.759(3)$ and $c =$

6.936(1) Å. In Table 3.64 selected crystallographic data of the refinement for the compound K_3InAs_2 is listed. Atomic parameters and anisotropic displacement parameters are listed in Table 3.65 and Table 3.66, respectively. Interatomic distances are given in Table 6.9 (Appendix). In the structure of the K_3InAs_2 four crystallographically independent positions are fully occupied by In (position 4*a*), As (8*j*) and two by K atoms (8*j* and 4*b*), resulting in four formula units per unit cell.

EXD analysis (Table 3.67) confirmed presence of all three elements with the expected stoichiometry.

Table 3.64 Crystallographic data and data and selected details of structure refinement for the compound.

Formula	K_3InAs_2
Formula weight ($g \cdot mol^{-1}$)	190.98
Space group	<i>Ibam</i> (no. 72)
Z	4
Unit cell parameters (Å)	$a = 7.821(2)$ $b = 14.759(3)$ $c = 6.936(1)$
Volume (Å ³)	800.7(3)
$D_{calcd.}$ ($g \cdot cm^{-3}$)	3.169
Abs. Coeff. (mm^{-1})	12.599
$F(000)$ (e)	688
Crystal shape/color	block/grey
Temperature (K)	150
θ range (deg)	2.948 – 29.993
Range in <i>hkl</i>	$\pm 10, \pm 20, \pm 9$
Reflections collected	14688 ($R_\sigma = 0.0254$)
Unique reflections	628 ($R_{int} = 0.1015$)
Data / parameter	628/ 19
GOF on F ²	1.014
R_1, wR_2 ($I > 2 \sigma(I)$)	0.0315, 0.0794
R_1, wR_2 (all data)	0.0355, 0.0770
Largest diff. peak/hole ($e \text{ \AA}^{-3}$)	1.435 and -1.562

Table 3.65 Atom coordinates and equivalent isotropic displacement parameters (Å²) for the compound K_3InAs_2 .

Atom	Wyck.	S.O.F.	x	y	z	U_{eq}
In	4 <i>a</i>	1	0	0	1/4	0.0100(2)
As	8 <i>j</i>	1	0.19243(7)	0.09871(4)	0	0.0122(2)
K1	8 <i>j</i>	1	0.2987(2)	0.31754(9)	0	0.0224(3)
K2	4 <i>b</i>	1	1/2	0	1/4	0.0182(4)

Table 3.66 Anisotropic displacement parameters (\AA^2) for the compound K_3InAs_2 .

Atom	U_{11}	U_{22}	U_{33}	U_{12}	U_{13}	U_{23}
In	0.0125(2)	0.0119(3)	0.0056(3)	0.000	0.000	0.000
As	0.0138(3)	0.0144(3)	0.0083(3)	0.000	0.000	-0.0027(2)
K1	0.0249(6)	0.0193(6)	0.0230(6)	0.000	0.000	-0.0067(5)
K2	0.0154(7)	0.0298(9)	0.0094(8)	0.000	0.000	0.000

Table 3.67 Results of the EDX analysis of the crystal with the refined composition K_3InAs_2 from the sample ' $\text{K}_7\text{In}_4\text{As}_6$ '. Significant deviation in potassium content is caused by the oxidation of the surface of the crystal.

	K (at. %)	In (at. %)	As (at. %)
EDX	62(4)	14(6)	25(4)
K_3InAs_2	50.0	16.7	33.3

Thermal Behavior

The thermal behavior of the 82 mg of the sample 'K₇In₄As₆' was determined with a Netzsch DSC 404 Pegasus apparatus. During the experiment, the sample was heated in an argon flow with a heating/cooling rate of 10 °C/min to 1000°C in two cycles. DSC analysis of the sample 'K₇In₄As₆' showed that after the heating in the first cycle compound K₇In₄As₆ is irreversibly decomposing between 730 and 760°C (Figure 3.69). Signals that appear during cooling in the first cycle are visible again in the second cycle. The major signal at 552.0°C in the first cycle (550.4 and 532.6°C in the second cycle) should occur due to the melting/crystallization of the investigated phase K₃InAs₂. Effects at 470.1°C (cycle 1) as well as at 459.1 and 468.5°C (cycle 2) indicate melting/crystallization of the K₂₂In₃₉ (see K-In binary phase diagram in Figure 6.3, d).

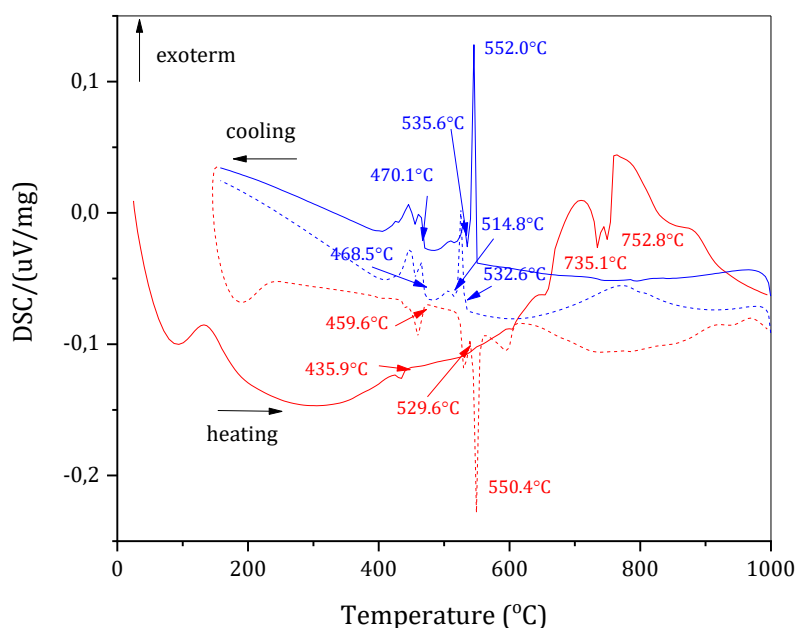


Figure 3.69 Thermogram of the sample 'K₇In₄As₆'. Heating curves are shown in red and cooling in blue (First cycle – solid line, second cycle – dashed line).

Crystal Structure

K_3InAs_2 , as it was mentioned, is isostructural to K_3InP_2 [182], and crystallizes in structure type Na_3AlAs_2 [202] – the unit cell is shown in Figure 3.70. The anionic substructure of the compound consists of In-centered As_4 tetrahedra (Figure 3.71, a) with In-As distance of 2.719 Å (Table 3.68), which is significantly longer than $d_{In-P} = 2.639$ Å in K_3InP_2 . Tetrahedra are interconnected through common edges and are forming infinite chains in [001] direction (Figure 3.71, b). Similar rods of Si-centered S_4 tetrahedra were first observed in SiS_2 [203].

In the structure of the K_3InAs_2 with four-bonded In and two-bonded As atoms are forming $\{InAs_2\}$ rods. K atoms in two independent Wyckoff positions are separating the rods. K1 is coordinated by four arsenic ($d_{K-As} = 3.304-3.335$ Å) and two indium atoms ($d_{K-In} = 3.569$ Å); K2 atoms are surrounded by four As atoms with K-As interatomic distance of 3.304 Å.

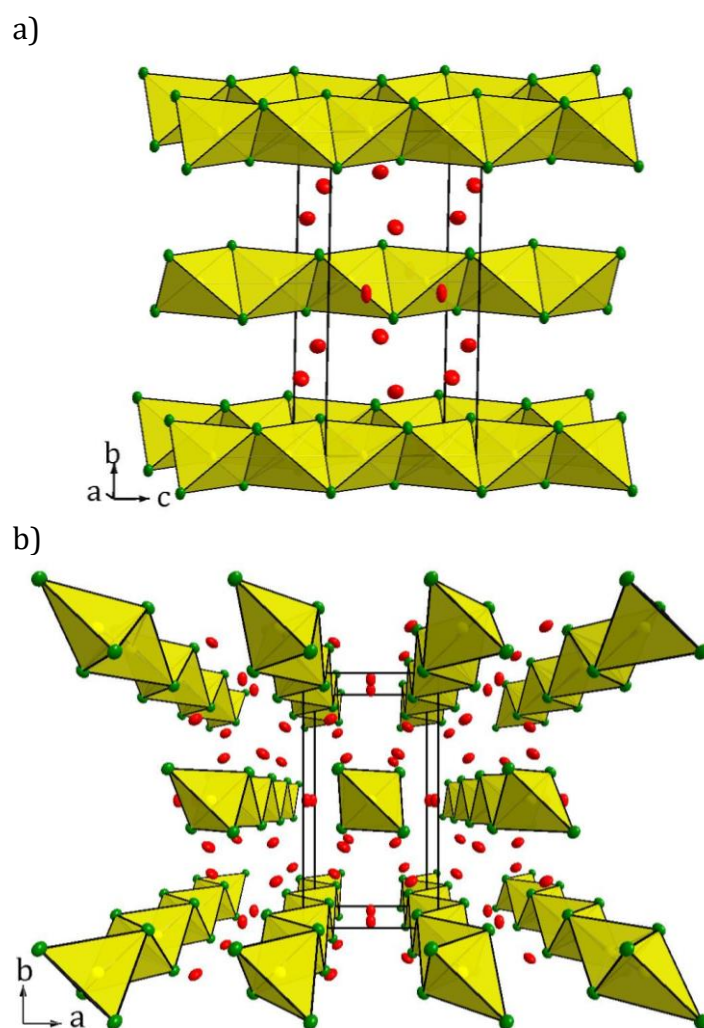


Figure 3.70 Unit cell of the K_3InAs_2 . Indium atoms (centering As_4 tetrahedra) are shown in yellow, arsenic atoms – in green and potassium atoms – in red color, the thermal ellipsoids are drawn at 90% probability level.

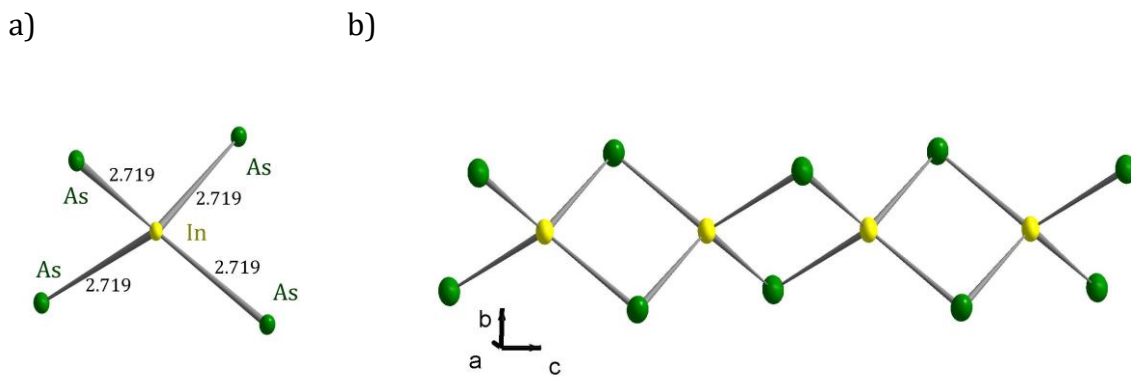


Figure 3.71 Surroundings of the In-atom in K_3InAs_2 (a) and stacking of the In-centered tetrahedra along [001] direction forming one-dimensional chains (b).

Table 3.68 Selected interatomic distances in K_3InAs_2 .

Atom types		Distance range(Å)	Atom types		Distance range(Å)
In	-In	3.4681(5)	K	-In	3.569(1)-3.9106(8)
In	-As	2.7193(5)	K	-As	3.3039(6)-3.335(1)

Electronic Situation

According to LMTO calculations (Figure 3.72), compound K_3InAs_2 , like K_3InAs_2 is a semiconductor with the band gap between the valence and conductive bands of 0.6 eV.

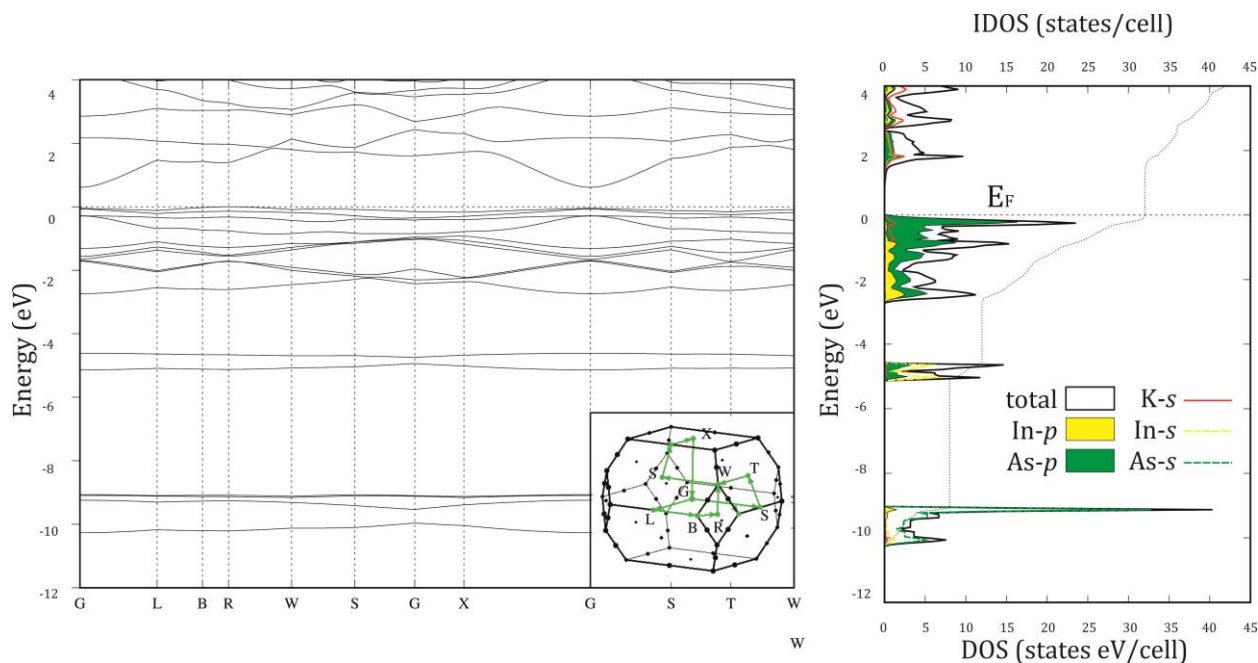


Figure 3.72 The band structures as well as the total Density of States (DOS) with orbital projected DOS calculated for the K_3InAs_2 .

The band structure was calculated along the main directions of the reciprocal lattice for the K_3InAs_2 gain a more deep insight view of bonding. The choice of the lattice vectors was implemented path (G-L-B-R-W-S-G-X-G-S-T-W) was selected as it was suggested in [200] for the orthorhombic Brillouin zone of $ORCF_2$ lattice using Bilbao Crystallographic Server [201].

The density of states (DOS) plot and the separate contributions from the constituting elements is also represented in Figure 3.72. The two peaks with the lowest energies in the DOS are the arsenic *s*-orbitals at around -10eV and arsenic as well as indium *p*-orbitals at around -5 eV. The continuous region following them (-3.0 to 0 eV) contains predominantly contributions from the *p*-orbitals of As with participation of the *s*-orbitals of potassium and *p*-orbitals of indium. The conduction band, which starts at around 2eV for K_3InAs_2 mainly consists of contributions from As *p*-orbitals and K *s*-orbitals.

K_3InAs_2 is an electronically balanced Zintl phase, with four-bonded In^{3+} and two-bonded As^{7-} atoms forming $\{InAs_2\}^{3-}$ rods. The formal charge of $\{InAs_2\}^{3-}$ anions is compensated by K cations in two independent Wyckoff positions, which are separating the rods. Electron count for the K_3InAs_2 can be written as $(K^+)_3(In^{3+})_1(As^{3-})_2$.

3.3.5 Novel In-rich Icosahedral Phase $K_{144}In_{192}As_{37}$

Synthesis and Characterization

To investigate the phase transition observed during the DSC analysis of the sample ' $K_7In_4As_6$ ' (Figure 3.69) a new sample the same K:In:As ratio of 7:4:6 was synthesized from pure elements (127.3 mg of K, 194.3 mg of In and 190.2 mg of As) in sealed niobium ampoule with the different temperature program: heating up with 5°C/min to 850°C, holding the temperature for 200 hours and quenching to the room temperature. The aim of this experiment was to find out what is happening in the system above 730-750°C. The main phase according to the PXRD analysis (Figure 3.73), along with other ternary phases, turned out to be novel In-rich phase $K_{144}In_{192}As_{37}$.

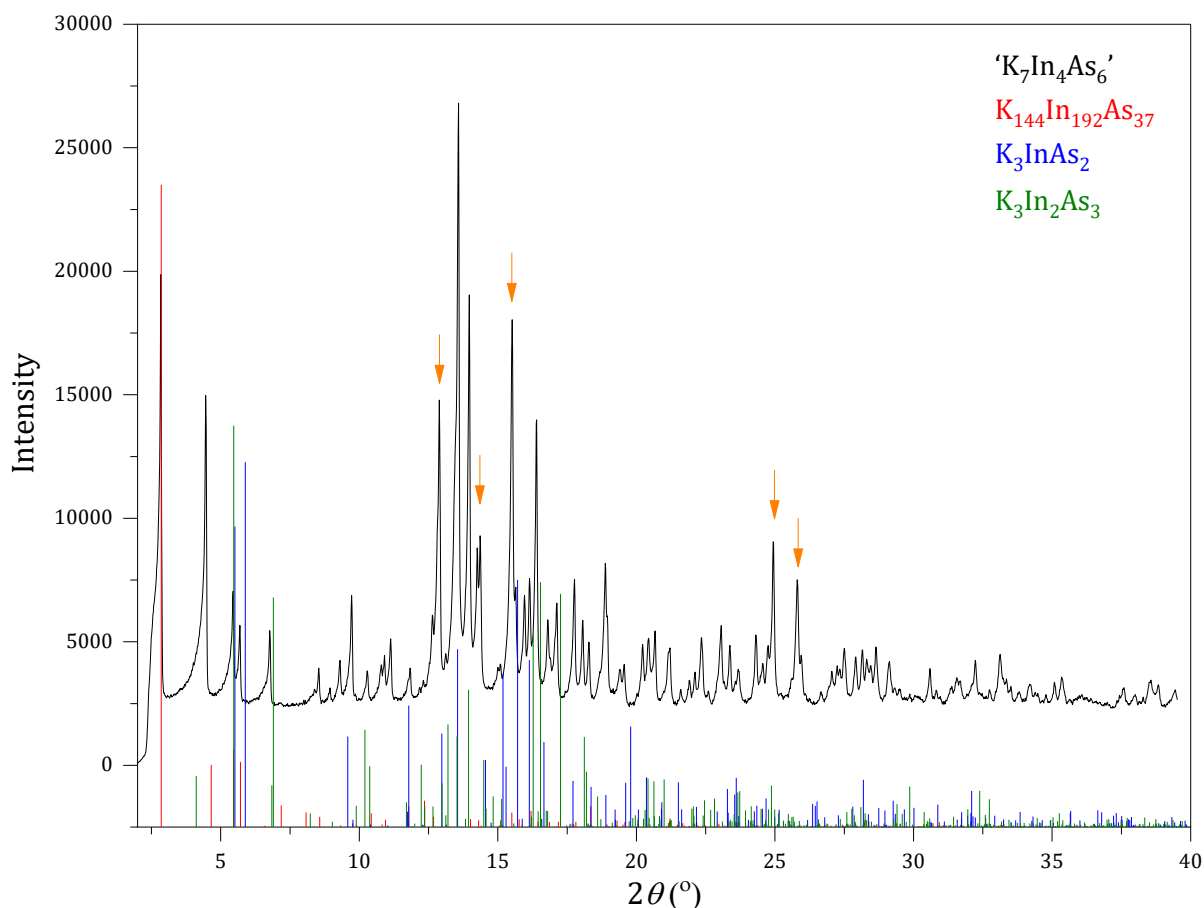


Figure 3.73 Experimental X-ray powder diffractogram (black) of the sample ' $K_7In_4As_6$ ', annealed at 850°C, with the theoretical pattern of the $K_{144}In_{192}As_{37}$ (red), K_3InAs_2 (blue) and $K_3In_2As_3$ (green). Unindexed reflexes are marked with an orange arrow.

To characterize the structure of the compound several dark grey single crystals were picked and checked for singularity. The best one was measured at Stoe Stadivari diffractometer with 50 seconds exposure time and 60 mm detector distance, at the temperature of 150 K. The unit cell of the compound was indexed in the cubic space group $Fd\bar{3}m$ with $a = 24.6407(5)$ Å. Selected crystallographic data and details of the structure refinement are listed in Table 3.69. Both of the two crystallographically independent As positions (Wyckoff positions $96g$ and $16c$ for the As1 and As2, respectively) are lacking electron density and were refined as defects with As occupancy 0.258(7) and 0.79(4) for As1 and As2, respectively. Because of the specific coordination environment, discussed later, Arsenic atoms in the As2 position have quite high values of the isotropic (and anisotropic) displacement parameters.

The atomic parameters and equivalent isotropic and anisotropic displacement parameters for all the atoms in the compound $K_{144}In_{192}As_{37(1)}$ are presented in Table 3.70 and Table 3.71, respectively. Interatomic distances in the compound $K_{144}In_{192}As_{37}$ are listed in Table 6.11 (Appendix).

EDX analysis of the crystal, characterized by the single crystal X-ray analysis confirmed the presence of all three elements in an expected ratio (Table 3.72).

Table 3.69 Crystallographic data and selected details of structure refinement for the compound $K_{144}In_{192}As_{37(1)}$.

Formula	$K_{144}In_{192}As_{37(1)}$
Formula weight ($g \cdot mol^{-1}$)	30483.2
Space group	$Fd\bar{3}m$ (no. 227)
Z	1
Unit cell parameters (Å)	$a = 24.6407(5)$
Volume (Å ³)	14961.0(9)
$D_{calcd.}$ ($g \cdot cm^{-3}$)	3.383
Abs. Coeff. (mm^{-1})	10.295
$F(000)$ (e)	13381
Crystal shape/color	block/dark grey
Temperature (K)	150
θ range (deg)	2.864 – 29.973
Range in hkl	$\pm 34, -34 \div 29, -33 \div 34$
Reflections collected	87423 ($R_6 = 0.0078$)
Unique reflections	1086 ($R_{int} = 0.0475$)
Data / parameter	1086/34
GOF on F2	1.130
R_1, wR_2 ($I > 2 \sigma(I)$)	0.0499, 0.1397
R_1, wR_2 (all data)	0.0539, 0.1426
Largest diff. peak/hole ($e \text{ \AA}^{-3}$)	5.018 and -2.755

Table 3.70 Atom coordinates and equivalent isotropic displacement parameters (\AA^2) for the compound $\text{K}_{144}\text{In}_{192}\text{As}_{37(1)}$.

Atom	Wyck.	S.O.F.	<i>x</i>	<i>y</i>	<i>z</i>	<i>U_{eq}</i>
In1	96 <i>g</i>	1	0.08146(2)	0.08146(2)	0.49335(3)	0.0155(2)
In2	96 <i>g</i>	1	0.03695(2)	0.03695(2)	0.38821(4)	0.0234(3)
As1	96 <i>g</i>	0.258(7)	0.0663(2)	0.0666(5)	0.3001(2)	0.032(2)
As2	16 <i>c</i>	0.79(4)	0	0	0	0.18 (1)
K1	32 <i>e</i>	1	0.2804(1)	0.2804(1)	0.28044(1)	0.0217(8)
K2	8 <i>b</i>	1	0.8750	0.8750	0.8750	0.040(3)
K3	96 <i>g</i>	1	0.3164(1)	0.3164(1)	0.12808(2)	0.0413(8)
K4	8 <i>c</i>	1	1/8	1/8	0.6250	0.013(1)

Table 3.71 Anisotropic displacement parameters (\AA^2) for the $\text{K}_{144}\text{In}_{192}\text{As}_{37(1)}$ (in \AA^2).

Atom	<i>U₁₁</i>	<i>U₂₂</i>	<i>U₃₃</i>	<i>U₁₂</i>	<i>U₁₃</i>	<i>U₂₃</i>
In1	0.0158(3)	0.0158(3)	0.0150(4)	-0.0006(2)	-0.0006(2)	-0.0032(2)
In2	0.0203(3)	0.0203(3)	0.0296(5)	-0.0067(2)	-0.0067(2)	-0.0022(3)
As1	0.033(2)	0.033(2)	0.028(3)	-0.002(1)	-0.002(1)	-0.018(2)
As2	0.18(1)	0.18(1)	0.18(1)	-0.010(9)	-0.010(9)	-0.010(9)
K1	0.0217(8)	0.0217(8)	0.0217(8)	0.004(1)	0.004(1)	0.004(1)
K2	0.040(3)	0.040(3)	0.040(3)	0.000	0.000	0.000
K3	0.041(1)	0.041(1)	0.043(2)	-0.001(1)	-0.001(1)	0.013(1)
K4	0.013(1)	0.013(1)	0.013(1)	0.000	0.000	0.000

Table 3.72 Results of the EDX analysis of the crystal compared to the refined composition of the compound $\text{K}_{144}\text{In}_{192}\text{As}_{37}$ from the sample 'K₇In₄As₆'.

	K (at. %)	In (at. %)	As (at. %)
EDX	46(6)	48(6)	6(4)
$\text{K}_{144}\text{In}_{192}\text{As}_{37}$	38.6	51.5	9.9

Crystal Structure

Compound $K_{144}In_{192}As_{37}$ is the In-riches phases within *A-Tr-Pn* ternary systems. The unit cell of the title compound, shown in Figure 3.74, consists of interconnected $\{In_{12}\}$ icosahedra and isolated by potassium As2 atoms. Icosahedra clusters are built by In atoms in two crystallographically independent fully occupied $96g$ positions ($d_{In-In} = 3.020-3.181 \text{ \AA}$, Table 3.73), with all atoms building exo-bonds: with six As1 atoms (with very short $d_{In2-As1} = 2.400 \text{ \AA}$) and six In1 atoms ($d_{In1-In1} = 3.035 \text{ \AA}$) – Figure 3.75, a.

Isolated As2 atoms are located in the hexagonal voids formed by icosahedra network, which explains high values of both iso- and anisotropic displacement parameters, and are surrounded by twelve As1 atoms building hexagonal prism with As1-As2 distances of 4.969 \AA , which is too long to claim any kind of interactions – Figure 3.75, b).

Exo-bonded icosahedra form a three-dimensional network (Figure 3.76, a), resembling those in the *A-In* binary phases ($K_{21.33}In_{39.67}$ ^[105], $Na_7In_{11.8}$ ^[155], $Na_{15}In_{27.4}$ ^[112], $K_{39}In_{80}$ ^[110] and $K_{17}In_{41}$ ^[106]) featuring Kagome nets as in Cu-substructure of $MgCu_2$ structure type. This relation can be visualized by connecting the centers of the icosahedra as in Figure 3.3.5.3, c and c). Unlike the binary *A-In* binary phases, where other polyhedra are occupying Mg position of $MgCu_2$, for $K_{144}In_{192}As_{37}$ the voids formed within Kagome nets are filled by isolated As2 atoms. This results in Kagome nets of As atoms, forming their own As-substructure (Figure 3.3.5.3, b) again resembling Cu-substructure of $MgCu_2$ structure type. Both networks of $\{In_{12}\}$ icosahedra and As atoms are intercalating forming the anionic structure of the $K_{176}In_{192}As_{31}$.

The structurally closest relative to the compound $K_{144}In_{192}As_{37}$ is binary $K_{17}In_{41}$ ^[106], which crystallizes in the same space group with a bit smaller cell parameters. Both compounds have layered structures (Figure 3.77 a, b), that are formed by two types of layers, A and B. A-type layers consist of icosahedral $\{In_{12}\}$ clusters building Kagome nets (Figure 3.77 c, d), in case of $K_{144}In_{192}As_{37}$ additionally including As atoms centering hexagonal channels. B-type layers feature triangle nets of $\{In_{12}\}$ icosahedra for both compounds, but in case of $K_{144}In_{192}As_{37}$ icosahedra are centering hexagonal channels of the Kagome nets of As atoms (reverse to layer A Figure 3.77, e) and for $K_{17}In_{41}$ inside of triangles are In-centered $\{In_{15}\}$ clusters (Figure 3.77, f).

The cationic substructure of the $K_{144}In_{192}As_{37}$ (Figure 3.78) consists of two cages: $\{K_{20}\}$ pentagonal dodecahedron, encapsulating $\{In_{12}\}$ icosahedra, with K-In distances between 3.545 and 3.813 Å, and K2-centered $\{K_{30}\}$ polyhedra surrounding As1 and As2 atoms. The individual potassium environments of As1 and As2 two atoms are featuring $\{K_6\}$ pentagonal pyramid and $\{K_8\}$ hexagonal bipyramid, respectively. The distances of the potassium atoms in the pentagonal prism of As1 atom are $d_{K3-As1} = 3.471$ Å (pentagonal ring) and $d_{K2-As1} = 4.775$ Å. The same K2 atoms are in the same time distant vertices of the hexagonal bipyramid, surrounding As2 atoms with $d_{K2-As2} = 5.335$ Å. The distances between the K3 atoms of the hexagonal ring, centered by As2 atoms are $d_{K3-As2} = 3.914$ Å. The pyramids stacked together via K2 vertices and sharing trigonal faces are forming $\{K_{30}\}$ cage.

Table 3.73 Selected interatomic distances in $K_{144}In_{192}As_{37}$.

Atom types			Distance range(Å)			Atom types			Distance range(Å)		
In	-In	3.020(1)-3.181(1)	K	-In	3.545(3)-3.813(4)	K	-In	3.545(3)-3.813(4)	K	-As	3.405(5)-5.3349(1)
In	-As	2.400(5)	K	-As	3.405(5)-5.3349(1)	K	-As	3.405(5)-5.3349(1)	K	-K	3.958(4)-4.0357(3)
As	-As	4.969(5)	K	-K	3.958(4)-4.0357(3)	K	-K	3.958(4)-4.0357(3)			

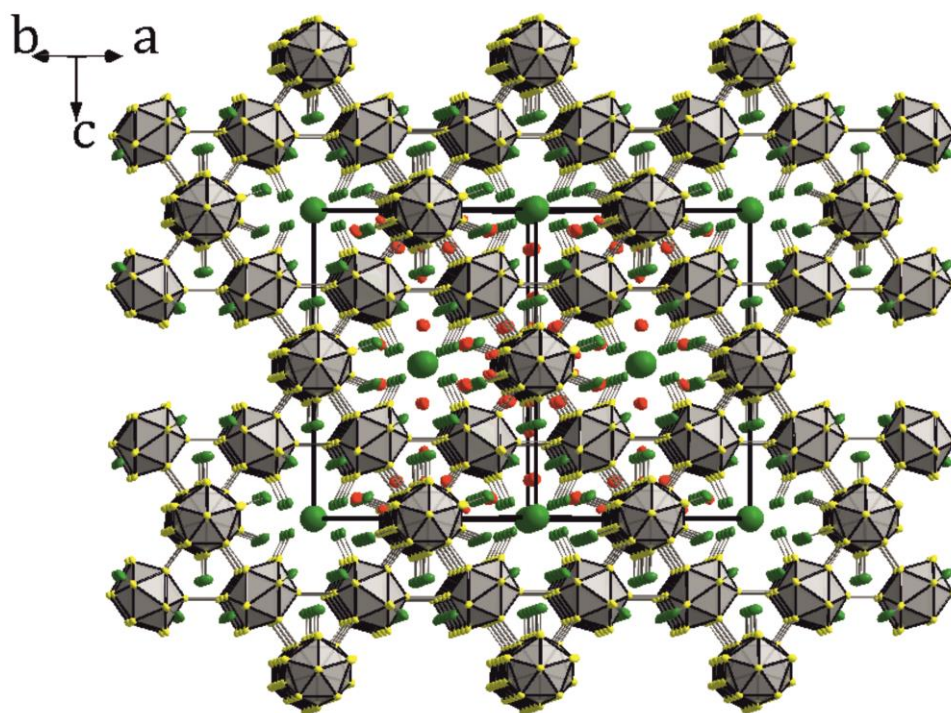
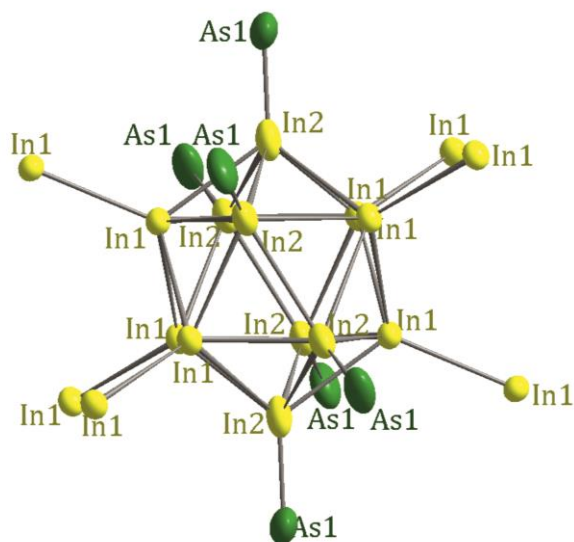


Figure 3.74 Unit cell of the $K_{144}In_{192}As_{37}$. K atoms are shown in red, In in yellow and As in green, the thermal ellipsoids are drawn with the 90% probability level.

a)



b)

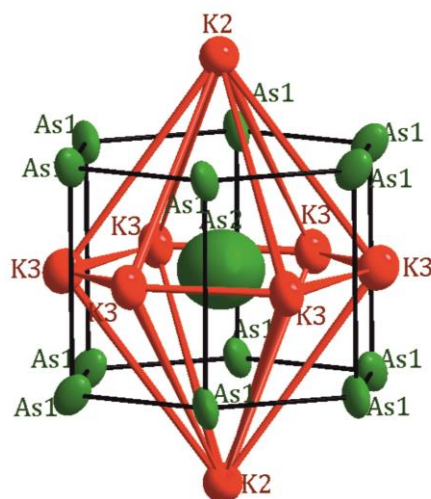


Figure 3.75 Fragments of the cationic structure of the compound $K_{144}In_{192}As_{37}$: $\{In_{12}\}$ icosahedron (a) and hexagonal prism of As1 atoms around As2 (b).

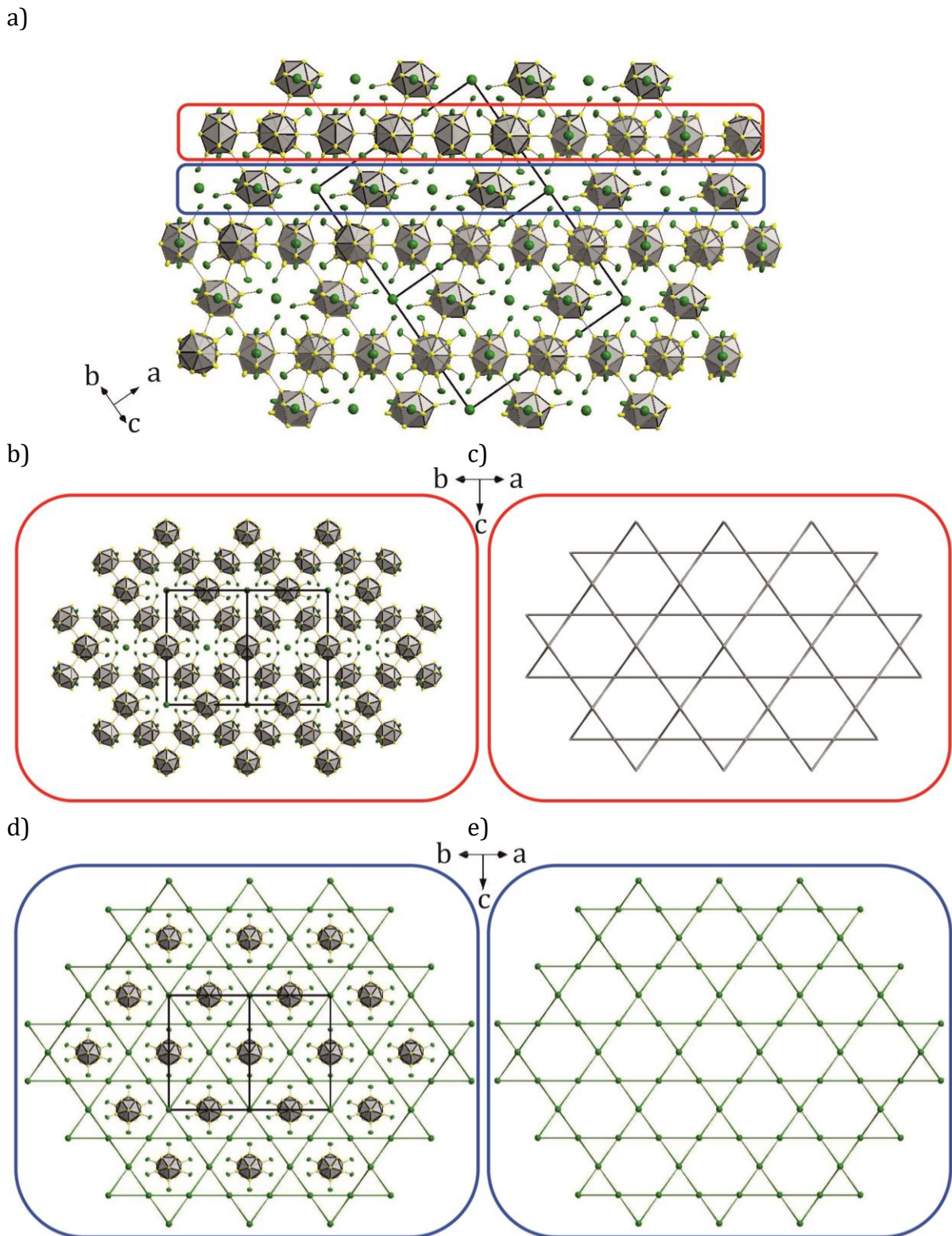


Figure 3.76 Anionic network within the structure of the $K_{144}In_{192}As_{37}$ (a); projection in $[110]$ direction of individual Kagome nets formed by $\{In_{12}\}$ icosahedra (b, c) and As-atoms (d, e).

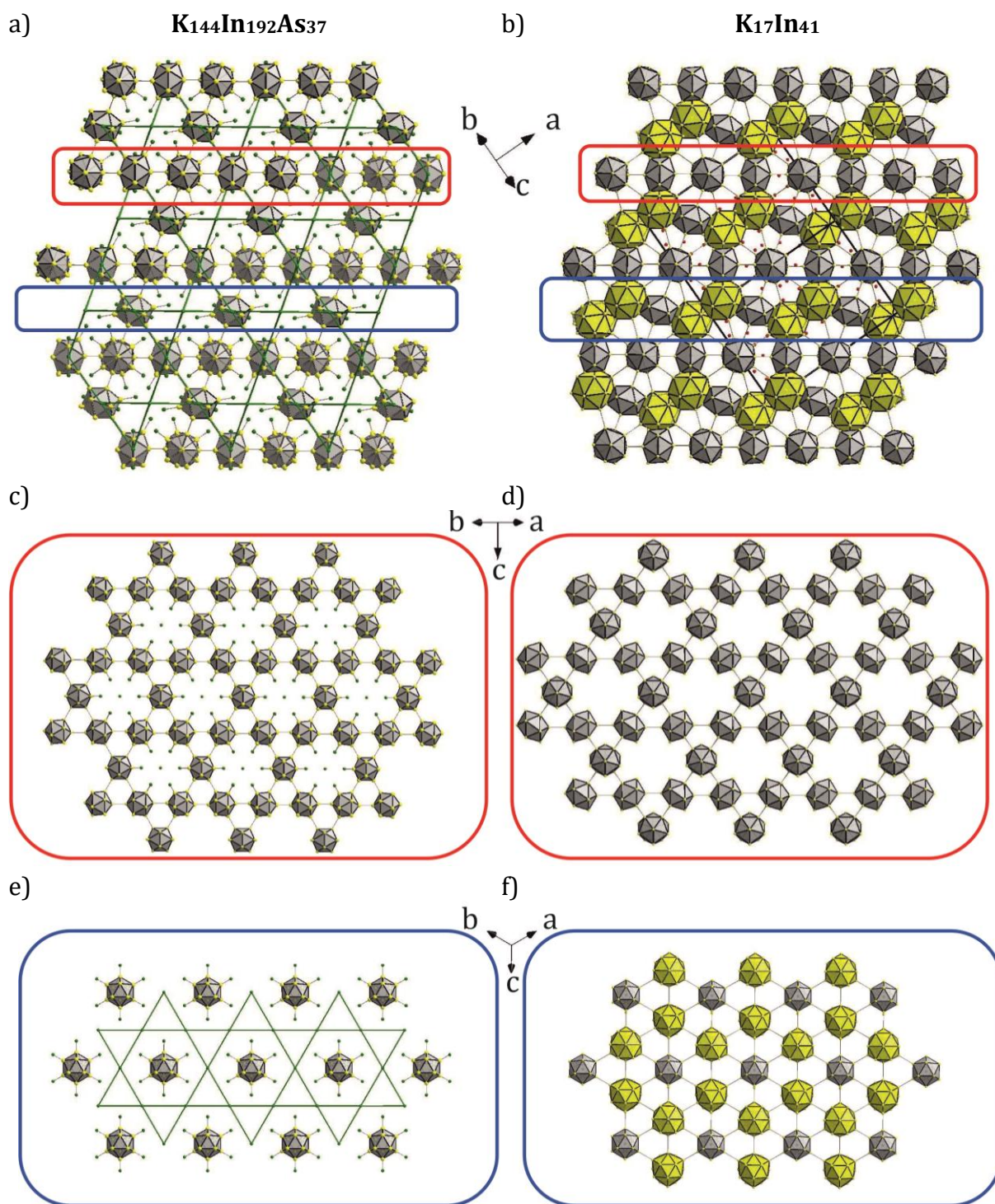


Figure 3.77 Comparison of the anionic structures of the icosahedral ternary $K_{144}In_{192}As_{37}$ (left) and binary $K_{17}In_{41}$ ^[106] (right) compounds: by two types of layers in $K_{144}In_{192}As_{37}$ (a) and $K_{17}In_{41}$ (b), A (marked in red) and B (blue). A-type layers: icosahedral $\{In_{12}\}$ clusters building Kagome nets (c, d), additionally including As atoms: exo-bonded to $\{In_{12}\}$ icosahedra and centering hexagonal channels in $K_{144}In_{192}As_{37}$. B-type layers featuring triangle nets of $\{In_{12}\}$ icosahedra for both compounds, in case of $K_{144}In_{192}As_{37}$ icosahedra have exo-bonds with As atoms and are centering hexagonal channels of the Kagome nets of As atoms (reverse to layer A), for $K_{17}In_{41}$ inside of triangles are In-centered $\{In_{15}\}$ clusters (f).

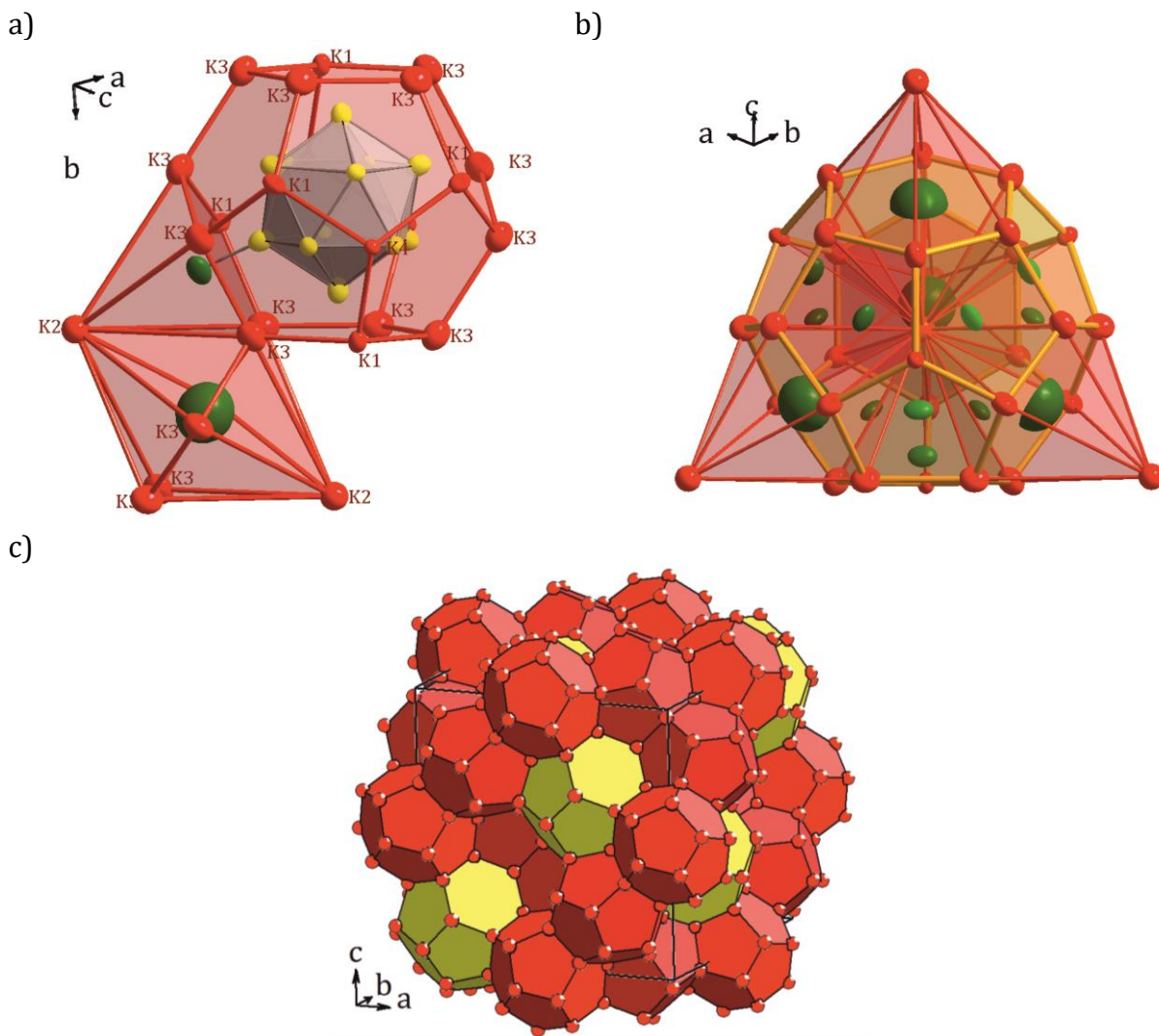


Figure 3.78 Cationic substructure of the $K_{144}In_{192}As_{37}$. $\{In_{12}\}$ icosahedra surrounded by $\{K_{26}\}$ forming a pentagonal dodecahedron, As1 atom encapsulated in $\{K_6\}$ pentagonal pyramid, whereas As2 atom – in $\{K_8\}$ hexagonal bipyramid (a), sharing trigonal faces; $\{K_{28}\}$ polyhedra around arsenic atoms (b); space filling by two types of $\{K_{20}\}$ (red) and $\{K_{30}\}$ (yellow) polyhedra.

Based on the refined empirical formula, with respect to the site occupancy factors for the As1 and As2 position the average electron count for $K_{144}In_{192}As_{37(1)}$ can be performed as follows. $\{In_{12}\}$ icosahedra as *closo* cluster with $6+6 \times 0.258 = 7.548$ exo-bonds has to be presented as $\{In_{12}\}^{-6.452}$ which, together with one-bonded As1 (As^{-2}) and isolated As2 (As^{-3}), gives us average negative charge of $6.452 \times 16 + 2 \times 0.79 \times 16 + 3 \times 0.258 \times 96 = 202.816$. With 144 K^+ atoms the structure of the $K_{144}In_{192}As_{37}$ is extremely electron-poor.

4 Summary and Conclusion

The goal of this thesis was to develop a rational approach in the syntheses of new polar intermetallic phases on the Zintl border by applying substitution effects in the binary alkali metal-tin systems. Through adding transition metal (Ag or elements of the platinum group), *p*-block metal (Bi) or completely substituting tin in the Na-Sn system by the combination of group 13 and 15 metals (Ga and Bi or In and As) new polar intermetallic phases in the respective ternary systems were obtained. All of these compounds are polar intermetallics, which belong to the class that is electronically situated in the middle, between Hume-Rothery and Zintl phases. It means that the combination of structural and bonding features from both phases are typical for these compounds. Among partial electron transfer induced by the difference in electronegativity of the elements between anionic and cationic substructures, covalent interactions can be also observed within formal anions.

All compounds were synthesized using individually optimized high temperature solid-state reactions directly from the elements or first obtaining binary precursors by pre-melting of the *d*- and *p*-metal components as well as flux synthesis. Among the standard characterization methods, like powder and single crystal XRD, EDX, DSC, and magnetometry, Raman spectroscopy was applied for the first time for the characterization of the solid-state compounds $A_{12+n}T_xSn_{17}$ containing endohedrally filled by the transition metal tin clusters $\{T@Sn_9\}$.

4.1 Na-Ag-Sn Ternary System

The systematical investigation of the Na-Ag-Sn ternary system revealed its close relation to both Na-Zn-Sn and Na-Au-Sn ternary systems but showed no similarities to Na-Cu-Sn. Introducing electron deficiency to the Na-Sn binary system through adding Ag (as it was shown in case of Zn), results in phases with structures similar to the binary (and ternary) compounds of the elements group 13, indides and gallides, with alkali metals (and transition metals), featuring different types of the icosahedral networks.

Compounds of the Na-Ag-Sn are between (almost) electron balanced phases in Na-Zn-Sn and complex polar intermetallic phases in the Na-Au-Sn. Similar to the Na-Zn-Sn system, there is an obvious correlation between the degree of reduction (alkali metal content) and the type of the atomic network in the compounds in the Na-Ag-Sn ternary system: the transition from

the compounds with an open anionic network of four bonded atoms to less reduced icosahedral phases.

Three phases, $\text{Na}_{29}\text{Ag}_{21}\text{Sn}_{39}$, $\text{Na}_{13}\text{Ag}_{5.5}\text{Sn}_{21.2}$, and $\text{Na}_{230.45}\text{Ag}_{274}\text{Sn}_{136}$, have very close Na content in the concentration triangle of the Na-Ag-Sn ternary system – Figure 4.1, a. It shows, that only by tuning Ag:Sn ratio in this row with around 32 at. % Na content, it is possible to control the structure of the outcoming compound. Compound $\text{Na}_{29}\text{Ag}_{21}\text{Sn}_{39}$ with a clearly defined anionic and cationic network is situated between $\text{Na}_{13}\text{Ag}_{5.5}\text{Sn}_{21.2}$ and $\text{Na}_{230.45}\text{Ag}_{274}\text{Sn}_{136}$, both Frank-Kasper phases.

The ability of Ag to form statistical mixtures with both Sn and Na makes it difficult to understand the chemical interactions between the components within the system, showing the similarity to the complex polar intermetallic phases in the Na-Au-Sn system.

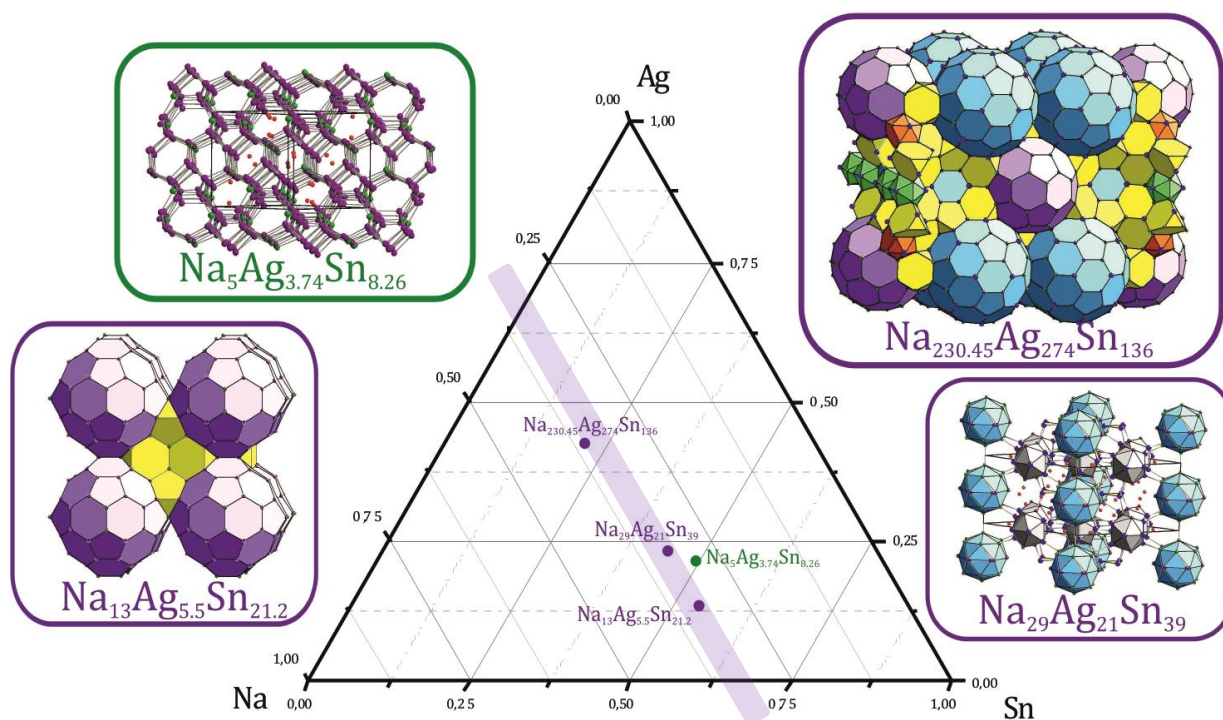
$\text{Na}_5\text{Ag}_{3.74}\text{Sn}_{8.26}$, as well as Sn-rich compounds in the Na-Sn-Bi ternary system (Figure 4.1, b) have a three-dimensional open framework structure. In case of $\text{Na}_5\text{Ag}_{3.74}\text{Sn}_{8.26}$ the atoms of the anionic substructure are exclusively four-bonded, which makes the structure related to the half-Heusler alloys, an intermediate between unfilled and stuffed diamond structures.

LMTO band structure calculations revealed the rather metallic character of the $\text{Na}_{29}\text{Ag}_{21}\text{Sn}_{39}$ and $\text{Na}_5\text{Ag}_{3.74}\text{Sn}_{8.26}$ compared to the binary Na-Sn compounds.

4.2 Compounds with Anionic Networks in the Na-Sn-Bi Ternary System

The Substitution of Sn in the Na-Sn binary system by small amounts of Bi leads to the formation of two phases, $\text{Na}_{13}\text{Sn}_{25.73}\text{Bi}_{1.27}$ and $\text{Na}_{27.4}\text{Sn}_{47.33}\text{Bi}_{0.57}$. Both compounds are almost electron balanced Zintl phases. It was established, that bismuth atoms tend to substitute tin only in positions, where atoms are two-bonded, preserving the integrity of the initial network of tin atoms, as it was observed in both $\text{Na}_{13}\text{Sn}_{25.73}\text{Bi}_{1.27}$ and $\text{Na}_{27.4}\text{Sn}_{47.33}\text{Bi}_{0.57}$ (ternary substitution variant of the binary Zintl Phase $\text{Na}_7\text{Sn}_{12}$). Alternatively, modify the structure in a way that allows cages to be formed, where Bi atoms can be encapsulated, having a formal charge of 3- – in $\text{Na}_{13}\text{Sn}_{25.73}\text{Bi}_{1.27}$.

a)



b)

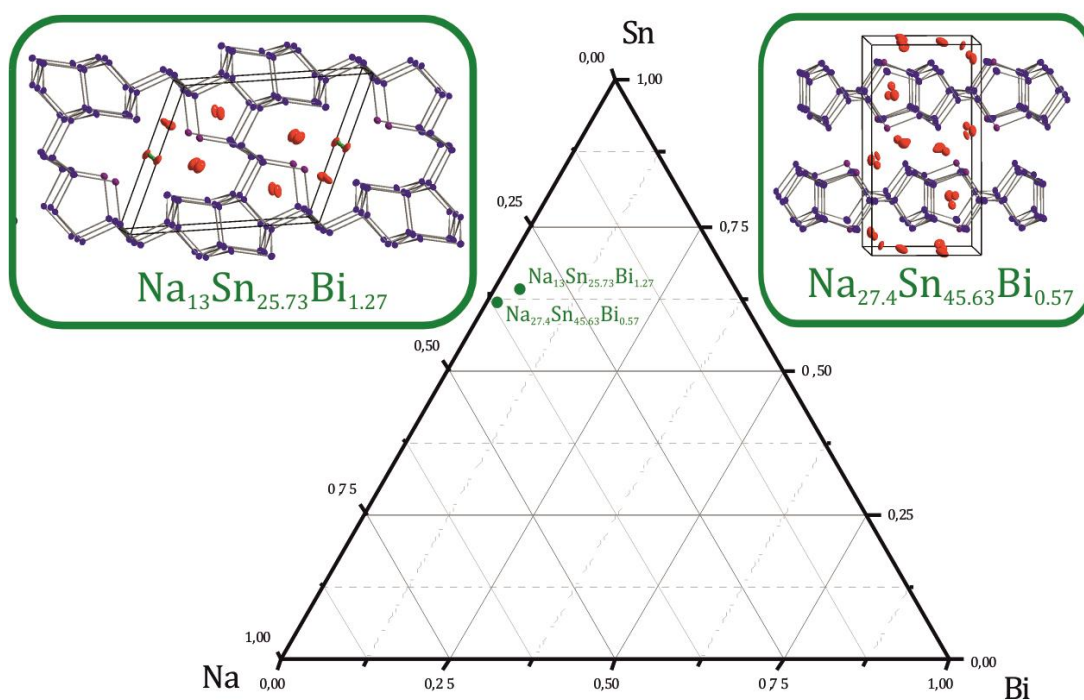


Figure 4.1 New compounds in the Na-Ag-Sn (a, for the details see Chapter 3.1.2 and 3.1.3) ternary system and tin-rich area of the Na-Sn-Bi (b, see Chapter 3.1.4) ternary systems: icosahedral $Na_{29}Ag_{21}Sn_{39}$, $Na_{13}Ag_{5.5}Sn_{21.2}$ and $Na_{230.45}Ag_{274}Sn_{136}$ (violet frame), as well as $Na_5Ag_{3.74}Sn_{8.26}$, $Na_{13}Sn_{25.73}Bi_{1.27}$ and $Na_{27.4}Sn_{45.63}Bi_{0.57}$ with the three-dimensional framework (green frame).

4.3 Endohedral Cluster Compounds in *A-T-Sn* Systems

New endohedrally filled $\{\text{Sn}_9\}^{4-}$ clusters with the elements of the platinum group were synthesized in the systems *A-T-Sn* ($A = \text{Na}, \text{K}; T = \text{Ru}, \text{Rh}, \text{Pd}, \text{Os}, \text{and Pt}$). It was possible to characterize the structure of the compounds $\text{K}_{12}\text{Pd}_{0.47}\text{Sn}_{17}$ with the single crystal diffraction experiments, which showed partial occupancy of the all four Pd atom sites between 25 and 60 %. Although no structure solution for the Ru, Rh, Os, and Pt filled clusters was possible, the XRPD measurements, EDX analysis together with Raman spectroscopy indicated the presence of the transition elements in all compounds.

Interesting is the fact that only iridium is an exception in the row of elements of the platinum group, not forming such cluster compounds.

The clusters $\{\text{Ru}@\text{Sn}_9\}^{6-}$ - $\{\text{Rh}@\text{Sn}_9\}^{5-}$ were obtained by dissolving the samples in the liquid ammonia and this indicates the possibility of using such neat solids as precursors for further modification.

4.4 New Ternary Compounds in *K-Tr-Pn* Systems

A summary of the all obtained new ternary compounds in the *A-Tt-Pn* ternary systems ($A = \text{K}; Tr = \text{Ga}, \text{In}; Pn = \text{As}, \text{Bi}$) is shown in Figure 4.2. It confirms that in the dimensionality of the compounds correlates with the alkali metal content: alkali metal rich compound $\text{K}_{20}\text{Ga}_6\text{Bi}_{13.294}$ contains 0-D isolated Bi-Bi dumbbells and $\{\text{Ga}_3\text{Bi}_6\}$ fragments, K_3InAs_2 comprises one-dimensional chains $\{\text{InAs}_2\}$, while decreasing alkali metal content leads to $\text{K}_{144}\text{In}_{192}\text{As}_{37}$ have a three-dimensional icosahedral. Alkali metals are playing the role of 'atomic scissors' within those structures.

Until now, no phases with high *Tr* content was reported, but the ratio between *Tr* and *Pn* atoms within the *A-Tt-Pn* phases also have a direct impact on the structure of the compounds: higher *Pn* content leads to formation *Pn* bridges between the tetrahedra, whereas higher *Tr* metal content results in forming *Tr-Tr* bonds and intercalated tetrahedra and more condensed systems in general. In this context, another interesting conclusion can be drawn from the results of Chapter 3.3.5. Significantly higher In content enabled the formation of the icosahedral phase $\text{K}_{144}\text{In}_{192}\text{As}_{37}$ with a complex structure, similar to the binary *A-In* compounds, additionally containing rather isolated As atoms.

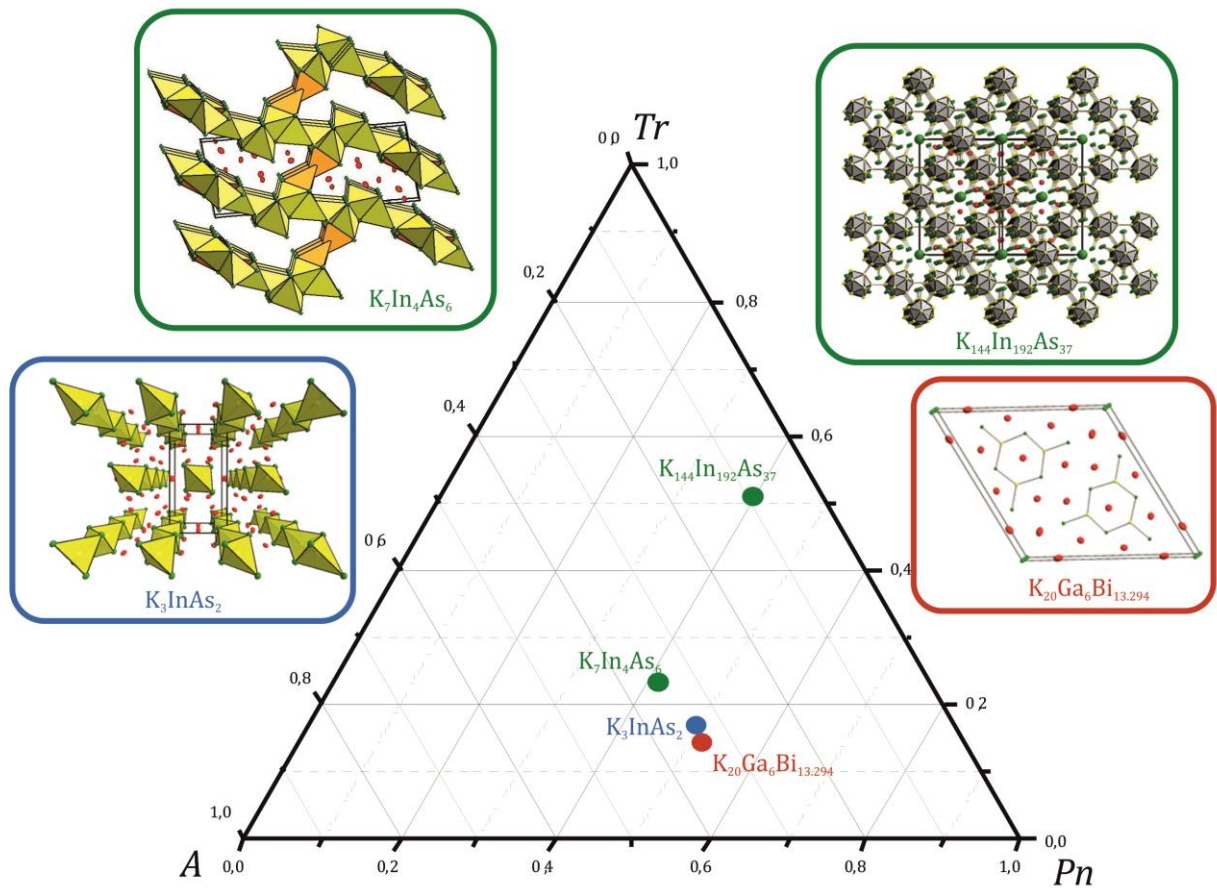


Figure 4.2 New ternary phases in the A - Tr - Pn ternary systems: $K_{20}Ga_6Bi_{13.294}$ with isolated Bi-Bi dumbbells and $\{Ga_3Bi_6\}$ fragments, K_3InAs_2 with one-dimensional chains, $K_7In_4As_6$ and $K_{144}In_{192}As_{37}$ with three-dimensional tetrahedral and icosahedral structures, respectively (for the details see Chapter 3.3.2, 3.3.3, 3.3.4 and 3.3.5).

4.5 Conclusion

The partial or full substitution as well as addition effects in the A -Sn systems ($A = \text{Na}, \text{K}$) by introducing a third component (d - or p -metal) or completely exchanging tin atoms by the combination of the p -block elements of the group 13 and 15 proved to be an incredibly efficient way of obtaining fascinating new polar intermetallic compounds. Several key principles have to be considered while trying to construct them:

- By varying the alkali metal content construction of the phases with different dimensionality is possible (compounds $\text{K}_{20}\text{Ga}_6\text{Bi}_{13.294}$, K_3InAs_2 , $\text{K}_7\text{In}_4\text{As}_6$, and $\text{K}_{144}\text{In}_{192}\text{As}_{37}$).
- The small amounts of p - or d -metals usually preserve the network of tin atoms, forming statistical mixtures and/or modifying its fragments (compounds $\text{Na}_5\text{Ag}_{3.74}\text{Sn}_{8.26}$, $\text{Na}_{13}\text{Sn}_{25.73}\text{Bi}_{1.27}$, and $\text{Na}_{27.4}\text{Sn}_{47.33}\text{Bi}_{0.57}$). Another scenario is possible for the elements of the platinum group: intercalation in the structure of the binary A -Sn, filling the cluster units ($\text{K}_{12}\text{Pd}_{0.47}\text{Sn}_{17}$).
- Increasing the content of the transition metals in the A - T -Sn systems leads away from the Zintl border, resulting in complex icosahedral structures as in quasicrystal approximants $\text{Na}_{13}\text{Ag}_{5.5}\text{Sn}_{21.2}$ and $\text{Na}_{230.45}\text{Ag}_{274}\text{Sn}_{136}$.

These principles could be applied in further attempts of the synthesis of the new polar intermetallic phases. It could be reached by going above the scope of the current work: introducing new components (e.g. d -block metals) or exploring other compositions (e.g. triel-rich area of the A - Tr - Pn phase diagrams).

5 References

- [1] A. Faghri, Y. Zhang, in *Transport Phenomena in Multiphase Systems*, Academic Press, Boston, **2006**, pp. 107-176.
- [2] A. M. Guloy, in *Inorganic Chemistry in Focus III*, Wiley, Weinheim, **2006**, pp. 157-171.
- [3] M. Nakamura, *MRS Bull.* **1995**, *20*, 33-39.
- [4] J. D. Corbett, *Inorg. Chem.* **2010**, *49*, 13-28.
- [5] W. B. Pearson, *The Crystal Chemistry and Physics of Metals and Alloys*, Wiley-Interscience, New York, **1972**.
- [6] J. K. Burdett, *Molecular shapes: Theoretical models of inorganic stereochemistry*, Wiley Interscience, New York, **1980**.
- [7] a. H. Jones, *Proc. Chem. Soc.* **1937**, *49*, 250-257; b. E. Zintl, *Angewandte Chemie* **1939**, *52*, 1-6; c. W. Klemm, E. Busmann, *Zeitschrift für anorganische und allgemeine Chemie* **1963**, *319*, 297-311; d. H. Schäfer, B. Eisenmann, W. Müller, *Angew. Chem., Int. Ed.* **1973**, *12*, 694-712; e. T. B. Massalski, U. Mizutani, *Prog. Mater. Sci.* **1978**, *22*, 151-262; f. J. Beck, *Coord. Chem. Rev.* **1997**, *163*, 55-70; g. G. A. Papoian, R. Hoffmann, *Angew. Chem., Int. Ed.* **2000**, *39*, 2408-2448; h. S. C. Sevov, J. M. Goicoechea, *Organometallics* **2006**, *25*, 5678-5692; i. S. M. Kauzlarich, S. R. Brown, J. G. Snyder, *Dalton Trans.* **2007**, 2099-2107; j. J. Köhler, M.-H. Whangbo, *Solid State Sci.* **2008**, *10*, 444-449; k. S. Scharfe, T. F. Fässler, *Philos. Trans. Royal Soc. A* **2010**, *368*, 1265-1284; l. E. S. Toberer, A. F. May, G. J. Snyder, *Chem. Mater.* **2010**, *22*, 624-634; m. J.-M. Dubois, E. Belin-Ferré, *Complex Metallic Alloys: Fundamentals and Applications*, Wiley-VCH Publishers GmbH & Co., Weinheim, Germany, **2011**; n. S. Scharfe, F. Kraus, S. Stegmaier, A. Schier, T. F. Fässler, *Angewandte Chemie International Edition* **2011**, *50*, 3630-3670; o. G. J. S. Miller, M.W.; Wang, F.; You, T.-S., in *Struct. Bond., Vol. 139* (Ed.: T. Fässler), Springer, Berlin/Heidelberg, Germany, **2011**, pp. 1-55; p. R. Nesper, *Z. Anorg. Allg. Chem.* **2014**, *640*, 2639-2648; q. U. Mizutani, H. Sato, *Crystals* **2017**, *7*, 9.
- [8] F. C. Gladisch, S. Steinberg, *Crystals* **2018**, *8*, 80.
- [9] a. W. Hume-Rothery, M. Powell Herbert, *Z. Kristallogr.* **1935**, *91*, 23; b. W. Hume-Rothery, R. W. Smallman, C. W. Haworth, *The Structure of Metals and Alloys*, Metals & Metallurgy Trust, **1969**.
- [10] D. G. Pettifor, R. W. Cahn, P. Haasen, *Physical Metallurgy*, Elsevier, Amsterdam **1983**.
- [11] L. M. Hoistad, S. Lee, *J. Am. Chem. Soc.* **1991**, *113*, 8216-8220.
- [12] a. F. Laves, H. Witte, *Metallwirtschaft* **1935**, *14*, 645-649; b. F. Laves, *Naturwiss.* **1939**, 65-73.
- [13] F. C. Frank, J. S. Kasper, *Acta Crystallogr.* **1958**, *11*, 184-190.
- [14] J. H. Westbrook, R. L. Fleischer, *Intermetallic Compounds: Structural Applications, Vol. 3*, Wiley, Chichester, United Kingdom, **2000**.
- [15] B. T. Matthias, T. Geballe, S. Geller, E. Corenzwit, *Physical Review - PHYS REV X* **1954**, *95*, 1435-1435.
- [16] J. B. Friauf, *J. Am. Chem. Soc.* **1927**, *49*, 3107-3114.
- [17] D. J. Thoma, in *Encyclopedia of Materials: Science and Technology* (Eds.: K. H. J. Buschow, R. W. Cahn, M. C. Flemings, B. Ilschner, E. J. Kramer, S. Mahajan, P. Veyssi re), Elsevier, Oxford, **2001**, pp. 4205-4213.
- [18] C. S. Barrett, T. B. Massalski, *Structure of Metals: Crystallographic Methods, Principles and Data*, Pergamon, **1980**.
- [19] J. H. Zhu, C. T. Liu, L. M. Pike, P. K. Liaw, *Intermetallics* **2002**, *10*, 579-595.
- [20] H. G. Grimm, A. Sommerfeld, *Z. Phys.* **1926**, 36-59.

- [21] a. E. Zintl, G. Brauer, *Z. Phys. Chem.* **1933**, *20B*, 245-271; b. E. Zintl, W. Dullenkopf, in *Z. Phys. Chem., Vol. 16B*, **1932**, p. 183; c. E. Zintl, S. Neumayr, in *Z. Phys. Chem., Vol. 20B*, **1933**, p. 272.
- [22] F. T. F., *Zintl Phases: Principles and Recent Developments*, Springer, Heidelberg, **2011**.
- [23] L. Pauling, *The nature of the chemical bond*, Cornell University Press, Ithaca, New York, **1960**.
- [24] E. Zintl, A. Woltersdorf, *Z. Electrochem.* **1935**, *41*, 876-879.
- [25] S. Sevov, in *Intermetallic Compounds - Principles and Practice* (Eds.: H. Westbrook, R. L. Fleischer), Wiley, Hoboken, New Jersey, United States, **2002**, pp. 113-132.
- [26] a. W. Klemm, *Proc. Chem. Soc.* **1959**, 329; b. W. Klemm, *Naturwis.* **1950**, 150-155.
- [27] E. Busmann, *Z. Anorg. Allg. Chem.* **1961**, *313*, 90-106.
- [28] K. Wade, *J. Chem. Soc.* **1971**, 792-793.
- [29] D. M. P. Mingos, *Nat. Phys. Sci.* **1972**, *236*, 99-102.
- [30] A. J. Welch, *ChemComm.* **2013**, *49*, 3615-3616.
- [31] Y. Grin, M. Baitinger, R. Kniep, H. G. Von Schnering, *Z. Kristallogr. - New Cryst. Struct.* **1999**, *214*, 453-454.
- [32] V. Quéneau, E. Todorov, S. C. Sevov, *J. Am. Chem. Soc.* **1998**, *120*, 3263-3264.
- [33] C. Hoch, M. Wendorff, C. Rohr, *Acta Crystallogr. C* **2002**, *58*, I45-I46.
- [34] A. Ugrinov, S. C. Sevov, **2003**, *17*, 373-376.
- [35] W. Blase, G. Cordier, *Z. Kristallogr.* **1991**, *194*, 150.
- [36] S. Stegmaier, T. F. Fässler, *J. Am. Chem. Soc.* **2011**, *133*, 19758-19768.
- [37] S.-J. Kim, S. D. Hoffman, T. F. Fässler, *Angew. Chem.* **2007**, *46*, 3144-3148.
- [38] D. M. Flot, M. M. Tillard-Charbonnel, C. H. E. Belin, *J. Am. Chem. Soc.* **1996**, *118*, 5229-5235.
- [39] J. D. Corbett, *Angew. Chem. Int. Ed.* **2000**, *39*, 670-690.
- [40] Q. Lin, G. J. Miller, *Acc. Chem. Res.* **2018**, *51*, 49-58.
- [41] G. J. Miller, *Eur. J. Inorg. Chem.* **1998**, *1998*, 523-536.
- [42] Stoe & Cie GmbH, Darmstadt, **2011**.
- [43] Version 1.48 ed., STOE & Cie GmbH, Darmstadt, Germany, **2008**.
- [44] Version 2.11 ed., STOE & Cie GmbH, Darmstadt, Germany, **2008**.
- [45] G. M. Sheldrick, University of Goettingen: Goettingen, Germany, **2014**.
- [46] Netzsch-Gerätebau GmbH, Selb, Germany, **2006**.
- [47] Q. D. Inc., *Vol. 1.61*, San Diego, USA, **2013**.
- [48] OriginLabCorp., 9.3.226 ed., Northampton, MA, **2018**.
- [49] G. A. Bain, J. F. Berry, *J. Chem. Educ.* **2008**, *85*, 532.
- [50] Renishaw, 4.2 build 5037 ed., **2002**.
- [51] M. v. Schilfgaarde, O. Jepsen, O. K. Andersen, A. Burkhardt, T. A. Paxton, G. Krier, Version 4.7 ed., Max-Planck-Institut für Festkörperforschung, Stuttgart (Germany), **1997**.
- [52] U. V. Barth, L. Hedin, *J. Phys. Chem. C* **1972**, *5*, 1629-1642.
- [53] O. Jepsen, O. K. Andersen, *Z. Phys. B* **1995**, *97*, 35-47.
- [54] B. Predel, in *Li-Mg - Nd-Zr* (Ed.: O. Madelung), Springer Berlin Heidelberg, Berlin, Heidelberg, **1997**, pp. 1-4.
- [55] W. Müller, K. Volk, *Z. Naturforsch. B Chem. Sci.* **1978**, 275-278.
- [56] W. Müller, K. Volk, *Z. Naturforsch. B* **1975**, 30.
- [57] Z. Du, R. A. Dunlap, M. N. Obrovac, *J. Alloys Compd.* **2014**, *617*, 271-276.
- [58] T. F. Fässler, S. Hoffmann, *Inorg. Chem.* **2003**, *42*, 5474-5476.
- [59] F. Dubois, M. Schreyer, T. F. Fässler, *Inorg. Chem.* **2005**, *44*, 477-479.
- [60] J. T. Vaughey, J. D. Corbett, *Inorg. Chem.* **1997**, *36*, 4316-4320.
- [61] T. F. Fässler, C. Kronseder, *Angew. Chem.* **1998**, *110*, 1641-1644.

- [62] S. Scharfe, F. Kraus, S. Stegmaier, A. Schier, T. F. Fässler, *Angew. Chem. Int. Ed.* **2011**, *50*, 3630-3670.
- [63] S.-J. Kim, F. Kraus, T. F. Fässler, *J. Am. Chem. Soc.* **2009**, *131*, 1469-1478.
- [64] R. Matthes, H. U. Schuster, *Z. Naturforsch., B: Chem. Sci.* **1980**, 778-780.
- [65] S. Stegmaier, T. F. Fässler, *Angew. Chem. Int. Ed.* **2012**, *51*, 2647-2650.
- [66] V. Hlukhyy, S. Stegmaier, L. van Wüllen, T. F. Fässler, *Chem. Eur. J.* **2014**, *20*, 12157-12164.
- [67] W. Thronberens, H.-D. Sinnen, H.-U. Schuster, *J. Alloys Compd.* **1980**, *76*, 99-108.
- [68] G. Wrobel, H. U. Schuster, *Z. Anorg. Allg. Chem.* **1977**, *432*, 95-100.
- [69] U. Zachwieja, *Z. Anorg. Allg. Chem.* **2001**, *627*, 353-356.
- [70] Q. Lin, V. Smetana, G. J. Miller, J. D. Corbett, *Inorg. Chem.* **2012**, *51*, 8882-8889.
- [71] W. Döring, W. Seelentag, W. Buchholz, H.-U. Schuster, in *Z. Naturforsch., B: Chem. Sci., Vol. 34*, **1979**, p. 1715.
- [72] S.-J. Kim, *PhD Dissertation: Substitution Effects in Binary Intermetallic Compounds: Investigations in the System Alkali and Alkaline-Earth Metal – Tin and Alkaline-Earth Metal – Bismuth*, Munich, **2007**.
- [73] S. Stegmaier, S.-J. Kim, A. Henze, T. F. Fässler, *J. Am. Chem. Soc.* **2013**, *135*, 10654-10663.
- [74] S. Ponou, S.-J. Kim, T. F. Fässler, *J. Am. Chem. Soc.* **2009**, *131*, 10246-10252.
- [75] S. J. Kim, T. F. Fässler, *J. Solid State Chem.* **2009**, *182*, 778-789.
- [76] E. Todorov, S. C. Sevov, *J. Am. Chem. Soc.* **1997**, *119*, 2869-2876.
- [77] G. M. Sheldrick, University of Goettingen: Goettingen, Germany, **2014**.
- [78] W. R. L. Lambrecht, O. K. Andersen, *Phys. Rev. B* **1986**, *34*, 2439-2449.
- [79] A. Henze, *PhD dissertation: Synthesis and Characterization of Lithium- and Sodium-Rich Transition-Metal Germanides and Stannides*, Munich, TUM, **2016**.
- [80] E. A. Tsukeva, E. Tsakin, S. K. Peneva, K. D. Djuneva, *Z. Kristallogr.* **1989**, *187*, 63.
- [81] C. W. Fairhurst, J. B. Cohen, *Acta Crystallogr., Sect. B: Struct. Sci.* **1972**, *28*, 371-378.
- [82] R. W. Henning, J. D. Corbett, *Z. Anorg. Allg. Chem.* **2002**, *628*, 2715-2723.
- [83] V. Smetana, G. J. Miller, J. D. Corbett, *Inorg. Chem.* **2013**, *52*, 12502-12510.
- [84] M. Tillard-Charbonnel, A. Chahine, C. Belin, in *Z. Kristallogr. Cryst. Mater., Vol. 208*, **1993**, p. 372.
- [85] M. Tillard-Charbonnel, N. Chousibi, C. Belin, *C.R. Acad. Sci., Ser. IIc: Chim.* **1992**, *315*, 661-665.
- [86] M. Tillard-Charbonnel, N. Chouaibi, C. Belin, J. Lapasset, *J. Solid State Chem.* **1992**, *100*, 220-228.
- [87] M. Tillard-Charbonnel, A. Manteghetti, C. Belin, *Inorg. Chem.* **2000**, *39*, 1684-1696.
- [88] G. Kienast, J. Verma, W. Klemm, *Z. Anorg. Allg. Chem.* **1961**, *310*, 143-169.
- [89] G. Bergman, J. L. T. Waugh, L. Pauling, *Acta Crystallogr.* **1957**, *10*, 254-259.
- [90] J. Dshemuchadse, D. Y. Jung, W. Steurer, *Acta Crystallogr., Sect. B: Struct. Sci.* **2011**, *67*, 269-292.
- [91] S. Sevov, J. Corbett, *Science* **1993**, *262*, 880-883.
- [92] S. C. Sevov, J. D. Corbett, *J. Solid State Chem.* **1996**, *123*, 344-370.
- [93] R. Nesper, *Angew. Chem., Int. Ed.* **1994**, *33*, 843-846.
- [94] C.-S. Lee, G. J. Miller, *Inorg. Chem.* **2001**, *40*, 338-345.
- [95] C. A. Guryan, P. W. Stephens, A. I. Goldman, F. W. Gayle, *Phys. Rev. B* **1988**, *37*, 8495-8498.
- [96] B. Li, J. D. Corbett, *Inorg. Chem.* **2004**, *43*, 3582-3587.
- [97] E. Todorov, S. C. Sevov, *Inorg. Chem.* **1997**, *36*, 4298-4302.
- [98] U. Frank-Cordier, G. Cordier, H. Schäfer, *Z. Naturforsch., B: Chem. Sci.* **1982**, *37*, 119.
- [99] B. Li, J. D. Corbett, *Inorg. Chem.* **2006**, *45*, 8958-8964.

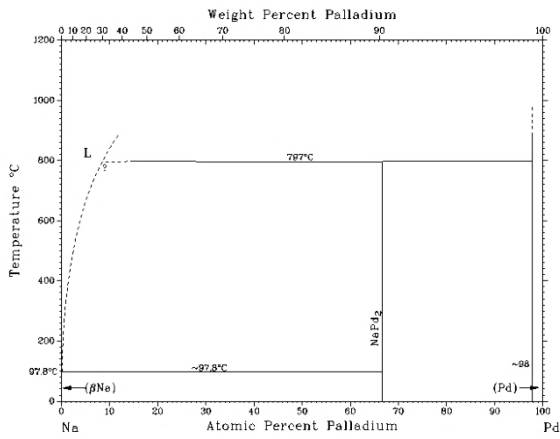
- [100] R. G. Ling, C. Belin, *Acta Crystallogr., Sect. B: Struct. Sci.* **1982**, *38*, 1101-1104.
- [101] M. Tillard-Charbonnel, C. Belin, C. N., in *Z. Kristallogr. Cryst. Mater., Vol. 206*, **1993**, p. 310.
- [102] W. Doering, W. Seelentag, W. Buchholz, H. U. Schuster, *Z. Naturforsch., B: Chem. Sci.* **1979**, *34*, 1715-1718.
- [103] M. Elding-Pontén, S. Lidin, *J. Solid State Chem.* **1995**, *115*, 270-273.
- [104] M. Tillard-Charbonnel, C. Belin, *J. Solid State Chem.* **1991**, *90*, 270-278.
- [105] G. Cordier, V. Müller, *Z. Kristallogr.* **1992**, *198*, 302-303.
- [106] G. Cordier, V. Müller, *Z. Naturforsch., B: Chem. Sci.* **1994**, *49*, 721.
- [107] G. Cordier, V. Müller, *Z. Kristallogr.* **1993**, *205*, 133.
- [108] M. Tillard-Charbonnel, C. Belin, *Mater. Res. Bull.* **1992**, *27*, 1277-1286.
- [109] M. Tillard-Charbonnel, A. Chahine, C. Belin, *Z. Kristallogr.* **1994**, *209*, 280.
- [110] B. Li, J. D. Corbett, *Inorg. Chem.* **2003**, *42*, 8768-8772.
- [111] M. Tillard-Charbonnel, A. Chahine, C. Belin, *Mater. Res. Bull.* **1993**, *28*, 1285-1294.
- [112] S. C. Sevov, J. D. Corbett, *J. Solid State Chem.* **1993**, *103*, 114-130.
- [113] T. F. Fässler, C. Kronseder, *Z. Anorg. Allg. Chem.* **1998**, *624*, 561-568.
- [114] M. Asbrand, B. Eisenmann, *Z. Naturforsch., B: Chem. Sci.* **1993**, *48*, 452.
- [115] B. Eisenmann, J. Klein, *Z. Naturforsch., B: Chem. Sci.* **1988**, *43*, 1156.
- [116] B. Eisenmann, U. Rößler, *Z. Kristallogr. - New Cryst. Struct.* **1998**, *213*, 28.
- [117] M. Asbrand, B. Eisenmann, J. Klein, *Z. Anorg. Allg. Chem.* **1995**, *621*, 576-582.
- [118] aB. Eisenmann, J. Klein, M. Somer, *Z. Kristallogr.* **1991**, *197*, 269; bJ. Klein, B. Eisenmann, *Z. Kristallogr.* **1991**, *196*, 213.
- [119] S. Ponou, *PhD Dissertation: Germanides, Germanide-Tungstate Double Salts and Substitution Effects in Zintl Phases*, TUM, Munich, **2006**.
- [120] P. Pyykkö, M. Atsumi, *Chem. Eur. J.* **2009**, *15*, 186-197.
- [121] B. Predel, in *Hg-Ho - La-Zr* (Ed.: O. Madelung), Springer Berlin Heidelberg, Berlin, Heidelberg, **1997**, pp. 1-2.
- [122] S. Miyazaki, K. Kawashima, T. Ipponjima, M. Fukuma, D. Hyakumura, J. Akimitsu, M. Yoshikawa, *J. Korean Phys. Soc.* **2013**, *63*, 475-476.
- [123] C. Hoch, M. Wendorff, C. Röhr, *Z. Anorg. Allg. Chem.* **2003**, *629*, 2391-2397.
- [124] J.-T. Zhao, J. D. Corbett, *Inorg. Chem.* **1994**, *33*, 5721-5726.
- [125] J. Gallmeier, H. Schäfer, A. Weiss, *Z. Naturforsch., B: Chem. Sci.* **1969**, *24*, 665-671.
- [126] S. Scharfe, T. F. Fassler, S. Stegmaier, S. D. Hoffmann, K. Ruhland, *Chem. Eur. J.* **2008**, *14*, 4479-4483.
- [127] V. Hlukhyy, H. He, L.-A. Jantke, T. F. Fässler, *Chem. Eur. J.* **2012**, *18*, 12000-12007.
- [128] B. Corain, G. Schmid, N. Toshima, *Metal Nanoclusters in Catalysis and Materials Science: The Issue of Size Control*, Elsevier Amsterdam, **2008**.
- [129] aB. A. Inc., Madison, Wisconsin, USA, **2012**; bB. A. Inc., Madison, Wisconsin, USA, **2012**.
- [130] B. A. Inc., Madison, Wisconsin, USA, **2001**.
- [131] G. Sheldrick, *Acta Crystallogr., Sect. C: Cryst. Struct. Commun.* **2015**, *71*, 3-8.
- [132] H. Jin, *PhD dissertation: Synthesis of intermetallic clusters in the ternary systems A-T-E (A=alkali metal; T=transition metal; E=Sn, Pb, Ge)*, TUM, Munich, **2013**.
- [133] K. Momma, F. Izumi, *J. Appl. Crystallogr.* **2011**, *44*, 1272-1276.
- [134] K. Momma, F. Izumi, *J. Appl. Crystallogr.* **2014**, *46*, 1070-1078.
- [135] B. J. L. Witzel, W. Klein, J. V. Dums, M. Boyko, T. F. Fässler, *Angew. Chem.* **2019**.
- [136] H. G. Von Schnering, M. Baitinger, U. Bolle, W. Carrillo-Cabrera, J. Curda, Y. Grin, F. Heinemann, J. Llanos, K. Peters, A. Schmeding, M. Somer, *Z. Anorg. Allg. Chem.* **1997**, *623*, 1037-1039.

- [137] M. J. Frisch, G. W. Trucks, H. B. Schlegel, G. E. Scuseria, M. A. Robb, J. R. Cheeseman, G. Scalmani, V. Barone, B. Mennucci, G. A. Petersson, H. Nakatsuji, M. Caricato, X. Li, H. P. Hratchian, A. F. Izmaylov, J. Bloino, G. Zheng, J. L. Sonnenberg, M. Hada, M. Ehara, K. Toyota, R. Fukuda, J. Hasegawa, M. Ishida, T. Nakajima, Y. Honda, O. Kitao, H. Nakai, T. Vreven, J. A. Montgomery Jr., J. E. Peralta, F. Ogliaro, M. Bearpark, J. J. Heyd, E. Brothers, K. N. Kudin, V. N. Staroverov, T. Keith, R. Kobayashi, J. Normand, K. Raghavachari, A. Rendell, J. C. Burant, S. S. Iyengar, J. Tomasi, M. Cossi, N. Rega, J. M. Millam, M. Klene, J. E. Knox, J. B. Cross, V. Bakken, C. Adamo, J. Jaramillo, R. Gomperts, R. E. Stratmann, O. Yazyev, A. J. Austin, R. Cammi, C. Pomelli, J. W. Ochterski, R. L. Martin, K. Morokuma, V. G. Zakrzewski, G. A. Voth, P. Salvador, J. J. Dannenberg, S. Dapprich, A. D. Daniels, O. Farkas, J. B. Foresman, J. V. Ortiz, J. Cioslowski, F. D. J., *Vol. Revision B.01*, Wallingford CT, **2009**.
- [138] a. D. Andrae, U. Häussermann, M. Dolg, H. Stoll, H. Preuss, *Theor. Chim. Acta* **1990**, *77*, 123; b. F. Weigend, R. Ahlrichs, *Phys. Chem. Chem. Phys.* **2005**, *7*, 3297-3305.
- [139] B. Metz, H. Stoll, M. Dolg, *J. Chem. Phys.* **2000**, *113*, 2563.
- [140] V. Barone, M. Cossi, *J. Phys. Chem. A* **1998**, *102*, 1995-2001.
- [141] Jmol: an open-source Java viewer for chemical structures in 3D. <http://www.jmol.org/>
- [142] a. G. Knizia, J. E. M. N. Klein, *Angew. Chem.* **2015**, *127*, 5609-5613; b. G. Knizia, J. E. M. N. Klein, *Angew. Chem., Int. Ed.* **2015**, *54*, 5518.
- [143] M. L. Laury, M. J. Carlson, A. K. Wilson, *J. Comput. Chem.* **2012**, *33*, 2380-2387.
- [144] S. Bobev, S. C. Sevov, *Inorg. Chem.* **1999**, *38*, 2672-2675.
- [145] V. G. Tissen, V. F. Degtyareva, M. V. Nefedova, E. G. Ponyatovskii, W. B. Holzapfel, *J. Phys. Condens. Matter* **1998**, *10*, 7303-7308.
- [146] L. Xu, S. C. Sevov, *Inorg. Chem.* **2000**, *39*, 5383-5389.
- [147] S. Bobev, S. C. Sevov, *J. Solid State Chem.* **2002**, *163*, 436-448.
- [148] G. Bruzzone, *Acta Crystallogr., Sect. B: Struct. Sci.* **1969**, *25*, 1206-1207.
- [149] a. R. W. Henning, J. D. Corbett, *Inorg. Chem.* **1997**, *36*, 6045-6049; b. G. Cordier, V. Müller, *Z. Kristallogr.* **1993**, *203*, 154.
- [150] a. R. W. Henning, J. D. Corbett, *Inorganic Chemistry* **1999**, *38*, 3883-3888; b. G. Cordier, V. Müller, *Z. Kristallogr.* **1993**, *203*, 150; c. S. P. Yatsenko, K. A. Tschuntonow, A. N. Orlov, Y. P. Yarmolyuk, Y. N. Hryn, *J. Alloys Compd.* **1985**, *108*, 339-343.
- [151] a. J. H. N. Van Vucht, *J. Alloys Compd.* **1985**, *108*, 163-175; b. R. G. Ling, C. Belin, *Z. Anorg. Allg. Chem.* **1981**, *480*, 181-185; c. K. A. Tschuntonow, S. P. Yatsenko, Y. N. Hryn, Y. P. Yarmolyuk, A. N. Orlov, *J. Alloys Compd.* **1984**, *99*, 15-21.
- [152] U. Frank-Cordier, G. Cordier, H. Schäfer, *Z. Naturforsch., B: Chem. Sci.* **1982**, *37*, 127.
- [153] C. Belin, *Acta Crystallogr., Sect. B: Struct. Sci.* **1980**, *36*, 1339-1343.
- [154] C. Belin, *Acta Crystallogr., Sect. B: Struct. Sci.* **1981**, *37*, 2060-2062.
- [155] S. C. Sevov, J. D. Corbett, *Inorg. Chem.* **1992**, *31*, 1895-1901.
- [156] a. G. Brauer, E. Zintl, in *Z. Phys. Chem., Vol. 37B*, **1937**, p. 323; b. H. Kerber, H. J. Deiseroth, R. Walther, *Z. Kristallogr. - New Cryst. Struct.* **1998**, *213*, 501; c. K. A. Chuntonov, S. P. Yatsenko, A. N. Kuznetsov, S. I. Alyamovskii, K. K. Abrashev, *Sov. Phys. - Crystallogr.* **1977**, *367*; d. E. D. Sands, H. D. Woods, J. W. Ramsey, *Acta Crystallogr.* **1963**, *16*, 316-316; e. G. Gnutzmann, F. Wilhelm Dorn, W. Klemm, *Z. Anorg. Allg. Chem.* **1961**, *309*, 210-225.
- [157] F. Gascoin, S. C. Sevov, *J. Am. Chem. Soc.* **2000**, *122*, 10251-10252.
- [158] F. Gascoin, S. C. Sevov, *Inorg. Chem.* **2001**, *40*, 5177-5181.
- [159] F. Emmerling, C. Röhr, *Z. Naturforsch., B: Chem. Sci.* **2002**, *57*, 963.
- [160] S. Burtzclaff, M. Hołyńska, S. Dehnen, *Z. Anorg. Allg. Chem.* **2010**, *636*, 1691-1693.

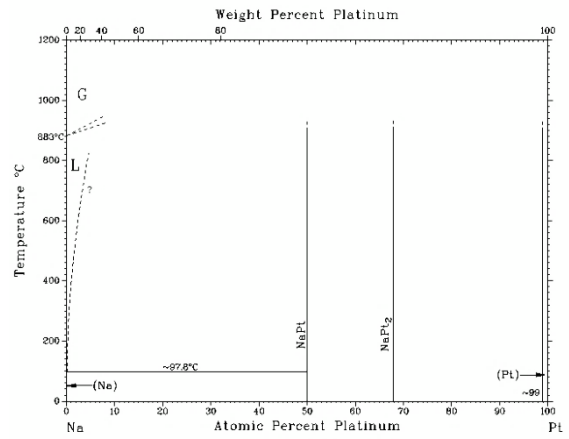
- [161] F. Emmerling, N. Längin, D. Petri, M. Kroeker, C. Röhr Prof. Dr.-Ing, *Z. Anorg. Allg. Chem.* **2004**, *630*, 171-178.
- [162] W. Höhle, G. Krogull, K. Peters, H. G. v. Schnering, *Z. Kristallogr. - New Cryst. Struct.* **1999**, *214*, 17.
- [163] W. Höhle, J. Buresch, K. Peters, J. H. Chang, H. G. v. Schnering, *Z. Kristallogr. - New Cryst. Struct.* **2002**, *217*, 487.
- [164] T. Hanauer, N. Korber, *Z. Anorg. Allg. Chem.* **2006**, *632*, 1135-1140.
- [165] B. Predel, in *B-Ba - C-Zr* (Ed.: O. Madelung), Springer Berlin Heidelberg, Berlin, Heidelberg, **1992**, pp. 1-1.
- [166] B. Predel, in *Ac-Ag ... Au-Zr: Supplement to Subvolume IV/5A* (Ed.: B. Predel), Springer Berlin Heidelberg, Berlin, Heidelberg, **2006**, pp. 1-2.
- [167] S. Massidda, A. Continenza, A. J. Freeman, d. Pascale Tm, F. Meloni, M. Serra, *Phys. Rev. B: Condens. Matter* **1990**, *41*, 12079-12085.
- [168] J. Beister Heinz, K. Syassen, J. Klein, *Z. Naturforsch., B: Chem. Sci.* **1990**, *45*, 1388.
- [169] Y. K. Vohra, S. T. Weir, A. L. Ruoff, *Phys. Rev. B* **1985**, *31*, 7344-7348.
- [170] L. Chi, J. D. Corbett, *Inorg. Chem.* **2001**, *40*, 2705-2708.
- [171] a. W. Blase, G. Cordier, *Z. Kristallogr.* **1993**, *206*, 143; b. W. Blase, G. Cordier, *Z. Kristallogr.* **1993**, *206*, 145.
- [172] a. W. Blase, G. Cordier, M. Somer, *Z. Kristallogr.* **1993**, *206*, 141; b. W. Blase, G. Cordier, M. Somer, *Z. Kristallogr.* **1991**, *195*, 121.
- [173] G. Cordier, W. Blase, *Z. Kristallogr.* **1992**, *199*, 277.
- [174] M. Somer, D. Thiery, M. Hartweg, L. Walz, K. Peters, H. G. v. Schnering, *Z. Kristallogr.* **1990**, *193*, 287.
- [175] M. Somer, K. Peters, D. Thiery, H. G. v. Schnering, *Z. Kristallogr.* **1990**, *192*, 271.
- [176] M. Somer, K. Peters, T. Popp, H. G. v. Schnering, *Z. Kristallogr.* **1990**, *192*, 273.
- [177] G. Cordier, H. Ochmann, *Z. Naturforsch., B: Chem. Sci.* **1990**, *45*, 277.
- [178] W. Blase, G. Cordier, M. Somer, *Z. Kristallogr.* **1991**, *195*, 115.
- [179] a. G. Cordier, H. Ochmann, *Z. Kristallogr.* **1991**, *195*, 111; b. G. Cordier, H. Ochmann, *Z. Kristallogr.* **1991**, *195*, 113.
- [180] a. G. Cordier, H. Ochmann, H. Schäfer, *J. Alloys Compd.* **1986**, *119*, 291-296; b. G. Cordier, H. Ochmann, *Z. Kristallogr.* **1991**, *195*, 125; c. G. Cordier, H. Ochmann, *Z. Kristallogr.* **1991**, *195*, 310.
- [181] B. Li, L. Chi, J. D. Corbett, *Inorg. Chem.* **2003**, *42*, 3036-3042.
- [182] W. Blase, G. Cordier, M. Somer, *Z. Kristallogr.* **1991**, *195*, 109.
- [183] a. M. Somer, W. Carrillo-Cabrera, E. M. Peters, K. Peters, H. G. Von Schnering, *Z. Kristallogr. - New Cryst. Struct.* **1998**, *213*, 5-6; b. W. Blase, G. Cordier, M. Somer, *Z. Kristallogr.* **1991**, *195*, 123.
- [184] F. Gascoin, S. C. Sevov, *Inorg. Chem.* **2001**, *40*, 6254-6257.
- [185] F. Gascoin, S. C. Sevov, *Angew. Chem., Int. Ed.* **2002**, *41*, 1232-1234.
- [186] G. Cordier, H. Ochmann, *Z. Kristallogr.* **1991**, *197*, 291.
- [187] G. Cordier, H. Ochmann, *Z. Kristallogr.* **1991**, *197*, 295.
- [188] T. L. T. Birdwhistell, E. D. Stevens, C. J. O'Connor, *Inorg. Chem.* **1990**, *29*, 3892-3894.
- [189] a. G. Cordier, H. Ochmann, *Z. Kristallogr.* **1991**, *197*, 293; b. T. Birdwhistell, C. Klein, T. Jeffries, E. Stevens, C. O'Connor, *J. Mater. Chem.* **1991**, *1*, 555-558.
- [190] G. Cordier, H. Ochmann, *Z. Kristallogr.* **1991**, *197*, 287.
- [191] G. Cordier, H. Ochmann, *Z. Kristallogr.* **1991**, *197*, 289.
- [192] O. Gourdon, F. Boucher, J. Gareh, M. Evain, C. Oconnor, J.-S. Jung, *Acta Crystallogr., Sect. C: Cryst. Struct. Commun.* **1996**, *52*, 2963-2964.
- [193] G. Cordier, O. H., *Z. Kristallogr.* **1991**, *197*, 297.
- [194] G. Cordier, H. Ochmann, H. Schafer, *Mater. Res. Bull.* **1986**, *21*, 331-336.

- [195] a. W. Blase, G. Cordier, M. Somer, *Z. Kristallogr.* **1991**, 195, 119; b. G. Cordier, H. Ochmann, *Z. Kristallogr.* **1991**, 195, 105; c. G. Cordier, H. Ochmann, *Z. Kristallogr.* **1991**, 195, 107.
- [196] G. Cordier, H. Ochmann, *Z. Kristallogr.* **1991**, 195, 306.
- [197] G. Cordier, H. Ochmann, *Z. Kristallogr.* **1991**, 197, 285.
- [198] W. Blase, G. Cordier, *Z. Kristallogr.* **1991**, 195, 117.
- [199] W. Blase, G. Cordier, *Z. Kristallogr.* **1995**, 210, 60.
- [200] W. Setyawan, S. Curtarolo, *Comput. Mater. Sci.* **2010**, 49, 299-312.
- [201] a. M. I. Aroyo, D. Orobengoa, G. de la Flor, E. S. Tasci, J. M. Perez-Mato, H. Wondratschek, *Acta Crystallogr., Sect. A: Found. Crystallogr.* **2014**, 70, 126-137; b. E. S. Tasci, G. de la Flor, D. Orobengoa, C. Capillas, J. M. Perez-Mato, M. I. Aroyo, *EPJ Web Conf.* **2012**, 22, 00009.
- [202] G. Cordier, H. Ochmann, *Z. Naturforsch., B: Chem. Sci.* **1989**, 43b, 1538-1540.
- [203] J. Peters, B. Krebs, *Acta Crystallogr., Sect. B: Struct. Sci.* **1982**, 38, 1270-1272.
- [204] A. D. Pelton, *Bull. All. Ph. Diagr.* **1986**, 7, 133-136.
- [205] C. S. G. T. E. (SGTE), *Bull. All. Ph. Diagr.* **1987**, 8, 401-402.
- [206] B. Predel, in *B-Ba - C-Zr* (Ed.: O. Madelung), Springer Berlin Heidelberg, Berlin, Heidelberg, **1992**, pp. 1-3.
- [207] H. Okamoto, *J. Phase Equilib.* **2012**, 33.
- [208] B. Predel, in *Li-Mg - Nd-Zr* (Ed.: O. Madelung), Springer Berlin Heidelberg, Berlin, Heidelberg, **1997**, pp. 1-1.
- [209] B. Predel, in *Li-Mg - Nd-Zr* (Ed.: O. Madelung), Springer Berlin Heidelberg, Berlin, Heidelberg, **1997**, pp. 1-1.
- [210] B. Predel, in *Pu-Re - Zn-Zr* (Ed.: O. Madelung), Springer Berlin Heidelberg, Berlin, Heidelberg, **1998**, pp. 1-2.
- [211] B. Predel, in *Pu-Re - Zn-Zr* (Ed.: O. Madelung), Springer Berlin Heidelberg, Berlin, Heidelberg, **1998**, pp. 1-2.
- [212] F. Predel, in *Phase Equilibria, Crystallographic and Thermodynamic Data of Binary Alloys: K-O ... Y-Zr* (Ed.: F. Predel), Springer Berlin Heidelberg, Berlin, Heidelberg, **2016**, pp. 170-173.
- [213] H. Okamoto, *J. Phase Equilib.* **1996**, 17, 463-463.
- [214] B. Predel, in *Dy - Er ... Ir - Y: Supplement to Subvolumes IV/5B, IV/5C and IV/5D* (Ed.: B. Predel), Springer Berlin Heidelberg, Berlin, Heidelberg, **2013**, pp. 89-89.
- [215] B. Predel, in *B - Ba ... Cu - Zr: Supplement to Subvolumes IV/5B, IV/5C and IV/5D* (Ed.: B. Predel), Springer Berlin Heidelberg, Berlin, Heidelberg, **2012**, pp. 111-112.
- [216] B. Predel, in *Ac-Ag ... Au-Zr: Supplement to Subvolume IV/5A* (Ed.: B. Predel), Springer Berlin Heidelberg, Berlin, Heidelberg, **2006**, pp. 1-2.
- [217] B. Predel, in *Hg-Ho - La-Zr* (Ed.: O. Madelung), Springer Berlin Heidelberg, Berlin, Heidelberg, **1997**, pp. 1-4.

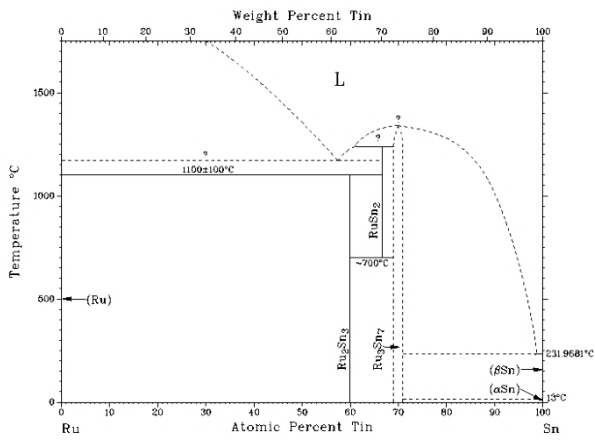
a)



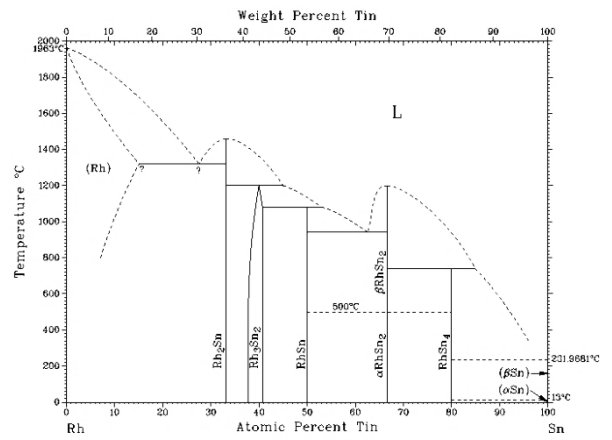
b)



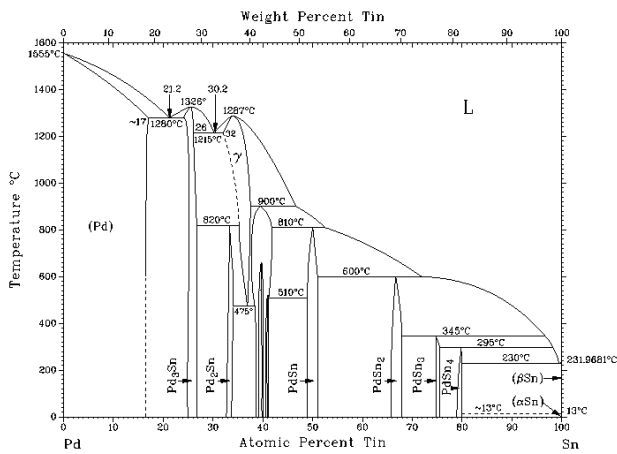
c)



d)



e)



f)

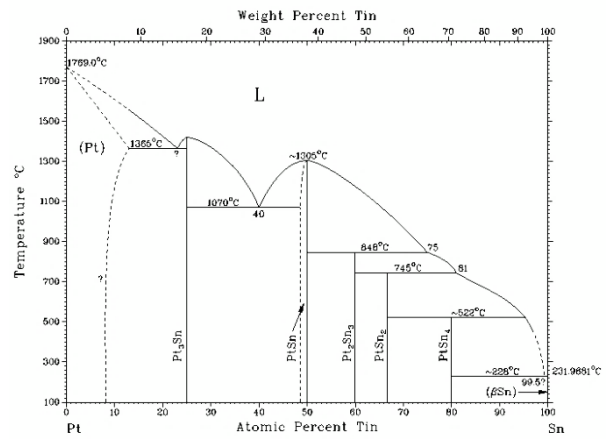


Figure 6.2 Phase diagram of the Na-Pd^[208] (a), Na-Pt^[209] (b), Ru-Sn^[210] (c), Rh-Sn^[211](d), Pd-Sn^[212](e) and Pt-Sn^[213](f) binary systems.

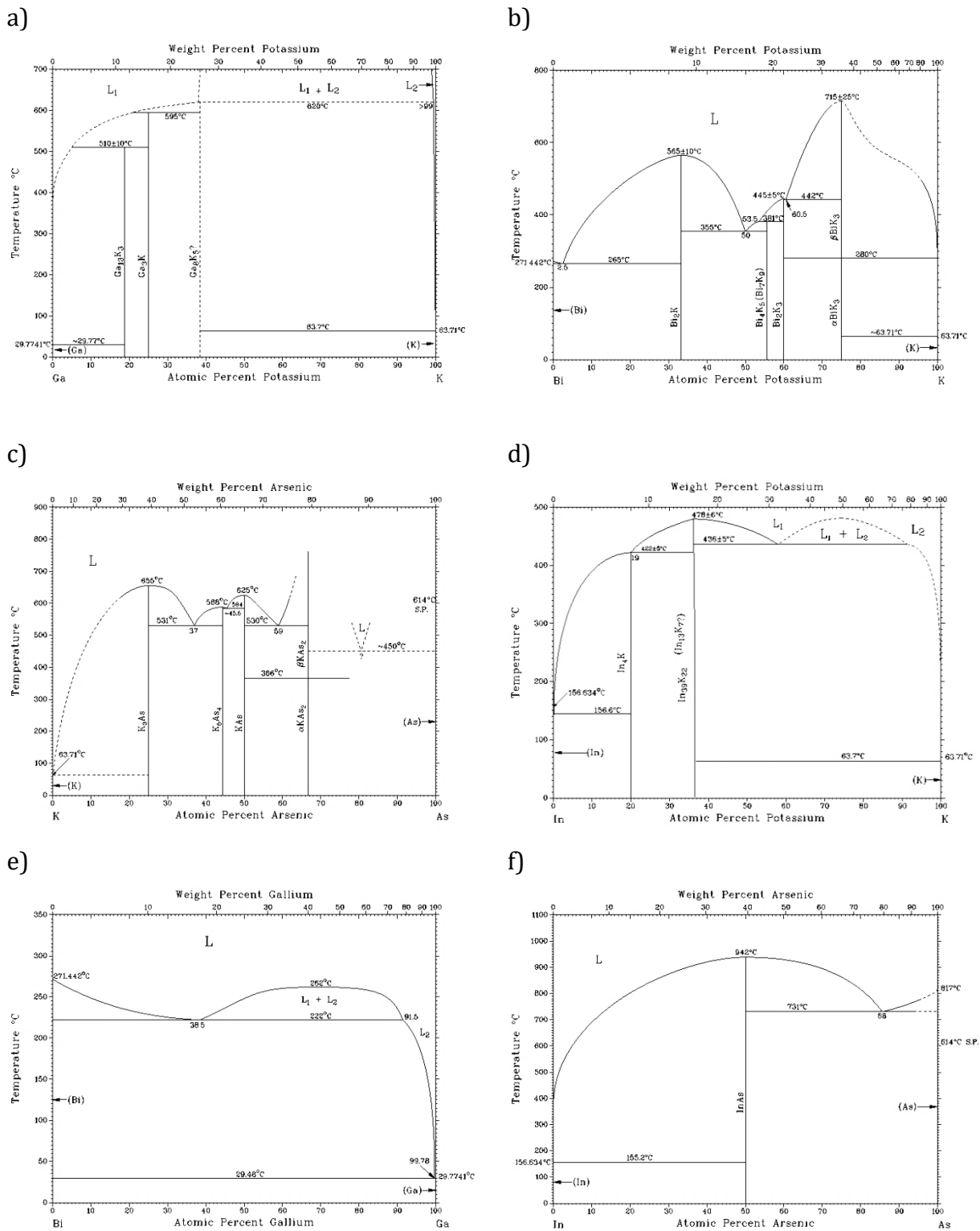


Figure 6.3 Phase diagram of the K-Ga^[214] (a), K-Bi^[215] (b), K-As^[216] (c), K-In^[217] (d), Bi-Ga^[165] (e) and In-As^[166] (f) binary systems.

Table 6.1 Interatomic distances in the Na₂₉Ag₂₁₍₁₎Sn₃₉₍₁₎.

Atom types		Distance (Å)	Atom types		Distance (Å)
Sn-Sn, Sn-Ag, Ag-Ag					
Ag1	Ag1	2.8612(3)	Ag2	2× M4	2.7254(2)
	6× Ag2	3.1162(1)		2× Ag2	2.8830(8)
Sn1	2× M5	2.8500(7)	Sn3	Sn3	2.8957(1)
	2× Sn1	2.9864(1)		Ag1	3.1162(1)
Sn3	Ag2	2.8957(1)	Sn2	Sn2	2.7727(1)
	2× Sn2	2.9119(6)		2× Sn2	2.8662(1)
	M5	2.9986(7)		2× Sn3	2.9119(6)
	M5	2.9987(8)		2× M5	2.9488(8)
	Sn3	3.1123(8)	M4	2× Ag2	2.7254(1)
M5	2.8493(8)	2× Ag2		2.9739(2)	
M5	Sn1	2.8500(7)			
	2× Sn2	2.9488(8)			
	Sn3	2.9986(7)			
	Sn3	2.9987(8)			
	Na-Sn, Na-Ag, Na-Na				
Na1	2× M5	3.2838(1)	Na2	2× Ag1	3.4387(2)
	M5	3.2852(1)		6× M4	3.4589(3)
	2× Sn2	3.3734(4)		12× Ag2	3.6607(1)
	2× Sn2	3.3741(4)	Na4	4× Ag2	3.8293(6)
	2× Sn2	3.3748(4)		4× Sn3	3.2140(2)
	2× Sn1	3.4739(6)		2× Sn2	3.3922(5)
	Sn1	3.4746(6)		2× Na4	3.4548(7)
	Na3	3.5089(5)	2× Na3	3.6890(9)	
	2× Na3	3.5103(5)	Na5	2× Sn3	3.3617(1)
	Na1	3.7065(9)		2× M4	3.3927(6)
Na3	M4	3.1791(4)		4× M5	3.3983(4)
	M5	3.3209(5)		2× Sn1	3.4997(4)
	M5	3.3210(2)		2× Na3	3.6795(3)
	Sn3	3.3236(3)		2× Na3	3.6798(3)
	Sn3	3.3239(4)		Na5	3.8276(9)
	Sn2	3.3796(4)			
	Sn2	3.3797(4)			
	2× Sn1	3.4639(5)			
	Na1	3.5103(5)			
	Na5	3.6795(4)			
Na4	3.6798(5)				

Table 6.2 Interatomic distances in the Na₁₃Ag_{5.5(5)}Sn_{21.2(5)}. *M* = Sn/Ag statistical mixture.

Atom types		Distance (Å)	Atom types		Distance (Å)
Sn-Sn, Sn-Ag, Ag-Ag					
Sn1	<i>M3</i>	2.7784(5)	<i>M2</i>	<i>M3</i>	2.8407(4)
	Sn1	2.9128(5)		<i>M3</i>	2.9111(4)
	4× Sn1	2.9331(3)		<i>M2</i>	2.9150(5)
<i>M3</i>	Sn1	2.7784(5)		2× <i>M2</i>	2.9704(5)
	2× <i>M2</i>	2.8407(4)		Ag4	3.1739(5)
	2× <i>M2</i>	2.9111(4)		Ag4	2.9875(9)
	Ag4	3.2305(7)		4× <i>M2</i>	3.1739(5)
			2× <i>M3</i>	3.2305(4)	
Na-Sn, Na-Ag, Na-Na					
Na1	Ag4	3.188(3)	Na2	Na2	3.3054(2)
	2× Na3	3.266(1)		3× Sn1	3.311(1)
	4× <i>M2</i>	3.309(1)		3× <i>M2</i>	3.380(1)
	4× <i>M2</i>	3.3547(6)		3× <i>M2</i>	3.408(1)
	2× Ag4	3.410(2)		3× <i>M3</i>	3.474 (1)
	2× <i>M3</i>	3.491(1)			
Na3	Na1	3.266(3)			
	2× Sn1	3.308(2)			
	Sn1	3.332(2)			
	2× <i>M3</i>	3.340(1)			
	2× <i>M2</i>	3.387(2)			
	2× <i>M2</i>	3.390(1)			
	<i>M3</i>	3.564(2)			
	Na3	3.597 (3)			
2× Na2	3.618(2)				

Table 6.3 Interatomic distances in the Na_{230.45}Ag₂₇₄Sn₁₃₆. *M* = Sn/Ag, *N* = Ag/Na statistical mixtures.

Atom types		Distance (Å)	Atom types		Distance (Å)	
Sn-Sn, Sn-Ag, Ag-Ag, M-Sn, M-Ag, M-M, N-Sn, N-Ag, N-M, N-N						
Sn1	2× Ag14	2.751(1)	Sn2	Ag17	2.865(1)	
	2× Sn/Ag35	2.7611(7)		Ag19	2.883(3)	
Sn3	2× Ag8	2.7420(9)		<i>M</i> 30	2.949(1)	
	2× Ag9	2.7653(7)		2× <i>M</i> 29	2.9605(7)	
	2× Na8	3.291(3)		2× <i>M</i> 36	2.9928(7)	
Sn5	Ag7	2.730(1)		Ag20	2.998(5)	
	Ag10	2.7336(8)		Sn4	Ag11	2.7361(8)
	<i>M</i> 36	2.7782(6)			Ag2	2.7698(8)
	<i>M</i> 29	2.789(1)			Ag3	2.8182(7)
Sn7	2× Ag13	2.742(1)			Ag18	3.2166(7)
Sn7	2× <i>M</i> 32	2.7954(9)	Sn6	Ag4	2.7148(8)	
	Sn9	2× Ag12		2.7534(5)	2× Ag5	2.8031(5)
Sn9	<i>M</i> 30	2.781(1)		2× Ag7	2.811(1)	
	2× Ag2	2.799(1)		Ag8	2.8114(8)	
	Sn11	<i>M</i> 33		2.716(1)	Ag6	2.9848(8)
2× Ag12		2.7978(6)	Sn8	Ag5	2.7408(7)	
2× Ag10		2.8202(8)		Ag3	2.7477(9)	
Ag13		2.840(1)		Ag15	2.7693(8)	
Ag16		2.997(1)		<i>M</i> 34	2.793(1)	
Ag1	2× Ag14	2.7732(9)		<i>N</i> 38	3.2253(8)	
	4× Ag15	2.8275(6)	Sn10	Ag1	2.8821(9)	
	2× Sn10	2.8821(9)		Ag14	2.8916(9)	
	2× Ag9	2.958(1)		2× Ag15	2.9256(7)	
	2× <i>N</i> 37	3.113(1)		2× Ag9	2.9611(7)	
Ag3	Sn8	2.7477(9)	Sn12	Ag26	2.798(4)	
	Sn4	2.8182(7)		Ag17	2.9003(6)	
	Ag3	2.905(1)		<i>M</i> 36	2.9777(7)	
	Ag2	2.9198(7)		<i>M</i> 35	2.9816(6)	
	Ag5	2.9228(8)		<i>M</i> 34	2.983(1)	
Ag5	Sn8	2.7408(7)		<i>M</i> 32	2.9876(7)	
	Sn6	2.8031(5)		<i>M</i> 29	3.003(1)	
	Ag8	2.9203(7)		Ag2	Sn4	2.7698(8)
	Ag3	2.9228(8)	Sn9		2.799(1)	
	Ag7	2.923(1)	Ag2		2.8733(6)	
Ag7	Sn5	2.730(1)	Ag12		2.911(1)	
	Sn6	2.811(1)	Ag3		2.9198(7)	
	Ag7	2.9092(6)	Ag18	3.1084(8)		
	Ag10	2.9197(7)	Ag4	Sn6	2.7148(8)	
	Ag5	2.923(1)		Ag21	2.7579(6)	
	Ag6	2.9908(7)		2× <i>M</i> 33	2.8934(6)	
Ag9	Sn3	2.7653(7)		Ag4	2.898(1)	
	Ag9	2.9099(7)	2× Ag11	2.9062(7)		
	Ag1	2.958(1)	Ag6	<i>M</i> 31	2.7518(8)	
	2× Sn10	2.9611(7)		Sn6	2.9848(8)	

	2× Ag15	2.9660(8)		Ag8	2.991(1)	
Ag11	Sn4	2.7361(8)		2× Ag7	2.9908(7)	
	Ag21	2.7734(6)		2× Ag5	3.0012(7)	
	2× M33	2.9008(7)	Ag8	Sn3	2.7420(9)	
	2× Ag4	2.9062(7)		Sn6	2.8114(8)	
	Ag11	2.9198(7)		Ag8	2.914(1)	
Ag13	Sn7	2.742(1)		2× Ag5	2.9203(7)	
	Sn11	2.840(1)		Ag6	2.991(1)	
	2× Ag10	2.9050(7)	Ag10	Sn5	2.7336(8)	
	Ag13	2.9052(9)		Sn11	2.8202(8)	
	Ag16	2.9999(9)		Ag13	2.9050(7)	
Ag15	Sn8	2.7693(8)		Ag12	2.9169(8)	
	Ag1	2.8275(6)		Ag7	2.9197(7)	
	Sn10	2.9256(7)		Ag16	2.9887(7)	
	Ag9	2.9660(8)	Ag12	Sn9	2.7534(5)	
	Ag14	2.9728(7)		Sn11	2.7978(6)	
	Ag15	2.982(1)		Ag2	2.911(1)	
Ag17	2× M36	2.7823(7)		Ag10	2.9169(8)	
	M35	2.783(1)		Ag12	2.9381(7)	
	M30	2.783(1)		Ag16	2.983(1)	
	M32	2.787(1)	Ag14	Sn1	2.751(1)	
	2× M29	2.795(1)		Ag1	2.7732(9)	
	2× M34	2.799(1)		Ag14	2.8308(9)	
	Sn2	2.865(1)		Sn10	2.8916(9)	
		2× Sn12	2.9003(6)		2× Ag15	2.9728(7)
Ag19	Sn2	2.883(3)	Ag16	Ag22	2.756(1)	
	2× Ag22	2.883(2)		2× Ag12	2.983(1)	
Ag21	4× M33	2.7438(8)			2× Ag10	2.9887(7)
	4× Ag4	2.7579(6)			Sn11	2.997(1)
	4× Ag11	2.7734(6)			Ag13	2.9999(9)
Ag23	2× Ag26	2.90(1)	Ag18	Ag18	2.929(1)	
	Ag24	2.98(2)		2× Ag2	3.1084(8)	
	Ag28	3.08(1)	Ag20	Sn2	2.998(5)	
Ag25	Ag28	3.21(1)		Ag28	3.077(7)	
	Ag24	3.92(2)		Ag24	3.15(1)	
Ag27	Ag28	2.92(2)		2× Ag26	3.316(6)	
	Sn12	3.16(2)		M31	3.532(6)	
	M31	3.23(1)	Ag22	Ag16	2.756(1)	
	Ag22	3.35(1)		2× Ag19	2.883(2)	
	Ag19	3.44(1)		Ag22	3.269(1)	
M29	Sn5	2.789(1)	Ag24	2× Ag23	2.98(2)	
	Ag17	2.795(1)		2× Ag20	3.15(1)	
	M36	2.929(1)	Ag26	Sn12	2.798(4)	
	M29	2.9517(6)		Ag23	2.90(1)	
	M32	2.9565(8)		M31	3.163(5)	
	Sn2	2.9605(7)		Ag28	3.310(5)	
	Sn12	3.003(1)		Ag20	3.316(6)	
M31	Ag6	2.7518(8)	Ag28	4× Ag27	2.92(1)	
	2× Ag26	3.163(5)		2× Ag20	3.077(7)	

	2× Ag27	3.23(1)		2× Ag23	3.08(1)
	2× Na15	3.349(2)		2× Na15	3.207(8)
<i>M33</i>	Sn11	2.716(1)		2× Ag25	3.21(1)
	Ag21	2.7438(8)		4× Ag26	3.310(5)
	<i>M33</i>	2.8861(9)		2× Ag22	3.311(7)
	2× Ag4	2.8934(6)	<i>M30</i>	Sn9	2.781(1)
	2× Ag11	2.9008(7)		Ag17	2.783(1)
<i>M35</i>	Sn1	2.7611(7)		2× <i>M36</i>	2.9212(7)
	Ag17	2.783(1)		Sn2	2.949(1)
	<i>M32</i>	2.911(1)		2× <i>M34</i>	2.9773(8)
	2× <i>M34</i>	2.9200(7)	<i>M32</i>	Ag17	2.787(1)
	2× Sn12	2.9816(6)		Sn7	2.7954(9)
<i>N37</i>	<i>N37</i>	3.106(3)		<i>M35</i>	2.911(1)
	2× Ag1	3.113(1)		2× <i>M29</i>	2.9565(8)
	4× Ag14	3.235(1)		2× Sn12	2.9876(7)
	4× Ag15	3.3566(8)	<i>M34</i>	Sn8	2.793(1)
	2× <i>N38</i>	3.453(2)		Ag17	2.799(1)
<i>N39</i>	Ag24	2.48(2)		<i>M35</i>	2.9200(7)
	2× Ag16	3.232(1)		<i>M36</i>	2.929(1)
	4× Ag12	3.266(3)		<i>M34</i>	2.9414(6)
	2× Sn9	3.378(3)		<i>M30</i>	2.9773(8)
	2× Ag22	3.444(5)		Sn12	2.983(1)
			<i>M36</i>	Sn5	2.7782(6)
				Ag17	2.7823(7)
				<i>M30</i>	2.9212(7)
				<i>M29</i>	2.929(1)
				<i>M34</i>	2.929(1)
				Sn12	2.9777(7)
				Sn2	2.9928(7)
			<i>N38</i>	2× Ag15	2.993(1)
				2× Ag3	3.122(1)
				<i>N38</i>	3.136(1)
				2× Sn8	3.2253(8)
				<i>N37</i>	3.453(2)

Na-Sn, Na-Ag, Na-M, Na-N, Na-Na

<i>Na1</i>	2× <i>M29</i>	3.218(3)	<i>Na2</i>	2× <i>M34</i>	3.249(3)
	<i>M32</i>	3.233(3)		<i>M35</i>	3.278(3)
	<i>Na4</i>	3.337(5)		2× Ag14	3.313(3)
	2× Sn5	3.353(2)		2× Ag15	3.318(2)
	2× Ag10	3.357(2)		<i>N37</i>	3.336(3)
	2× Ag7	3.364(3)		2× Sn8	3.425(2)
	2× Ag13	3.382(3)		2× Na6	3.435(3)
	Sn7	3.409(3)		Sn1	3.438(3)
	2× Na20	3.499(3)		Na7	3.559(5)
	Na9	3.551(5)	<i>Na4</i>	Ag4	3.256(3)
<i>Na3</i>	4× Ag12	3.201(3)		2× <i>M33</i>	3.259(3)
	2× Na10	3.257(4)		2× Ag10	3.334(2)
	4× Ag2	3.322(1)		<i>Na1</i>	3.337(5)
	2× Sn9	3.349(2)		2× Ag7	3.343(3)

	<i>N</i> 39	3.352(7)		2× Ag13	3.350(3)
	2× Ag18	3.438(4)		2× Sn11	3.381(2)
Na6	Ag14	3.213(3)		Sn6	3.385(3)
	<i>M</i> 34	3.214(3)		Na4	3.550(5)
	<i>M</i> 35	3.241(3)		2× Na18	3.567(3)
	Ag15	3.259(3)	Na5	<i>M</i> 34	3.217(2)
	Sn12	3.317(3)		<i>M</i> 30	3.230(3)
	Sn10	3.319(3)		<i>M</i> 36	3.239(3)
	Sn1	3.349(2)		Na18	3.313(3)
	Sn8	3.412(3)		Ag7	3.339(3)
	Na2	3.435(3)		Ag5	3.355(3)
	Ag26	3.505(6)		Ag12	3.358(2)
	Na13	3.674(4)		Ag10	3.364(2)
	Na6	3.684(4)		Sn5	3.374(3)
	Na16	3.685(4)		Sn8	3.376(2)
	Na15	3.691(4)		Ag3	3.394(3)
	Na11	3.692(3)		Ag2	3.402(3)
Na8	Ag9	3.182(3)		Sn9	3.402(2)
	<i>N</i> 38	3.182(3)		Na7	3.484(3)
	2× Ag15	3.245(3)		Na21	3.505(3)
	2× Ag8	3.272(3)		Na16	3.530(3)
	Sn3	3.291(3)	Na7	2× <i>M</i> 34	3.224(3)
	Na12	3.303(5)		<i>M</i> 30	3.241(3)
	2× Ag5	3.353(2)		Na19	3.331(4)
	2× Ag3	3.438(3)		2× Ag3	3.350(2)
	2× Sn8	3.473(2)		2× Ag2	3.371(3)
	2× Na11	3.493(3)		Sn9	3.376(3)
Na10	2× Ag11	3.224(3)		2× Sn8	3.386(2)
	<i>M</i> 33	3.253(3)		2× Na5	3.484(3)
	Na3	3.257(4)		Na2	3.559(5)
	2× Ag2	3.329(2)		2× <i>N</i> 38	3.942(3)
	2× Sn4	3.357(2)	Na9	Ag6	3.246(3)
	2× Ag12	3.377(3)		2× Ag7	3.296(3)
	Sn11	3.390(3)		Sn2	3.319(3)
	Na10	3.492(5)		2× <i>M</i> 29	3.334(3)
	2× Na18	3.550(3)		2× Sn5	3.414(2)
Na12	Ag11	3.229(3)		<i>M</i> 31	3.509(3)
	2× Ag4	3.240(3)		2× Na16	3.542(3)
	Na8	3.303(5)		Na1	3.551(5)
	2× Ag5	3.337(2)		2× Na14	3.672(3)
	2× Ag8	3.356(4)	Na11	Ag6	3.229(2)
	2× Ag3	3.361(3)		Ag8	3.257(2)
	2× Sn6	3.382(2)		Ag5	3.283(2)
	Sn4	3.421(3)		Ag15	3.296(2)
	2× Na18	3.542(3)		Ag9	3.307(2)
	Na12	3.554(4)		Sn10	3.358(2)
Na14	<i>M</i> 29	3.196(3)		Sn3	3.402(2)
	<i>M</i> 29	3.210(3)		Sn8	3.427(2)
	<i>M</i> 36	3.219(3)		<i>M</i> 31	3.459(3)

	<i>M36</i>	3.222(3)		Na8	3.493(3)
	Sn2	3.269(3)		Na11	3.569(3)
	Sn12	3.277(3)		Na15	3.613(3)
	Na14	3.344(4)		Na16	3.615(3)
	Sn5	3.438(3)		Na17	3.668(3)
	Sn5	3.439(3)		Na6	3.692(3)
	Ag27	3.54(1)	Na13	Ag25	3.00(1)
	Ag26	3.538(8)		2× <i>M35</i>	3.249(2)
	Na20	3.669(5)		2× <i>M32</i>	3.265(2)
	Na9	3.672(3)		2× Sn12	3.283(8)
	Na21	3.675(3)		Sn1	3.349(4)
Na16	Ag26	3.206(8)		Na13	3.438(4)
	Ag6	3.209(3)		Sn7	3.452(4)
	Ag7	3.245(3)		2× Na6	3.674(4)
	Ag5	3.292(3)		2× Na20	3.710(4)
	<i>M34</i>	3.300(3)	Na15	Sn10	3.071(3)
	<i>M36</i>	3.319(3)		Ag28	3.207(8)
	Sn12	3.336(3)		Na15	3.235(4)
	Sn5	3.398(3)		2× Ag26	3.336(8)
	Sn8	3.429(3)		2× <i>M31</i>	3.349(2)
	<i>M31</i>	3.480(3)		2× Ag27	3.47(1)
	Na5	3.530(3)		2× Na11	3.613(3)
	Na9	3.542(3)		Na17	3.678(5)
	Na11	3.615(3)		2× Na6	3.691(4)
	Ag27	3.65(1)		Ag25	4.02(1)
	Na6	3.685(4)		Ag23	4.65(1)
Na18	Ag11	3.237(2)		2× Na11	4.960(3)
	Ag4	3.255(2)	Na17	4× Ag9	3.208(3)
	<i>M33</i>	3.258(2)		Na17	3.323(7)
	Na5	3.313(3)		2× Sn10	3.374(1)
	Ag2	3.319(2)		2× Sn3	3.384(3)
	Ag12	3.326(2)		4× Na11	3.668(3)
	Ag5	3.332(2)		2× Na15	3.678(5)
	Ag3	3.352(2)	Na19	Ag18	3.165(5)
	Ag7	3.360(2)		4× Ag2	3.257(3)
	Ag10	3.372(3)		4× Ag3	3.274(1)
	Sn11	3.378(2)		2× Na7	3.331(4)
	Sn6	3.390(2)		2× Sn4	3.390(3)
	Sn4	3.395(2)		2× <i>N38</i>	3.469(5)
	Na12	3.541(3)	Na21	Ag19	2.891(3)
	Na10	3.550(3)		Ag16	3.233(2)
	Na4	3.567(3)		Ag10	3.235(3)
Na20	Ag23	3.11(1)		<i>M30</i>	3.247(2)
	Ag25	3.18(1)		Ag12	3.275(3)
	Ag10	3.246(3)		<i>M36</i>	3.292(2)
	Ag13	3.262(3)		Sn2	3.340(2)
	Ag16	3.270(3)		Sn5	3.368(2)
	<i>M29</i>	3.292(3)		Sn9	3.403(3)
	<i>M32</i>	3.300(3)		Ag22	3.490(2)

Sn12	3.324(3)	Na5	3.505(3)
Sn5	3.379(3)	Na20	3.563(3)
Sn7	3.403(2)	Ag20	3.639(6)
Na1	3.499(3)	N39	3.652(2)
Na21	3.563(3)	Na14	3.675(3)
Ag22	3.592(3)	Na21	3.701(3)
Na20	3.649(4)		
Na14	3.669(4)		
Na13	3.710(4)		

Table 6.4 Interatomic distances in the Na₅Ag_{3.7(4)}Sn_{8.2(4)}.

Atom types		Distance (Å)	Atom types		Distance (Å)
Sn-Sn, Sn-Ag, Ag-Ag					
<i>M1</i>	Ag6	2.785(1)	<i>M2</i>	Ag6	2.8219(9)
	<i>M2</i>	2.8811(9)		<i>M5</i>	2.8755(9)
	<i>M3</i>	2.8858(9)		<i>M1</i>	2.8811(9)
	<i>M4</i>	2.923(1)		<i>M2</i>	2.951(1)
<i>M3</i>	<i>M1</i>	2.8858(9)	<i>M4</i>	<i>M5</i>	2.905(1)
	<i>M5</i>	2.8916(9)		Ag6	2.922(1)
	<i>M4</i>	2.9705(9)		<i>M1</i>	2.923(1)
	<i>M5</i>	3.051(1)		<i>M3</i>	2.9705(9)
<i>M5</i>	Ag6	2.800(1)	Ag6	<i>M1</i>	2.785(1)
	<i>M2</i>	2.8755(9)		<i>M5</i>	2.800(1)
	<i>M3</i>	2.8916(9)		<i>M2</i>	2.8219(9)
	<i>M4</i>	2.905(1)		<i>M4</i>	2.922(1)
Na-Sn, Na-Ag, Na-Na					
Na1	Ag6	3.112(5)	Na2	Ag6	3.154(5)
	<i>M4</i>	3.196(5)		<i>M4</i>	3.195(5)
	<i>M2</i>	3.244(5)		<i>M1</i>	3.296(5)
	<i>M5</i>	3.301(5)		<i>M5</i>	3.365(5)
	<i>M2</i>	3.369(5)		Ag6	3.388(4)
	<i>M1</i>	3.441(5)		<i>M2</i>	3.423(5)
	<i>M4</i>	3.494(5)		<i>M3</i>	3.431(5)
	Na3	3.502(7)		Na3	3.500(6)
	<i>M2</i>	3.588(5)		<i>M3</i>	3.500(5)
	<i>M5</i>	3.741(5)		<i>M3</i>	3.666(5)
	Na2	3.771(7)	<i>M1</i>	3.767(5)	
Na3	2× Ag6	3.164(3)		Na1	3.771(7)
	2× Na2	3.500(6)			
	2× Na1	3.503(6)			

Table 6.5 Interatomic distances in the Na₁₃Sn_{25.73(2)}Bi_{1.27(2)}.

Atom types		Distance (Å)	Atom types		Distance (Å)
Sn-Sn, Sn-Bi, Bi-Bi					
Bi1	Sn11	3.145(8)	Sn1	Sn7	2.889(1)
<i>M2</i>	Sn1	2.965(1)		Sn5	2.892(2)
	Sn10	2.985(1)		Sn1	2.911(1)
Sn4	Sn5	2.829(2)		<i>M2</i>	2.965(1)
	Sn3	2.837(2)	Sn3	Sn6	2.835(2)
	Sn6	2.843(2)		Sn4	2.837(2)
	Sn8	2.861(2)		Sn9	2.889(1)
Sn6	Sn5	2.822(1)		Sn7	2.947(2)
	Sn3	2.835(2)	Sn5	Sn6	2.822(1)
	Sn4	2.843(1)		Sn4	2.829(2)
	Sn11	2.854(2)		Sn12	2.848(1)
Sn8	Sn4	2.861(2)		Sn1	2.892(2)
	Sn12	2.878(2)	Sn7	Sn7	2.879(1)
	Sn9	2.880(1)		Sn1	2.889(1)
Sn10	Sn13	2.887(1)		Sn3	2.947(2)
	Sn12	2.900(2)	Sn9	Sn11	2.870(2)
	Sn10	2.936(1)		Sn8	2.880(1)
	<i>M2</i>	2.985(1)		Sn3	2.890(1)
Sn12	Sn5	2.848(1)		Sn13	2.907(2)
	Sn11	2.876(1)	Sn11	Sn6	2.854(2)
	Sn8	2.878(2)		Sn9	2.870(2)
	Sn10	2.900(2)		Sn12	2.877(1)
				Bi1	3.145(8)
			Sn13	Sn13	2.880(1)
				Sn10	2.887(1)
				Sn9	2.907(2)
Na-Sn, Na-Bi, Na-Na					
Na1	<i>M2</i>	3.298(7)	Na2	Bi1	3.20(1)
	Sn3	3.431(7)		<i>M2</i>	3.243(7)
	Sn11	3.457(8)		Sn13	3.250(8)
	Sn7	3.516(9)		Bi1	3.27(1)
	Na2	3.521(8)		Sn12	3.324(5)
	Sn6	3.614(6)		Sn11	3.377(7)
	Bi1	3.65(1)		Na1	3.521(8)
	Sn8	3.759(9)		Sn10	3.540(6)
	Sn4	3.804(8)		Na3	3.59(1)
	Bi1	3.89(1)		Na7	3.618(7)
	Na6	3.99(1)		Sn8	3.696(6)
	Na3	4.00(1)		Sn10	3.703(7)
	Na3	Sn13	3.271(7)		Na4
Sn7		3.288(5)	Na4	Bi1	3.22(3)
<i>M2</i>		3.302(8)		<i>M2</i>	3.246(6)
Sn3		3.332(7)		Sn13	3.262(7)
Sn1		3.365(7)		Sn9	3.274(5)
Sn9		3.387(8)		Bi1	3.30(2)

	Sn10	3.389(5)		Sn11	3.384(6)
	Sn5	3.513(7)		Sn13	3.527(7)
	Sn12	3.524(7)		Na6	3.534(8)
	Na2	3.59(1)		Na5	3.59(1)
	Na1	4.00(1)		Sn8	3.623(7)
Na5	Sn13	3.295(5)		Sn10	3.624(8)
	<i>M2</i>	3.298(7)		Na7	3.631(7)
	Sn3	3.315(7)		Na2	3.967(9)
	Sn7	3.319(7)	Na6	<i>M2</i>	3.298(9)
	Sn10	3.351(7)		Sn11	3.430(9)
	Sn9	3.439(7)		Sn5	3.463(6)
	Sn1	3.443(5)		Na4	3.534(8)
	Sn5	3.484(7)		Sn7	3.554(9)
	Sn12	3.550(8)		Sn6	3.623(8)
	Na4	3.59(1)		Bi1	3.62(1)
	Na6	3.97(1)		Sn8	3.833(9)
Na7	2× Sn8	3.186(8)		Bi1	3.86(1)
	2× <i>M2</i>	3.300(1)		Sn4	3.925(6)
	2× Na2	3.618(7)		Na5	3.97(1)
	2× Na4	3.631(7)		Na1	3.98(1)
	2× Na1	4.076(7)		Sn1	4.058(9)
	2× Na6	4.080(9)		Na7	4.080(9)

Table 6.6 Interatomic distances in the Na_{27.4(2)}Sn_{47.33(2)}Bi_{1.63(2)}.

Atom types		Distance (Å)	Atom types		Distance (Å)
Sn-Sn, Sn-Bi, Bi-Bi					
<i>M1</i>	Sn2	2.9333(9)	Sn2	Sn3	2.8434(8)
	Sn7	2.9339(8)		Sn12	2.8821(7)
Sn3	Sn4	2.8239(8)	Sn4	<i>M1</i>	2.9333(9)
	Sn2	2.8434(8)		Sn11	2.938(1)
	Sn13	2.8491(8)		Sn3	2.8239(8)
	Sn10	2.8551(9)		Sn8	2.8381(8)
Sn5	Sn7	2.8508(8)	Sn6	Sn6	2.8573(8)
	Sn12	2.8542(7)		Sn4	2.8573(8)
	Sn6	2.8952(8)		Sn5	2.8952(8)
Sn7	Sn5	2.8508(8)	Sn8	Sn11	2.9339(9)
	Sn10	2.8836(8)		Sn7	2.942(1)
	<i>M1</i>	2.9339(8)		Sn4	2.8381(8)
	Sn6	2.942(1)		Sn10	2.8986(8)
Sn9	Sn13	2.9271(8)	Sn10	Sn8	2.957(1)
	Sn8	2.9645(9)		Sn9	2.9645(9)
	Sn11	3.0776(9)		Sn3	2.8551(9)
Sn11	Na8	2.87(1)	Sn12	Sn7	2.8836(8)
	Sn6	2.9339(9)		Sn8	2.8986(8)
	Sn2	2.938(1)		2× Sn5	2.8542(7)
	Sn9	3.0776(9)		2× Sn2	2.8821(7)
Sn13	2× Sn3	2.8491(8)			
	2× Sn9	2.9271(8)			
Na-Sn, Na-Bi, Na-Na					
Na1	2× Sn2	3.293(5)	Na2	Sn8	3.122(4)
	2× Sn6	3.306(4)		Sn7	3.211(4)
	2× Sn7	3.388(4)		<i>M1</i>	3.263(4)
	2× <i>M1</i>	3.533(2)		Sn13	3.280(4)
	2× Sn11	3.698(2)		Sn2	3.293(4)
	2× Na5	4.094(7)		Sn11	3.297(4)
Na3	<i>M1</i>	3.219(4)	Na4	Sn9	3.331(4)
	<i>M1</i>	3.274(5)		Sn8	3.419(4)
	Sn10	3.277(4)		Sn6	3.442(4)
	Sn3	3.331(5)		Sn9	3.541(4)
	Sn9	3.333(4)		Na3	3.757(6)
	Na4	3.652(6)		Na4	3.831(7)
	Sn13	3.697(5)		Sn10	3.184(5)
	Na6	3.703(7)		Sn5	3.316(5)
	Na2	3.757(6)		<i>M1</i>	3.325(5)
	Na5	3.768(7)		Sn10	3.409(5)
	Sn2	3.827(5)		Na3	3.652(6)
	Na4	3.909(7)		Sn8	3.708(5)
	Na3	3.990(7)		Sn9	3.740(5)
Na5	Sn11	3.216(5)	Sn7	3.784(5)	
	<i>M1</i>	3.223(5)	Na5	3.800(7)	
	Sn5	3.264(5)	Sn7	3.815(5)	

	Na8	3.37(1)		Na2	3.831(7)
	Sn12	3.443(5)		Na3	3.909(7)
	Sn9	3.601(5)	Na6	<i>M1</i>	3.245(5)
	Na6	3.604(7)		Sn5	3.266(6)
	Na7	3.665(7)		Sn4	3.305(5)
	Na8	3.75(1)		Na8	3.32(1)
	Na3	3.768(7)		Sn10	3.485(5)
	Na4	3.799(7)		Na5	3.604(7)
	Sn2	3.828(5)		Sn11	3.606(6)
	Sn2	3.924(5)		Sn6	3.664(5)
Na7	Sn9	3.186(6)		Na3	3.703(7)
	Sn5	3.207(5)		Sn7	3.722(5)
	Na8	3.21(1)	Na7	3.726(8)	
	Sn11	3.254(6)	Na8	Na8	2.78(1)
	Sn4	3.259(5)		Sn11	2.87(1)
	Sn4	3.277(6)		Sn4	3.08(1)
	Na7	3.503(8)		Sn9	3.10(1)
	Na5	3.665(7)		Sn11	3.15(1)
	Sn8	3.666(5)		Na7	3.21(1)
	Sn6	3.718(5)		Na6	3.32(1)
Na6	3.726(8)	Na5		3.37(1)	
Sn6	3.860(6)	Na5	3.75(1)		

Table 6.7 Interatomic distances of the K₁₂Pd_{0.46}Sn₁₇.

Atom types		Distance (Å)	Atom types		Distance (Å)
Pd-Sn distances					
Pd1	Sn44	2.560(7)	Pd2	Sn13	2.553(6)
	Sn40	2.571(6)		Sn51	2.573(7)
	Sn39	2.579(6)		Sn15	2.580(6)
	Sn38	2.588(6)		Sn10	2.592(6)
	Sn34	2.624(6)		Sn37	2.616(6)
	Sn25	2.633(6)		Sn46	2.628(6)
	Sn11	2.636(6)		Sn24	2.651(6)
	Sn12	2.646(6)		Sn43	2.673(6)
	Sn36	2.791(6)		Sn45	2.766(6)
	Pd3	Sn55		2.47(1)	Pd4
Sn57		2.47(1)	/Sn69	2.672(9)	
Sn14		2.49(1)	Sn70	2.61(1)	
Sn53		2.54(1)	/Sn71	2.534(9)	
Sn54		2.55(1)	Sn72	2.69(1)	
Sn52		2.58(1)	/Sn73	2.74(1)	
Sn49		2.63(1)	Sn74	2.54(1)	
Sn50		2.64(1)	/Sn75	2.56(1)	
Sn47		2.78(1)	Sn76	2.807(9)	
			/Sn77	2.624(8)	
		Sn59	2.559(6)		
		Sn58	2.587(6)		
		Sn56	2.588(6)		
		Sn42	2.605(6)		
Sn-Sn distances within tetrahedral cluster					
Cluster 4A			Cluster 4B		
Sn1	Sn4	2.927(3)	Sn5	Sn7	2.911(4)
	Sn3	2.956(4)		Sn8	2.932(4)
	Sn2	2.986(4)		Sn6	2.934(4)
Sn2	Sn3	2.914(4)	Sn6	Sn8	2.929(4)
	Sn4	2.926(4)		Sn5	2.934(4)
	Sn1	2.986(4)		Sn7	2.941(4)
Sn3	Sn2	2.914(4)	Sn7	Sn5	2.911(4)
	Sn4	2.948(4)		Sn8	2.932(4)
	Sn1	2.956(4)		Sn6	2.941(4)
Sn4	Sn2	2.926(4)	Sn8	Sn6	2.929(4)
	Sn1	2.927(3)		Sn7	2.932(4)
	Sn3	2.948(4)		Sn5	2.932(4)
Cluster 4C			Cluster 4D		
Sn9	Sn11	2.927(4)	Sn13	Sn15	2.921(4)
	Sn10	2.930(4)		Sn14	2.923(4)
	Sn12	2.954(4)		Sn16	2.947(4)
Sn10	Sn9	2.930(4)	Sn14	Sn16	2.916(4)
	Sn11	2.932(4)		Sn13	2.923(4)
	Sn12	2.941(4)		Sn15	2.928(4)
Sn11	Sn12	2.912(4)	Sn15	Sn13	2.921(4)

Sn12	Sn9	2.927(4)	Sn16	Sn16	2.927(4)
	Sn10	2.932(4)		Sn14	2.928(4)
	Sn11	2.912(4)		Sn14	2.916(4)
	Sn10	2.941(4)		Sn15	2.927(4)
	Sn9	2.954(4)		Sn13	2.947(4)
Cluster 4E			Cluster 4F		
Sn17	Sn19	2.914(4)	Sn21	Sn24	2.883(4)
	Sn20	2.914(4)		Sn23	2.936(4)
	Sn18	2.940(4)		Sn22	2.939(4)
Sn18	Sn19	2.932(4)	Sn22	Sn24	2.906(4)
	Sn17	2.940(4)		Sn23	2.938(4)
	Sn20	2.948(4)		Sn21	2.939(4)
Sn19	Sn20	2.913(4)	Sn23	Sn24	2.923(4)
	Sn17	2.914(4)		Sn21	2.936(4)
	Sn18	2.932(4)		Sn22	2.938(4)
Sn20	Sn19	2.913(4)	Sn24	Sn21	2.883(4)
	Sn17	2.914(4)		Sn22	2.906(4)
	Sn18	2.948(4)		Sn23	2.923(4)
Cluster 4G					
Sn25	Sn28	2.908(4)	Sn27	Sn28	2.910(4)
	Sn26	2.922(4)		Sn25	2.938(4)
	Sn27	2.938(4)		Sn26	2.953(4)
Sn26	Sn28	2.922(4)	Sn28	Sn25	2.908(4)
	Sn25	2.922(4)		Sn27	2.910(4)
	Sn27	2.953(4)		Sn26	2.922(4)
Distorted Cluster 4H					
Cluster 4H ₁			Cluster 4H ₂		
Sn29	Sn30	2.940(4)	/Sn33	Sn34	2.887(4)
	Sn31	2.942(5)		Sn35	2.923(4)
	Sn32	2.951(5)		Sn36	2.931(4)
Sn30	Sn32	2.904(5)	/Sn34	Sn33	2.887(4)
	Sn31	2.909(4)		Sn35	2.917(4)
	Sn29	2.940(4)		Sn36	3.028(4)
Sn31	Sn30	2.909(4)	/Sn35	Sn34	2.917(4)
	Sn32	2.925(5)		Sn36	2.922(4)
	Sn29	2.942(5)		Sn33	2.923(4)
Sn32	Sn30	2.904(5)	/Sn36	Sn35	2.922(4)
	Sn31	2.925(5)		Sn33	2.931(4)
	Sn29	2.951(5)		Sn34	3.028(4)
Sn-Sn distances within 9-atomic cluster					
Cluster 9A			Cluster 9B		
Sn37	Sn42	2.989(4)	Sn46	Sn50	2.954(4)
	Sn38	3.004(4)		Sn51	3.015(4)
	Sn39	3.019(4)		Sn49	3.044(4)
	Sn44	3.057(4)		Sn48	3.123(4)
Sn38	Sn37	3.004(4)	Sn47	Sn51	2.984(4)
	Sn45	3.028(4)		Sn52	3.055(4)
	Sn44	3.034(4)		Sn53	3.129(4)
	Sn40	3.084(4)		Sn54	3.146(5)

Sn39	Sn37	3.019(4)		Sn48	3.353(4)
	Sn43	3.025(4)	Sn48	Sn51	2.981(5)
	Sn42	3.082(4)		Sn52	3.006(4)
	Sn40	3.117(4)		Sn46	3.123(4)
Sn40	Sn43	3.009(4)		Sn50	3.216(4)
	Sn45	3.039(4)		Sn47	3.353(4)
	Sn38	3.084(4)	Sn49	Sn46	3.044(4)
	Sn39	3.117(4)		Sn54	3.073(4)
Sn41	Sn42	2.977(4)		Sn50	3.078(4)
	Sn43	2.985(4)		Sn53	3.080(4)
	Sn45	3.026(4)	Sn50	Sn46	2.954(4)
	Sn44	3.031(4)		Sn48	2.972(4)
Sn42	Sn41	2.977(4)		Sn52	3.006(4)
	Sn37	2.989(4)		Sn49	3.078(4)
	Sn39	3.082(4)	Sn51	Sn48	2.981(5)
	Sn44	3.246(4)		Sn47	2.984(4)
Sn43	Sn41	2.985(4)		Sn46	3.015(4)
	Sn40	3.009(4)		Sn53	3.033(4)
	Sn39	3.025(4)	Sn52	Sn50	3.006(4)
	Sn45	3.432(4)		Sn48	3.006(4)
	Sn42	3.505(4)		Sn47	3.055(4)
Sn44	Sn41	3.031(4)		Sn54	3.3071(5)
	Sn38	3.034(4)	Sn53	Sn54	2.944(5)
	Sn37	3.057(4)		Sn51	3.033(4)
	Sn42	3.246(4)		Sn49	3.080(4)
	Sn45	3.310(4)		Sn47	3.129(4)
Sn45	Sn41	3.026(4)	Sn54	Sn53	2.944(5)
	Sn28	3.028(4)		Sn52	3.071(5)
	Sn40	3.039(4)		Sn49	3.073(4)
	Sn44	3.310(4)		Sn47	3.146(5)
	Sn43	3.432(4)		Sn50	3.872(5)
Cluster 9C					
Sn55	Sn56	2.945(5)	Sn60	Sn63	2.933(6)
	Sn60	3.011(5)		Sn61	2.986(5)
	Sn57	3.012(4)		Sn57	3.006(5)
	Sn59	3.111(5)		Sn55	3.011(5)
	Sn63	3.344(5)	Sn61	Sn62	2.956(5)
Sn56	Sn55	2.945(5)		Sn63	2.975(5)
	Sn59	2.959(6)		Sn60	2.986(5)
	Sn63	2.961(5)		Sn58	3.043(5)
	Sn62	2.980(5)	Sn62	Sn58	2.910(5)
Sn57	Sn58	2.982(4)		Sn61	2.956(5)
	Sn60	3.006(5)		Sn56	2.980(5)
	Sn59	3.007(5)		Sn63	3.304(5)
	Sn55	3.013(4)		Sn59	3.329(6)
Sn58	Sn62	2.910(5)	Sn63	Sn60	2.933(6)
	Sn57	2.982(4)		Sn56	2.961(5)
	Sn59	3.018(5)		Sn61	2.975(5)
	Sn61	3.043(4)		Sn62	3.304(6)
Sn59	Sn56	2.959(6)		Sn60	3.344(6)

	Sn57	3.007(5)		Sn55	3.345(5)
	Sn58	3.018(5)			
	Sn55	3.111(5)			
	Sn62	3.328(6)			
Sn-Sn distances between common atoms for disordered cluster 9D ₁ and 9D ₂					
Sn64	Sn73	2.891(7)	Sn66	Sn70	2.787(8)
	Sn65	3.040(5)		Sn71	2.99(1)
	Sn66	3.040(4)		Sn65	2.997(6)
	Sn69	3.061(9)		Sn64	3.040(4)
Sn65	Sn77	2.920(7)		Sn75	3.107(8)
	Sn76	2.97(1)	Sn67	Sn72	2.830(9)
	Sn66	2.997(6)		Sn75	2.891(8)
	Sn64	3.040(5)		Sn69	3.03(1)
	Sn71	3.18(1)		Sn68	3.112(9)
				Sn73	3.153(9)
Sn-Sn distances in disordered 9D atomic cluster					
Cluster 9D ₁			Cluster 9D ₂		
Sn68	Sn72	2.96(1)	/Sn73	Sn64	2.891(7)
	Sn69	3.01(1)		Sn74	2.98(1)
	Sn67	3.112(9)		Sn77	3.01(1)
	Sn64	3.113(8)		Sn67	3.153(9)
	Sn65	3.658(9)	/Sn74	Sn75	2.97(1)
Sn69	Sn68	3.01(1)		Sn73	2.98(1)
	Sn67	3.03(1)		Sn64	3.155(8)
	Sn70	3.05(1)		Sn67	3.258(9)
	Sn64	3.061(9)		Sn66	3.394(8)
Sn70	Sn66	2.787(8)	/Sn75	Sn67	2.891(8)
	Sn71	3.04(1)		Sn74	2.97(1)
	Sn69	3.05(1)		Sn76	2.99(1)
	Sn67	3.215(8)		Sn66	3.107(8)
Sn71	Sn72	2.97(1)	/Sn76	Sn65	2.97(1)
	Sn66	2.99(1)		Sn75	2.99(1)
	Sn70	3.04(1)		Sn77	3.01(1)
	Sn65	3.17(1)		Sn67	3.19(1)
	Sn67	3.41(1)		Sn66	3.63(1)
Sn72	Sn67	2.830(9)	/Sn77	Sn65	2.920(7)
	Sn68	2.96(1)		Sn76	3.01(1)
	Sn71	2.97(1)		Sn73	3.01(1)
	Sn65	3.245(8)		Sn67	3.165(7)

Table 6.8 Interatomic distances of the $K_{20}Ga_6Bi_{13.294(8)}$.

Atom types		Distance (Å)	Atom types		Distance (Å)
Bi-Bi, Bi-Ga, Ga-Ga					
Bi1	Ga1	2.705(1)	Bi2	Ga1	2.647(1)
	Ga1	2.710(1)		Ga1	Bi2
Bi3	2× Bi3	2.7345(2)	Bi1	Bi1	2.705(1)
	2× Bi3	3.7928(9)		Bi1	2.7096(9)
K-Ga, K-Bi, K-K					
K1	2× Ga1	3.7938(6)	K2	2× Bi2	2.647(4)
	2× Ga1	3.7940(7)		2× Bi3	3.606(1)
	2× Ga1	3.8980(3)		Bi2	3.647(3)
	2× Bi1	3.8982(2)		K3	3.666(3)
	2× Bi1	3.8992(3)		2× K4	4.261(4)
	Bi1	4.424(2)		4× K2	4.276(3)
	K3	4.424(2)		K4	4.348(2)
	K3	4.425(3)	K4	2× Ga1	4.366(3)
	K3	4.473(3)		2× Bi1	3.720(2)
	K4	4.475(2)		Bi2	3.726(1)
	K4	4.475(2)		2× Bi2	3.730(3)
	K4	5.4689(3)		2× K2	3.758(2)
	2× K1	3.649(2)		2× K3	4.276(3)
	K3	Bi1		3.689(2)	K3
2× Ga1		3.704(1)	K2	4.316(4)	
2× Bi1		3.739(2)	K1	4.366(3)	
2× Bi2		4.261(4)	K3	4.475(2)	
K2		4.293(2)			
2× K4		4.316(4)			
K4		4.424(2)			
K1		4.550(3)			
2× K3		4.582(3)			
K4		5.4689(3)			
2× K3		2.705(1)			

Table 6.9 Interatomic distances of the K_3InAs_2

Atom types		Distance (Å)	Atom types		Distance (Å)
In-In, In-As, As-As					
In	4× As	2.7193(5)	As	2× In	2.7193(5)
	2× In	3.4681(5)			
K-In, K-As, K-K					
K2	4× As	3.3039(6)	K1	As	3.318(2)
	2× K2	3.4681(5)		As	3.335(2)
	2× In	3.9106(8)		2× In	3.569(1)
	4× K1	3.964(1)		2× As	3.6824(7)
				2× K2	3.964(1)
		2× K1	4.072(1)		

Table 6.10 Interatomic distances of the K₇In₄As₆.

Atom types		Distance (Å)	Atom types		Distance (Å)
In-In, In-As, As-As					
In1	As9	2.662(1)	In2	As7	2.652(1)
	As12	2.674(1)		As4	2.653(1)
	As5	2.682(1)		As7	2.750(1)
	As2	2.720(1)		As1	2.751(1)
	In3	3.178(1)		In6	3.249(1)
In3	As11	2.592(1)		In5	3.369(1)
	As4	2.743(1)		In2	3.414(1)
	As9	2.752(1)	In4	As6	2.682(1)
	As5	2.854(1)		As8	2.758(1)
	In1	3.178(1)		As3	2.805(1)
In5	As10	2.694(1)		In4	2.833(1)
	As7	2.780(1)		In8	3.333(1)
	As1	2.791(1)	In6	As5	2.633(1)
	In5	2.838(1)		As10	2.650(1)
	In6	3.319(1)		As4	2.732(1)
	In2	3.369(1)		As1	2.768(1)
In7	As2	2.659(1)		In2	3.249(1)
	As8	2.659(1)		In5	3.319(1)
	As8	2.742(1)	In8	As12	2.612(1)
	As3	2.743(1)		As6	2.657(1)
	In8	3.270(1)		As2	2.795(1)
	In4	3.3383(9)		As3	2.801(1)
	In7	3.475(1)		In7	3.270(1)
As1	In2	2.751(1)		In4	3.333(1)
	In6	2.768(1)	As2	In7	2.659(1)
	In5	2.791(1)		In1	2.720(1)
As3	In7	2.743(1)		In8	2.795(1)
	In8	2.801(1)	As4	In2	2.653(1)
	In4	2.805(1)		In6	2.732(1)
As5	In6	2.633(1)		In3	2.743(1)
	In1	2.682(1)	As6	In8	2.657(1)
	In3	2.854(1)		In4	2.682(1)
As7	In2	2.652(1)	As8	In7	2.659(1)
	In2	2.750(1)		In7	2.742(1)
	In5	2.780(1)		In4	2.758(1)
As9	In1	2.662(1)	As10	In6	2.650(1)
	In3	2.752(1)		In5	2.694(1)
As11	In3	2.592(1)	As12	In8	2.612(1)
				In1	2.674(1)
K-In, K-As, K-K					
K1	As9	3.286(3)	K2	As11	3.271(2)
	As6	3.374(2)		As10	3.390(2)
	As2	3.383(3)		As4	3.451(2)
	In7	3.484(2)		In2	3.510(2)
	As3	3.573(3)		As1	3.542(2)
	In4	3.594(2)		In5	3.592(2)
	K13	3.709(4)		K9	3.746(3)
	In7	3.739(2)		K5	3.748(3)
	As8	3.755(2)		In2	3.751(2)
	K8	3.770(3)		In5	3.814(2)

K3	K14	3.811(4)	K4	As7	3.827(2)	
	As7	3.290(2)		As7	3.832(2)	
	As11	3.420(3)		K11	3.848(3)	
	In3	3.426(2)		K3	3.957(3)	
	As1	3.443(3)		As8	3.214(3)	
	As5	3.614(3)		In1	3.321(2)	
	K11	3.677(4)		As3	3.512(3)	
	K3	3.692(3)		As9	3.557(2)	
	K9	3.700(3)		As3	3.633(2)	
	As1	3.735(3)		As12	3.649(2)	
	In2	3.802(2)		In8	3.687(2)	
	In6	3.821(2)		K4	3.769(3)	
	As4	3.862(2)		As2	3.774(3)	
	K2	3.957(3)		K14	3.793(4)	
K5	As5	3.374(3)	K6	K8	3.819(4)	
	As7	3.467(3)		As10	3.321(2)	
	As1	3.656(3)		As11	3.323(3)	
	As1	3.668(3)		As5	3.331(3)	
	As11	3.679(3)		In8	3.450(2)	
	K11	3.714(4)		K8	3.603(4)	
	In5	3.731(3)		As2	3.605(2)	
	K2	3.748(3)		As6	3.703(2)	
	K6	3.908(3)		In1	3.727(2)	
	K7	As12		3.298(3)	K9	3.729(4)
		As9		3.316(3)	As12	3.795(3)
		In6		3.436(3)	K12	3.898(3)
		As10		3.628(3)	K5	3.908(3)
		K12		3.633(4)	K10	3.970(4)
As6		3.659(3)	K7	3.980(4)		
In1		3.754(3)	K8	As12	3.352(3)	
In8		3.812(3)		As8	3.411(2)	
As4		3.829(3)		As2	3.443(3)	
K9		3.846(4)		As9	3.473(2)	
K9		As5		3.251(2)	As11	3.559(2)
		As4		3.314(2)	K6	3.603(4)
		As7		3.321(2)	K10	3.675(3)
		As12		3.351(2)	K1	3.770(3)
	K3	3.700(3)		K4	3.819(4)	
	K6	3.729(4)		As6	3.866(2)	
	K10	3.742(4)		In3	3.871(2)	
	K2	3.746(3)		K12	3.914(3)	
	As11	3.761(3)		K10	As4	3.225(3)
	As10	3.821(3)			As6	3.406(3)
	K7	3.846(4)	As12		3.487(3)	
	K11	As10	3.455(3)		As9	3.491(3)
		As4	3.462(3)		K8	3.675(3)
		As11	3.657(3)		K9	3.742(4)
K3		3.677(4)	K12		3.820(4)	
As7		3.682(3)	K6		3.970(4)	
K5		3.714(4)	K13		3.972(4)	
In5		3.738(3)	K12		As11	3.378(3)
K2		3.848(3)			As2	3.412(3)
In2		3.853(3)			As5	3.490(3)
As1		3.938(3)			K7	3.633(4)

K13	K12	3.964(3)	K14	In3	3.679(3)
	As12	3.297(3)		As10	3.708(3)
	As8	3.446(3)		K10	3.820(4)
	As3	3.592(3)		In6	3.887(3)
	In4	3.646(3)		K6	3.898(3)
	K1	3.709(4)		K8	3.914(4)
	As9	3.840(3)		K11	3.964(3)
	K14	3.850(4)		As6	3.491(3)
	As6	3.886(3)		As2	3.511(3)
	K10	3.972(4)		As8	3.623(3)
			In4	3.659(3)	
			K4	3.793(4)	
			K1	3.811(4)	
			In7	3.824(3)	
			As3	3.829(3)	
			K13	3.850(4)	

Table 6.11 Interatomic distances of the $K_{144}In_{192}As_{37(1)}$.

Atom types		Distance (Å)	Atom types		Distance (Å)
In-In, In-As, As-As					
In1	In2	3.020(1)	In2	As1	2.400(5)
	In1	3.0345(7)		In1	3.020(1)
	2× In1	3.0704(9)		2× In1	3.1031(7)
	2× In2	3.1031(7)		2× In2	3.181(1)
As1	In2	2.400(5)			
K-In, K-As, K-K					
K1	3× As1	3.405(5)	K2	12× As1	4.775(4)
	3× In2	3.545(3)		4× As2	5.3349(1)
	6× In1	3.741(3)	K4	12× In1	3.5812(5)
	3× K3	3.958(4)		4× K1	4.036(3)
	K4	4.036(3)		12× In2	5.6529(5)
K3	2× As1	3.471(5)			
	2× As1	3.568(5)			
	2× In2	3.694(3)			
	2× In2	3.742(3)			
	2× In1	3.813(4)			
	As2	3.914(4)			
	2× K3	3.916(4)			
	K1	3.958(5)			
K3	4.083(4)				

7 List of Publications

1. Marina Boyko, Viktor Hlukhyy, Thomas F. Fässler **Na₂₉Ag_{20.6}Sn_{39.7} - a Cluster Interconnected Compound as a Hierarchical Variant of CaCu₅-type.**
19. Vortragstagung für Anorganische Chemie der Fachgruppen Wöhler-Vereinigung und Festkörperchemie und Materialforschung, Regensburg, 24.09.2018.
2. Benedikt J. L. Witzel, Wilhelm Klein, Jasmin V. Dums, Marina Boyko and Thomas F. Fässler **Metallocages for Metal Anions: Highly Charged [Co@Ge₉]⁵⁻ and [Ru@Sn₉]⁶⁻ Clusters Featuring Spherically Encapsulated Co⁻ and Ru²⁻ Anions**
Angewandte Chemie, accepted manuscript, 2019.